Fall 12-17-2022

INHIBITION OF RAD18 BY ARSENIC

Lindsay B. Volk
University of New Mexico

Lindsay Volk

Candidate

Biomedical Sciences

Department

This dissertation is approved, and it is acceptable in quality and form for publication:

Approved by the Dissertation Committee:

Dr. Laurie Hudson, Chairperson

Dr. Mary Ann Osley

Dr. Alan Tomkinson

Dr. Debra MacKenzie

INHIBITION OF RAD18 BY ARSENIC

by

LINDSAY B. VOLK

B.A., Biology, Castleton University, 2012

DISSERTATION

Submitted in Partial Fulfillment of the
Requirements for the Degree of

Doctor of Philosophy
Biomedical Sciences

The University of New Mexico
Albuquerque, New Mexico

December, 2022

DEDICATION

I dedicate this dissertation to my family for their support and encouragement,

to my mentor for her exceptional guidance,

and to my dogs for making me smile,

Thank You.

ACKNOWLEDGEMENTS

First, I would like to acknowledge my mentor, Dr. Laurie Hudson. Her guidance has elevated my research capabilities by teaching me important skills such as being mindful of the big picture. Dr. Hudson is a gifted mentor in that she balances independence and guidance as needed. She supported my individual growth as a research scientist by allowing me to develop my own research project and experimental designs. She has also encouraged a well-rounded graduate experience that includes both research and professional development opportunities to facilitate my career success. Altogether, I am extremely fortunate to have a mentor that supports my personal and professional growth, as well as provides opportunities for me to independently develop as a research scientist.

Secondly, I would like to acknowledge the individuals that made a significant contribution to this dissertation and to my graduate career. I am exceptionally grateful for the support provided by Dr. Karen Cooper over the past 5 years. Whether it was teaching me to run a comet assay, splitting my cells when I could not make it into the lab, or proofreading a grant application, Dr. Cooper was always happy and willing to help. My dissertation committee composed of Dr. Mary Ann Osley, Dr. Alan Tomkinson, and Dr. Debra MacKenzie enhanced my research project by offering important guidance and recommendations. In addition, Dr. Osley provided me with excellent teaching opportunities to fulfill the requirements of my Certificate in University Science Teaching. For technical

support, Dr. Michael Paffett from The UNM Fluorescence Microscopy and Cell Imaging Shared Resource, Dr. Ting Jiang from The UNM Integrative Molecular Analysis Core, and Dr. Yinsheng Wang from the University of California Riverside were instrumental in the design and execution of experiments performed in this dissertation.

Lastly, I would like to acknowledge support from the National Institutes of Health 1R01ES030993, 1R21ES021499, UNM METALS Superfund Research Program 1P42ES025589, and the UNM Center for Metals in Biology and Medicine P20GM130422. This research was partially supported by the UNM Comprehensive Cancer Center P30CA118100 through Trainee Matching Funds and made use of the UNMCCC Fluorescence Microscopy and Cell Imaging shared resource. I give special thanks to The UNM Integrative Molecular Analysis Core within the UNM Center for Metals in Biology and Medicine. Several figures presented in this dissertation were created with Biorender from BioRender.com.

INHIBITION OF RAD18 BY ARSENIC

by

Lindsay B. Volk

B.A., Biology, Castleton University, 2012

Ph.D., Biomedical Sciences, University of New Mexico, 2022

ABSTRACT

Arsenite exposure leads to the retention of UV-induced DNA damage, thus burdening translesion synthesis (TLS). Rad18 is an essential factor in initiating TLS through PCNA monoubiquitination and is implicated in homologous recombination. It contains two functionally and structurally distinct zinc fingers that are potential targets for arsenite binding. Results from this study reveal arsenite binding to both zinc fingers of Rad18 and a corresponding loss of domain function. Importantly, arsenite inhibited Rad18 RING-dependent PCNA monoubiquitination and polymerase eta recruitment to DNA damage. Further analysis demonstrated multiple effects of arsenite, including the reduction in the nuclear localization and UV-induced chromatin recruitment of Rad18. Arsenite and Rad18 knockdown in UV exposed keratinocytes significantly increased markers of replication stress and DNA strand breaks to a similar degree, suggesting arsenite mediates its effects through Rad18. Altogether, this dissertation supports a mechanism by which arsenite inhibits TLS through the altered activity and regulation of Rad18.

TABLE OF CONTENTS

LIST OF FIGURES

CHAPTER 1

CHAPTER 2

CHAPTER 3

LIST OF TABLES

ABBREVIATIONS

6-4 PPs, pyrimidine (6-4) pyrimidone photoproducts; 8-OHdG, 8-Hydroxy-2'-deoxyguanosine; AQP, aquaporin; As(III), arsenite; ATO, arsenic trioxide; BaP, benzo(a)pyrene; BER: base excision repair; BPDE, benzo(a)pyrene diolepoxide; BSA, bovine serum albumin; CPD, cyclobutane pyrimidine dimer; Da, Dalton; DAPI, 4',6-Diamidino-2-Phenylindole Dihydrochloride; DBD, DNA binding domain; DDT, DNA damage tolerance; DMA, dimethylarsonous acid; DMSO, dimethyl sulfoxide; DSB, double-strand break; DSBR, double-strand break repair; EdU, 5-Ethynyl-2'-deoxyuridine; EGFR, epidermal growth factor receptor; EPA, Environmental Protection Agency; H3K36me3, tri-methylation of histone H3 on lysine 36; H3K9me2, di-methylation of histone H3 on lysine 9; HEK-293T, human embryonic kidney (HEK) 293T cells; HEKn, normal human neonatal epidermal keratinocytes; HR, homologous recombination; ESI, electrospray ionization; IR, ionizing radiation; LC, liquid chromatography; MALDI-TOF, matrix-assisted laser desorption/ionization – time of flight; MCL, maximum contaminant level; MIP, max intensity projection; MMA(III): monomethylarsonous acid; MMR, mismatch repair; MS, mass spectrometry; mtDNA: mitochondrial DNA; ND, no damage; NER, nucleotide excision repair; NHEJ, non-homologous end joining; NOS, nitric oxide synthase; NOX, NADPH oxidase; NT, no treatment; PAHs, polycyclic aromatic hydrocarbons; PARP, poly(ADP-ribose)polymerase; PCNA, proliferating cell nuclear antigen; PH2AX, phospho-histone H2A.X (Ser139); PTPs, protein tyrosine phosphatases; Polη, DNA polymerase eta; RING, really interesting new gene;

RNS, reactive nitrogen species; ROS, reactive oxygen species; RPA, replication protein A; SCR, scrambled; SEM, standard error of the mean; siRNA, small interfering RNA; ssDNA, single-stranded DNA; TLS, translesion synthesis; TPEN, N,N,N′,N′-tetrakis(2-pyridinylmethyl)-1,2-ethanediamine; UBZ, ubiquitin-binding zinc finger; UV, ultraviolet radiation; WHO, World Health Organization; XPA, xeroderma pigmentosum complementation group A; XPC, xeroderma pigmentosum complementation group C

CHAPTER 1

INTRODUCTION

This chapter contains a slightly modified version of "Arsenic co-carcinogenesis: inhibition of DNA repair and interaction with zinc finger proteins" by Zhou X, Speer RM, Volk LB (co-first author), Hudson LG, Liu KJ published in Seminars in Cancer Biology (doi: 10.1016/j.semcancer.2021.05.009), "Arsenic and cancer: evidence and mechanisms" by Speer RM, Zhou X, Volk LB, Liu KJ, Hudson LG accepted to Advances in Pharmacology, and "The impact of arsenic on Rad18 and translesion synthesis" by Volk LB, Cooper KL, Jiang T, Paffett ML, and Hudson LG in revision for Toxicology and Applied Pharmacology.

1.1 Introduction to the carcinogenicity of arsenic

Arsenic is ubiquitous in the environment and exposures occur through water, soil, dust, and food. Arsenic is a class I human carcinogen and independently a weak mutagen at environmentally relevant concentrations. Arsenic is the first substance listed on the 2019 Substance Priority List of U.S. Agency for Toxic Substances and Disease Registry [https://www.atsdr.cdc.gov/spl/index.html]. The Environmental Protection Agency (EPA) and World Health Organization (WHO) set a maximum contaminant level (MCL) for arsenic at 10 ppb, which was based on data for arsenic as a single agent exposure and did not consider coexposures (2000). Additionally, recent studies suggest arsenic may affect human health at levels lower than this limit (Ahmad and Bhattacharya, 2019; Saint-Jacques et al., 2018). There is strong experimental and epidemiological evidence that arsenic in

combination with other environmental insults, such as ultraviolet radiation (UV), increases carcinogenesis at low concentrations. Thus, the affected population in the U.S. and around the world may be significantly larger than current estimates when considering that many rural populations rely on well water with arsenic levels above the EPA and WHO standard and are at a greater risk for arsenic-associated diseases.

Arsenic is known to generate multiple types of DNA damage including oxidative DNA damage and strand breaks. At lower concentrations, studies show that arsenic functions as a cocarcinogen enhancing the genotoxicity of other DNA damaging agents (Hartwig et al., 2020; Salnikow and Zhitkovich, 2008). Mechanisms associated with reactive oxygen species (ROS) generation and DNA repair inhibition play important roles in arsenic cocarcinogenicity (Tam et al., 2020). Certain zinc finger DNA repair proteins, such as poly(ADP-ribose)polymerase-1 (PARP-1), are sensitive arsenic targets at low and non-cytotoxic concentrations, which indicates the interaction of arsenic with these protein targets may play an important role in its cocarcinogenesis mechanism.

Arsenic exists in various forms, and metabolic processes generate multiple organic and inorganic arsenic forms at trivalent and pentavalent states. However, trivalent inorganic arsenic (As(III), arsenite) is most relevant to environmental exposure from drinking water, soil, and food. This chapter will focus on the molecular mechanisms that contribute to arsenic carcinogenesis and cocarcinogenesis (highlighting trivalent arsenite) with a particular emphasis on arsenic-mediated DNA damage and repair inhibition. Current research

demonstrating zinc finger proteins as key molecular targets of arsenic will be described. The impact of DNA repair inhibition by arsenic on replication stress has not been thoroughly investigated and is the focus of the dissertation research described later in this chapter.

1.2 Arsenic exposure and uptake

The majority of human population studies focus on chronic arsenic ingestion through drinking water as the predominant exposure route (Andrew et al., 2003; ATSDR, 2016, 2007; Banerjee et al., 2007; Podgorski and Berg, 2020; World Health Organization, 2018). Many parts of the world have high levels of arsenic in groundwater and aquifers with populations that use these water sources for household needs. One arsenic prediction model based on household groundwater-usage statistics estimates that between 94 and 220 million people may be exposed to high arsenic concentrations (Podgorski and Berg, 2020). Indeed, many seminal health studies have focused on populations in areas of the world with high levels of arsenic in water sources including, but not limited to, Bangladesh, India, Taiwan and Chile (ATSDR, 2016, 2007; Banerjee et al., 2017; Farzan et al., 2021; Moore et al., 2002). Some studies have established the relationship between arsenic levels in water and arsenic in biological specimens such as urine, hair, and nails (Mahata et al., 2003; Mäki-Paakkanen et al., 1998; Ruíz-Vera et al., 2019).

More recently, greater attention has been paid to food as a source of arsenic exposure (Arslan et al., 2017; Gundert-Remy et al., 2015; Oberoi et al., 2014;

Wong et al., 2022). Food crops may contain elevated arsenic levels through irrigation with arsenic-containing water, cultivation in arsenic contaminated fields, or use of agricultural products containing arsenic (Gundert-Remy et al., 2015; Wong et al., 2022). Rice has become a notable concern due to arsenic's uptake and accumulation in this plant compared to other common grains such as wheat (Karagas et al., 2019). There is evidence of greater urinary arsenic in individuals reporting higher rice consumption compared to those with low rice consumption even in areas of low arsenic drinking water exposure (Gossai et al., 2017).

Arsenic exposure is mainly in the form of trivalent inorganic arsenic through gastrointestinal absorption. Trivalent arsenic uptake into eukaryotes is mediated mainly by proteins in the aquaporin superfamily (AQPs) (Agre et al., 2002). Mammalian AQPs were first identified to transport trivalent arsenic in rat and mice as AQP9 and AQP7, respectively (Liu et al., 2002). Meanwhile, trivalent arsenic has also been shown to be taken up by glucose transporters such as GLUT1 (Liu et al., 2006) and hexose permeases (Liu et al., 2004). Both aquaglyceroporins and glucose permeases are bidirectional routes of trivalent arsenic into and out of cells.

Organic arsenic forms contribute to arsenic toxicity mainly through metabolic pathways. The metabolism of arsenic after absorption consists of two major types of reactions; oxidative methylation and reduction (Hughes et al., 2011; Li et al., 2017) (**Figure 1.1**). First, arsenite is oxidatively methylated into monomethylarsonic acid (MMA(V)). MMA(V) is thus reduced into monomethylarsonous acid (MMA(III)). Second, MMA(III) is oxidatively methylated

into dimethylarsonic acid (DMA(V)), then reduced into dimethylarsonous acid (DMA(III)). The metabolism of arsenic plays a critical role in toxicity and carcinogenesis. The exact mechanisms of action of different arsenic forms are still unclear, but various hypotheses have been proposed.

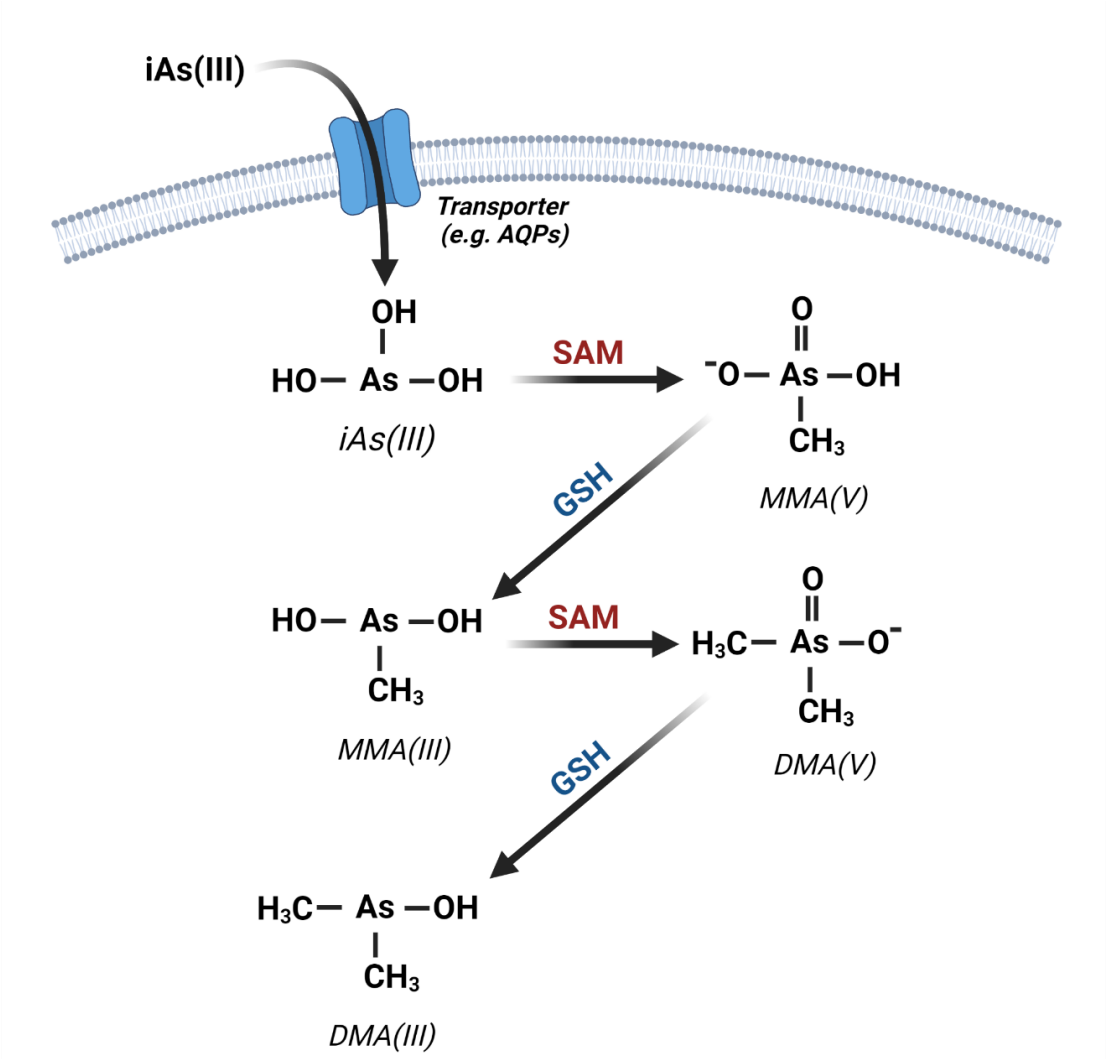

Figure 1.1: The metabolism of arsenic. The uptake of trivalent arsenic into eukaryotes is mediated through several transporters such as AQPs. Trivalent arsenic is metabolized by successive oxidative methylation and reduction reactions. First, iAs(III) is oxidatively methylated into MMA(V) by S-adenosyl methionine (SAM), then reduced into MMA(III) by glutathione (GSH). Second, MMA(III) is oxidatively methylated into DMA(V), then reduced into DMA(III).

Under drinking water exposure, an animal study of organ distribution of arsenicals suggested that kidney, lung, and liver contain the highest levels of arsenic (H. Li et al., 2013). Arsenic is also found in other organs including skin (Hughes et al., 2003; Palma-Lara et al., 2020). In lung, the major form is DMA(III) at almost all time points (Kenyon et al., 2005). At early stages of exposure, liver and kidney contain all forms of arsenicals, such as MMA(III), MMA(V), DMA(III), DMA(V), and inorganic arsenic. At later stages, both liver and kidney show an increase in the percentage of DMA(III) in arsenicals (Kenyon et al., 2005). In contrast, blood and brain contains the lowest level of all arsenic forms compared to other organs across all time points. Inorganic and organic arsenicals were also reported to be strongly accumulated in reproductive organs (Pant et al., 2004).

The carcinogenicity of various arsenic forms and oxidative states largely depend on the tissue/cell type. Intriguingly, in bladder or human urothelial cells, DMA(III) and MMA(III) are the most hazardous arsenicals when considering cytotoxicity and genotoxicity (Bailey et al., 2012; Wang et al., 2007). However, in lung and skin cells, trivalent arsenicals show higher potency for DNA damage (Bolt and Hengstler, 2018; Sattar et al., 2016). This may be because of a difference in metabolism or cellular arsenic uptake.

1.3 Arsenic carcinogenesis

The relationships between arsenic exposure and cancer are clear. Cancer is one of the health effects of concern; arsenic is classified as a Class I human carcinogen by the International Agency for Research on Cancer (IARC) with

strong experimental and human population evidence to support arsenic carcinogenicity (IARC, 2004; Moore et al., 2002; Srinivas et al., 2019; Tam et al., 2020). The strongest evidence for organ-specific arsenic carcinogenicity is in skin, lung, bladder, and kidney with evidence for arsenic contributions to other cancers (ATSDR, 2016, 2007; Palma-Lara et al., 2020; World Health Organization, 2018) (**Figure 1.2**).

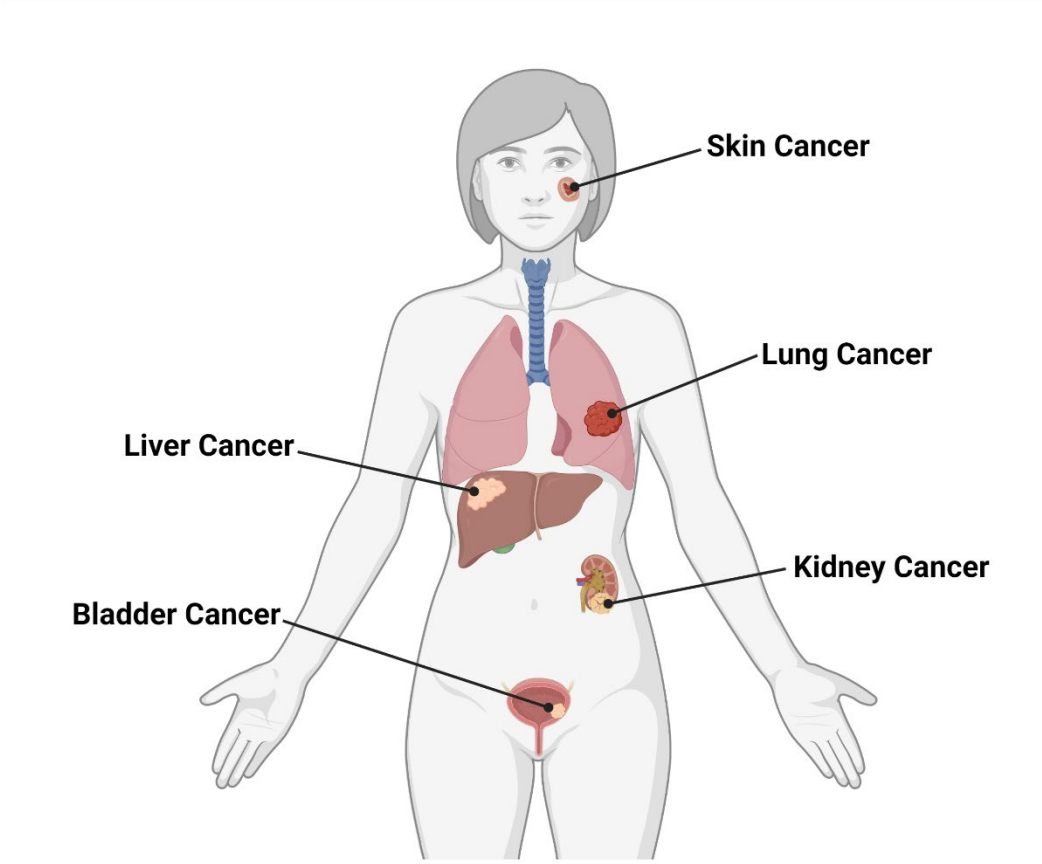

Figure 1.2: Cancers associated with arsenic exposure. Epidemiology studies support the association of arsenic exposure through drinking water with increased risk of developing skin, lung, bladder, kidney, and liver cancers.

Skin Cancer

Various non-cancerous skin lesions are associated with long term exposure to inorganic arsenic including changes in pigmentation, plantar-palmar hyperkeratinization and hyperkeratotic warts and corns (ATSDR, 2007; Hunt et al., 2014). These skin changes are most common in areas with high arsenic levels in drinking water and are viewed as sensitive indicators of chronic arsenic exposure (ATSDR, 2007; Cheng et al., 2016; Hunt et al., 2014). Skin lesions and cancer appear to be more prevalent at exposures to drinking water levels in excess of 50 µg/L and evidence linking arsenic to skin cancer is less conclusive at lower arsenic levels (Boffetta et al., 2020; Karagas et al., 2015; Lamm et al., 2021). Recent findings suggest that ingestion of arsenic containing foods in the diet such as rice may also contribute to skin cancer risk (Gossai et al., 2017; Karagas et al., 2019).

The most common tumors associated with arsenic exposure are keratinocytic tumors including squamous cell carcinomas, which may develop from hyperkeratotic warts or corns, and basal cell carcinomas (ATSDR, 2007; Karagas et al., 2015; Palma-Lara et al., 2020). There is less consistent evidence for arsenic-associated melanoma although it has been reported in Bangladesh (Choudhury et al., 2018), but not in the United States (Bedaiwi et al., 2022; Langston et al., 2022; Yager et al., 2016) or there are too few studies to draw firm conclusions (Matthews et al., 2019).

Lung Cancer

Epidemiological evidence indicates increased incidence of lung cancer in workers exposed to arsenic in the copper mining and smelting industry and ingestion through contaminated water (ATSDR, 2007; Palma-Lara et al., 2020; Smith et al., 2012; Steinmaus et al., 2014). Studies conducted in Chilean cohorts born during periods of low versus high arsenic exposure from water reveal increased incidence of several cancers, including lung cancer, associated with the high exposure period (ATSDR, 2016, 2007; Smith et al., 2006). Similarly, mitigation efforts to decrease arsenic ingestion from contaminated water in Taiwan led to reduction in lung cancer rates (Su et al., 2011). No associations were identified for lung cancer and arsenic in soil in Taiwan despite reported associations between lung cancer and other metals in the same soils (Huang et al., 2013). These findings and others support the conclusion that lung cancer is increased upon chronic exposure to arsenic in drinking water (ATSDR, 2007; Chen et al., 2010; Heck et al., 2009; Kuo et al., 2017; Su et al., 2011). There is evidence for dose dependence (Chen et al., 2010); however, the associations are less strong at low arsenic exposures (Shao et al., 2021; Tsuji et al., 2019).

The most common type of lung cancer associated with arsenic exposure is squamous cell carcinoma (Heck et al., 2009; Kuo et al., 2017; Taeger et al., 2009). The correlation between arsenic and squamous cell carcinoma was more pronounced at higher exposure levels; adenocarcinoma and small cell carcinoma of the lung were not associated with arsenic level in the drinking water in a Taiwan population (Kuo et al., 2017) although other investigators reported

increased adenocarcinoma and small cell carcinomas of the lung with arsenic exposure (Chen et al., 2010; Guo et al., 2004). A study of former German uranium miners exposed to arsenic found that the arsenic-related type of lung cancer differed in miners based on evidence of silicosis. Arsenic was associated with increased squamous cell carcinoma in miners without silicosis. In contrast non-small cell lung cancer was related to arsenic exposure in miners with silicosis (Taeger et al., 2009) suggesting that other underlying factors may influence the specific lung cancer arising because of arsenic exposure.

Bladder Cancer

Population studies identify a clear relationship between elevated arsenic levels in drinking water and bladder cancer (ATSDR, 2007; IARC, 2004; Krajewski et al., 2021; Smith et al., 2012). A recent study found evidence for oxidative DNA damage in residents exposed to arsenic from artesian well-water in Taiwan and concluded that arsenic exposure and DNA damage predicted the risk of bladder cancer (Tsai et al., 2021). In the US, arsenic concentrations in drinking water were positively associated with bladder cancer in both men and women (Baris et al., 2016; Mendez et al., 2017) and a spatial cluster analysis of bladder cancer mortality identified significant hot spots. Further studies concluded that there was a significant association between bladder cancer mortality and arsenic intake from well water (Amin et al., 2019; Baris et al., 2016). Notably, well water is not subject to federal regulation and can exceed the EPA recommended MCL. As with other arsenic-associated cancers, there is not

uniform agreement on risks linked to lower exposures (Kayajanian, 2003) although a meta-analysis suggested that exposure to 10 µg/L of arsenic in drinking water may double the risk of bladder cancers (Saint-Jacques et al., 2014). Arsenic ingestion through food is also considered a potentially important source of exposure that may contribute to bladder and other cancers (Gundert-Remy et al., 2015; Karagas et al., 2019; Oberoi et al., 2014).

There are several studies that indicate arsenic exposure may influence bladder cancer progression and clinical outcomes. Comparisons of clinicopathological characteristics in bladder cancer patients from an arsenic contaminated region versus two reference areas found significantly greater proportions of locally advanced and high-grade tumors in the arsenic-exposed patients (Fernández et al., 2020). Patients from areas of high arsenic exposure in Taiwan versus low arsenic exposure found worse prognosis in the patients from areas of high arsenic and this was most pronounced in the disease-free survival of early-stage disease (Chang et al., 2021). Similar findings were reported for patients in West Bengal, India where measured arsenic accumulation in bladder tumor tissue was associated with advanced tumors, poor prognosis, and disease recurrence after treatment (Ghosh et al., 2021). These observations may be related to distinct mechanisms of arsenic carcinogenesis (Palma-Lara et al., 2020; Zhou et al., 2021).

Additional Cancers and Cancer Risk Due to Prenatal and Early Life Exposure

Although the evidence for arsenic-associated cancers is strongest for skin, lung, and bladder tumors, there are other cancers that are linked to arsenic exposure. There is significant evidence for arsenic induced kidney cancer (Chen and Costa, 2021; Ferreccio et al., 2013a; Krajewski et al., 2021; Naujokas et al., 2013; Palma-Lara et al., 2020; Saint-Jacques et al., 2014; Smith et al., 2012) and liver cancer (ATSDR, 2016, 2007; Chen and Costa, 2021; Naujokas et al., 2013; Palma-Lara et al., 2020). There is more limited evidence for increased gastrointestinal tract (ATSDR, 2016, 2007; Krajewski et al., 2021), laryngeal (Smith et al., 2012), prostate (Lamm et al., 2021), and breast cancer (Moslehi et al., 2021) risk with elevated arsenic exposure (Abuawad et al., 2021). In the case of breast cancer, it appears that genetic factors may play an important modifying role in arsenic-associated risk (Moslehi et al., 2021).

Gestational and early life exposure to arsenic is associated with a variety of long-term health effects including increased risk of cancer in humans (Martinez and Lam, 2021; Smeester and Fry, 2018). This observation is supported by research demonstrating increased cancer in mice following pre- and perinatal arsenic exposures (Boekelheide et al., 2012; Nohara et al., 2017). Studies conducted in Northern Chile provide strong evidence for the cancer consequences of prenatal and early life arsenic exposures. In 1958, the levels of arsenic in drinking water increased nearly 10-fold to 870 ppb and remediation efforts in the 1970s reduced arsenic in drinking water to near pre-1958 levels.

This led to human cohorts with different levels and timing of arsenic exposure (Smith et al., 2012). Increased mortality rates were observed for bladder, laryngeal, lung, kidney, liver, and other cancers (Ferreccio et al., 2013b; Smith et al., 2012; Steinmaus et al., 2014). Long latency patterns of 25 years or more after early life exposure have been reported for liver, kidney, and bladder cancers, often accompanied by evidence for higher incidence and cancer mortality in children and young adults (Liaw et al., 2008; Marshall et al., 2007; Yuan et al., 2010). These findings point to arsenic cancer risks that can persist decades after exposure in early life stages. Given evidence from experimental animal models that prenatal arsenic exposure elevates cancer development (Martinez and Lam, 2021; Waalkes et al., 2007), arsenic exposures across the entire lifespan are a concern.

Modifying Factors of Arsenic Carcinogenesis

Arsenic is one of a limited number of metals or metalloids that is metabolized to methylated forms (Roy et al., 2020). Biotransformation of inorganic arsenic to mono and dimethyl forms (MMA and DMA, respectively) occurs through the enzyme arsenic methyltransferase and arsenic is excreted as a mixture of inorganic and methylated forms (**Figure 1.1**) (Roy et al., 2020). Population studies suggest that the different forms of arsenic are not equivalent in carcinogenic potential. Studies of the proportion of inorganic and methylated arsenic species found that individuals with high percent urinary inorganic arsenic or low DMA present were more likely to develop bladder cancer (Chung et al.,

2013) and a meta-analysis found that bladder and lung cancer were increased significantly with increasing MMA percent in the urine (Melak et al., 2014). Positive associations between percent urinary MMA and cancers of the breast and skin in addition to lung and bladder also have been reported (Abuawad et al., 2021; Gamboa-Loira et al., 2017; Huang et al., 2018). There is increasing evidence that polymorphisms and expression levels of arsenic methyltransferase may lead to differences in arsenic metabolism (Delgado et al., 2021) and are important factors in arsenic-related cancer risk and outcomes (de la Rosa et al., 2017; Huang et al., 2018; Lin et al., 2018; Song et al., 2020).

Coexposures of arsenic and DNA damaging agents can amplify carcinogenesis with the greatest evidence in human populations for skin, lung, and bladder cancers. The risk of arsenic-associated skin lesions that can be precursors to cancer was greater with sun exposure (Chen et al., 2006). Furthermore, arsenic exposure and smoking increase risk of lung and bladder cancers with evidence for a significant arsenic dose effect (Chen et al., 2010, 2004; Ferreccio et al., 2013b; Karagas et al., 2004; Koutros et al., 2018; Tsuda et al., 1995). These population-based findings are consistent with experimental findings of arsenic cocarcinogenesis (Zhou et al., 2021). Cumulatively, the evidence derived from studies of human populations exposed to arsenic indicate that arsenic is a human carcinogen both as a single agent and the carcinogenic effects can be modified by multiple factors including genetic polymorphisms and toxic coexposures.

1.4 Arsenic-induced oxidative stress

Arsenic exposure induces oxidative stress and ROS, which are commonly associated with carcinogenic mechanisms. ROS induce DNA damage and alter DNA repair (Hayes et al., 2020; Hou et al., 2018; Tehrani et al., 2019), which are main concerns for arsenic exposure and carcinogenesis. Such effects on cellular processes take place in both direct and indirect mechanisms. This section will discuss how arsenic exposure induces oxidative stress, and how arsenic leads to DNA damage and alters DNA repair.

Mechanisms of oxidative stress induced by arsenic

Oxidative stress is caused by either the induction of ROS or impairment of the antioxidant response system. Arsenic exposure induces oxidative stress through both mechanisms. There are several mechanisms underlying arsenic-induced ROS generation, and their contributions can depend on arsenic concentration and cell type. Studies show arsenic ROS generation occurs in the mitochondria through inhibition of succinic dehydrogenase activity (Corsini et al., 1999). Additionally, at environmentally relevant levels of arsenic, oxidative damage can occur through arsenic-induced activation of NADPH oxidase (NOX) and nitric oxide synthase (NOS) (**Figure 1.3; Appendix A**) (Barchowsky et al., 1999; Cooper et al., 2022, 2009; Smith et al., 2001). ROS generation also occurs directly through the process of arsenic metabolism within the cell (Ahmad et al., 2000; Kato et al., 1994). Arsenic directly induces the generation of oxygen derived radicals including superoxide anions and hydrogen peroxide (Tam et al.,

2020). Specifically, the arsenic metabolite, dimethylarsine, is shown to interact with molecular oxygen to produce a superoxide anion (Yamanaka et al., 1990). Arsenic increases the formation of peroxyl radicals, singlet oxygen, and hydroxyl radicals among others via Fenton type reactions (Jomova et al., 2011; Shi et al., 2004b). While treatment with dimethyl sulfoxide (DMSO) was shown to inhibit the effects of arsenic-induced ROS by reducing oxygen radicals (Hei et al., 1998), other types of oxidative stress were not attenuated by this type of treatment. These results indicate arsenic oxidative stress occurs through several different mechanisms.

Antioxidant imbalance through altered mitochondrial function and inhibition of ROS scavengers may also serve as main sources of arsenic oxidative stress (**Figure 1.3**). In the cell glutathione serves as an electron donor during arsenic metabolism thereby depleting glutathione leading to antioxidant imbalances (Drobna et al., 2009; Hayakawa et al., 2005; Hughes, 2002). Arsenic-induced antioxidant imbalances have been demonstrated in other studies, which show alterations to superoxide dismutase, catalase, glutathione peroxidase, and glutathione S-transferase (Ćavar et al., 2010; Flora, 1999; Samuel et al., 2005). In addition to directly affecting antioxidant enzyme function, arsenic may alter synthesis of antioxidants including glutathione (Thompson et al., 2009) and superoxide dismutase 1 (Yin et al., 2019). These mechanisms of altered antioxidant response with the concurrent increase in ROS generation likely play important roles in carcinogenic mechanisms of arsenic exposure related to oxidative stress.

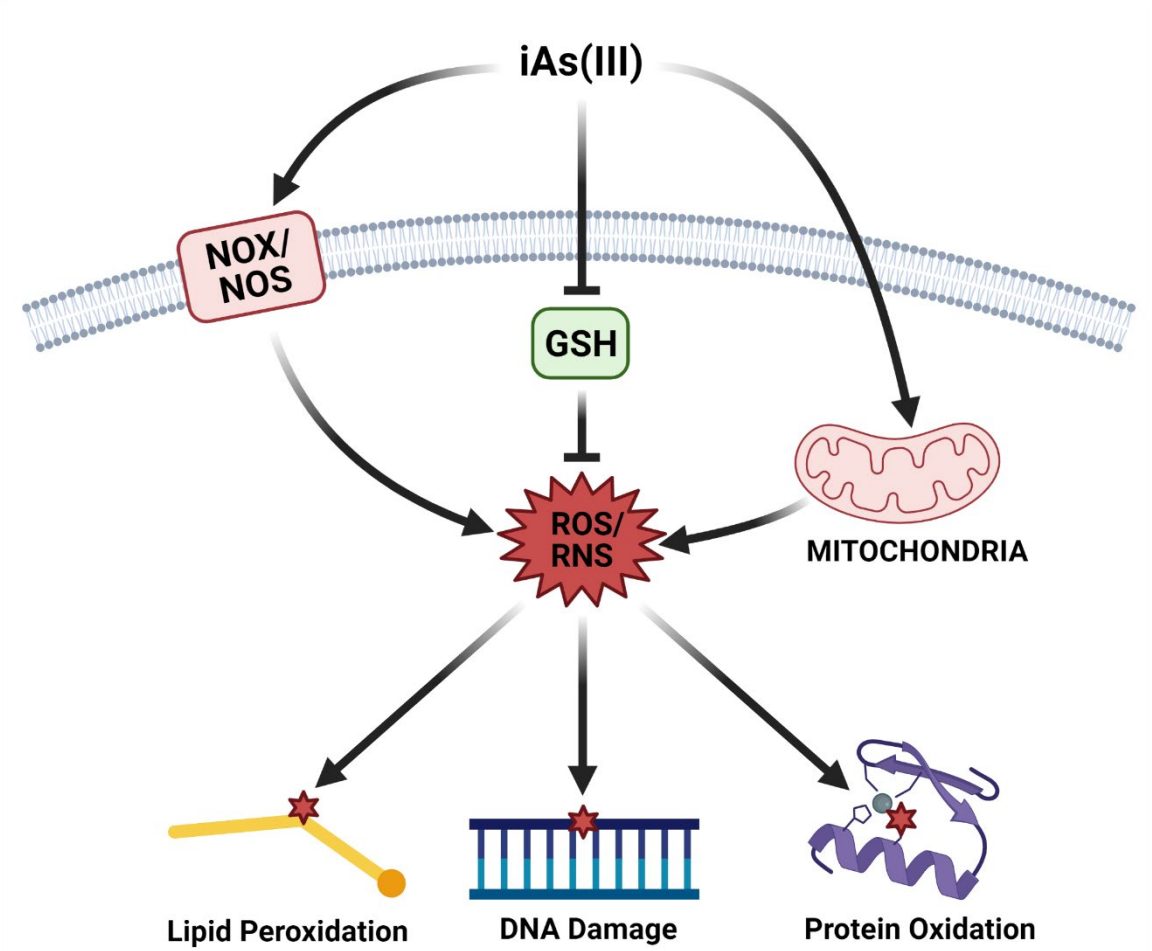

Figure 1.3: Mechanism of arsenic-induced ROS and oxidative damage to macromolecules. Arsenic exposure stimulates the production of ROS/RNS through mechanisms such as the dysregulation of the electron transport chain and stimulation of enzymes such as NOX and NOS. The depletion of glutathione (GSH) through the metabolism of arsenic further promotes redox imbalance. Consequently, macromolecules such as DNA, protein, and lipids are damaged by arsenic-induced ROS/RNS.

Molecular targets of oxidative damage

Consequences of oxidative stress include damage to major macromolecules in the cell including lipids, proteins, and DNA (**Figure 1.3**). Arsenic exposure has been associated with lipid peroxidation in conjunction with ROS generation and DNA damage (Biswas et al., 2010). Arsenic-induced lipid peroxidation was also associated with decreased glutathione and glutathione peroxidase activity likely

further contributing to oxidative stress in cells (Manna et al., 2008). Recent studies show several molecules are capable of reducing arsenic-induced lipid peroxidation including chlorogenic acid and allicin by attenuating ROS and upregulating antioxidant response. Arsenic-induced oxidative damage to lipids may exacerbate oxidative stress in the cell and lead to further perturbations of other components such as DNA. For example, when lipids are oxidized in the cell additional bioactive ROS molecules are generated (Jomova et al., 2011). These bioactive molecules can then perpetuate further lipid damage and target DNA or protein.

DNA is considered a major target of oxidative damage and arsenic-induced oxidative DNA damage has been well studied (Bach et al., 2016; Li et al., 2001; Wei et al., 2019). As a result of increased oxidative stress, arsenic can induce several types of DNA lesions, including strand breaks. One mechanism of arsenic-induced oxidative DNA damage is through NOX activation leading to increased superoxide production (Lynn Shugene et al., 2000). Additionally, arsenic exposure can produce hydroxy radicals that react with DNA nucleobases producing DNA lesions including 8-Hydroxy-2'-deoxyguanosine (8-OHdG), 5-hydroxycytosine, and 5-hydroxyuracil (Huang et al., 2004). While arsenic can induce DNA damage through direct oxidative stress, oxidative damage or alterations to DNA repair proteins can lead to altered DNA repair and therefore additional or unrepaired DNA damage.

Oxidative stress is also associated with protein modifications after arsenic exposure. Direct damage to proteins by arsenic-induced oxidative damage has

been demonstrated by an increase in carbonyl residues, which are used as a biomarker for arsenic oxidative protein damage and a decrease in protein thiols (Biswas et al., 2008; Mahata et al., 2007; Samuel et al., 2005). A recent study also demonstrated a significant association of oxidized low-density lipoprotein with arsenic intake from drinking water in a cohort from the Navajo Nation (Harmon et al., 2018). Several studies have investigated how arsenic-induced oxidative stress alters post-translational modifications of proteins (Howe and Gamble, 2016). Specifically, studies show certain posttranslational modifications to proteins are sensitive to redox states (Duan et al., 2017; Petushkova and Zamyatnin, 2020), which may be altered by arsenic-induced oxidative stress. Tu et al., 2018 (Tu et al., 2018) found arsenic significantly alters histone modifications associated with the transformation of bronchial epithelial cells, and this finding is supported by other studies (Bhattacharjee et al., 2018a; Chervona et al., 2012; Pournara et al., 2016). Arsenic has been found to alter phosphorylation status of proteins leading to changes in signaling pathways and protein function (Alp et al., 2010; Hayakawa et al., 2005; Sheldon, 2017; Shen et al., 2017). Other studies have examined changes in posttranslational modifications of cysteines on proteins by arsenic associated with altered DNA repair protein function (Ding et al., 2009; Wang et al., 2013). Arsenic oxidative stress leads to modification of cysteine residues, especially those containing zinc finger proteins, which are likely targets of arsenic-induced ROS (Nandi et al., 2005; Zhou et al., 2019, 2015). Arsenic is also thought to affect protein tyrosine

phosphorylation due to its effects on redox-sensitive cysteines (Natarajan V et al., 1998; Souza et al., 2001; Wetzler et al., 2006).

Signaling pathways in oxidative stress

Arsenic-induced oxidative stress affects signaling pathways for cell cycle, apoptosis, and gene transcription related to DNA damage and repair. All these pathways have the potential to promote carcinogenic mechanisms and studies show arsenic-induced ROS affect signaling in many of these pathways specifically related to DNA damage (Ganapathy et al., 2019; Medda et al., 2021). For example, although arsenic induces DNA damage, studies show arsenic allows cell cycle checkpoint bypass resulting in unregulated cell proliferation and perpetuation of DNA damage (Beezhold et al., 2017; Hassani et al., 2018; Vogt and Rossman, 2001). In addition to altering cell cycle control, arsenic has also been shown to promote proliferation and survival through extracellular signal-regulated kinase, epidermal growth factor receptor (EGFR) and mitogen-activated protein kinase pathways while simultaneously inhibiting cell death pathways, including apoptosis, although the cells are under increased oxidative stress (Dreval et al., 2018; Germolec et al., 1996; Gu et al., 2017). EGFR may also be activated without EGF binding due to transient inactivation of protein tyrosine phosphatases (PTPs). Because PTPs have preserved cysteine residues sensitive to ROS, and EGFR transactivation is negatively regulated by PTPs, arsenic-induced oxidative stress could inhibit PTPs, thus activating downstream tyrosine kinases (Kumagai and Sumi, 2007). Interestingly, a recent study

demonstrated melatonin was able to overcome arsenic-induced oxidative stress associated with upregulation of pro-inflammatory pathways as well as DNA damage (Abdollahzade et al., 2021). All these mechanisms promote survival of arsenic exposed cells despite DNA damage and increased oxidative stress potentially promoting tumorigenesis.

In addition to affecting proteins in signaling pathways, arsenic may also affect transcription of genes in those pathways resulting in altered function. For example, arsenic activates the E2F family of transcription factors contributing to altered cell cycle regulation and uncontrolled cell proliferation (Kao et al., 2017). Similarly, arsenic affects expression of proteins involved in apoptosis, for example, increasing Bax (pro-apoptotic) and decreasing Bcl2 (antiapoptotic), and these effects occurred despite persistently increased DNA damage (Singh et al., 2011). The combination of transcriptional effects with direct alteration of proteins in these pathways contributes to arsenic carcinogenic mechanisms and tumor progression.

1.5 DNA Damage Induced by Arsenic Exposure

The effects of arsenic on DNA damage and repair underly the carcinogenic and cocarcinogenic mechanisms of arsenic. Unrepaired or incorrectly repaired DNA damage leads to various types of mutations across the genome, which increases the risk of developing cancer. Arsenic exposure can not only cause DNA damage, but also inhibit DNA repair. When coexposed with other DNA damaging agents, DNA repair inhibition by arsenic leads to the retention of DNA

damage and enhanced mutagenesis (Hartwig et al., 2020). Arsenic-induced DNA damage is predominantly mediated through oxidative dependent mechanisms, but other mechanisms also play roles which will be discussed in this section.

Arsenic induces DNA damage and alters DNA methylation

Chromosome instability

Common features of genome instability associated with cancer development include changes to chromosome structure or copy number (Bhatia and Kumar, 2013; Thompson and Compton, 2011; Ye et al., 2020). Several *in vitro*, *in vivo,* and *ex vivo* studies have identified chromosome aberrations, copy number alterations, and micronuclei in association with arsenic exposure (Bustaffa et al., 2014; Dong et al., 2019; Faita et al., 2013). A study on primary human lymphocytes discovered sub-micromolar arsenite treatment resulted in a concentration-dependent increase in abnormal metaphase cells. The most prevalent chromosomal aberrations found in the arsenite exposed lymphocytes were chromatid breaks and aneuploidy (Chakraborty and De, 2009). Aneuploidy is a common characteristic of cancer cells arising from aberrant cell division. A study assessing lung squamous cell carcinoma tumors found an association between arsenic exposure and DNA copy number alterations. Arsenic induced DNA losses in several chromosomes and a gain at chromosome 19q13.33, which is known to contain oncogenes (Martinez et al., 2010). Colognato et al. found arsenic-induced aneuploidy led to the development of micronuclei in arsenic exposed human peripheral lymphocytes (Colognato et al., 2007).

Micronuclei are associated with DNA damage and cancer and have been found to promote tumorigenesis (Bhatia and Kumar, 2013; Kwon et al., 2020). An epidemiology study of a population in Southern Assam, India, linked arsenic exposure through drinking water with enhanced cytogenetic damage. More specifically, cytome assay analysis of buccal epithelial cells revealed arsenic exposure increased the percentage of micronuclei, nuclear buds, binucleated, and pyknotic cells correlating with greater levels of DNA damage in lymphocytes measured via comet assay (Roy et al., 2016). These findings indicate that arsenic can induce genome instability leading to the development of a variety of changes to chromosome structure and copy number, all of which can promote tumorigenesis.

Oxidative DNA damage

There is a vast amount of literature demonstrating the capability of arsenic to generate ROS leading to oxidative stress and DNA damage. As discussed in **Section 1.4**, oxidative damage via arsenic can occur through various mechanisms including mitochondrial dysfunction, antioxidant imbalance, and the activation of NOX and NOS (Cooper et al., 2009; Ding et al., 2005a; Hu et al., 2020). Arsenic-induced ROS and reactive nitrogen species (RNS) attack DNA bases producing lesions such as 8-OHdG and 8-nitroguanine, respectively. Indeed, 8-OHdG has widely been used to measure oxidative DNA damage after arsenic exposure (Chayapong et al., 2017; Cooper et al., 2014; Ding et al., 2005a; Dutta et al., 2015; Mar Wai et al., 2019; Navasumrit et al., 2019). A study

on human *in utero* arsenic exposure showed a significant increase in both 8-OHdG and 8-nitroguanine DNA lesions in arsenic exposed newborns. The study also revealed a significant increase in DNA strand breaks associated with *in utero* arsenic exposure which could arise from unrepaired damage (Navasumrit et al., 2019).

Arsenic-induced oxidative damage to DNA can be enhanced with coexposure to a DNA damaging agent. For example, 10 μM arsenite treatment of HaCaT cells is required for a significant increase in 8-OHdG lesions, whereas the addition of UV leads to enhanced oxidative damage with only 2 μM arsenite (Ding et al., 2005a; Sun et al., 2014). Additionally, a recent epidemiology study found that ROS induced by chronic low levels of arsenic in drinking water correlated with DNA damage (by comet assay) in airway cells and 8-OHdG DNA damage in plasma (Dutta et al., 2015). Further evidence of ROS-induced DNA damage after arsenic exposure is illustrated by a reduction in DNA damage with the addition of free radical scavenging enzymes such as SOD and catalase and treatments upregulating antioxidant responses (Cooper et al., 2013; Ince et al., 2019; Kessel et al., 2002; Zhou et al., 2019). These findings exemplify arsenic as a cocarcinogen.

DNA Methylation

DNA methylation influences gene expression and is mediated through DNA methyltransferases (DNMTs) that catalyze the addition of a methyl group to cytosine. CpG island methylation within promoter regions is generally associated

with decreased gene transcription. DNA methylation patterns are often altered in cancer cells supporting gene-specific promoter hypermethylation and global genome hypomethylation. These alterations can lead to the downregulation of tumor suppressor genes, such as p53 and p16, and the activation of transposable elements and proto-oncogenes promoting carcinogenesis (Brocato and Costa, 2013; Martin and Fry, 2018). P53 and p16 are DNA damage response factors capable of initiating cell cycle arrest in the presence of DNA damage. These mechanisms are essential for preventing the propagation of genetically damaged cells that could lead to the development of cancer. Blood samples from individuals chronically exposed to arsenic in West Bengal, India, revealed a dose-dependent increase in hypermethylation of tumor suppressor genes p53 and p16. However, a small subgroup of individuals exposed to high levels of arsenic displayed hypomethylation of p53, which is a common duality of arsenic on DNA methylation (Chanda et al., 2006; Reichard and Puga, 2010).

Various studies have demonstrated arsenic induced global genome hypomethylation, which may occur as a result of arsenic metabolism. The biotransformation of arsenic can deplete S-Adenosyl methionine levels which is also required for DNA methylation via DNMTs. This can lead to genomic hypomethylation, especially in the context of nutritional deficiencies that limit the synthesis and reutilization of S-Adenosyl methionine (Bustaffa et al., 2014; Martin and Fry, 2018; Reichard and Puga, 2010; Saxena et al., 2018). In addition, several studies demonstrate the ability of arsenite to reduce both transcript and protein levels of DNMT1, DNMT3A, and DNMT3B in HaCaT and lung epithelial

cells, potentially leading to global hypomethylation (Mauro et al., 2016; Rea et al., 2017; Reichard et al., 2007). Gestational arsenic exposure increases global DNA hypomethylation in the sperm of C3H mice, particularly at the retrotransposon LINEs and LTRs. This arsenic mediated effect can lead to an increase in retrotransposon activity which is known to induce various types of cancer (Cajuso et al., 2019; Nohara et al., 2020). Several epidemiology studies have also shown hypomethylation of transposable elements with arsenic exposure (Bustaffa et al., 2014). As mentioned previously, hypomethylation of proto-oncogenes has been reported with arsenic exposure. Proto-oncogene c-Myc and c-Ha-ras hypomethylation and the resulting increase in expression was demonstrated in arsenic treated Syrian hamster embryo cells (Takahashi et al., 2002). C-Myc upregulation is heavily associated with cancer contributing to the development of over 40% of tumors (Miller et al., 2012). Activating mutations within H-ras are commonly found within tumors promoting cancer cell proliferation and survival (Fernández-Medarde and Santos, 2011). Altogether, alterations in DNA methylation patterns by arsenic can lead to gene expression changes that promote carcinogenesis.

Mitochondrial DNA

Mitochondrial DNA (mtDNA) encodes for products involved in cellular respiration and protein synthesis and is vulnerable to oxidative damage. Mitochondria have limited DNA repair capabilities compared to DNA in the nucleus and mtDNA lacks the protective features provided by histones and

nucleosome assembly. ROS generated through the electron transport chain is a common cause of oxidative damage to mtDNA and the development of somatic mutations. Mutations within mtDNA can further disrupt oxidative phosphorylation resulting in heightened ROS production, rate of DNA mutations, and risk for cancer induction (Tseng et al., 2006). Arsenic is known to disrupt the electron transport chain which can enhance the levels of mitochondrial ROS leading to direct mtDNA damage. A concentration-dependent increase in oxidative damage to mtDNA was observed in arsenic exposed human keratinocytes, which was partially rescued with antioxidant treatment. Additionally, elevated levels of mtDNA oxidative damage and mutations were found in lesional skin tissue of individuals with arsenic-induced Bowen's disease compared to perilesional tissue (Lee et al., 2013). Another study showed arsenic trioxide (ATO) treatment of human acute promyelocytic leukemia cells resulted in an increase in mtDNA mutation spots corresponding with an increase in cellular apoptosis. The types of mutations that arose from ATO exposure included transitions, transversions, and codon insertions and deletions (Meng et al., 2010).

In addition to mutations, alterations in mtDNA copy number are also linked to cancer development (Sun et al., 2018; Yu et al., 2007). The D-loop region of mtDNA regulates replication and transcription and D-loop hypomethylation can lead to an increase in mtDNA copy number (Gao et al., 2015). An epidemiology study on a population in West Bengal, India, demonstrated an increase in D-loop hypomethylation in blood samples of individuals exposed to arsenic through drinking water. These findings corresponded with an arsenic-induced increase in

mtDNA copy number (Sanyal et al., 2018). Alternatively, studies have also found an arsenic-induced increase in mtDNA deletions and decrease in mtDNA copy number, which can also support carcinogenesis (Partridge et al., 2007; Zhang et al., 2011). Altogether, these findings demonstrate the genotoxicity of arsenic not only affects nuclear DNA, but also alters the integrity of mtDNA, which is known to be associated with cancer development.

Somatic Mutations

Arsenic is known to induce mutations, which may be in part due to ROS generation (Hei et al., 1998). A study utilizing the mouse lymphoma TK assay revealed a significantly increase in mutation frequency with exposure to at least 10 μM arsenic. This effect was observed with various arsenic species including arsenite, ATO, monomethylarsonic acid, and dimethylarsinic acid (Soriano et al., 2007). Even at low concentrations, arsenite treatment of normal human neonatal epidermal keratinocytes (HEKn) showed a concentration-dependent increase in HPRT mutations from 0.1 to 1 μM arsenite, however the most significant differences were observed with coexposure to UV (Cooper et al., 2013). The role of arsenic-enhanced mutations in carcinogenic mechanisms is a promising trajectory for arsenic research. There is little information on specific site mutations induced by arsenic, and a majority of the literature on this topic is focused on the effect of arsenic in cases of pre-existing mutations (Chang et al., 2009; Nohara et al., 2012). To date, studies have focused on site mutations in specific genes limiting the ability to determine the mechanisms leading to these

events. To better understand arsenic cocarcinogenesis, whole-genome or whole-exome sequencing can be used to determine mutational processes by analyzing mutational signatures.

Arsenic synergy with DNA damaging agents

Ultraviolet radiation (UV)

Arsenic exposure increases the risk of developing skin lesions and several types of skin cancer including squamous cell carcinoma *in situ*, invasive squamous cell carcinoma, and basal cell carcinoma (Kim et al., 2017; Naujokas et al., 2013). In the United States, nonmelanoma skin cancer is the most prevalent malignancy and is associated with increased cost, morbidity, and mortality. Over 3 million people in the United States were treated for nonmelanoma skin cancer in 2012, a substantial increase from 2006 (Rogers et al., 2015). Approximately 90% of nonmelanoma skin cancers are caused by exposure to UV (Kim and He, 2014). In 2004, Burns et al. discovered environmentally relevant levels of arsenic greatly enhanced the carcinogenicity of UV leading to increased cancer yield in mice (Burns et al., 2004). An epidemiology study by Chen et al. also revealed this association in humans (Chen et al., 2006). The link between consumption of arsenic contaminated drinking water and the development of skin cancer is apparent even at concentrations below the EPA MCL of 10 µg/L (Mayer and Goldman, 2016).

UV exposure produces various types of DNA damage depending on wavelength. UVA can generate ROS leading to DNA single strand breaks and

oxidized DNA bases, whereas UVB predominantly contributes to the generation of cyclobutane pyrimidine dimers (CPDs) and pyrimidine (6-4) pyrimidone photoproducts (6-4 PPs) (Cadet and Douki, 2018). Various repair pathways are activated to remove damage caused by UV, such as single strand break repair and base excision repair (BER) for remediating DNA single strand breaks and oxidized DNA bases, respectively. For bulkier DNA lesions such as CPDs and 6-4 PPs, recognition and repair are facilitated by nucleotide excision repair (NER) (Chatterjee and Walker, 2017). Exposure to low levels of arsenic can lead to the inhibition of BER and NER, thus reducing the repair capacity for UV generated DNA lesions (Tam et al., 2020). Studies on UV exposed HEKn cells revealed a significant increase in the levels of 8-OHdG, CPDs, DNA strand break marker phospho-histone H2A.X (Ser139) (PH2AX), and HPRT mutations with only 1 μM arsenite treatment (Cooper et al., 2014, 2013). Levels of UV induced CPDs, 6-4 PPs, and PH2AX were also significantly increased in SHK-1 mice treated with 5 mg/L of arsenite in their drinking water for 28 days (Cooper et al., 2013). Evidence suggests arsenic generated ROS and RNS play a role in the synergistic effects of arsenic and UV through the inhibition of PARP-1 (**Appendix A**) (Cooper et al., 2009, 2022; Ding et al., 2008, 2009; Qin et al., 2008b; Wang et al., 2013). In addition, many studies have found arsenic can regulate the expression of various NER and BER proteins impacting the ability of cells to repair UV generated DNA lesions (Muenyi et al., 2015; Tam et al., 2020). Altogether, the synergy between arsenic and UV provides a clear example of how arsenic can function as a co-carcinogen.

Polycyclic aromatic hydrocarbons (PAHs)

Exposure to PAHs, such as benzo(a)pyrene (BaP), are linked with the development of skin, lung, and bladder cancers and are derived from both natural and anthropogenic sources (Rengarajan et al., 2015). For example, cigarette smoke contains BaP, along with other carcinogens as discussed below (Ma et al., 2019). Exposure to BaP can also occur from emissions from fossil fuel combustion, release of hazardous waste, and ultimately through drinking water. These sources concurrently serve as common sources of arsenic, and therefore, result in BaP-arsenic coexposures. Reactive metabolites of BaP, such as benzo(a)pyrene diolepoxide (BPDE), generate helix distorting DNA lesions at concentrations as low as 10 nM (Piberger et al., 2018). The dominant DNA adduct formed with exposure to BaP is BPDE-N^2-dG, which can lead to G to T transversions in DNA if unrepaired (Tran et al., 2002). These transversions are often found within the p53 gene of lung cancer patients and are associated with PAH exposure through cigarette smoking (Pfeifer and Hainaut, 2003).

Studies have demonstrated the ability of arsenic to promote BaP-induced DNA damage. For example, the addition of arsenite to BaP exposed mouse hepatoma cells enhanced the number of BaP-DNA lesions by as much as 18-fold. Given alone, 0.5 μM BaP and 2.5 μM arsenite did not induce HPRT mutations, but together increased the mutation frequency by 8-fold (Maier et al., 2002). Another study found Sprague–Dawley rats treated with BaP and arsenite displayed an increase in the retention of DNA adducts compared to BaP alone, suggesting the inhibition of DNA repair (Tran et al., 2002). More recent studies by

Burchiel et al. have demonstrated a synergy between arsenic and PAHs in the suppression of immune cells (Ezeh et al., 2015; Xu et al., 2016). Arsenite promoted the genotoxicity of BaP metabolites in mouse thymus cells. Further investigation revealed mechanisms underlying the observed effect may include PARP inhibition and increased BaP metabolism (Xu et al., 2016). Altogether, studies have provided evidence for the synergism of arsenic and BaP leading to increased DNA damage, mutagenesis, and altered immune functions.

Tobacco

Cigarette smoke contains an assortment of carcinogens including PAHs, aromatic amines, and nitrosamines, and can generate ROS leading to oxidative damage to DNA (Ma et al., 2019). Arsenic has been shown to increase genotoxicity and lung cancer risk in cigarette smokers (Chen et al., 2004; Ferreccio et al., 2013b; Roy et al., 2016). *In vivo* studies have demonstrated an increase in oxidative DNA damage with co-exposure to arsenic and cigarette smoke. For example, the addition of aerosolized arsenic compounds to Syrian golden hamsters exposed to cigarette smoke led to a 5-fold increase in 8-oxo-2'-deoxyguanosine, predominantly in the nuclei of airway epithelium and sub-adjacent interstitial cells (Hays et al., 2006). Another study revealed an arsenite-induced increase in plasma 8-OHdG levels within cigarette smoke exposed mice (Wang et al., 2012). An epidemiology study of tobacco chewers in Southern Assam, India, revealed a significant increase in cytogenetic damage when coexposed to arsenic. More specifically, arsenic enhanced the percentage of

buccal epithelial cells containing micronuclei and nuclear buds in tobacco chewers signifying chromosomal damage (Roy et al., 2016). Altogether, these findings demonstrate the ability of arsenic to enhance the genotoxicity of tobacco products resulting in genomic instability and carcinogenesis.

Ionizing radiation (IR)

Radiotherapies utilizing X-ray or gamma radiation generate DNA double-strand breaks (DSBs), which can be lethal or mutagenic if not repaired correctly thus making an effective treatment against cancer (Borrego-Soto et al., 2015). Though a number of cancers can be treated with radiation alone, some require co-therapy to improve treatment outcomes (Baskar et al., 2012). ATO has been shown to significantly increase IR-induced apoptosis of endothelial HDMEC and tumor OSCC-3 cells, while protecting osteoblasts. This arsenic effect was also demonstrated *in vivo*, where the addition of ATO to IR treated mice inhibited tumor growth, angiogenesis, and metastasis, as well as protected against radiation-induced bone loss (Kumar et al., 2008). A study on IR exposed glioblastoma multiforme cells found treatment with ATO upregulated Bax and caspase-3 and downregulated Bcl-2 leading to cellular apoptosis (Moloudi et al., 2017). Arsenic exposure has been shown to inhibit DNA double-strand break repair (DSBR) leading to the retention of DNA damage which can result in the activation of p53 and the induction of apoptosis (Cooper et al., 2014; De Zio et al., 2013; Lieber et al., 2010; Morales et al., 2016; Norbury and Zhivotovsky,

2004; Selmin et al., 2019; Zhang et al., 2014). These findings may support the usefulness of arsenic and IR as a cancer co-therapy.

Cisplatin

Cisplatin is a DNA crosslinking agent used in the treatment of several different types of cancers including carcinomas, germ cell tumors, lymphomas, and sarcomas. Cisplatin crosslinks purine bases within DNA, activating a number of DNA repair pathways (Dasari and Tchounwou, 2014). NER, mismatch repair (MMR), homologous recombination (HR), translesion synthesis (TLS), and Fanconi anemia pathway all play a role in the repair of cisplatin generated DNA lesions (Rocha et al., 2018). The disadvantages of cisplatin as a chemotherapy are the development of cisplatin resistant cancer cells and the various side effects of the treatment (Dasari and Tchounwou, 2014). Combination therapies can often be more effective at lower doses decreasing potential side effects and increasing cytotoxicity towards drug resistant cancer cells (Mokhtari et al., 2017). The synergistic nature of arsenic and cisplatin has sparked many investigations into the co-therapeutic potential of arsenic in the treatment of cancer (Miodragović et al., 2019). The addition of ATO to cisplatin treated human ovarian cancer cells resulted in a concentration-dependent decrease in proliferation and increase in apoptosis. The synergistic effect of arsenic and cisplatin treatment was evident in both cisplatin sensitive and resistant ovarian cancer cell lines, demonstrating the usefulness of arsenic in the treatment of ovarian cancer (Zhang et al., 2009). A number of mechanisms are involved in

cisplatin resistance, including upregulation of DNA repair pathways. The addition of arsenite to cisplatin treated mice increased platinum accumulation in tumors and prevented the upregulation of NER factor Xeroderma Pigmentosum Complementation Group C (XPC), suggesting arsenite may sensitize cancer cells to cisplatin through its ability to suppress NER and increase platinum uptake in tumors (Muenyi et al., 2011).

1.6 Arsenic regulation of DNA repair

At environmentally relevant concentrations, arsenic acts mainly as a cocarcinogen enhancing the carcinogenic effects of other carcinogens. One of the most important mechanisms of arsenic cocarcinogenesis is the inhibition of DNA repair. Epidemiology studies show arsenic-exposed populations have reduced DNA repair capacity (Andrew et al., 2003). While not fully understood, arsenic orchestrates a multitude of different effects on cellular function that decrease DNA repair and promote the carcinogenicity of DNA damaging agents. Indeed, evidence of arsenic mediated changes in the levels and recruitment of NER, BER, DSBR, and MMR proteins have been reported (**Figure 1.4**) (Andrew et al., 2006, 2003; Bhattacharjee et al., 2018b; Ding et al., 2020; Ebert et al., 2011; Holcomb et al., 2017; Hossain et al., 2012; Mauro et al., 2016; Mo et al., 2006; Nollen et al., 2009; Osmond et al., 2010; Selmin et al., 2019; Sykora and Snow, 2008; Zhang et al., 2017). In addition, arsenic can alter the activity of DNA repair proteins such as through direct binding to critical zinc finger domains, further discussed in **Section 1.7** (Tam et al., 2020). For example, DNA repair

pathways depend on DNA ligases for the sealing of undamaged DNA, and arsenite is known to inhibit the activity of both DNA ligase I and III (**Figure 1.4**) (Hu et al., 1998).

Retained DNA damage from arsenic inhibition of DNA repair can result in the generation of DNA DSBs when encountered by the DNA replication fork (Alexander and Orr-Weaver, 2016; Ying et al., 2009). Arsenic is known to induce DNA strand breaks, particularly in conjunction with a DNA damaging agent (Qin et al., 2008b; Tam et al., 2020; Ying et al., 2009). DNA DSBs are a common cause of chromosomal rearrangements and can also occur through improper DNA repair. Studies have shown alterations in DSBR by arsenic favor error prone pathways, such as non-homologous end joining (NHEJ) (**Figure 1.4**), and are associated with structural changes to chromosomes including chromosomal translocations (Lieber et al., 2010; Morales et al., 2016; Selmin et al., 2019; Zhang et al., 2014). The following sections summarize and review recent advances in arsenic inhibition of DNA repair, showing the effects at all levels, from transcription to post-translation.

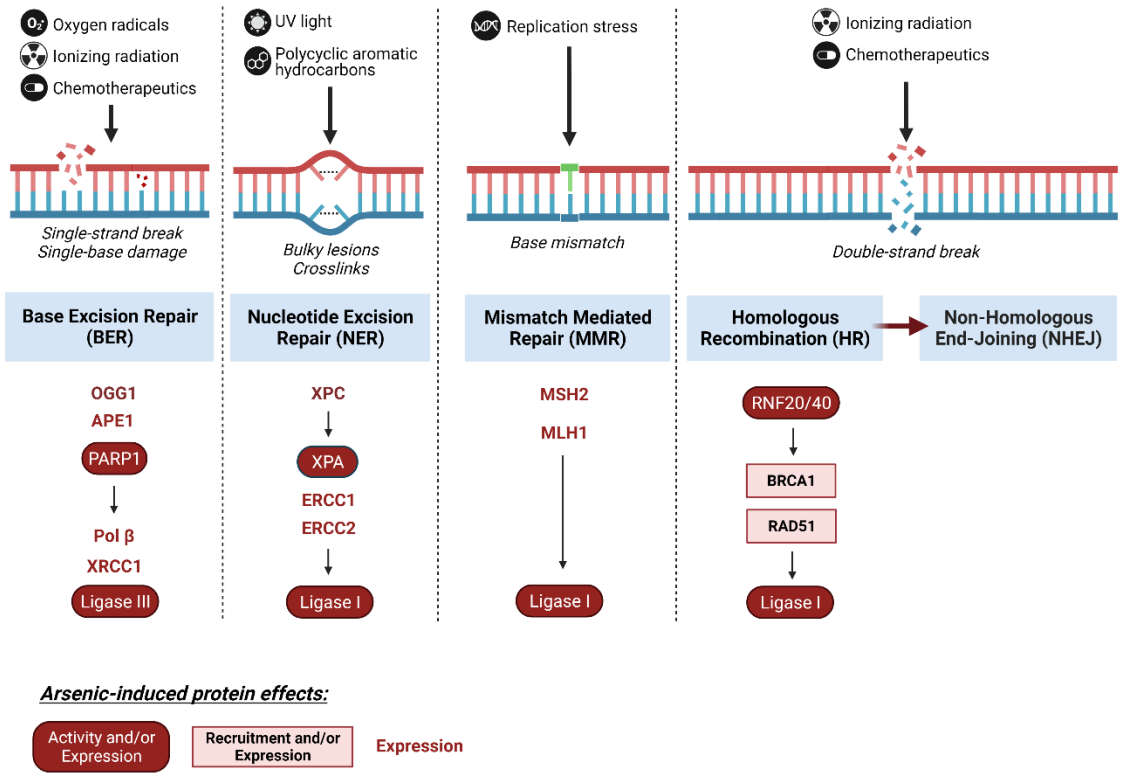

Figure 1.4: Arsenic inhibits DNA repair. Various DNA lesions are generated by both endogenous and exogenous sources of DNA damage. These types of damage are remediated by repair pathways which contain critical DNA repair proteins that facilitate the recruitment of repair proteins, removal of damage, and the synthesis and sealing of undamaged DNA. Arsenic alters the function of key DNA repair proteins by several means: zinc finger domain inhibition leading to loss of activity, disruption in recruitment to DNA damage, and/or the suppression of expression by altering transcription and protein turnover.

Transcriptional regulation

Canonical pathways of protein expression begin with changes in mRNA at the transcriptional level. Several studies have demonstrated arsenic-induced alterations in transcript levels of DNA repair genes, particularly those involved in NER and BER (Ebert et al., 2011; Holcomb et al., 2017). Mechanistically, arsenic may alter the expression of DNA repair genes by affecting DNA methylation and histone modifications. Importantly, arsenic-induced changes in gene expression can depend on various conditions. A study conducted by Osmond et al.

investigated arsenite regulation of BER gene transcript levels in mice. Transcript levels of BER genes APE1, LIG1, OGG1, PARP1, and POLB were all significantly reduced in 24-week-old mice treated with 2 ppm arsenite for 2 weeks compared to untreated mice (**Figure 1.4**). However, acute 24hr arsenite treatment *increased* BER genes APE1, LIG3, and POLB. These findings along with the significant differences between transcript levels in 24-week-old versus 1-week-old mice, highlights the complexity of arsenic and the potential reasoning behind the diverse and sometimes conflicting results seen in arsenic research (Osmond et al., 2010). Many studies have demonstrated arsenic may impact DNA repair directly at the transcriptional level, though much of the research has been conducted using arsenic levels significantly higher than environmentally relevant. Detailed mechanisms, such as DNA methylation and histone modifications, will be discussed in this section.

DNA Methylation

As mentioned in **Section 1.5**, arsenic can downregulate DNA damage response genes and upregulate proto-oncogenes and transposons by altering DNA methylation patterns. Additionally, arsenic is associated with the downregulation of DNA repair genes via promoter hypermethylation. BRCA1 is an essential DNA repair protein involved in HR, an error free DSBR pathway, and promoter hypermethylation is commonly linked with sporadic breast tumors and estrogen receptor negativity (Birgisdottir et al., 2006). Arsenite treatment led to BRCA1 hypermethylation and decreased BRCA1 and estrogen receptor alpha

expression in both MCF7 cells and MCF7 cell mammary tumor xenografts (**Figure 1.4**) (Selmin et al., 2019). These findings may demonstrate a mechanism by which arsenic promotes cancer through the inhibition of an error free DSBR pathway. Indeed, a study utilizing DSBR reporter assays showed arsenic exposure influences pathway choice favoring more error prone repair mechanisms, such as NHEJ, which are associated with chromosomal aberrations (Lieber et al., 2010; Morales et al., 2016).

Arsenic-induced changes in DNA methylation are also linked with the downregulation of MMR genes. Arsenite treatment of HaCaT cells has been shown to increase promoter hypermethylation of the MMR gene MSH2 resulting in decreased expression (Mauro et al., 2016). In addition, a study evaluating the impact of arsenic on individuals within West Bengal, India, revealed significant promoter hypermethylation of both MLH1 and MSH2 genes and a corresponding downregulation in gene transcript levels (**Figure 1.4**) (Bhattacharjee et al., 2018b). MMR is an important pathway in the recognition and remediation of DNA replication and recombination generated base mismatches, insertions, and deletions (Li, 2008). Recombination events can occur from unrepaired DNA lesions, particularly when encountered by the replication fork (Alexander and Orr-Weaver, 2016). Arsenic exposure leads to the retention of unrepaired DNA lesions which may increase replication stress and DNA strand breaks, thus increasing the requirement of MMR (Alexander and Orr-Weaver, 2016; Li, 2008, p. 200; Tam et al., 2020). Therefore, the loss of MMR in the context of arsenic exposure may have a great effect on genome stability. The impacts of arsenic-

induced promoter hypermethylation are broad, altering the function of other DNA repair pathways such as NER through the hypermethylation of ERCC1 and ERCC2 (**Figure 1.4**) (Zhang et al., 2017).

Histone Modifications

Chromatin structure is tightly regulated by the methylation of histones, such as di-methylation of histone H3 on lysine 9 (H3K9me2), which is most often found within heterochromatin and is associated with gene silencing (Bannister and Kouzarides, 2011). Recently, Ding et al. discovered an arsenite induced increase in H3K9me2 levels within promoter regions of BER genes MPG, XRCC1, and PARP1, which corresponded with a decrease in transcript and protein levels of each gene (**Figure 1.4**) (Ding et al., 2020). Partial rescue of protein levels was achieved with methyltransferase inhibitor treatments, indicating the role of histone methylation in the mechanism of action of arsenic (Ding et al., 2020). BER is an essential pathway for the removal of oxidized DNA bases, particularly in the context of arsenic exposure which stimulates the production of ROS (Whitaker et al., 2017). Without this protective mechanism, mutations may arise and promote tumorigenesis (Sakumi et al., 2003, p. 1).

Post-translational regulation

Degradation

Arsenic regulates proteasomal-mediated degradation of proteins through various means (Di and Tamás, 2007; Holcomb et al., 2017; Jacobson et al.,

2012; Tamás et al., 2014; Watanabe et al., 2014; Yan et al., 2014; Yang et al., 2019). For example, ATO is used in the treatment of acute promyelocytic leukemia due to its ability to bind PML-RARα oncoprotein and stimulate ROS leading to the formation of PML-RARα multimers and targeted degradation (Jeanne et al., 2010). Arsenic binding also contributes to the degradation of TIP60 involved in DSBR (Tam et al., 2017). The mechanism and consequences of arsenic binding to proteins is further discussed in **Section 1.7**. Another mechanism by which arsenite influences protein degradation is through the upregulation of E3 ubiquitin ligases. A study on p53 mutant expressing HaCaT and MIA PaCa-2 cell lines revealed ATO transcriptionally increased the levels of an E3 ubiquitin ligase, Pirh2, which in turn increased the polyubiquitination and degradation of mutant p53 (Yan et al., 2014). XPC is an integral factor in global genome NER and can bind to a variety of DNA lesions such as those caused by exposure to UV, chemotherapy drugs, and tobacco smoke (Ma et al., 2019; Schärer, 2013). High concentrations of arsenite decreased XPC protein levels in human lung fibroblasts and primary mouse keratinocytes (**Figure 1.4**). XPC expression in human lung fibroblasts was partially rescued with the addition of a proteasome inhibitor, MG-132, suggesting levels of XPC were regulated via arsenite-induced proteasomal degradation (Holcomb et al., 2017). In addition to specific targets, global levels of polyubiquitinated proteins were increased in ATO treated mouse cardiomyocytes. These findings corresponded with a concentration-dependent increase in proteasome activity with ATO exposure, which was found to play a protective role against arsenic mediated cell death

(Watanabe et al., 2014). In addition to transcriptional regulation, these findings demonstrate arsenite can alter the levels of DNA damage response and repair genes via protein degradation.

Recruitment

Protein phosphorylation is a post-translational modification which can induce changes in protein activity, stability, binding, and cellular localization. Arsenic is known to regulate several different signaling pathways via mechanisms such as generating ROS, binding to sulfhydryl groups, and altering gene expression. EGFR signaling mediates DNA repair pathways such as MMR (Ortega et al., 2015). The activation of EGFR leads to the phosphorylation of the DNA sliding clamp, proliferating cell nuclear antigen (PCNA), which in turn inhibits the binding and activation of MMR factors by PCNA (Tong et al., 2015). PCNA is a critical processivity factor that facilitates DNA replication and replication-coupled DNA repair pathways by acting as a scaffold for the recruitment of proteins (Mailand et al., 2013). HeLa cells treated with 5, 10, and 15 μM arsenite resulted in a concentration-dependent increase in EGFR levels in which corresponded with an increase in the phosphorylation of PCNA. Whole cell extracts from arsenite treated HeLa cells had reduced MMR activity which was partially restored by the addition of exogenous PCNA (Tong et al., 2015). These findings demonstrate a mechanism by which arsenic alters the activity of MMR through PCNA phosphorylation (Ortega et al., 2015; Tong et al., 2015).

As mentioned previously, Bhattacharjee et al. demonstrated hypermethylation of MMR genes in individuals chronically exposed to arsenic in West Bengal, India. In addition to this finding, the authors discovered another mechanism by which arsenic inhibits the activity of MMR, alterations in histone methylation. The study found that arsenic exposure was associated with the reduction in tri-methylation of histone H3 on lysine 36 (H3K36me3), particularly in the subpopulation with skin lesions (Bhattacharjee et al., 2018b). H3K36me3 is required for the recruitment of MMR machinery to chromatin, and thus, its function. Loss of H3K36me3 is linked with microsatellite instability and enhanced spontaneous mutation frequency, as seen in cells deficient in MMR (F. Li et al., 2013, p. 36). Alterations in histone acetylation and ubiquitination have also been demonstrated with arsenic exposure. Arsenite can bind and inhibit histone modifiers such as TIP60 histone acetyltransferase and RNF20-RNF40 histone E3 ubiquitin ligase resulting in a decrease in acetylation of lysine 16 on histone H4 and monoubiquitination of lysine 120 on histone H2B respectively. These histone modifications are important in the recruitment of DSBR factors such as BRCA1 and RAD51 by relaxing chromatin around DNA DSBs (Tam et al., 2020, 2017; Zhang et al., 2014). Altogether, the different mechanisms in arsenic mediated regulation of DNA repair proteins illustrates the multifaceted effects of arsenic on cell function and genome stability (**Figure 1.4**).

1.7 Mechanisms of arsenic-induced zinc finger protein disruption

The DNA repair system is highly sensitive to arsenic exposure. Even at low, non-cytotoxic concentrations, arsenic exposure inhibits DNA repair activity coinciding with inhibition of specific zinc finger DNA repair proteins that are sensitive to arsenic exposure. In this section, we will summarize and review recent advances on arsenic inhibition of zinc finger DNA repair proteins. In addition, we will discuss how this mechanism works in concert with oxidative stress mechanisms, creating a cohesive picture of arsenic cocarcinogenesis.

Zinc finger proteins: key role of the zinc ion

Zinc finger proteins form a large family that function in various physiological and pathological processes (Cassandri et al., 2017; Razin et al., 2012). Zinc fingers are small, folded motifs thermodynamically held together by the coordination of a zinc ion with a combination of four cysteine and/or histidine residues (Eom et al., 2016; Klug, 2010). Zinc plays an important role in the structure and function of zinc fingers, as well as protecting the sensitive thiol groups from oxidation (Krishna et al., 2003; Zhou et al., 2015). Zinc finger proteins can be categorized by the number of cysteine and histidine residues they contain. For example, the “classical” zinc finger consists of 2 cysteine and 2 histidine residues, designated a C2H2 conformation (Razin et al., 2012). Other non-classical zinc finger proteins have different combinations of cysteine and histidine residues, such as C3H1 and C4 (Cassandri et al., 2017; Eom et al., 2016). Zinc finger proteins can also have more complicated structures, such as

RING (really interesting new gene), PHD, and LIM types (Borgel et al., 2017; Gibson et al., 1988; Linke et al., 2008; Nunez et al., 2011; Turner and Miller, 1994), however, these complex structures are in reality combinations of C3H1 or C4 zinc fingers (Cassandri et al., 2017; Eom et al., 2016; Linke et al., 2008; Matthews et al., 2009). Over 80% of zinc finger proteins are found in the C2H2 conformation, while a minority are categorized as the C3H1 and C4 conformations (Cassandri et al., 2017).

Over five percent of human proteins contain zinc finger domains that perform various functions including binding to DNA, RNA, lipids, proteins, and are involved in post translational modifications (Vilas et al., 2018). Recognizing and binding to other macro-molecules are mediated by zinc finger motifs (Eom et al., 2016; Fu and Blackshear, 2017; Linke et al., 2008; Razin et al., 2012). Removing the zinc ion from zinc fingers results in conformational changes and loss of function. As a result, arsenic displacement of zinc ion, through direct or indirect mechanisms, could severely disrupt zinc finger protein function, which will be discussed in following sections.

Zinc finger DNA repair proteins as an arsenic target

PARP-1 has two C3H1 zinc fingers in its DNA binding domain (DBD) and is an essential DNA repair protein that is recognized as a highly sensitive target of arsenic exposure (Tam et al., 2020). Early studies show low levels of arsenic not only inhibit PARP-1 expression, but also its function, setting the stage for future investigation into how arsenic affects zinc finger proteins (Hartwig et al., 2003;

Walter et al., 2007). PARP-1 binds to DNA strand breaks via its zinc fingers in the DNA-binding domain, stimulating poly ADP-ribosylation, recruitment of DNA repair factors, and the initiation of repair pathways such as BER, NER, single-strand break repair, and DSBR (Ray Chaudhuri and Nussenzweig, 2017; Reynolds et al., 2015). These pathways are required for the repair of UV generated DNA damage and therefore, PARP-1 is an essential protein for maintaining genome stability in the context of UV exposure (Chatterjee and Walker, 2017). Indeed, knockdown of PARP-1 significantly increases the retention of UV-induced 8-OHdG and DNA strand breaks in HaCaT cells (Ding et al., 2009; Qin et al., 2008b).

Arsenite treatment of HEKn cells results in a concentration-dependent decrease in PARP-1 zinc content, signifying arsenite mediated displacement of zinc from the PARP-1 zinc fingers (Cooper et al., 2014). The mechanism of zinc displacement from PARP-1 was revealed by MALDI-TOF-MS analysis demonstrating arsenite binding to the PARP-1 zinc finger peptide, even in the presence of excess zinc (Ding et al., 2009; Zhou et al., 2011). Arsenite was shown to reduce chromatin bound PARP-1 and UV stimulated poly ADP-ribosylation in HEKn cells providing evidence for arsenite mediated inhibition of the zinc finger containing DBD of PARP-1 (**Figure 1.4**) (Cooper et al., 2014; Ding et al., 2017). PARP-1 inhibition by arsenite may also be a mechanism underlying the enhancement of UV-induced 6-4 PPs, CPDs, 8-OHdG, PH2AX, and gene mutations in HEKn cells exposed to arsenite (Cooper et al., 2013). Arsenite treatment of SHK-1 mice also led to an increase in UV-induced 6-4 PPs, CPDs,

and PH2AX. Furthermore, zinc supplementation reduced arsenic enhancement of DNA damage both *in vitro* and *in vivo* (Cooper et al., 2013). These findings support a mechanism of arsenite-induced zinc loss from PARP-1 leading to DBD inhibition and the retention of DNA damage with coexposure to UV.

PARP-1 is not a unique DNA repair protein target for arsenic. Xeroderma Pigmentosum Complementation group A (XPA) is an essential NER factor that binds to DNA lesions via its C4 zinc finger domain and acts as a scaffold to mediate repair (Fadda, 2015). Arsenite treatment of both HaCaT and HEKn cells leads to a significant reduction in XPA zinc content (Ding et al., 2017; Zhou et al., 2011). The loss of zinc in XPA corresponds with increased cysteine oxidation and decreased chromatin recruitment of XPA in HEKn cells exposed to arsenite (**Figure 1.4**) (Ding et al., 2017; Zhou et al., 2015). The inhibition of XPA by arsenic may contribute to the retention of UV induced 6-4 PPs, CPDs, and DNA strand breaks in cells (Cooper et al., 2013; Fadda, 2015). In addition, XPA inhibition by arsenic could hinder the removal of bulky DNA lesions caused by cisplatin and BaP, thus supporting the observed synergistic effects described in **Section 1.5** (Ma et al., 2019; Schärer, 2013). Several studies by Wang et al. demonstrate arsenic targeting RING finger containing DNA repair proteins. The RING finger is distinct from the zinc finger domains of XPA and PARP-1 in that it is composed of two interdigitated zinc-binding sites. Upon DNA damage, the RNF20-RNF40 E3 ubiquitin ligase complex is responsible for the monoubiquitination of histone H2B which leads to chromatin relaxation and facilitates DSBR factor recruitment (Zhang et al., 2014). Both RNF20 and RNF40

RING fingers contain C4 and CHC2 zinc binding sites (Foglizzo et al., 2016). MALDI-TOF-MS and UV absorption spectra analyses of RNF20 and RNF40 RING finger peptides revealed direct arsenite binding resulting in conformational changes of the zinc finger domain (**Figure 1.4**). A decrease in the monoubiquitination of H2B was observed in several different cell lines after 24 h exposure to 5 μM arsenite. In addition, 5 μM arsenite treatment of HeLa cells displayed decreased recruitment of DSBR factors BRCA1 and RAD51 to laser-induced DNA DSB sites (**Figure 1.4**) (Zhang et al., 2014). These findings are consistent with the observation that arsenic inhibits the repair of IR induced DNA DSBs (Takahashi et al., 2000). Another study revealed arsenite binding to the RING finger containing DNA repair protein FANCL. FANCD2 monoubiquitination by the E3 ubiquitin ligase, FANCL, is a critical step during DNA interstrand crosslink repair. This repair pathway is necessary for the removal of interstrand crosslinks generated by DNA damaging agents such as cisplatin and endogenous metabolites (Clauson et al., 2013). Arsenite exposure of HeLa cells resulted in decreased FANCD2 monoubiquitination and chromatin recruitment (Jiang et al., 2017). Altogether, these findings illustrate a mechanism of arsenic cocarcinogenicity via the inhibition of DNA repair zinc finger domains.

Arsenic directly and selectively binds to zinc fingers

Arsenic can react with the sulfur of thiol group in cysteine to form As-S bond. Therefore, proteins with free cysteine residues are potential arsenic targets. However, arsenic does not show significant binding to free cysteine or thiol-

containing small molecules *in vivo*. Protein studies indicate low reactivity of arsenic to proteins with single cysteine or two cysteine residues (Asmuss et al., 2000). Kinetics experiments show arsenic binding to one or two cysteine residues have a higher dissociation rate constant than three or four cysteine residues (Kitchin and Wallace, 2006a, 2006b). It was demonstrated that the half-life of the arsenite-trithiol peptide complex is two orders of magnitude greater than that of the corresponding arsenite-dithiol peptide complex. This dramatic difference in chemical kinetics implies that trivalent arsenite may be capable of interacting with single or two cysteine residues, but a more stable interaction of arsenite with a C3 or C4 zinc finger protein may be necessary to sustain biological impact. Furthermore, trivalent arsenic appears to have a spatial requirement for binding with three cysteines simultaneously. Reactivity of arsenite to cysteine requires at least 3 cysteines to be present with a strict spatial requirement of 3 cysteine thiols oriented towards the same center within the radius of the arsenic atom. Cysteine in zinc finger motifs naturally fulfill this spatial requirement, where all cysteine thiols point to and bind with the zinc ion in the center.

The differential reactivity of arsenic to different numbers of cysteine residues in zinc finger motif suggests arsenic binding selectivity. Trivalent arsenic selectively binds to C3H1 and C4 zinc fingers, but not C2H2 zinc fingers, as demonstrated by mass spectrometry (MS) and site direct mutation studies (Zhou et al., 2014, 2011). When inorganic arsenite is metabolized to become MMA(III), the methyl group will occupy one of the three binding sites. As expected,

MMA(III) not only binds with C3H1 and C4 zinc fingers, but also C2H2 (Zhou et al., 2014, 2011). Even more interestingly, two MMA(III) were found on the same C4 zinc finger motif. These findings provide consistent evidence that arsenic binding selectivity is determined chemically by its valence state.

Since a majority of zinc finger proteins in biological systems are of C2H2 configuration, selective binding of trivalent arsenic with the minority C3H1 and C4 zinc finger proteins may make them particularly targeted. For example, PARP-1 can be inhibited by arsenite at concentrations as low as 0.1 μM in cells (Ding et al., 2009), leading to zinc release and DNA binding activity inhibition. GATA-1, a transcription factor regulating red blood cell differentiation, can be inhibited by arsenic exposure starting from the concentration of 0.1 μm in cellular and animal models (Zhou et al., 2020). This selective binding may explain why arsenic shows a co-carcinogenesis effect at environmentally relevant concentrations. Moreover, C4 configuration zinc fingers may be more sensitive to arsenic exposure compared to the C3H1 configuration due to higher number of available cysteine residues (Ding et al., 2017).

A kinetic and thermodynamic study revealed that zinc and arsenic have relatively similar binding affinities towards zinc finger peptides, suggesting that zinc finger occupancy in a cellular system may be strongly influenced by the relative concentrations of each metal (Huestis et al., 2016). A slight kinetic advantage for arsenic over zinc may lead to significant arsenic binding to newly synthesized zinc finger proteins, especially during the process of significant induction of protein expression, such as during a DNA damage response with

significant PARP-1 induction. Similarly, this may occur in red blood cell differentiation when a large amount of GATA-1 is induced. Thus, under these circumstances, certain zinc finger protein targets may be highly sensitive to arsenic exposure.

Arsenic indirectly disrupts zinc fingers through ROS/RNS

Arsenic induces oxidative and nitrosative stress, affecting related enzymes and protein targets such as HO-1 (Shi et al., 2004a). Specifically, zinc finger proteins containing redox sensitive cysteine residues are molecular targets of ROS induced by arsenic. The number of cysteine residues in certain proteins is a factor of the likelihood of oxidation by ROS. Thus, C4 zinc finger proteins are more likely to be oxidized by ROS than C3H1 and C2H2. Oxidative modification on cysteine residues in a zinc finger motif leads to zinc release, conformational change, and ultimately functional loss of certain zinc finger protein targets (Wang et al., 2013; Zhou et al., 2015). Zinc finger protein targets such as PARP-1 are highly sensitive to arsenic-induced ROS. For example, PARP-1 can be inhibited by arsenite as low as 0.1 μM, while the effect can be rescued by antioxidants (Wang et al., 2013).

There are different types of oxidative modifications on cysteine residues; some are reversible (i.e. -SOH and -SO_2H) while others are irreversible (i.e. -SO_3H and -SS-). Arsenic-induced ROS leads to both types of modifications (Zhou et al., 2015), suggesting that some oxidative changes induced by arsenic might be reversed by antioxidants or zinc supplement, but in certain conditions

the damage could be permanent. Arsenic also induces nitric oxide production at low and environmentally relevant concentrations (Ding et al., 2008; L. Zhou et al., 2016). Nitrosative stress can lead to nitrostative modification of zinc finger proteins such as PARP-1 (X. Zhou et al., 2016). Furthermore, ROS and RNS mechanisms may occur at the same time and synergistically. For example, superoxide and nitric oxide produce a peroxynitrite, which inhibits PARP-1 activity (Zhou et al., 2019). Therefore, arsenic-generated ROS/RNS not only can directly cause DNA damage, but also inhibit DNA repair through oxidative or nitrosative modifications to key DNA repair zinc finger proteins.

The interplay between direct and indirect mechanisms

Zinc binding protects cysteine residues within a zinc finger motif from being oxidized easily. Under increased oxidative stress, free cysteine should be oxidized prior to zinc-protected cysteine on zinc finger motifs (Ray Chaudhuri and Nussenzweig, 2017). Taking PARP-1 as an example: its regulatory domain responsible for enzyme activity contains 2 free cysteines, while the cysteines in its DBD are all located in zinc fingers which are bound to zinc ions (Ray Chaudhuri and Nussenzweig, 2017). Therefore, when ROS levels increase, PARP-1 DNA binding activity should be less sensitive to oxidative damage than the enzyme activity. However, while the two free cysteines in the regulatory domain remain unchanged, arsenic is able to cause oxidation of the cysteines on PARP-1 zinc finger and inhibit PARP-1 activity at low and non-cytotoxic concentrations (Zhou et al., 2015). This result suggests that arsenic

displacement of zinc from the zinc finger configurations eliminates zinc protection of the zinc finger cysteine residues, thus rendering these cysteines vulnerable to attack by arsenite-generated ROS.

Under oxidative stress, arsenic binding to zinc fingers is unstable. When arsenic replaces zinc from zinc finger motifs, thiol groups on the cysteines becomes vulnerable to oxidative modification, making arsenic binding to zinc fingers a transient process (Zhou et al., 2015). Arsenic presence in zinc finger proteins increases at the beginning of exposure, but then decreases quickly while oxidative modifications on zinc finger proteins persist and continue to increase (Zhou et al., 2015). These results indicate that cysteine oxidation further disrupts arsenite binding to the zinc finger motif, thereby releasing arsenite to interact with another target protein. Because the released arsenite would be free to interact with another target protein and then repeat this cycle, it effectively functions in a catalyst-like manner for oxidation of targeted proteins. The bind-and-release model could explain why a very low concentration of arsenite (e.g. submicromolar) is capable of causing significant inhibition of PARP-1 activity in cells. Since a significant portion of arsenic-induced oxidative damage to zinc fingers is likely permanent, it explains why adding antioxidants only partially reverses the impact of arsenic exposure (Shi et al., 2004a).

Arsenic selectively binds to specific zinc finger proteins, making these proteins vulnerable to oxidative damage. The interplay and the unified mechanisms of arsenic binding (direct mechanism) and oxidation (indirect mechanism) of zinc fingers by arsenic explains the high sensitivity of certain zinc

finger proteins to arsenic exposure, and more importantly, sheds light on prevention and intervention strategies by utilizing zinc supplements and antioxidants.

1.8 Summary of the carcinogenicity of arsenic

Arsenic carcinogenesis and cocarcinogenesis present a significant risk to human health at environmentally relevant concentrations. Research on the molecular mechanisms of arsenic cocarcinogenesis should be of great help in prevention and intervention of the impact of arsenic exposure. In addition to the many other effects of arsenic exposure such as DNA damage, epigenetic alterations, and gene regulation, inhibition of DNA repair plays a central role in arsenic cocarcinogenesis. Recent work revealed a clear mechanism of selective binding of arsenic to zinc finger proteins, as well as the interplay of binding and ROS. The overall concept of the molecular mechanism is summarized in **Figure 1.5**. This illustrated mechanism not only demonstrates how arsenic inhibits DNA repair but is also meant to inspire future research on arsenic interacting with zinc fingers as a key molecular mechanism involved in the cocarcinogenicity of other environmental toxicants (Zhou et al., 2020) or to be applied to pharmaceutical applications (Cao et al., 2011).

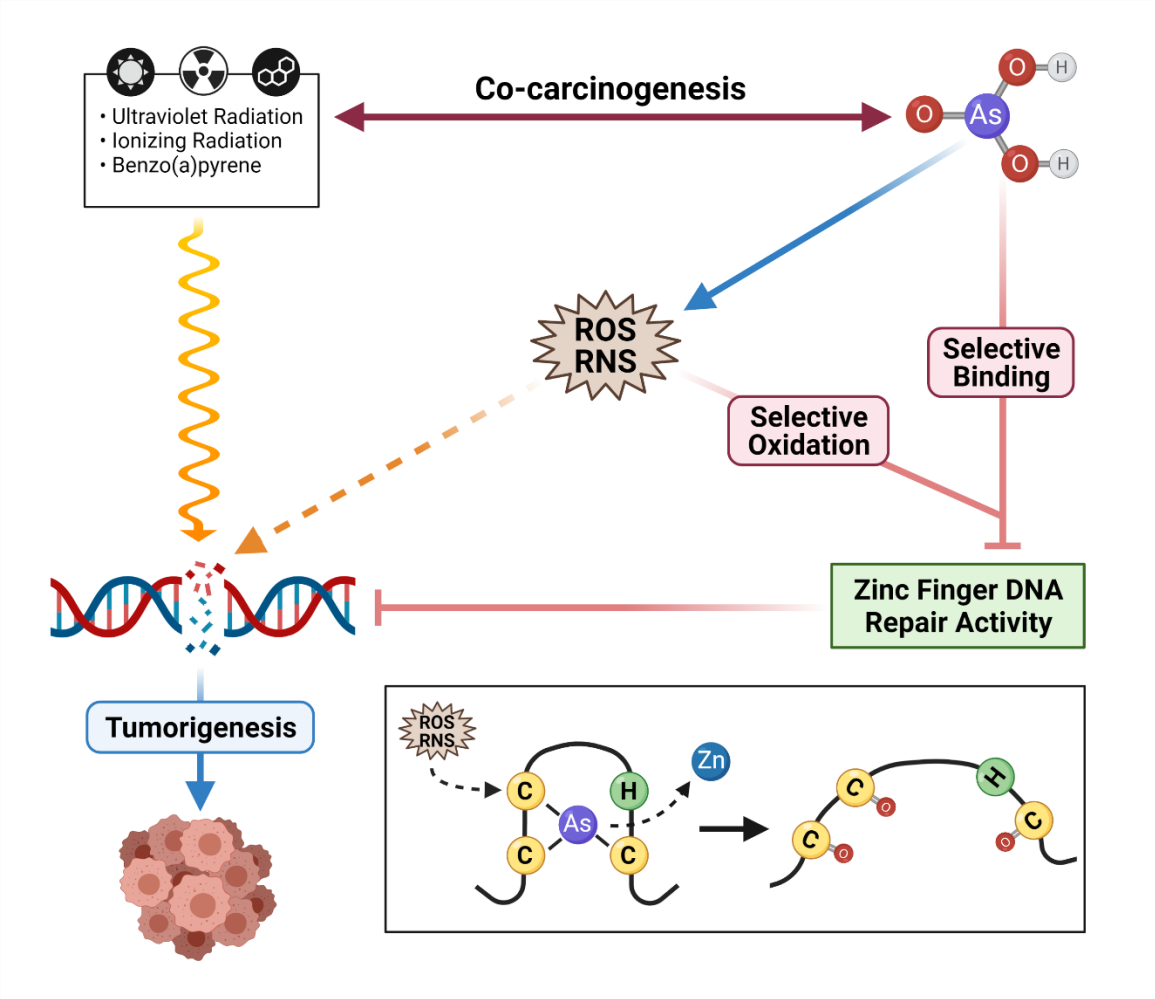

Figure 1.5: Schematic illustration of arsenic cocarcinogenesis

Meanwhile, there are still many important gaps in our understanding of the mechanisms of arsenic carcinogenesis and cocarcinogenesis. One of the major gaps of knowledge is how arsenic is involved in mutagenic processes that lead to cancers. For example, while there are many types of environmental mutagens, why does arsenic exposure and coexposure lead to cancers at such low concentrations? Also, UV exposure results in certain mutational processes leading to unique mutational patterns in the genome. Whether arsenic coexposure alters such patterns, and how such potential changes lead to strong

cocarcinogenesis effects is still unclear. In particular, the impact of arsenite-induced DNA damage retention on downstream mechanisms involved in replication stress, such as TLS, has not been thoroughly examined. TLS alleviates replication stress by bypassing DNA damage at replication forks and gaps (Ma et al., 2020). Whether promoting or suppressing, alterations in the activity of TLS by arsenic can elevate genomic instability and underly the carcinogenicity of arsenic.

1.9 The implications of arsenite-induced DNA damage retention on replication stress

As mentioned in the previous sections, arsenic is an established human skin carcinogen and acts as a cocarcinogen by enhancing the DNA damage, mutagenicity, and tumor formation of UV. UV is a complete carcinogen capable of initiating and promoting tumors. Exposure to UV produces various types of DNA damage, including UVA-induced DNA single-strand breaks and oxidized DNA bases and UVB-induced CPDs and 6-4 PPs (Cadet and Douki, 2018). Arsenic exposure has been shown to reduce the repair capacity for UV generated lesions by inhibiting repair pathways such as BER and NER involved in the remediation of oxidized bases and bulky DNA lesions, respectively (Chatterjee and Walker, 2017; Tam et al., 2020). For example, the DNA of keratinocytes coexposed to arsenite and UV have significantly elevated levels of oxidative damage, bulky lesions, strand breaks, and mutations compared to UV alone (**Section 1.5**) (Cooper et al., 2014, 2013).

A proposed mechanism underlying arsenic cocarcinogenicity is the disruption of DNA repair leading to the retention of UV-induced DNA damage (Muenyi et al., 2015; Tam et al., 2020; Zhou et al., 2021). Arsenic inhibits DNA repair through multiple mechanisms including altered DNA repair protein expression, post translational modifications, subcellular localization, recruitment to DNA damage, and enzymatic activity (**Figure 1.4**). Many of these mechanisms are dependent upon the function of zinc finger domains for protein:protein and protein:DNA interactions (Holcomb et al., 2017; Muenyi et al., 2015; Tam et al., 2020; Zhou et al., 2021). DNA repair proteins PARP-1 and XPA are involved in BER and NER respectively, and contain zinc finger DBDs which have been well characterized for arsenite binding and zinc displacement (**Section 1.7**) (Muenyi et al., 2015; Tam et al., 2020; Zhou et al., 2021).

The inhibition of DNA repair by arsenic increases UV-induced DNA damage retention and the likelihood of unrepaired DNA lesions present during replication, particularly in actively dividing keratinocytes (Holcomb et al., 2017; Muenyi et al., 2015; Tam et al., 2020; Zhou et al., 2021). These lesions are circumvented through the activation of DNA damage tolerance (DDT) pathways such as TLS (**Figure 1.6**) (Ma et al., 2020; Vaziri et al., 2016). When replication forks encounter DNA damage, the replicative polymerase and helicase become uncoupled. Consequently, a stretch of single-stranded DNA (ssDNA) is exposed and is subsequently bound with replication protein A (RPA). Regions of ssDNA and RPA assist in the recruitment of the E3 ubiquitin ligase RAD18 in complex with the E2 ubiquitin conjugating enzyme human Rad6 (homologs Rad6A/B). The

Rad18 RING finger facilitates the monoubiquitination of PCNA, a processivity factor necessary for coordinating DNA replication. Monoubiquitinated PCNA enhances the recruitment and retention of alternative polymerases with larger, more accommodating active sites to bypass the damage by inserting nucleotides opposite the DNA lesion. Bypass of UV-induced CPDs by DNA polymerase eta (Polη) is viewed as an error-free process; however, other TLS polymerases are more error prone (Lou et al., 2021; Ma et al., 2020; Vaziri et al., 2016). An alternative DDT pathway, template switching (TS), involves the extension of monoubiquitinated PCNA to polyubiquitinated PCNA via a Rad5 complex. TS is relatively error free and is mediated by strand invasion of the sister chromatid. Both TLS and TS depend on the E3 ubiquitin ligase activity of the Rad18 RING finger for the monoubiquitination of PCNA (Gaillard et al., 2015; Ma et al., 2020; Vaziri et al., 2016).

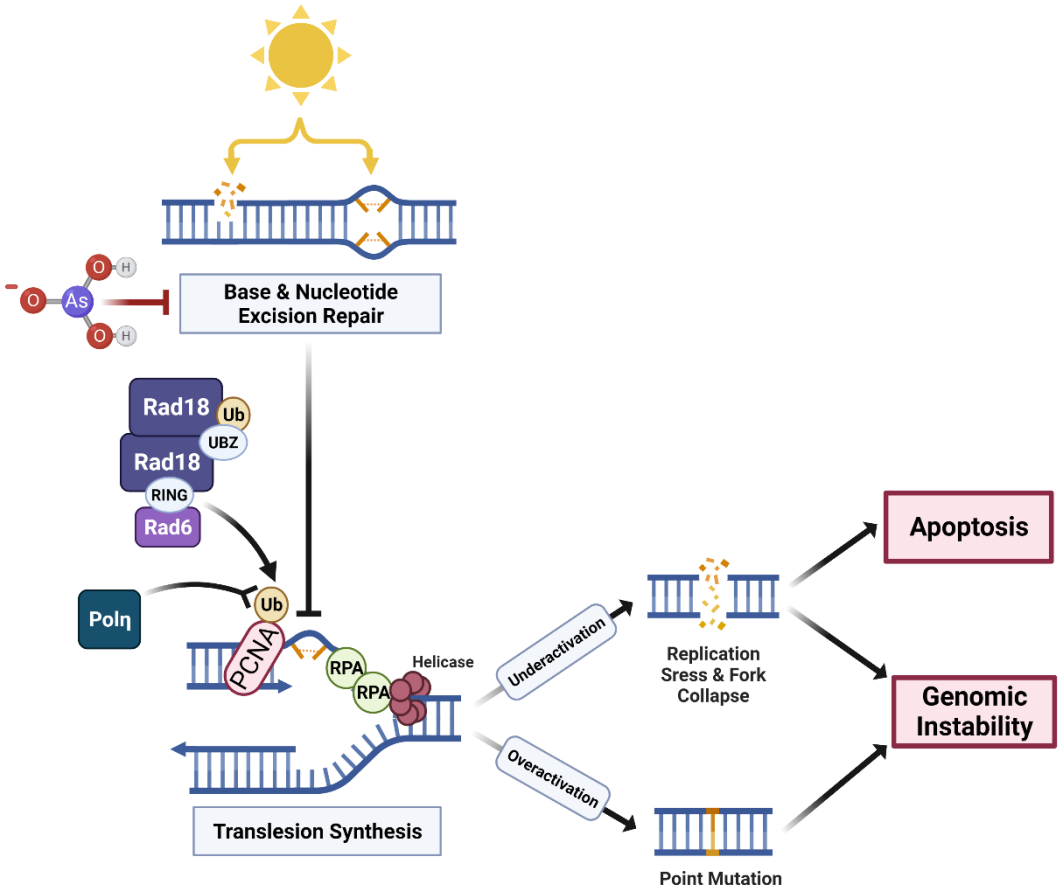

Figure 1.6: Arsenic burden on TLS. Arsenite inhibits various proteins involved in BER and NER, thus leading to the retention of UV-induced DNA damage. If not repaired, retained DNA damage must be bypassed by DDT mechanisms such as TLS to prevent replication stress and fork collapse. TLS is initiated through the monoubiquitination of PCNA by the Rad18-Rad6 complex to facilitate the recruitment of alternative polymerases to stalled replication forks. TLS is tightly regulated as either the over- or under-activation of TLS can promote genomic instability.

One mechanism by which arsenic may alter TLS is through the binding and disruption of the Rad18 zinc fingers. Several studies have demonstrated arsenite targeting of RING finger containing proteins resulting in protein degradation or inhibition (Muenyi et al., 2015; Tam et al., 2020; Zhou et al., 2021). The loss of Rad18 or Rad18 RING function substantially reduces UV-induced PCNA monoubiquitination and thus the initiation of TLS (Huang et al., 2009; Inagaki et al., 2011; Miyase et al., 2005; Shiomi et al., 2007; Watanabe et al., 2004). In

contrast, no ubiquitin-binding zinc finger (UBZ) domains have been evaluated as potential arsenite targets. The Rad18 UBZ domain prevents the overactivation of TLS by facilitating the monoubiquitination of Rad18 and the subsequent formation of the Rad18 homodimer (Inagaki et al., 2011; Miyase et al., 2005; Zeman et al., 2014). High levels of Rad18 are known to overactivate TLS leading to mutagenesis and the development of treatment resistant cancers, demonstrating the importance of proper TLS regulation to prevent mutagenesis (Ma et al., 2020; Vaziri et al., 2016).

The impact of arsenic on TLS is unknown and may represent an avenue for the cocarcinogenicity of arsenic as both the overactivation and underactivation of TLS can promote genomic instability (Gaillard et al., 2015; Ma et al., 2020; Vaziri et al., 2016). In the context of UV exposure, TLS is well characterized for inducing mutations when error-prone TLS polymerases replace the function of Polη. Indeed, the debilitating disorder xeroderma pigmentosum is associated with mutations in the gene coding for Polη. Though error prone in certain conditions, TLS is necessary for bypassing unresolved lesions during replication to prevent mutagenic replication gaps and fork collapse events (**Figure 1.7**) (Gaillard et al., 2015; Ma et al., 2020; Vaziri et al., 2016). The loss of TLS is associated with an increase in DNA damage induced s-phase arrest, DNA strand breaks, chromosomal aberrations, and >4 bp genomic deletions (Bi et al., 2005; Lou et al., 2021; Ma et al., 2020; Saberi et al., 2007; Sasatani et al., 2015; Shiomi et al., 2007; Tateishi et al., 2003; Vaziri et al., 2016). If arsenic disrupts TLS, these adverse effects on genomic integrity may be exacerbated due to the arsenic-

induced retention of DNA damage and suppression of HR which is often involved in alternative pathways for remediating stalled replication forks (Gaillard et al., 2015; Muenyi et al., 2015; Tam et al., 2020; Zhou et al., 2021). Although several *in vitro*, *in vivo*, and *ex vivo* studies have reported an increase in DNA strand breaks, chromosome aberrations, and genomic deletions with arsenic exposure (Muenyi et al., 2015; Tam et al., 2020; Zhou et al., 2021), the mechanisms have not been well-defined and arsenic disruption of TLS may be involved.

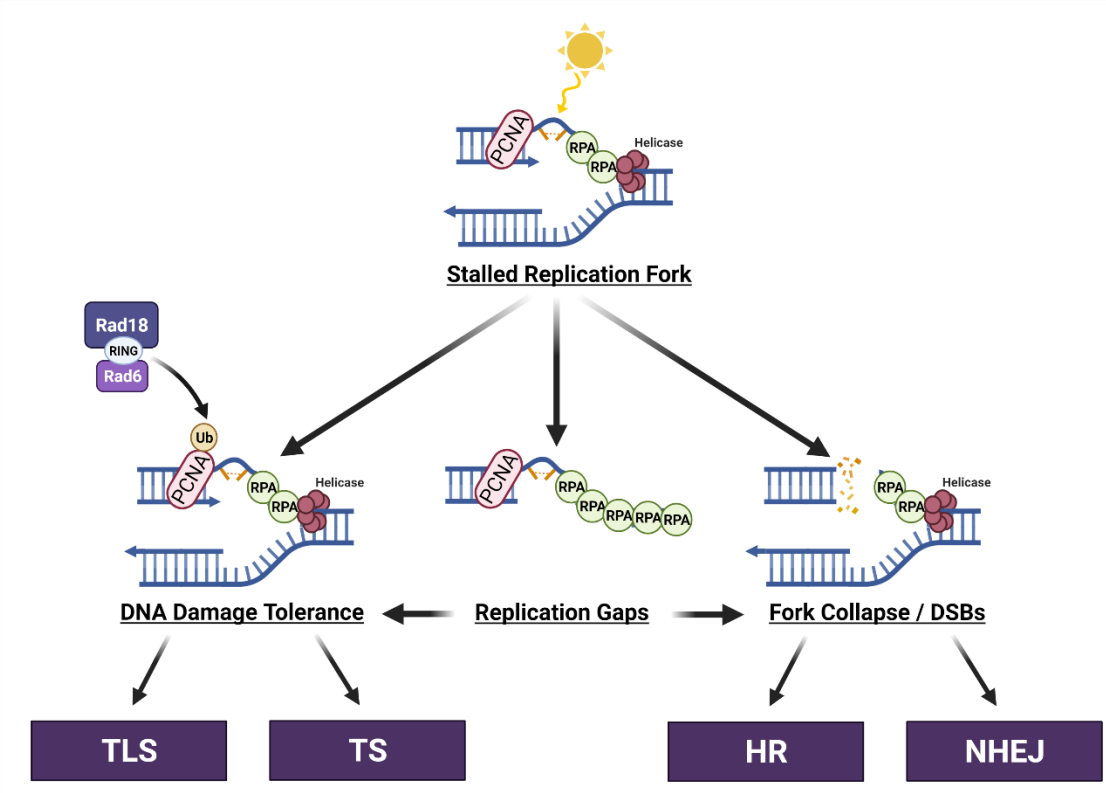

Figure 1.7: Dynamics of stalled replication forks. Stalled replication forks and gaps can be resolved by DDT pathways TLS and TS or lead to the formation of DNA DSBs requiring DSBR mechanisms.

In the context of UV-induced CPDs, TLS is the predominant tolerance pathway and remarkably accurate (Cohen et al., 2015). However, depending on the lesion, alternative pathways involving HR factors can resolve stalled

replication forks. In addition, HR can repair DSBs resulting from the breakdown of replication forks or gaps (**Figure 1.7**) (Costes and Lambert, 2012). Evidence supports the inhibition of HR by arsenic, thus promoting the more error prone pathway NHEJ (Tam et al., 2020; Zhou et al., 2021). As several studies indicate a role of Rad18 in HR (Huang et al., 2009; Inagaki et al., 2011; Kobayashi et al., 2015; Szüts et al., 2006; Vaziri et al., 2016; Watanabe et al., 2009), any arsenic mediated disruption of Rad18 may contribute to the inhibition of HR by arsenic.

One mechanism by which Rad18 assists in HR is by binding to ubiquitinated factors near DNA break sites through its UBZ domain, then binding to factors that promote HR such as RAD51C and FANCD2 through its RING finger (Federico et al., 2016; Huang et al., 2009; Inagaki et al., 2011; Williams et al., 2011). UBZ domain knockout or mutations inhibit Rad18, RAD51C, and Rad9 IR-induced foci formation, indicating a loss of recruitment to DNA damage (Huang et al., 2009; Inagaki et al., 2011). One study demonstrated that knockout of Rad18 and RNF8 (ring finger protein 8) significantly decreased IR-induced Rad51 foci formation and enhanced NHEJ toxicity (Kobayashi et al., 2015). Rad18 deficient cells display elevated levels of chromosomal aberrations and micronuclei with IR exposure, signifying genomic instability (Bhatia and Kumar, 2013; Sasatani et al., 2015; Smith et al., 2004; Thompson and Compton, 2011; Yamashita et al., 2002). Loss of Rad18 or its zinc fingers decreases survival against DNA strand break generating IR and camptothecin (Huang et al., 2009). Similar to the function of PARP1, studies suggest Rad18 promotes HR thereby suppressing NHEJ toxicity at stalled replication forks (Kobayashi et al., 2015; Saberi et al.,

2007; Szüts et al., 2006)

In conclusion, Rad18 contains structurally and functionally distinct zinc finger domains which are conducive to arsenite binding and disruption, ***supporting the hypothesis that arsenic inhibits Rad18*** (**Figure 1.8**). Rad18 is an important factor in TLS and has been implicated in HR. These pathways play a significant role in mitigating replication stress by resolving stalled replication forks and replication gaps. Replication stress is associated with carcinogenesis, which can be further promoted in the event of TLS or HR inhibition through chromosomal aberrations (Gaillard et al., 2015). No studies have evaluated the impact of arsenite on TLS in keratinocytes and therefore, this study can reveal a novel mechanism underlying the carcinogenicity of arsenic.

1.10 Dissertation Overview

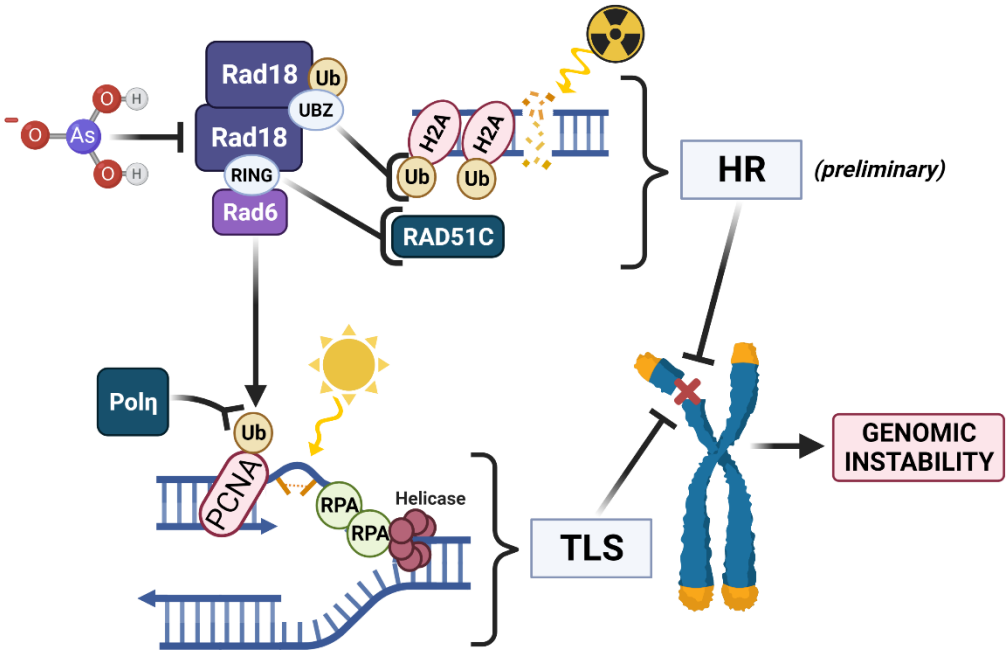

Figure 1.8: Dissertation overview. The UBZ domain locates Rad18 to strand breaks where the RING finger binds DSBR factors such as RAD51C. In addition, the RING finger monoubiquitinates PCNA during TLS to facilitate the recruitment of alternative TLS polymerases such as Polη. These mechanisms suppress chromosomal aberrations and genomic instability.

<u>Specific Aim 1 (Chapter 3):</u> Test the hypothesis that arsenite binds to and disrupts the function of Rad18 zinc fingers.

The purpose of aim 1 is to evaluate the zinc fingers of Rad18 as targets of arsenite. Results reveal zinc loss from endogenous Rad18 in arsenite treated HEKn cells, which is suggestive of loss of structure and function in one or both of Rad18 zinc fingers. To elucidate the mechanism by which zinc is released from Rad18, peptide metal binding assays were utilized. Results demonstrate arsenite binding to the Rad18 RING and UBZ peptides. Arsenite treatment of HEKn cells resulted in decreased PCNA and Rad18 monoubiquitination, indicating a loss of function of the Rad18 RING finger and UBZ domain, respectively (Miyase et al., 2005). Rad18 and Rad6 colocalization was significantly disrupted by arsenite exposure which is partially dependent on a functional RING finger domain. Additionally, arsenite decreased Rad18 foci formation in IR exposed HEKn cells, showing a disruption in Rad18 recruitment to DNA DSBs and indicating UBZ domain inhibition. Altogether, findings from aim 1 demonstrate an arsenite mediated loss of Rad18 RING E3 ubiquitin ligase activity and protein-protein interactions which are important to DDT and DSBR (**Figure 1.8**). Arsenite binding to the Rad18 UBZ domain is a novel finding supporting the observed arsenite-induced inhibition of Rad18 monoubiquitination and foci formation, which are necessary for Rad18 sequestration and recruitment of DSBR factors (Huang et al., 2009; Zeman et al., 2014). These effects can have consequences on the

maintenance of genome integrity.

<u>Specific Aim 2 (Chapter 4):</u> Investigate mechanisms of arsenite regulation of Rad18.

In the context of DNA repair, arsenite regulates DNA repair pathways and the expression, localization, and recruitment of various DNA repair proteins (Tam et al., 2020; Zhou et al., 2021). Keratinocytes exposed to arsenite displayed a significant reduction in the nuclear localization of DDT factors Rad18, Rad6, PCNA, and Polη. Rad6 depends on the nuclear localization signal of Rad18 for translocation and the arsenite-induced disruption of Rad18 may have influenced the localization of Rad6 (Hedglin and Benkovic, 2015, p. 6). In addition to cellular localization, the UV-induced chromatin recruitment of Rad18 and Rad6 were both significantly decreased with arsenite exposure, which may be in part due to the arsenite-induced reduction in chromatin bound RPA. RPA contains a zinc finger DBD that is structurally conducive to arsenite binding, which may explain the loss of RPA on chromatin with arsenite exposure. The loss of PCNA monoubiquitination in aim 1 supports the observed arsenite mediated reduction in both Polη UV-induced recruitment to chromatin and colocalization with PCNA (**Figure 1.8**). Arsenite treatment significantly reduced Rad18 recruitment to IR-induced PH2AX and ubiquitin foci, supporting the disruption of the Rad18 UBZ domain. Findings from aim 2 illustrate the diverse implications of arsenite exposure on Rad18 and Rad18 dependent mechanisms.

<u>Specific Aim 3 (Chapter 5):</u> Examine the impacts of arsenite exposure and Rad18 deficiency on TLS & DSBR.

No studies have evaluated the consequences of arsenite exposure on TLS and very few have assessed the modulation of DSBR by arsenite in keratinocytes. In addition, Rad18 is not an extensively studied protein. Therefore, it is important to assess the role of both arsenite and Rad18 in the disruption of TLS and DSBR. Experiments so far have demonstrated arsenite-induced alterations in localization, recruitment, and the activity of TLS factors which is expected to increase stalled replication forks, DNA damage, and apoptosis. Results demonstrate a significant reduction in the mean intensity of 5-Ethynyl-2'-deoxyuridine (EdU) staining in HEKn cells treated with arsenite or Rad18 siRNA to a similar degree, indicating arsenite mediates its impact on replication stress through Rad18. Arsenite treatment or knockdown of Rad18 in keratinocytes significantly increased UV-induced PH2AX, a marker of replication stress and DNA strand breaks, demonstrating the importance of Rad18 in the maintenance of genome stability and ability of arsenite to induce genomic instability (**Figure 1.8**). Additionally, arsenite increased the presence of both ssDNA and DNA DSBs as measured by neutral single-cell gel electrophoresis (comet assay).

Failure of TLS to bypass damage often results in apoptosis and the levels of UV-induced DNA damage response signaling and cleaved-caspase 3 (marker of apoptosis) were significantly elevated in Rad18 deficient cells. Interestingly, arsenite suppressed these responses to UV as has been shown by other studies (Chen et al., 2005; Qin et al., 2012; Sun et al., 2011; Wu et al., 2005; Zhou et al.,

2017). In addition to UV exposure, arsenite elevated the number of PH2AX foci in IR exposed HEKn cells, indicating DSBR inhibition (**Figure 1.8**). Future studies utilizing both the knockdown of Rad18 and arsenite treatment will reveal the role of Rad18 in the observed arsenite-induced effects with IR. Aim 3 findings have revealed a decrease in the size of replicated DNA post UV and increase in the levels of UV-induced DNA strand breaks and ssDNA gaps in arsenite exposed HEKn cells, suggesting inhibition of TLS. Furthermore, the inhibition of apoptosis by higher concentrations of arsenite in HEKn cells may increase carcinogenesis by allowing the survival of damaged cells.

CHAPTER 2

METHODS

This chapter contains a slightly modified version of "The impact of arsenic on Rad18 and translesion synthesis" by Volk LB, Cooper KL, Jiang T, Paffett ML, and Hudson LG in revision for Toxicology and Applied Pharmacology.

2.1 Reagents

Chemicals

Sodium arsenite (>99%) was purchased from Fluka Chemie (Buchs, Switzerland); zinc chloride (>98%) from Sigma (St. Louis, MO); Hydrogen peroxide 30% from J.T.Baker (Phillipsburg, NJ); 16% formaldehyde solution and carboxy- ",7'-dichlorodihydrofluorescein diacetate (DCFDA) from Thermo Scientific (Waltham, MA); N,N,N',N'-Tetrakis(2-pyridylmethyl)ethylenediamine (TPEN; ≥97%) from Tocris (Bristol, United Kingdom); mitomycin C from Enzo Biochem (Farmingdale, NY); and etoposide from Calbiochem (San Diego, CA).

Small interfering RNAs (siRNAs) & transfection reagent

The Rad18 Human siRNA Oligo Duplex kit was obtained from Origene (Rockville, MD) and contained 3 unique Rad18 27mer siRNA duplexes A-C #SR311213 (Locus ID 56852; RefSeq NM_020165), Trilencer-27 Universal Scrambled Negative Control siRNA Duplex #SR30004, and RNAse free siRNA Duplex Resuspension Buffer. The Trilencer-27 Fluorescent-labeled transfection control siRNA duplex #SR30002 and siTran 2.0 siRNA Transfection Reagent kit

#TT320001 containing siTran 2.0 Transfection Reagent and 5x Transfection Buffer were purchased from Origene. siRNA Duplex Resuspension Buffer was added to siRNA duplexes to a final concentration of 10 μM according to manufacturer's instructions and aliquots frozen at -20 °C.

Antibodies

Primary antibodies obtained from Cell Signaling (Danvers, MA) include Cleaved Caspase-3 (Asp175) (5A1E) Rabbit mAb #9664, DNA Polymerase η (E1I7T) Rabbit mAb #13848, GAPDH (D16H11) XP® Rabbit mAb #5174, Histone H3 (D1H2) XP® Rabbit mAb #4499, Histone H4 (L64C1) Mouse mAb #2935, HR6A/HR6B Rabbit Antibody #4944, PARP (46D11) Rabbit mAb #9532, PARP Rabbit Antibody #9542, PCNA (D3H8P) XP® Rabbit mAb #13110, PCNA (PC10) Mouse mAb #2586, Phospho-Histone H2A.X (Ser139) Antibody #2577, Phospho-Histone H2A.X (Ser139) (D7T2V) Mouse mAb #80312, Phospho-p53 (Ser15)(16G8) Mouse mAb #9286, Phospho-Rad18 (Ser403) Rabbit Antibody #8393, Rad18 (D2B8) XP® Rabbit mAb #9040, RPA70/RPA1 Rabbit Antibody #2267, and SP1 Rabbit Antibody #5931.

HR6B/UBE2B Mouse Antibody (PCRP-UBE2B-1C7) #NBP3-07169 was obtained from Novus Biologicals (Centennial, CO). POLH Rabbit Polyclonal Antibody #PA5-76055 was obtained from Thermo Fisher Scientific. Primary antibodies obtained from Bethyl Laboratories include BRCA1 Rabbit Polyclonal Antibodies #A301-377A and #A301-378A, DNL3 (LIG3) Rabbit Polyclonal Antibodies #A301-636A and #A301-637A, p53 Rabbit Polyclonal Antibodies

#A300-247A and #A300-248A, and Rad18 Rabbit Polyclonal Antibodies #A301-340A and #A301-339A. APTX Rabbit Polyclonal Antibody #ab31841, XPA (12F5) Mouse mAb #ab2352, XPA Rabbit Polyclonal Antibody #ab85914 were obtained from Abcam (Cambridge, United Kingdom). PML Rabbit Antibody (H-238) #sc-5621 was obtained from Santa Cruz Biotechnology (Dallas, TX). Mono- and Polyubiquitinylated Conjugates Mouse mAb (FK2) #BML-PW8810-0100 was obtained from Enzo Life Sciences.

Secondary antibodies used in near-infrared western blotting were obtained from LI-COR Biosciences (Lincoln, NE) and include IR Dye 680RD Goat anti-Mouse #925-68070, IR Dye 680RD Goat anti-Rabbit #925-68071, IR Dye 800CW Goat anti-Mouse #925-32210, and IR Dye 800CW Goat anti-Rabbit #925-32211. Invitrogen secondary antibodies used in immunocytochemistry were obtained through Thermo Fisher Scientific and include Goat anti-Mouse IgG (H+L) Alexa Fluor Plus 488 #A32723, Goat anti-Mouse IgG (H+L) Alexa Fluor Plus 647 #A32728, Goat anti-Rabbit IgG (H+L) Alexa Fluor Plus 488 #A32731, and Goat anti-Rabbit IgG (H+L) Alexa Fluor Plus 647 #A32733.

Peptides

The following peptides were ordered from Genemed Synthesis, Inc. (San Antonio, TX): TKVDCPVCGVNIPESHINKHLDSCLS (UBZ), TKVDCPVCGVNIPESHINKHLDSHLS (UBZ_{C2H2}), LRCGICFEY-FNIAMIIPQCSHNYCSLCIRKFLSYKTQCPTCCV (RING), LRHGIHFEYFNIAMIIPQHSHNYCSLCIRKFLSYKT-QCPTCCV ($RING_{H2C2}$).

Peptides were validated by the manufacturer using HPLC and purity was determined to be >95%.

2.2 Ultraviolet Radiation (UV)

UV exposures were conducted with two FS40 UVB broadband bulbs emitting wavelengths of light between 280 nm and 400 nm with a peak near 300 nm. The proportion and intensity of UVA/UVB is measured annually using an ILT2400 radiometer equipped with UVA (SED033) and UVB (SED240) detectors (International Light Technologies; Peabody, MA). The spectral emission profile for exposures described herein was 91% UVB, 9% UVA and <1% UVC. In experiments involving UV, HEKn cells in medium were exposed to 2.8 kJ/m^2 UVB. The dose of UVB was sufficient to induce CPDs (**Figure 2.1A**), PH2AX (**Figure 2.1B**), and replication stress (**Figure 2.1C**) 4 h post UV without significantly altering viability 24 h post UV (**Figure 2.1D**).

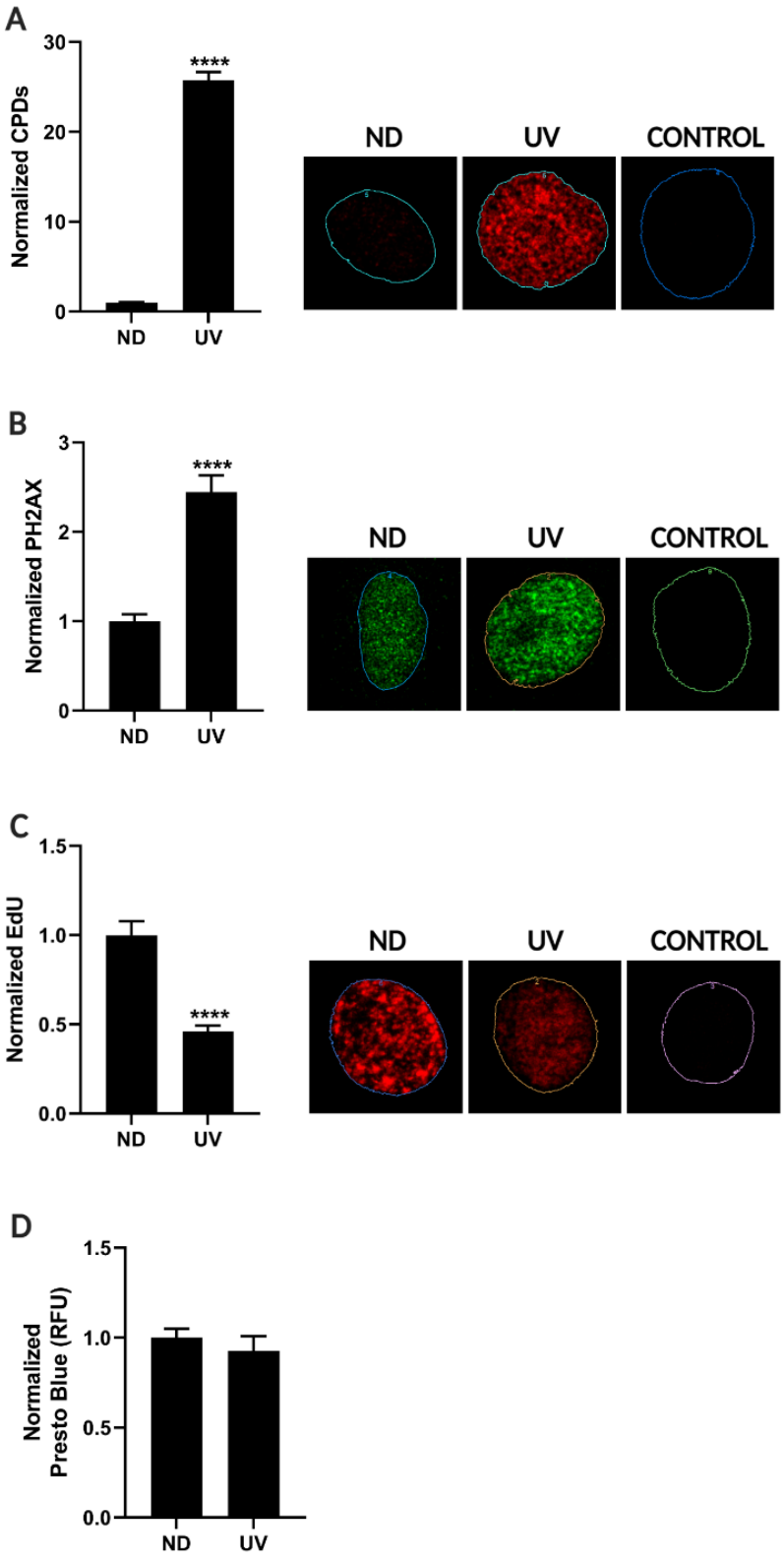
A
Normalized CPDs
30
20
10
0
****
ND
UV
ND
UV
CONTROL
B
Normalized PH2AX
3
2
1
0
****
ND
UV
ND
UV
CONTROL
C
Normalized EdU
1.5
1.0
0.5
0.0
****
ND
UV
ND
UV
CONTROL
D
Normalized Presto Blue (RFU)
1.5
1.0
0.5
0.0
ND
UV

Figure 2.1: UV response in HEKn cells. HEKn cells were exposed without (No Damage: ND) or with 2.8 kJ/m^2 UVB. Cells were fixed 4 h post UV exposure and immunocytochemistry was performed as described in Methods. Max intensity projections (MIPs) were analyzed for **(A)** CPDs and **(B)** PH2AX (Ser139) sum of intensity per nucleus normalized to ND with Slidebook 6. Nuclei are outlined in representative images and secondary only controls (CONTROL) are included. N≥120 nuclei. ****p<0.0001 compared to ND. **(C)** HEKn cells were treated with 10 μM 5-Ethynyl-2'-deoxyuridine (EdU) 1 h prior to exposure with 2.8 kJ/m^2 UVB. Cells were fixed 4 h post UV exposure and EdU detection was performed. MIPs were analyzed for EdU sum of intensity per nucleus normalized to ND with Slidebook 6. N≥421 nuclei. ****p<0.0001 compared to ND. **(D)** HEKn cells were exposed to 2.8 kJ/m^2 UVB and allowed to recover for 24 h before performing the PrestoBlue cell viability assay as described in Methods. Relative Fluorescence Units (RFU) were normalized to ND. N=3. There was no significant difference compared to ND. All values represent mean ± SEM.

2.3 Ionizing Radiation (IR)

IR exposures were conducted with a Faxitron MultiRad 225 Irradiator. In experiments involving IR, HEKn cells in medium were exposed to 5 Gy of X-ray at a rate of 2 Gy/min. The dose of IR was sufficient to induce PH2AX 2 h post IR with a significant recovery at 6 h post IR (**Figure 5.5**).

2.4 Cell Culture and Treatment

Cell culture

Pooled HEKn (lot #05461) and single donor HEKn cells (lot #00263; used only in zinc release assay) were purchased from Lifeline Cell Technologies (Oceanside, CA) and cultured in Lifeline DermaLife K culture medium and supplements without the addition of antibiotics. HEKn cells were subcultured for no more than 10 passages using Lifeline trypsin 0.05% EDTA 0.02%, Lifeline trypsin neutralization solutions, and Sigma Dulbecco's Phosphate Buffered Saline (DPBS). HEKn stocks were stored in Lifeline FrostaLife freezing medium in liquid nitrogen.

Human embryonic kidney (HEK) 293T cells were obtained from ATCC

(Manassas, VA) and cultured in Dulbecco's Modified Eagle's Medium (Sigma) with 10% fetal calf serum (Atlanta Biologicals; Flowery Branch, GA) and 2 mM L-Glutamine (Sigma). Human embryonic kidney (HEK) 293T cells were passaged using 0.25% Trypsin-EDTA 1x (VWR; Radnor, PA) and stocks stored in 90% complete medium and 10% DMSO in liquid nitrogen. Cells were used for no more than 20 passages from receipt. All cell lines were maintained at 37°C in a 95% air/5% CO_2 humidified incubator. All PBS buffers used in cell culture and in the following methods were calcium and magnesium free.

Cell treatment

Stock solutions were prepared as follows: 1 mM stock arsenite in milliQ water, 100 mM TPEN in ethanol, 100 mM DCFDA in DMSO, 100 mM etoposide in DMSO, and 1.5 mM mitomycin C in DPBS. Stock solutions were sterilized using a 0.22-μm syringe filter and aliquots stored at -20°C. DCFDA stocks were aliquoted in dark eppendorf tubes to protect from light and stored at -20°C in a desiccator. Working solutions were prepared by diluting the stock with complete cell culture medium. For experiments involving cell exposures, cells were placed in complete medium containing arsenite at the concentrations and times indicated in the figures and figure legends. Final concentration of ethanol in TPEN treatments was negligible (0.005%) and did not reveal any significant differences compared no treatment (NT) control.

Rad18 knockdown

HEKn cells were transfected with Trilencer-27 Fluorescent-labeled transfection control (TYE563 labeled siRNA), universal scrambled control (SCR), Rad18 siRNA-A (R18A), Rad18 siRNA-B (R18B), or Rad18 siRNA-C (R18C) according to the manufacturer's instructions. Briefly, cells were plated in Thermo Nunc Lab-Tek II 4-well slides at $2.5x10^4$ cells per well or Greiner Bio-One (Frickenhausen, Germany) CELLSTAR 100 mm cell culture plates at $4x10^5$ cells per plate. After 1 day of growth, medium was replaced with fresh medium 30-60 min prior to transfection. siRNA was diluted in 1x Transfection Buffer, then siTran 2.0 Reagent added, mixed, and incubated at room temperature for 15 min. The transfection mixture was added dropwise to cells, and slides or plates gently rocked. Final concentrations were 20 or 40 nM siRNA as reported in figure legends, 9% Transfection Buffer, and 0.055% siTran 2.0 Reagent. Medium containing transfection complex was removed 5-6 h later and replaced with fresh medium. Cells were treated as described in figure legends and fixed for immunocytochemistry or collected for western blot 2 days post transfection.

Transfection with 20 nM of TYE563 labeled siRNA demonstrates efficient uptake of siRNA with the transfection conditions described above (**Figure 2.2A**). HEKn cells transfected with 20 nM of R18A-C resulted in a 31% knockdown of Rad18 with R18A and 35% knockdown with R18B compared to 20 nM SCR control as measured by immunocytochemistry. No significant changes were observed with R18C and therefore this siRNA was excluded from the study (**Figure 2.2B**). Western blot analysis demonstrated a 30% and 45% knockdown with R18A and R18B respectively (**Figure 2.2C**), comparable to the findings

obtained by immunocytochemistry. HEKn cells transfected with 20 nM each of R18A and R18B (R18AB; 40 nM total) led to a 62% and 71% knockdown of Rad18 compared to 40 nM SCR control as measured by immunocytochemistry (**Figure 2.2D**) or western blot (**Figure 2.2E**), respectively.

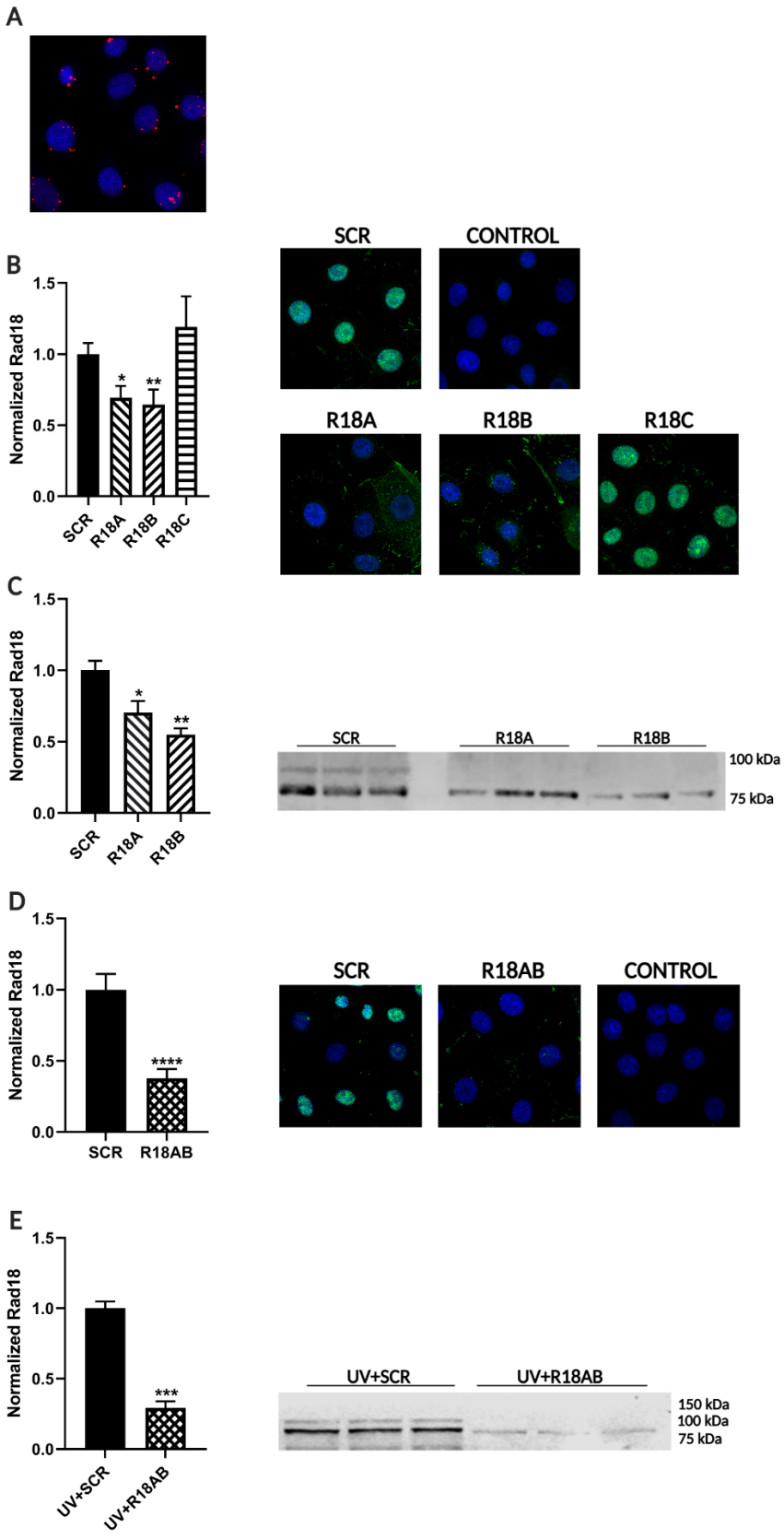
A
B
Normalized Rad18
1.5
1.0
0.5
0.0
*
**
SCR
R18A
R18B
R18C
SCR
CONTROL
R18A
R18B
R18C
C
Normalized Rad18
1.5
1.0
0.5
0.0
*
**
SCR
R18A
R18B
SCR
R18A
R18B
100 kDa
75 kDa
D
Normalized Rad18
1.5
1.0
0.5
0.0
****
SCR
R18AB
SCR
R18AB
CONTROL
E
Normalized Rad18
1.5
1.0
0.5
0.0
***
UV+SCR
UV+R18AB
UV+SCR
UV+R18AB
150 kDa
100 kDa
75 kDa

Figure 2.2: Rad18 knockdown by siRNA. HEKn cells were transfected with 20 nM of TYE563 labeled siRNA, universal scrambled control (SCR), Rad18 siRNA-A (R18A), Rad18 siRNA-B (R18B), or Rad18 siRNA-C (R18C) as described in Methods. Cells were fixed 48 h post transfection and immunocytochemistry performed. **(A)** Image demonstrates uptake of TYE563 siRNA (red) in HEKn cells with optimized transfection conditions (DAPI = blue). **(B)** MIPs were analyzed for Rad18 (green) sum of intensity normalized to number of cells and SCR control with Slidebook 6. Secondary only control (CONTROL) included with representative images. N≥15 images (≥5 cells per image). **p<0.01, *p<0.05 compared to SCR. **(C)** HEKn cells were transfected with 20 nM of SCR, R18A, or R18B. Whole cell lysates were collected 48 h post transfection and analyzed via western blot. Rad18 was normalized to total protein stain and SCR control. N=3. **p<0.01, *p<0.05 compared to SCR. **(D)** HEKn cells were treated and analyzed as described in **B**, except transfected with 40 nM universal scrambled control or 20 nM each of R18A and R18B (R18AB; 40 nM total). N≥15 images (≥5 cells per image). ****p<0.0001 compared to SCR. **(E)** HEKn cells were transfected with 40 nM universal scrambled control (SCR) or 20nM each of R18A and R18B (R18AB; 40 nM total) and exposed to 2.8 kJ/m^2 UVB 2 days post transfection. Whole cell lysates were collected 4 h post UV exposure and analyzed via western blot. Rad18 was normalized to total protein stain and UV+SCR control. N=3. ***p<0.001 compared to UV+SCR. All values represent mean ± SEM.

2.5 Cell Viability

PrestoBlue Cell Viability Reagent was obtained from Thermo Fisher Scientific. HEKn cells were plated in a 96 well plate at 2.5x10^3 cells per well. Two days later, cells were exposed with or without UV and allowed to recover for 24 hr. PrestoBlue cell viability assay was performed according to the manufacturer's instructions. Briefly, 1/10^{th} volume of cell viability reagent was added directly to cells in culture medium and incubated for 2 hr at 37°C in a humidified cell culture incubator. Plates were read on a SpectraMax i3x (Molecular Devices; San Jose, CA) equipped with SoftMax Pro 7.0 software. Well scan was performed using excitation wavelength of 560 nm (bandwidth 9 nm) and an emission of 585 nm (bandwidth 15 nm). Background fluorescence was subtracted from results. The cell viability assay was performed with 3 independent experimental replicates.

2.6 Western Blot

HEKn cells were plated in 100 mm plates at $1.4x10^5$ cells per plate and cultured for 4 days. Cells were treated as described in figure legends. Plates were washed 2 times with ice-cold 1xPBS, then scraped and collected in non-denaturing lysis buffer (20 mM TRIS pH 7.5, 150mM NaCl, 1% Triton X-100) with 1:100 Thermo Halt Protease and Phosphatase Inhibitor Cocktail on ice. Lysates were sonicated for 15 pulses (3 output control, 30% duty cycle) with a Branson Sonifier Cell Disruptor 200 and centrifuged at 14000xg for 15 min at 4°C. Supernatant was transferred to a fresh tube and frozen at -80°C. Protein concentration was determined using Thermo Scientific Pierce BCA Protein Assay Kit. Equal amounts of lysate (20-60µg protein) in laemmli buffer (5x: 10% SDS, 500mM DTT, 50% glycerol, 250mM Tris HCl, 0.5% Bromophenol Blue, pH 6.8) were loaded into a 10-15% SDS-PAGE gel along with Bio-Rad (Hercules, CA) Precision Plus Protein All Blue Prestained Protein Standards. Electrophoresis was performed in a Bio-Rad Mini-PROTEAN Tetra Cell or a C.B.S Scientific (San Diego, CA) Double-Wide Mini-Blotter at 120v for 1.5-2.5 h with a Bio-Rad PowerPac Basic Power Supply. Protein was transferred to LI-COR Odyssey Nitrocellulose Membrane at 30v overnight at 4°C. Membranes were allowed to dry for at least one h and then rehydrated in 1xTBS (20 mM Tris base, 150 mM NaCl, pH 7.6).

Blots were stained with LI-COR Revert 700 Total Protein Stain according to manufacturer's instructions and imaged with LI-COR Odyssey Fc or 9120 Imager. Blots were destained and blocked for 1 h at room temperature in LI-COR

Intercept Blocking Buffer TBS. Primary antibodies were diluted (according to manufacturer's recommendations for western blot) in Intercept Blocking Buffer with 0.2% Tween 20 and incubated overnight at 4°C on a rocker. Three washes were performed with 1xTBS 0.1% Tween-20 (TBST) before the addition of LI-COR IR Dye secondary antibody (1:15000) for 1 h at room temperature. Three washes were performed with TBST followed by 1 wash with TBS prior to imaging on a LI-COR Odyssey Fc or 9120 Imager.

No saturation was present in images collected for analysis. Target quantification was performed using LI-COR Image Studio Lite Ver 5.2. To calculate target signal, the product of background and area was subtracted from the sum of the pixel intensity values (Total). Signal = Total – (Background x Area). Results were normalized to Revert 700 Total Protein Stain. Blots were stripped with LI-COR NewBlot IR Stripping Buffer according to manufacturer's instructions. Stripping efficiency was assessed prior to experimentation. Depending on the experiment, blots were cut prior to imaging to fit on the imager tray, but blot sections were imaged at the same time and under the same imaging conditions. In experiments involving multiple blots, normalization controls were included. All western blot analysis was performed with ≥3 independent experimental replicates. Brightness and contrast were adjusted uniformly to enhance the visualization of representative blots.

2.7 Immunocytochemistry

Slide preparation

HEKn cells were plated in 4-well chamber slides at $1.25x10^4$ cells per well or $2.5x10^4$ cells per well (siRNA experiments only) and treated as described in figure legends. Cells were fixed in 3.7-4% paraformaldehyde for 15 min, washed 3 times in 1xPBS, then permeabilized with dry methanol at -20°C for 10 min. After 3 washes, cells were blocked in 1xPBS 5% normal goat serum (Thermo Scientific) 0.15% Triton X-100 (Fisher BioReagents) buffer for 1 h at room temperature. Slides were placed in humidity chambers and incubated with primary antibody 1xPBS 1% bovine serum albumin (BSA; Sigma) 0.15% Triton X-100 overnight at 4°C. Primary antibody concentrations were diluted according to manufacturer's recommendations for immunofluorescence (immunocytochemistry), except 1:200-1:400 was used for Rad18 (D2B8) XP® Rabbit mAb #9040 and 1:200 was used for RPA70/RPA1 Rabbit Antibody #2267. Slides were washed 3 times, then incubated with secondary antibodies (1:1000) in 1xPBS 1%BSA 0.15% Triton X-100 buffer for 1 h at room temperature. After 3 washes, slides were incubated with 0.5 µg/mL 4',6-Diamidino-2-Phenylindole Dihydrochloride (DAPI; Invitrogen) in 1xPBS for 10 min. After 3 more washes, slides were mounted with Invitrogen Prolong Glass Antifade Mountant, allowed to cure overnight at room temperature, then sealed with nail polish and stored at 4°C. All washes (5 min each) and incubations (except for the primary antibody incubation) were performed at room temperature on a rotator. For the CPD immunocytochemistry (**Figure 2.1**), cells were denatured in 2 N HCl for 30 min, then washed 5 times with 1xPBS prior to block.

Confocal microscopy

Sub-Airy unit (0.6AU) pinhole confocal microscopy was performed as previously described (Noureddine et al., 2021; Saha et al., 2022) with a Leica TCS-SP8 (Leica Microsystems; Wetzlar, Germany) controlled by LASX software version 3.5.7 and followed by computational image restoration (deconvolution) with Huygens Essential version 20.10 (Scientific Volume Imaging; Hilversum, Netherlands) utilizing a constrained maximum likelihood estimation algorithm. All 3D confocal scanning parameters (Z-stacks; 1.5 µm physical length, 11 slices) were obtained with a 63×/1.4NA apochromat oil objective in sequential scanning mode, a sub-Airy pinhole size of 0.6 AU, and image size of 92 µm x 92 µm. Both lateral and axial voxel dimensions were acquired at ideal Nyquist sampling rates (https://svi.nl/NyquistCalculator) using spectral hybrid detectors where fluorophore emission spectra bands-widths were precisely set in combination with sequential scanning to avoid any possibility of fluorophore cross-talk.
As stated above, quality control measures were undertaken to avoid fluorophore cross-talk by systematically validating no direct laser excitation of adjacent (red shifted) channels were observed during parameter optimization. Secondary only controls were included in each experiment to minimize background and determine appropriate values for background subtraction during image restoration and subsequent analysis. Replicate control wells were included to test the well-to-well variability of each antibody and analysis, and no significant differences were detected. Nuclear staining was utilized to select groups of cells (≥5 cells per image) as to avoid bias from antibody staining.

Maximum intensity projection (MIP) analysis

All post-processed (deconvolved) confocal images were converted to max intensity projections (MIPs) with LAS X software. Raw MIPs were imported into Intelligent Imaging Innovations (Denver, CO) Slidebook 6 version 6.0.6 for analysis. Masks were utilized to define whole cells, as well as the nuclear and cytoplasmic regions (**Figure 2.3A**). Subcellular localization analysis was performed by calculating the whole cell, nuclear, or cytoplasmic target sum of intensity per image, then was divided by the number of cells per image. Sum of intensity of CPD, PH2AX, EdU, and phospho-p53 targets utilized in UV experiments were calculated per nuclei. Object analysis was used to generate the number of Rad18, PH2AX, ubiquitin, Rad18+PH2AX, and Rad18+ubiquitin foci per image, then was divided by the number of cells per image (**Figure 2.3B**). Channel threshold and brightness were adjusted uniformly to enhance the visualization of representative images.

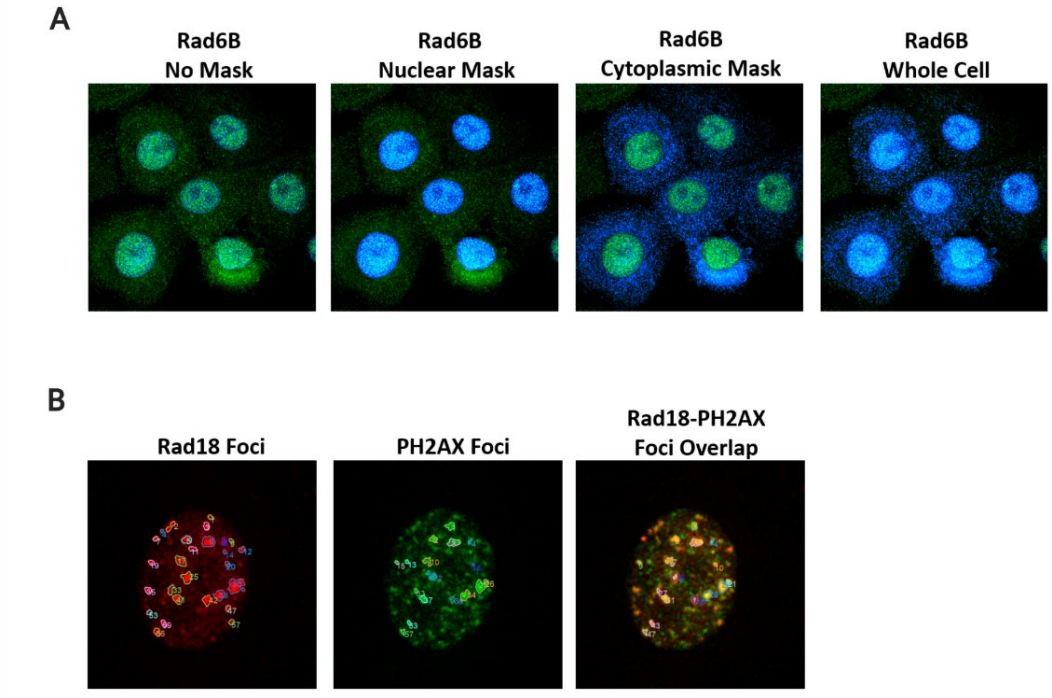

Figure 2.3: MIP Analysis. (A) Example mask highlighting (light blue) of the Rad6B (green) nuclear, cytoplasmic, and whole cell staining (DAPI = dark blue). **(B)** Example foci analysis of Rad18 (red), PH2AX (green), and Rad18-PH2AX (yellow) overlap.

Colocalization analysis

Deconvolved confocal images were analyzed for the spatial overlap between two targets using the Huygens Essentials Colocalization Analyzer. First, background was estimated from control images using the Costes method and the resulting channel thresholds were applied equally to all images in each experiment. Next, the Pearson's correlation coefficient was calculated for each image and colocalization maps in the form of iso-colocalization surfaces were generated. Colocalization maps were processed with MIP Renderer using false color to highlight the lowest to highest pixel values using the following color scheme: purple (lowest) < blue < green < yellow < orange < red (highest).

Brightness was adjusted uniformly to enhance the visualization of representative colocalization map MIPs.

2.8 Reactive Oxygen Species (ROS) Detection

HEKn cells were plated in 96 well plates at 1 x 10^4 cells per well and incubated overnight. Cells were then pretreated with 20 μM DCFDA for 30 min, then fresh medium with or without arsenite (1 or 5 μM) was added. Plates were incubated for an additional 1 h or 24 h before detection of ROS. Nuclei were stained with DAPI (0.7 μg/ml) and wells immediately imaged using an Olympus IX83 fluorescence microscope equipped with cellSens Dimension (Olympus; v 1.9) imaging software and a DP80 digital camera. A minimum of 10 images per treatment were collected and sum of intensity fluorescence was quantified using cellSens Dimension and Count & Measure imaging software (Olympus; v 1.9) and normalized to DAPI fluorescence. All images were acquired within 3 h of staining to minimize the possibility of signal degradation. ROS detection was performed with 3 independent experimental replicates. Brightness and contrast were adjusted uniformly to enhance the visualization of representative images.

2.9 Zinc Release Assay

Single donor HEKn cells were cultured in 150 mm plates to approximately 50% of confluence then treated with or without 1 μM arsenite for 24h. Total protein was collected, proteins of interest immunoprecipitated, and zinc content determined using 4,(2-pyridylazo)-resorcinol as previously described (Cooper et

al., 2013; Zhou et al., 2011). Antibodies utilized for the immunoprecipitation (IP) and/or immunoblotting (IB) of target proteins and their final concentrations are listed in **Table 2.1**. Zinc release assay was performed with ≥3 independent experimental replicates.

Target Protein	Manufacturer	Catalog Number	Dilution Used	
			IP	IB
APTX	Abcam	ab31841	1:500	1:1000
BRCA1	Bethyl Laboratories	A301-377A	1:150	
BRCA1	Bethyl Laboratories	A301-378A		1:1000
LIG3	Bethyl Laboratories	A301-637A	1:150	
LIG3	Bethyl Laboratories	A301-636A		1:2000
p53	Bethyl Laboratories	A300-247A	1:250	
p53	Bethyl Laboratories	A300-248A		1:5000
PARP-1	Cell Signaling	9532	1:200	
PARP-1	Cell Signaling	9542		1:1000
PML	Santa Cruz Biotech	sc-5621	1:100	1:500
RAD18	Bethyl Laboratories	A301-340A	1:100	
RAD18	Bethyl Laboratories	A301-339A		1:1000
SP-1	Cell Signaling	5931	1:200	1:1000
XPA	Abcam	ab85914	1:100	
XPA	Abcam	ab2352		1:500

Table 2.1: Zinc release assay antibodies and dilutions. Listed are the final dilutions used for the immunoprecipitation (IP) and immunoblotting (IB) of target proteins during the zinc release assay.

2.10 Peptide Analysis

Peptide stocks

The RING finger peptides were resuspended in 70% acetonitrile, 10% acetic acid, 20% milliQ water, and 250 μM dithiothreitol to a concentration of 1 mM and sonicated for 10 pulses. The UBZ domain peptides were resuspended in 50% acetonitrile, 50% milliQ water, and 250 μM dithiothreitol to a concentration of 1 mM and gently vortexed. Peptide stocks were stored in a desiccation chamber at -20°C.

Liquid Chromatography (LC) and Electrospray Ionization (ESI) MS

Stock peptides were added to 10 mM ammonium acetate (pH 7.2) and 250 μM dithiothreitol buffer to a final concentration of 100 μM. Aliquots of the 100 μM peptides were mixed with 400 μM arsenite and incubated at room temperature for ≥30 min. Coincubation experiments were conducted by incubating the peptide with arsenite and zinc at different molar ratios (ratio 1:2, 1:1, 2:1, respectively).

Both LC-MS experiments and ESI−MS direct infusion were performed on Q-exactive orbitrap classic mass spectrometer (Thermo Fisher Scientific; San Jose, CA) equipped with a HESI source (Thermo Fisher Scientific; San Jose, CA). For ESI-MS, samples from the metal binding assay were diluted 10-fold with 10 mM ammonia acetate and introduced into the MS source at 5 μL/min. The ESI source spray voltage, capillary temperature, sheath gas, auxiliary gas, S-lens RF level and mass resolution were maintained at 3.5 kV, 320°C, 5 psi, 0 psi, 50 V, and 17,500, respectively. For the LC-MS experiment, 1 μL of undiluted samples were injected using a Vanquish Flex Binary UHPLC (Thermo Fisher Scientific; San Jose, CA) equipped with a Biobasic 4 5 μm 50 x 2.1 mm column (Thermo Fisher

Scientific; San Jose, CA). Peptides were eluted using mobile phase A of 0.1% formic acid in water, mobile phase B of 0.1% formic acid in acetonitrile, and a 10 min gradient of 1) 3%-97% B over 6.5 min, 2) then a hold of B for 1.5 min, 3) return to A in 0.5 min and 4) a final hold of A for 1.5 min. MS data were acquired in the mass range of 400 – 4,000 m/z. For data analysis, intact peptide masses were deconvoluted using Unidec1 Version 5.0.2 (Marty et al., 2015).

Matrix-Assisted Laser Desorption/Ionization – Time of Flight (MALDI-TOF) MS

Peptide solution was diluted to a concentration of 25 μM in a buffer containing 5 mM Tris-HCl (pH 6.8) and 250 μM dithiothreitol. Aliquots of the 25 μM peptides were mixed with 200 μM arsenite and incubated in room temperature for 1 hr. Coincubation experiments were conducted by incubating the peptide with arsenite and zinc at different molar ratios (ratio 1:2, 1:1, 2:1, respectively).

MALDI-TOF MS analyses were performed using a MALDI TOF/TOF 5800 system (Applied Biosystems; Foster City, CA) equipped with a nitrogen laser in the positive-ion, reflectron mode. One μL of the above-mentioned peptide solution was mixed with an equal volume of 2,5-dihydroxybenzoic acid matrix solution and spotted onto a MALDI sample plate and dried completely prior to MS analysis. Each mass spectrum was acquired using 500 laser shots of random positions across a spot. Laser intensity was 5000 (arb. Unit), and the pulse rate was 400 Hz.

2.11 Chromatin Fractionation

HEKn cells were plated in 100 mm plates at $1.2x10^5$ cells per plate and cultured for 3 days, then treated with 1 μM or 5 μM arsenite for 24 h prior to UV exposure. Cells were lysed 4 h post UV exposure and proteins were fractionated as described previously (Lake et al., 2010). Briefly, cells were rinsed with 1xPBS, collected in 200 μl fractionation buffer (150 mM NaCl, 0.5 mM MgCl2, 20 mM HEPES pH 8.0, 10% glycerol, 0.5% Triton X-100, 1 mM DTT) on ice and centrifuged at 15,000xg for 20 min at 4°C. Resulting supernatant (roughly 300 μl) was removed and added to 75 μl of 5x laemmli buffer (soluble fraction). 125 μl of 2x laemmli buffer was added to the pellet (chromatin fraction). All samples were sonicated continuously for 10 seconds. The chromatin-enriched fraction was 3 times more concentrated than the soluble fraction. Equal volumes of samples were loaded onto 13-14% SDS-PAGE gels and western blot analysis performed as described in **Section 2.6**. Representative Revert 700 Total Protein Stain of samples is provided in **Figure 2.4A**. Fractionation efficiency was confirmed with histone H3 and histone H4 for the insoluble fraction and GAPDH for the soluble fraction (**Figure 2.4B**). The recruitment of PARP-1 to chromatin in arsenite and UV treated cells was used as a control and results were similar to previous findings (**Figure 2.4C**) (Ding et al., 2017). Chromatin fractionation was performed with 3 independent experimental replicates.

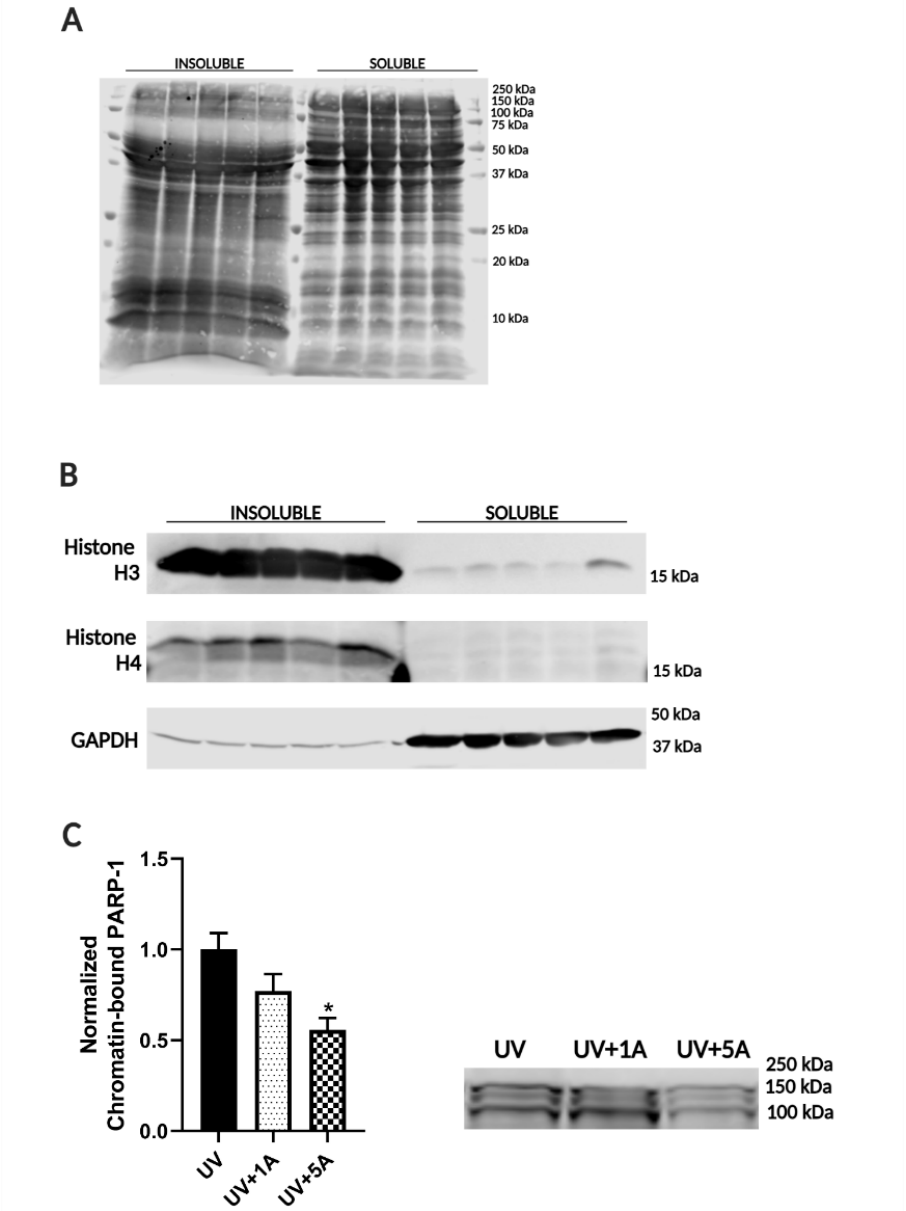

Figure 2.4: Chromatin fractionation controls. HEKn cells were treated and analyzed as described in **Figure 4.7** and Methods. Shown are representative western blots of chromatin fractionation **(A)** total protein stain and **(B)** fractionation controls. **(C)** HEKn cells were treated with 1 μM (UV+1A) or 5 μM (UV+5A) arsenite for 24 h prior to exposure with 2.8 kJ/m^2 UVB. Chromatin fractionation was performed 4 h post UV exposure as described in Methods. PARP-1 in the chromatin fraction was normalized to total protein stain and UV only control. N=3. Values represent mean ± SEM. *p<0.05 compared to UV.

2.12 DNA Synthesis Assay

Click-iT Plus EdU Cell Proliferation Kit for Imaging (Alexa Fluor™ 555 dye) was obtained from Thermo Fisher Scientific and reagents prepared according to manufacturer's instructions. HEKn cells plated in 4-well chamber slides at $1.25x10^4$ cells per well or $2.5x10^4$ cells per well (siRNA experiments only) and treated as described in figure legends. Ten μM 5-ethynyl-2'-deoxyuridine (EdU) added 1 h prior to UV exposure and cells were fixed 4 h post UV for a total EdU treatment of 5 h. Cells not exposed to UV were also treated with EdU for 5 h. EdU detection was performed according to manufacturer's instructions. Briefly, cells were fixed in 3.7% paraformaldehyde for 15 min, washed 2 times with 3% BSA in 1xPBS, then permeabilized with 0.5% Triton® X-100 in 1xPBS for 20 min. Cells were washed 2 times with 3% BSA in 1xPBS, then incubated with Click-iT Plus reaction cocktail for 20 min. Cell were washed once with 3% BSA in 1xPBS, then 2 times with 1xPBS prior to a 30 min incubation with Hoechst® 33342 in 1xPBS. Cells were washed 3 times with 1xPBS and mounted with Invitrogen Prolong Glass Antifade Mountant. All incubations were performed on a rotator at room temperature. Slides were allowed to cure overnight at room temperature, then sealed with nail polish and stored at 4°C. Imaging was performed as described in **Section 2.7**.

2.13 Comet Assay

Neutral comet assay was performed according to instructions included with Trevigen (Gaithersburg, MD) CometAssay #4250-050-K with the addition of an

S1 nuclease treatment as previously described (Quinet et al., 2016). Briefly, HEKn cells were plated in 100 mm plates at $1.4x10^5$ cells per plate and cultured for 3 days. Cells were treated with 1 μM or 5 μM arsenite for 24 h prior to UV exposure. Cells were collected 4 h post UV. For positive controls, HEKn cells were treated with 25 μM etoposide, 15 μM Mitomycin C, and serum starvation (Lifeline DermaLife medium without K supplements) for 4 h. Cells were collected by trypsinization, washed, and resuspended in ice cold 1xPBS, then counted and adjusted to $1x10^5$ cells per mL in ice cold 1xPBS. Cells were combined with 37°C molten LMAgarose (Trevigen) at a ratio of 1:10 (v/v), and 50 μl of the mixture was immediately pipetted onto each well of a Trevigen 20-well CometSlide. The slides were placed at 4°C for 30 min, then immersed in prechilled Trevigen Lysis Buffer at 4°C for 1 h. Slides with S1 nuclease treatment were washed 3 times with Promega (Madison, WI) 1x S1 Nuclease Reaction Buffer, then incubated for 30 min at 37°C in a humidity chamber with 40 U/mL of Promega S1 Nuclease in 1X Reaction Buffer. All slides were washed with prechilled 1x Neutral Electrophoresis Buffer (0.1 M Tris Base plus 0.3 M sodium acetate) for 30 minutes at 4°C

The slides were transferred to the CometAssay ES tank with prechilled 1x Neutral Electrophoresis Buffer. Electrophoresis was performed at 21v for 1 h at 4°C. Excess Neutral Electrophoresis Buffer was drained and slides immersed in DNA precipitation solution (1 M ammonium acetate in 95% ethanol) for 30 min at room temperature. Slides were then immersed in 70% ethanol for 30 min at room temperature. Slides dried overnight at room temperature in the dark. Diluted

Invitrogen SYBR Gold (1:10000 in TE buffer) was pipetted onto each well and incubated for 5 min at 4°C. Excess SYBR Gold was removed, slides dried at 37°C and wells imaged using an Olympus IX83 fluorescence microscope equipped with cellSens Dimension (Olympus; v 1.9) imaging software and a DP80 digital camera. Comets (22-70 per treatment) were analyzed for percent tail DNA using Comet Analysis Software (Trevigen) version 1.2. Comet assay was performed with ≥3 independent experimental replicates. Controls were performed. Etoposide demonstrated DNA DSBs captured by the neutral comet assay. DSBs were increased with S1 nuclease treatment of the replication stress positive controls mitomycin C and serum starvation (**Figure 2.5**).

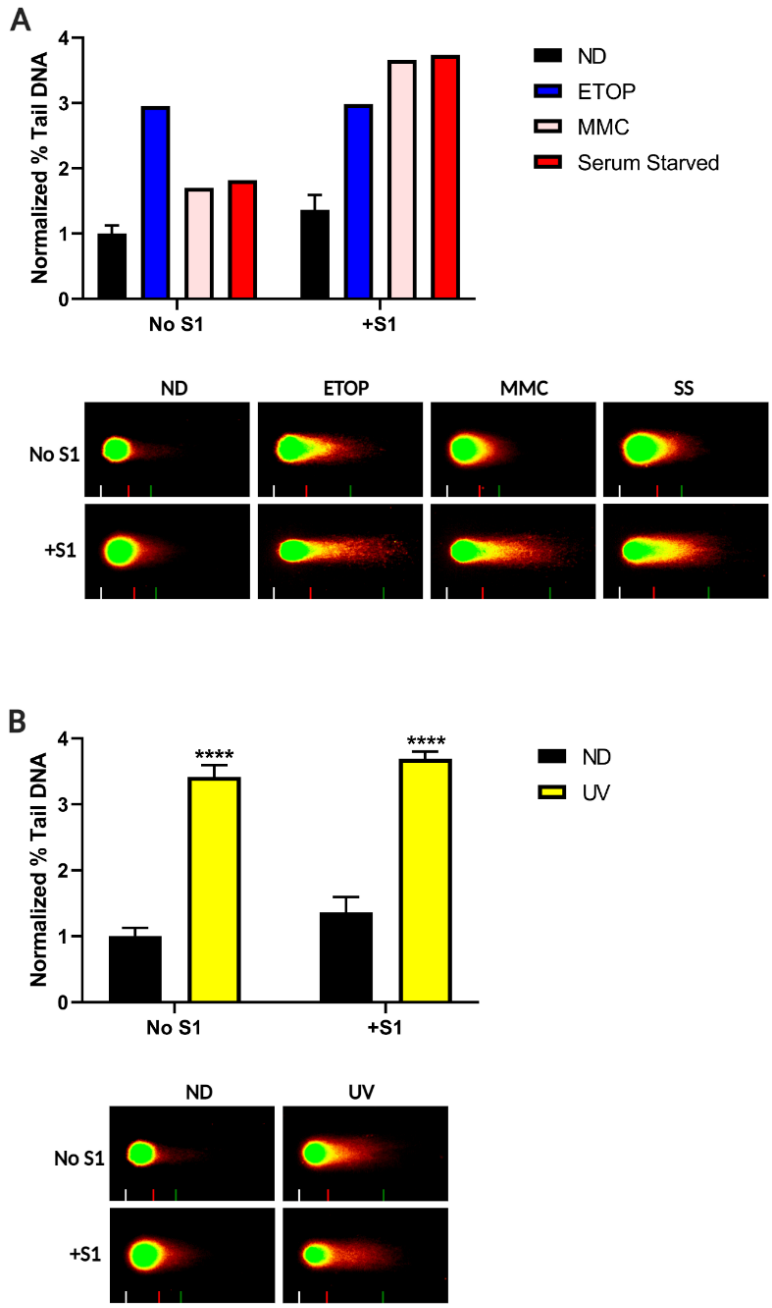

Figure 2.5: Neutral comet assay controls. (A) HEKn cells were treated without (ND) or with 25 μM etoposide (ETOP), 15 μM mitomycin C (MMC), or serum starved (Lifeline DermaLife medium without K supplements) for 4 h prior to collection. Neutral comet assay was performed with or without the addition of S1 nuclease as described in Methods and representative images are shown. Comets were analyzed for percent tail DNA using Trevigen Comet Analysis Software and normalized to NT control. N≥1. **(B)** HEKn cells were collected 4 h post 2.8 kJ/m^2 UVB. Comets were analyzed for percent tail DNA and normalized to NT control. N=3. ****p<0.0001 compared to corresponding ND control. No significant differences when comparing No S1 to +S1 for UV treatment matched groups. All values represent mean ± SEM.

2.14 Statistical Analysis

All graph values represent mean ± standard error of the mean (SEM). Statistical comparisons were performed by nonparametric, unpaired Student's 2-sample *t*-test using GraphPad Prism 5.0 & 8.0 (GraphPad Software Inc.; San Diego, CA). $p<0.05$ was considered to be statistically significant.

CHAPTER 3

AIM 1: ARSENITE BINDS TO AND DISRUPTS THE FUNCTION OF RAD18 ZINC FINGERS

This chapter contains a slightly modified version of "The impact of arsenic on Rad18 and translesion synthesis" by Volk LB, Cooper KL, Jiang T, Paffett ML, and Hudson LG in revision for Toxicology and Applied Pharmacology.

3.1 Rad18 is a target of arsenite

Arsenite preferentially binds to zinc fingers containing ≥3 zinc coordinating cysteine residues (Muenyi et al., 2015; Tam et al., 2020; Zhou et al., 2021). Based on this feature, the UBZ and RING zinc fingers of Rad18 are candidate targets for arsenite. The Rad18 RING finger is composed of two interdigitated zinc-binding sites, a C4 and a CHC2 (**Figure 3.1**) (Huang et al., 2011) and several RING finger containing proteins are known arsenite targets (Tam et al., 2020; Zhou et al., 2021). In comparison, the Rad18 UBZ domain coordinates one zinc ion with a C2HC zinc-binding site (**Figure 3.1**). The classical C2H2 zinc finger of aprataxin (APTX) is structurally comparable to the UBZ domain and does not bind arsenite; however, mutant CCHC APTX zinc finger peptides bind arsenite (Rizzo et al., 2014; Zhou et al., 2011).

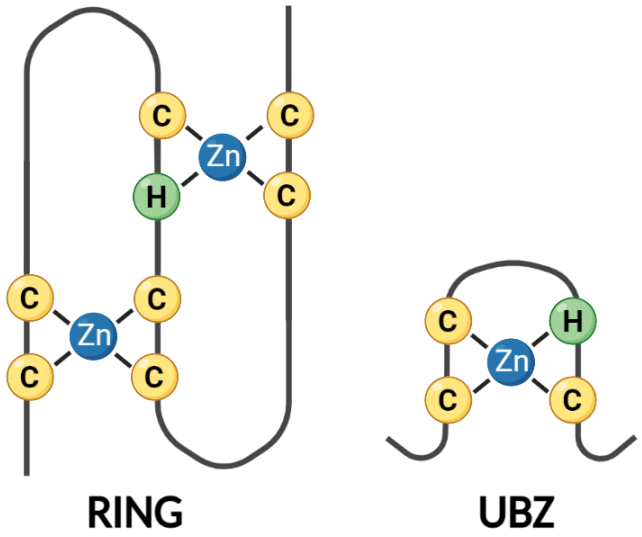

Figure 3.1: Rad18 zinc finger domains. Schematic of zinc binding sites within the Rad18 RING finger and UBZ domains.

Arsenite displaces zinc from Rad18

A zinc displacement assay was used to determine if Rad18 is a target of arsenite. HEKn cells were treated with 1 μM arsenite for 24 h and zinc finger proteins were isolated by immunoprecipitation. Zinc content was detected by incubation with a colorimetric zinc chelator, 4,(2-pyridylazo)-resorcinol). Arsenite exposure resulted in nearly 80% loss of zinc from endogenous Rad18, which was significantly greater than the loss from the APTX and SP1 C2H2 zinc finger controls and comparable to zinc loss from previously identified arsenite targets PARP-1 and XPA (**Figure 3.2**) (Zhou et al., 2011). Arsenite binding to PML has been well studied and underlies its use as a treatment for acute promyelocytic leukemia (**Section 1.6**) (Zhou et al., 2021).

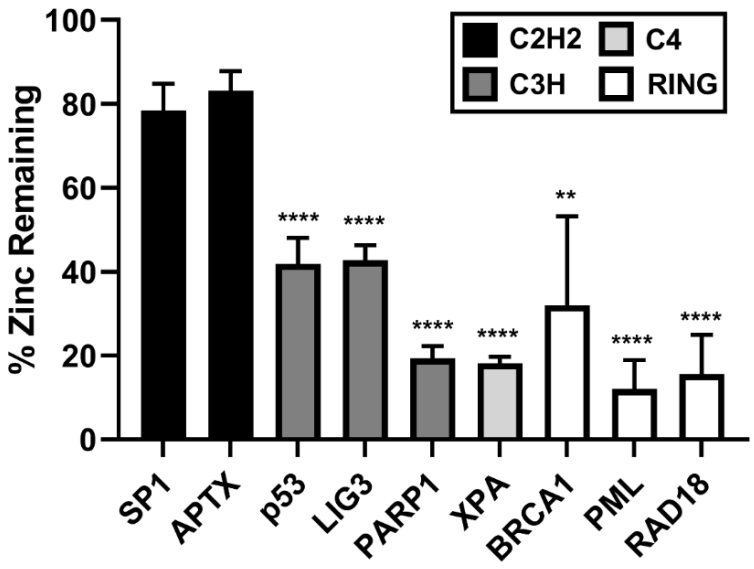

Figure 3.2: Arsenite-induced zinc release from proteins involved in DNA damage response. Single donor HEKn cells were treated with or without 1 μM arsenite for 24 h. The following targets were isolated by immunoprecipitation and free zinc detected by 4,(2-pyridylazo)-resorcinol chelation assay: specificity protein 1 (SP1), APTX, p53, DNA ligase 3 (LIG3), PARP-1, XPA, BRCA1, promyelocytic leukemia protein (PML), and Rad18. Results were normalized to NT control (defined as 100%) for each individual target. Values represent mean ± SEM. N≥3. ****p<0.0001, **p<0.01 compared to C2H2 zinc finger proteins (SP1 and APTX average).

Arsenite binds Rad18 RING peptide

More detailed analysis using MS was conducted to determine which of the Rad18 zinc fingers may be a target of arsenite. Peptides were synthesized containing the amino acid sequence for the Rad18 RING finger and UBZ domains, as well as mutants with only two cysteines per zinc-binding site (**Figure 3.3A**). Resuspended Rad18 zinc finger peptides were incubated with or without arsenite or zinc for LC-MS analysis. Arsenite incubation with the RING peptide revealed a +144 Dalton (Da) peak shift indicating peptide bound to two arsenic ions (**Figure 3.3B**) (binding of two arsenic ions and removal of four protons). The shift was evident even when peptide was coincubated with arsenite and excess zinc (**Figure 3.4A**). Interestingly, the H2C2 mutant RING peptide was still

capable of binding to one arsenic ion (giving +72 Da shift in the observed mass-to-charge value) (**Figure 3.3C**), perhaps due to the availability of ≥3 zinc coordinating cysteine residues retained between the two binding sites.

A

ZF peptide	Sequence	Results (Da)	
		Peptide	+As(III)
R18-RING	$CX_2CX_{12}CX_1HX_2CX_2CX_{10}CX_2C$	5014	+144
R18-RING $_{H2C2}$	$HX_2HX_{12}HX_1HX_2CX_2CX_{10}CX_2C$	5116	+72
R18-UBZ	$CX_2CX_{11}HX_3C$	2809	+72
R18-UBZ$_{C2H2}$	$CX_2CX_{11}HX_3H$	2843	+0

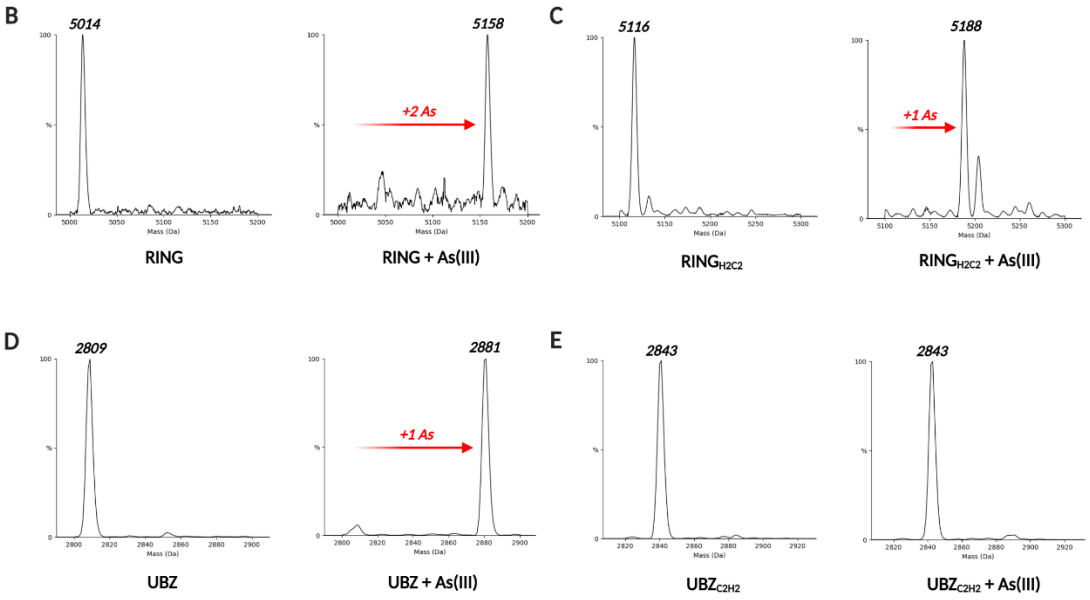

Figure 3.3: Arsenite binds Rad18 zinc finger domains. (A) Rad18 zinc finger (ZF) peptide sequence, corresponding peptide mass, and results are shown. **(B-E)** In an ammonium acetate buffered solution, 100 µM of each peptide was incubated with 400 µM arsenite (As(III)) for a minimum of 30 min at room temperature prior to LC-MS analysis. LC-MS results were obtained for **(B)** Rad18 RING, **(C)** RING$_{H2C2}$, **(D)** UBZ, and **(E)** UBZ$_{C2H2}$ peptides, respectively.

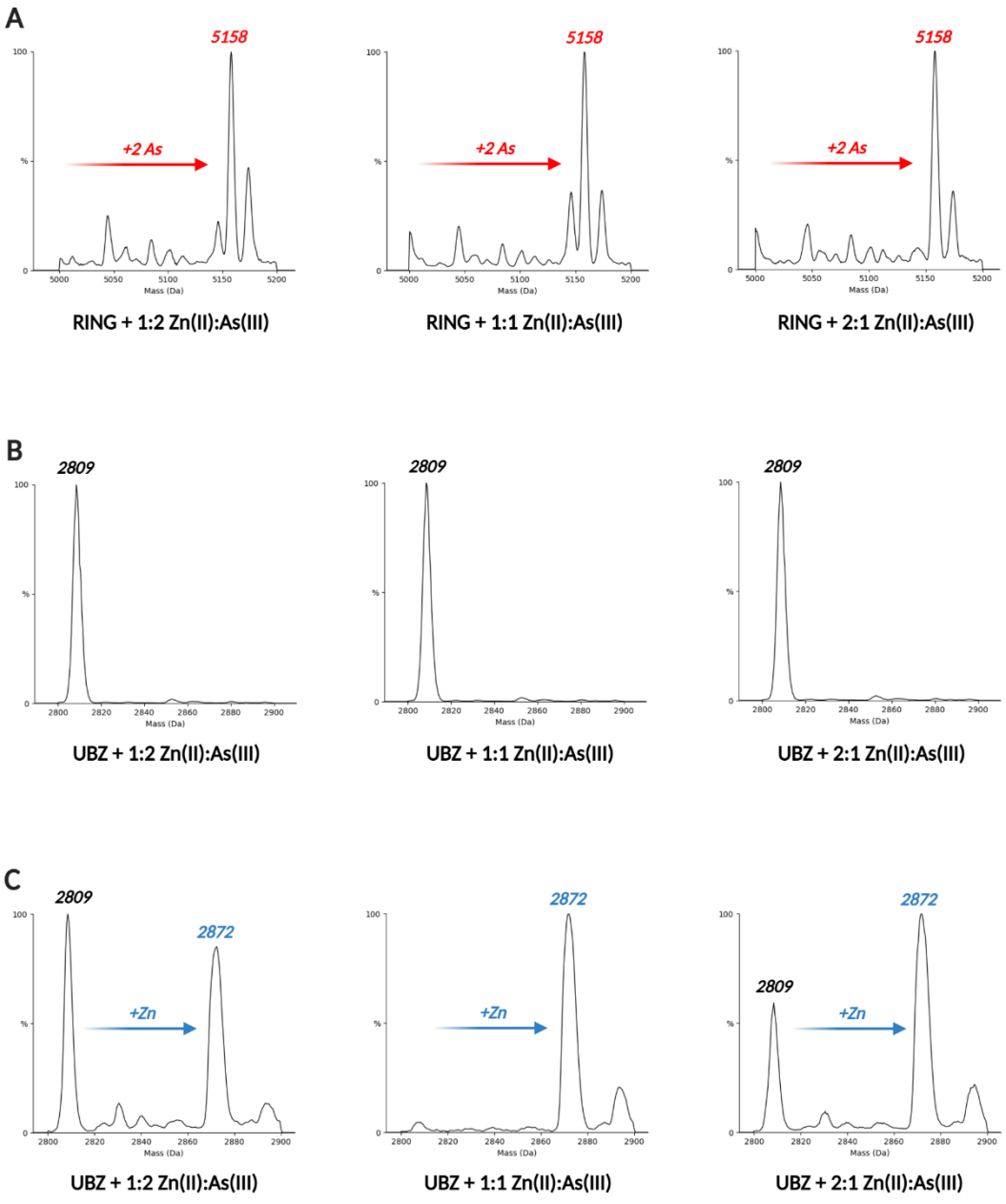

Figure 3.4: Zinc-arsenite coincubation assay with Rad18 zinc finger peptides. Peptide sequences are shown in **Figure 3.3**. In an ammonium acetate buffered solution, 100 μM of each peptide was coincubated with zinc (Zn(II)) and arsenite (As(III)) at one of the following concentrations: 200 μM zinc : 400 μM arsenite (1:2), 400 μM zinc : 400 μM arsenite (1:1), 800 μM zinc : 400 μM arsenite (2:1). Peptide-metal incubations proceeded for a minimum of 30 minutes at room temperature prior to MS analysis. LC-MS results of the zinc-arsenite coincubation assay were obtained for the **(A)** RING and **(B)** UBZ peptides and ESI-MS for the **(C)** UBZ peptide.

Arsenite binds Rad18 UBZ peptide

Incubation of the Rad18 UBZ peptide with arsenite resulted in a +72 Da peak shift corresponding to one bound arsenic ion (**Figure 3.3D**), which was absent with the C2H2 mutant UBZ peptide (**Figure 3.3E**), These findings were consistent with the matrix-assisted laser desorption/ionization - time of flight (MALDI-TOF) MS data (**Figure 3.5**). Arsenite binding to the UBZ domain was not evident when coincubated with zinc (**Figure 3.4B**). ESI-MS results showed peaks corresponding to free peptide and zinc bound peptide, but no peak corresponding to arsenic bound peptide (**Figure 3.4C**). Altogether, these data suggest greater sensitivity of the Rad18 RING finger for disruption by arsenic in comparison to the UBZ domain.

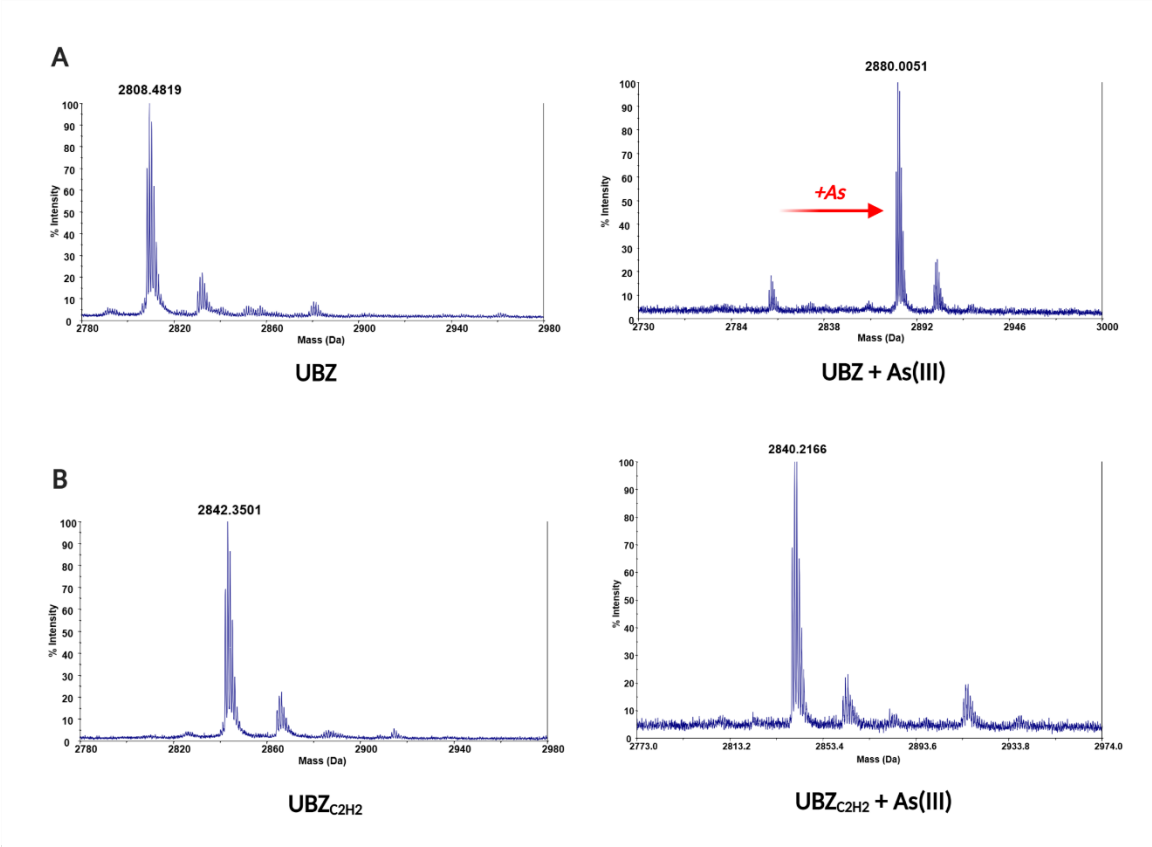

Figure 3.5: MALDI-TOF-MS analysis of the Rad18 UBZ peptide. Peptides sequences are shown in **Figure 3.3**. In a Tris-HCl buffered solution, 25 µM of each UBZ peptide was incubated with or without 200 µM arsenite for 1 h at room temperature prior to MALDI-TOF-MS analysis. MALDI-TOF-MS results were obtained for **(A)** UBZ and **(B)** UBZ_{C2H2} peptides.

Arsenite stimulates ROS production in HEKn cells

Previous studies have determined that the inhibition of zinc finger domains by arsenite is a dual mechanism. First, arsenite increases the vulnerability of the zinc coordinating cysteine residues to oxidative damage by zinc finger binding and zinc displacement. Second, arsenite-induced ROS oxidizes the sensitized cysteine residues releasing arsenite (Cooper et al., 2022; Tam et al., 2020; Zhou et al., 2021). These actions lead to domain loss of function and, consequently, inhibition of DNA repair (**Figure 1.4**). ROS production by arsenite through mechanisms such as NOX stimulation (**Appendix A**) is an important component

in the inhibition of zinc fingers and is evident in pooled HEKn cells (**Figure 3.6**) (Cooper et al., 2022; Tam et al., 2020; Zhou et al., 2021). To determine the consequences of the disruption of Rad18 by arsenite, Rad18 zinc finger function in the presence of arsenite was assessed in **Section 3.2**.

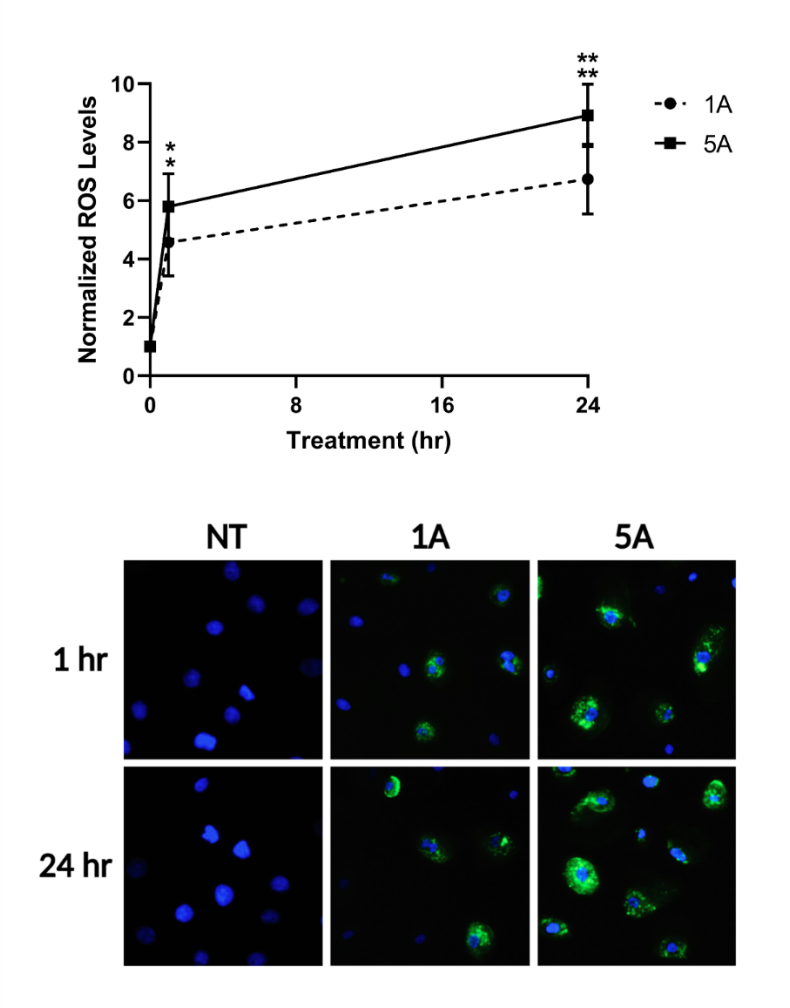

Figure 3.6: Arsenite-induced ROS in HEKn cells. HEKn cells were pretreated with 20 μM DCFDA for 30 min, then fresh medium without (NT) or with 1 μM (1A) or 5 μM arsenite (5A) was added. Plates were incubated for an additional 1 h or 24 h before detection of ROS as described in Methods. DCFDA sum of intensity (green) was normalized to DAPI (blue) and NT control using cellSens Dimension software as described in Methods. Values represent mean ± SEM. N=3. **p<0.01, *p<0.05 compared to NT.

3.2 Arsenite inhibits Rad18 zinc finger function

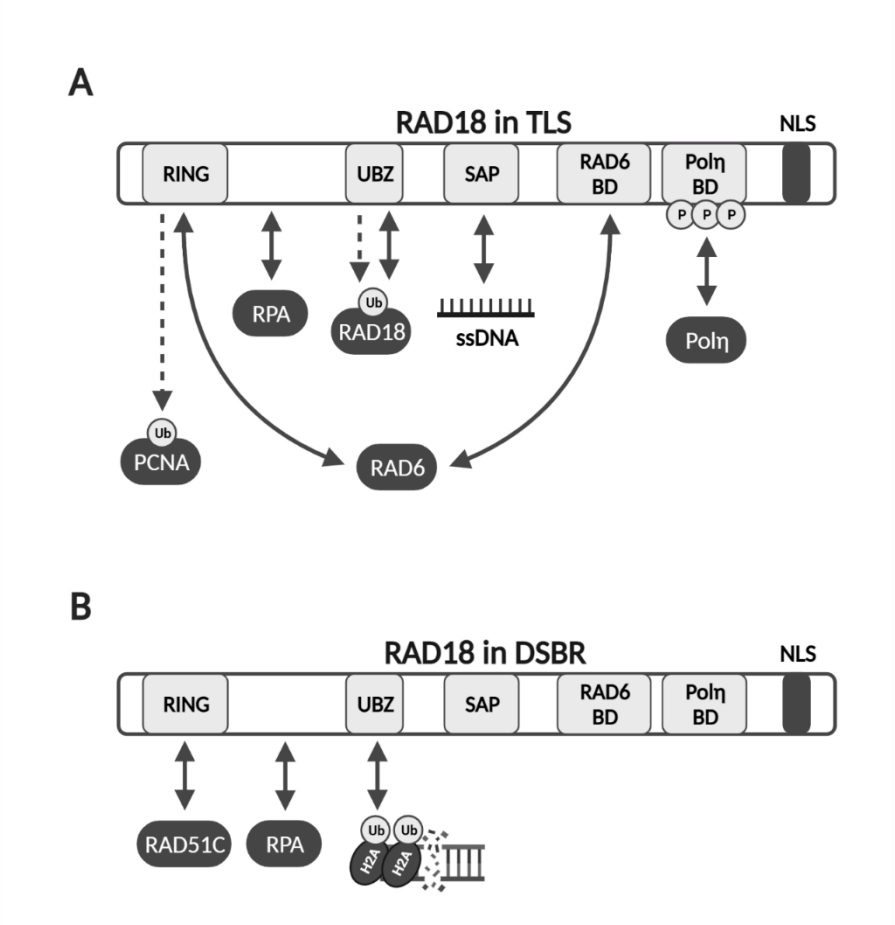

Figure 3.7: Rad18 domain schematic. Rad18 domains involved in (A) TLS and (B) DSBR. Dashed arrows represent Rad18 zinc finger mediated post translational modifications. Solid arrows represent Rad18 domain binding activity. BD = Binding domain. NLS = Nuclear Localization Signal.

Arsenite inhibits Rad18 RING finger function

The Rad18 RING finger is a multifunctional domain with E3 ubiquitin ligase and protein binding activities, and is involved in various pathways including TLS and DSBR (**Figure 3.7**) (Huang et al., 2009; Inagaki et al., 2011; Miyase et al., 2005; Song et al., 2010; Vaziri et al., 2016; Williams et al., 2011). Rad18 monoubiquitinates PCNA through its RING finger in response to DNA damage-induced stalled replication forks (**Figure 3.8A**) (Ma et al., 2020; Vaziri et al.,

2016). The monoubiquitination of PCNA enhances the recruitment and retention of TLS polymerases. Treatment of HEKn cells with arsenite for 24 h significantly reduced both basal and UV-induced PCNA monoubiquitination (Lys164) in a concentration-dependent manner suggesting a decrease in zinc finger domain function (**Figure 3.8B**). Knockdown of Rad18 significantly reduced UV-induced PCNA monoubiquitination in HEKn cells, confirming the importance of Rad18 in this response (**Figure 3.8C**).

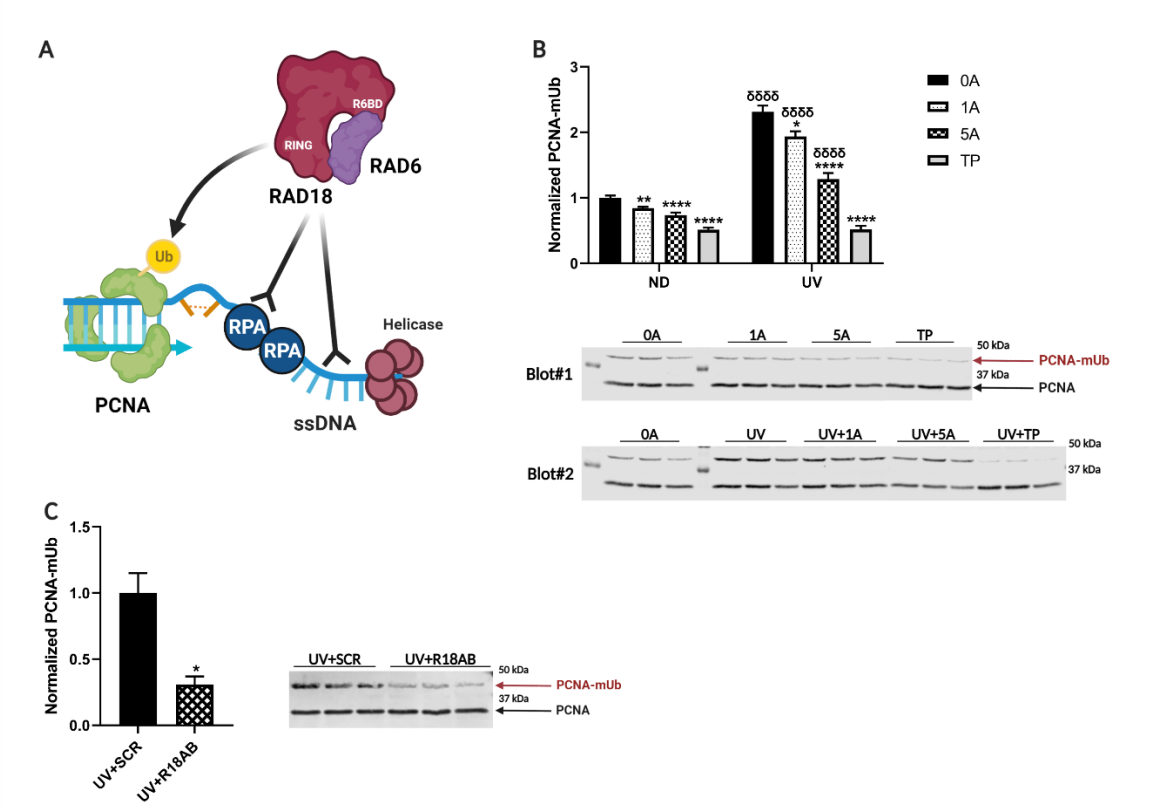

Figure 3.8: Arsenite reduces RING-dependent PCNA monoubiquitination in HEKn cells. (A) Schematic of Rad18 mediated PCNA monoubiquitination. R6BD = Rad6 Binding Domain. Ub = ubiquitin. **(B)** HEKn cells were treated without (0A) or with 1 μM (1A) or 5 μM arsenite (5A) for 24 h or 5 μM TPEN (TP) for 30 min prior to exposure without (ND) or with 2.8 kJ/m^2 UVB. Whole cell lysates were collected 4 h post UV exposure and analyzed via western blot. Monoubiquitinated PCNA (Lys164; PCNA-mUb) was normalized to total protein stain and NT control. N≥6. ****p<0.0001, **p<0.01, *p<0.05 compared to corresponding 0A control. $^{\delta\delta\delta\delta}$p<0.0001 comparing ND to UV for arsenite treatment matched groups. **(C)** HEKn cells were transfected with 40 nM SCR (SCR) or 20 nM each of R18A and R18B (R18AB; 40 nM total), then exposed to 2.8 kJ/m^2 UVB 2 days later. Whole cell lysates were collected 4 h post UV exposure and analyzed via western blot. Monoubiquitinated PCNA was normalized to total protein stain and UV+SCR control. N=3. *p<0.05 compared to UV+SCR. All values represent mean ± SEM.

The E3 ubiquitin conjugating enzyme, human Rad6 (homologs Rad6A/B), is required for the monoubiquitination of PCNA by Rad18. The interaction of Rad18 with Rad6 is dependent on the Rad18 RING finger and Rad6 binding domain (**Figure 3.7A, Figure 3.8A**) (Inagaki et al., 2011). Knockout or mutations in the Rad18 RING finger decrease the amount of Rad6 coimmunoprecipitated with Rad18 (Inagaki et al., 2011). Since the Rad18 RING finger is a target of arsenite

(**Figure 3.3**), it reasons that RING binding activity may be disrupted. To assess the impact of arsenite on the interactions between Rad18 and Rad6B, colocalization analysis was performed in arsenite treated HEKn cells. Results demonstrate a concentration dependent decrease in Rad18-Rad6B colocalization (**Figure 3.9**), suggesting a disruption in the interaction between Rad18 and Rad6. Altogether, findings from **Figures 3.8 and 3.9** support the inhibition of Rad18 RING finger function by arsenic, which can lead to reduced DDT activity and promote UV-induced replication stress.

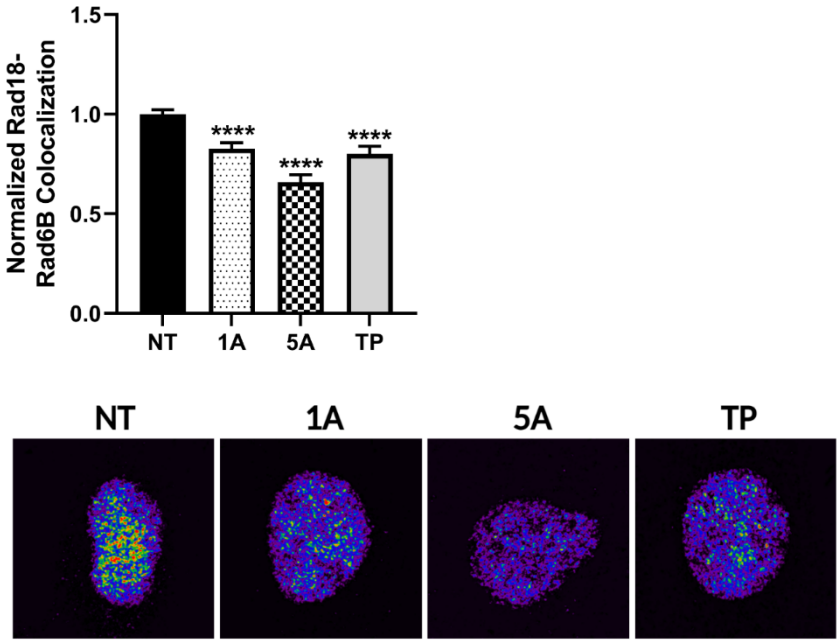

Figure 3.9: Arsenite disrupts RING-dependent colocalization of Rad18 and Rad6B. HEKn cells were treated without (0A) or with 1 μM (1A) or 5 μM arsenite (5A) for 24 h or 5 μM TPEN (TP) for 0.5 h prior to exposure without (ND) or with 2.8 kJ/m^2 UVB. Cells fixed 4 h post UV exposure and immunocytochemistry performed. Pearson's correlation coefficients and colocalization maps for Rad18 and Rad6B were obtained with Huygens Colocalization Analyzer as described in Methods. Results were normalized to NT control. Cells from representative colocalization map MIPs are provided and display false coloring to show pixel intensity from purple (lowest) < blue < green < yellow < orange < red (highest). N≥12 z-stacks (≥5 cells per z-stack). Values represent mean ± SEM. ****p<0.0001 compared to NT.

Arsenite inhibits Rad18 UBZ function

The Rad18 UBZ domain is involved in Rad18 ubiquitination and the localization of Rad18 to DSB sites (**Figure 3.7**) (Huang et al., 2009; Inagaki et al., 2011; Rizzo et al., 2014; Zeman et al., 2014). The monoubiquitination of Rad18 by Rad6 stimulates Rad18 homodimerization, which sequesters Rad18 from initiating TLS in undamaged cells. Rad18 monoubiquitination is reduced in response to some, but not all DNA damaging agents, freeing Rad18 to bind to other factors in order to promote DDT pathways (**Figure 3.10A**) (Zeman et al., 2014). Knockout or mutations in the Rad18 UBZ domain prevents monoubiquitination and impairs Rad18 homodimerization (Inagaki et al., 2011; Miyase et al., 2005; Zeman et al., 2014). Rad18 monoubiquitination was significantly reduced in HEKn cells exposed to 5 μM arsenite for 24 and 48 h suggesting impairment of the UBZ domain function (**Figure 3.10B**). These findings are expected to promote DDT, however, PCNA monoubiquitination was still suppressed in arsenite treated cells further supporting the arsenite mediated inhibition of the Rad18 zinc fingers.

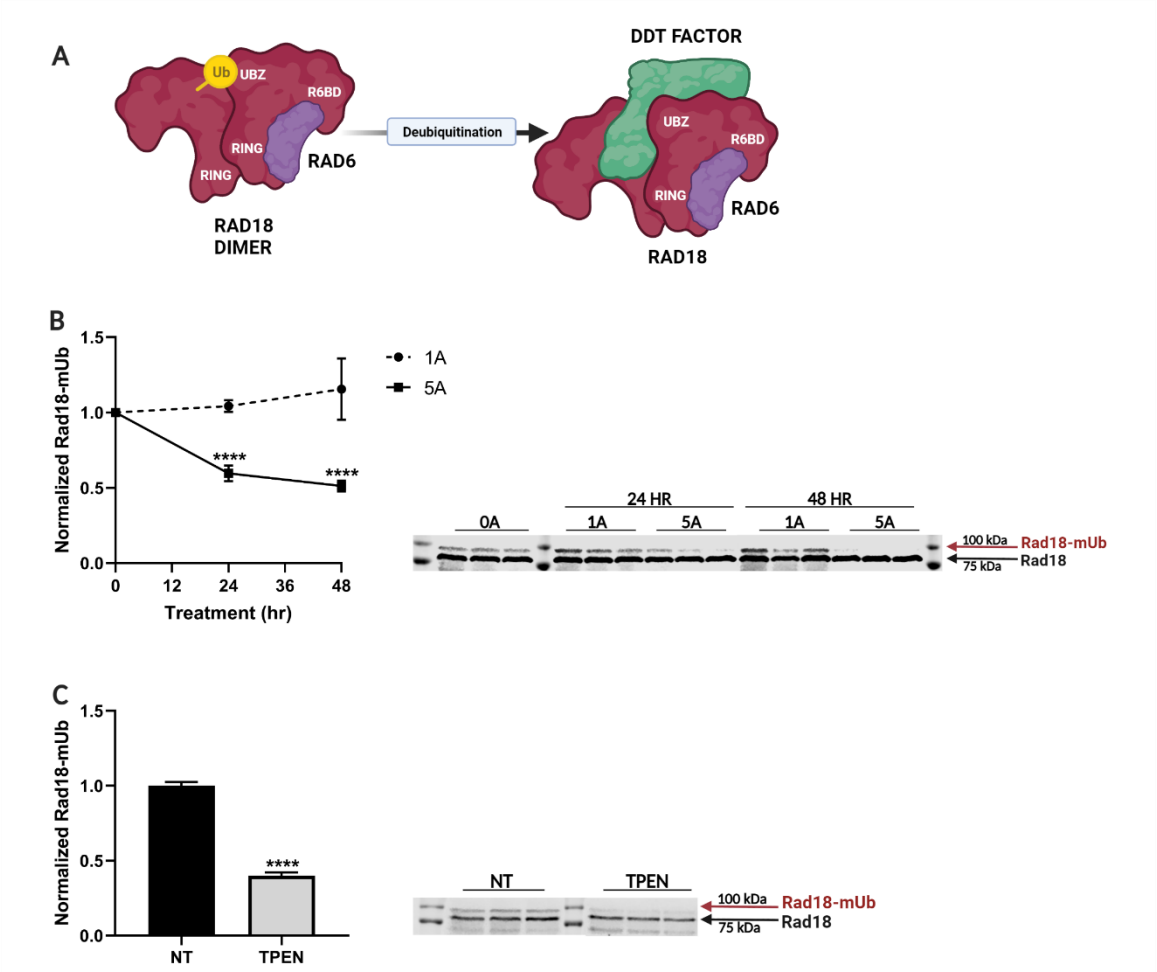

Figure 3.10: Arsenite decreases UBZ-dependent Rad18 monoubiquitination. (A) Schematic of Rad18 ubiquitination and homodimerization. **(B)** HEKn cells were treated without (0A) or with 1 μM (1A) or 5 μM arsenite (5A) for 24 and 48 h. Whole cell lysates were collected and analyzed via western blot. Monoubiquitinated Rad18 (Rad18-mUb) was normalized to total protein stain and NT control (0 h). N≥3. ****p<0.0001 compared to NT control. **(C)** HEKn cells were treated with 5 μM TPEN for approximately 4 h. Whole cell lysates were collected and analyzed via western blot. Monoubiquitinated Rad18 was normalized to total protein stain and NT control. N≥3. ****p<0.0001 compared to NT. All values represent mean ± SEM.

Several studies have identified roles Rad18 performs beyond TLS initiation including the recruitment of DSBR factors during HR (Huang et al., 2009; Inagaki et al., 2011; Vaziri et al., 2016). After exposure to IR, the Rad18 UBZ domain binds ubiquitinated factors near DNA break sites which results in the formation of Rad18 foci (**Figure 3.7B**) (Huang et al., 2009; Tian et al., 2013). Knockout of the

UBZ domain prevents IR-induced Rad18 foci and subsequent recruitment of DSBR factors via the Rad18 RING finger (Huang et al., 2009). To evaluate arsenite inhibition of the UBZ domain ubiquitin binding function, Rad18 foci formation in arsenite and IR exposed HEKn cells was assessed. The number of IR-induced Rad18 foci at both 2 h and 6 h post IR was significantly reduced in HEKn cells coexposed to 5 μM arsenite (**Figure 3.11**). These findings indicate a potential role of Rad18 in the inhibition of HR with exposure to higher concentrations of arsenite.

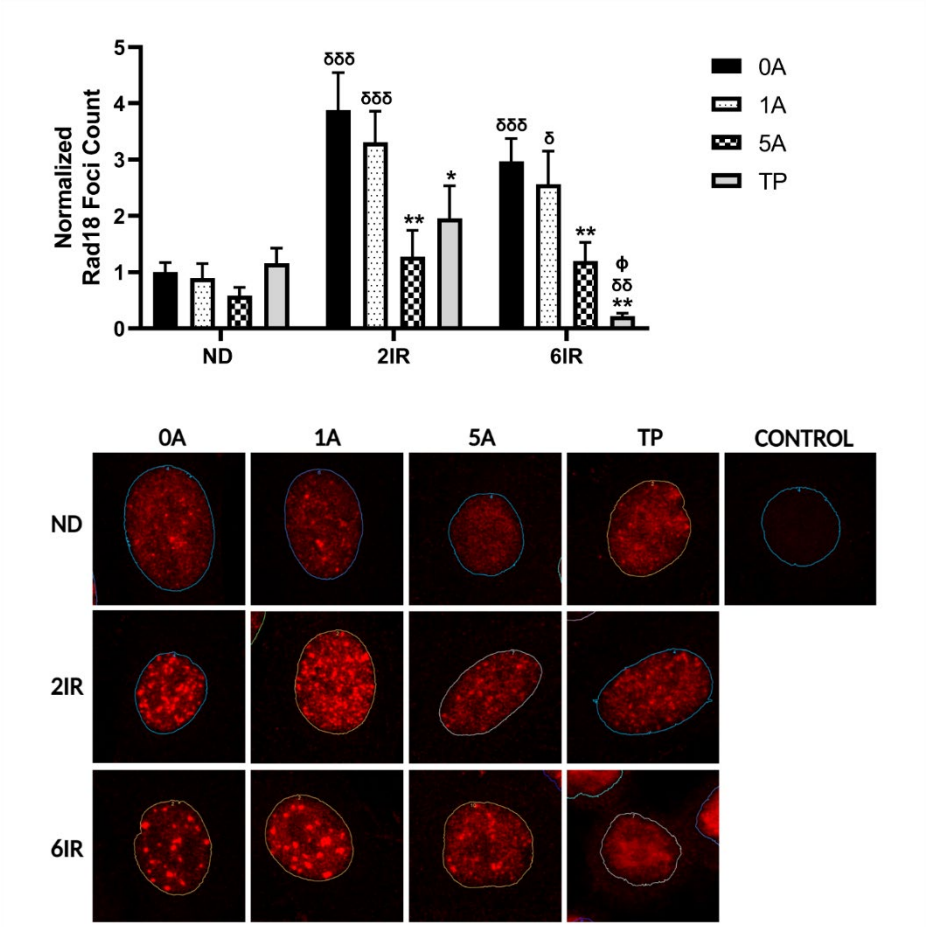

Figure 3.11: Arsenite reduces UBZ-dependent IR-induced Rad18 foci formation. HEKn cells were treated without (0A) or with 1 μM (1A) or 5 μM arsenite (5A) for 24 h or 5 μM TPEN (TP) for 0.5 h prior to exposure without (ND) or with 5 Gy X-rays. Cells fixed 2 (2IR) and 6 h (6IR) post IR exposure and immunocytochemistry performed. MIPs were analyzed for number of Rad18 foci per nuclei normalized to NT control with Slidebook6. Nuclei are outlined in representative images and a secondary only control (CONTROL) is included. N≥10 images (≥5 nuclei per image). **p<0.01, *p<0.05 compared to corresponding 0A control. $^{\delta\delta\delta}$p<0.001, $^{\delta\delta}$p<0.01, $^{\delta}$p<0.05 comparing 2IR and 6IR to ND for treatment matched groups. $^{\Phi}$p<0.05 comparing 6IR to 2IR for treatment matched groups.

Treatment with zinc chelator is similar to arsenite

Both the RING and UBZ domains of Rad18 are zinc binding motifs as previously described (**Figure 3.1**) (Inagaki et al., 2011). Treatment of HEKn cells with the membrane-permeable zinc chelator N,N,N′,N′-tetrakis(2-pyridinylmethyl)-1,2-ethanediamine (TPEN) significantly reduced RING-dependent PCNA

monoubiquitination (**Figure 3.8B**) and Rad18-Rad6 colocalization (**Figure 3.9**), as well as UBZ-dependent Rad18 monoubiquitination (**Figure 3.10C**) and IR-induced foci formation (**Figure 3.11**). The similarities in findings between arsenite and TPEN treatments (**Table 3.1**) strongly support arsenite disruption of the zinc-binding domains of Rad18 as has been reported for other zinc finger proteins (Muenyi et al., 2015; Tam et al., 2020; Zhou et al., 2021).

Domain	Function	Results from arsenite or TPEN treatments
RING	E3 ubiquitin ligase activity	Decreased PCNA monoubiquitination
	Protein binding	Decreased Rad18-Rad6B colocalization
UBZ	Rad18 monoubiquitination	Decreased Rad18 monoubiquitination
	Ubiquitin binding	Decreased IR-induced Rad18 foci formation

Table 3.1: Impacts of arsenite and TPEN on Rad18 zinc finger function.

Arsenite effect is cell line dependent

In contrast to HEKn cells, PCNA monoubiquitination was upregulated (**Figure 3.12A**) and Rad18 monoubiquitination unaltered (**Figure 3.12B**) in arsenite treated HEK-293T cells. The increase in UV-induced PCNA monoubiquitination is what would be expected with arsenite mediated DNA damage retention triggering DDT pathways. The difference between cell lines may be due to the level of Rad18, which is considerably higher in the immortalized HEK-293T cells compared to primary HEKn cells (**Figure 3.12C)**. Rad18 expression is regulated at both the transcription and protein level and is significantly greater in rapidly dividing cells (Miyase et al., 2005; Varanasi et al., 2012). The surplus of Rad18 in HEK-293T

cells may provide more protection from arsenite-induced changes. Mechanistic studies involving Rad18 or arsenite are known to be variable, partly due to the use of different cell types (Ma et al., 2020; Muenyi et al., 2015; Tam et al., 2020; Vaziri et al., 2016; Zhou et al., 2021). Therefore, this finding illuminates the importance of using an appropriate biological model for studying the cocarcinogenic activity of arsenite through TLS.

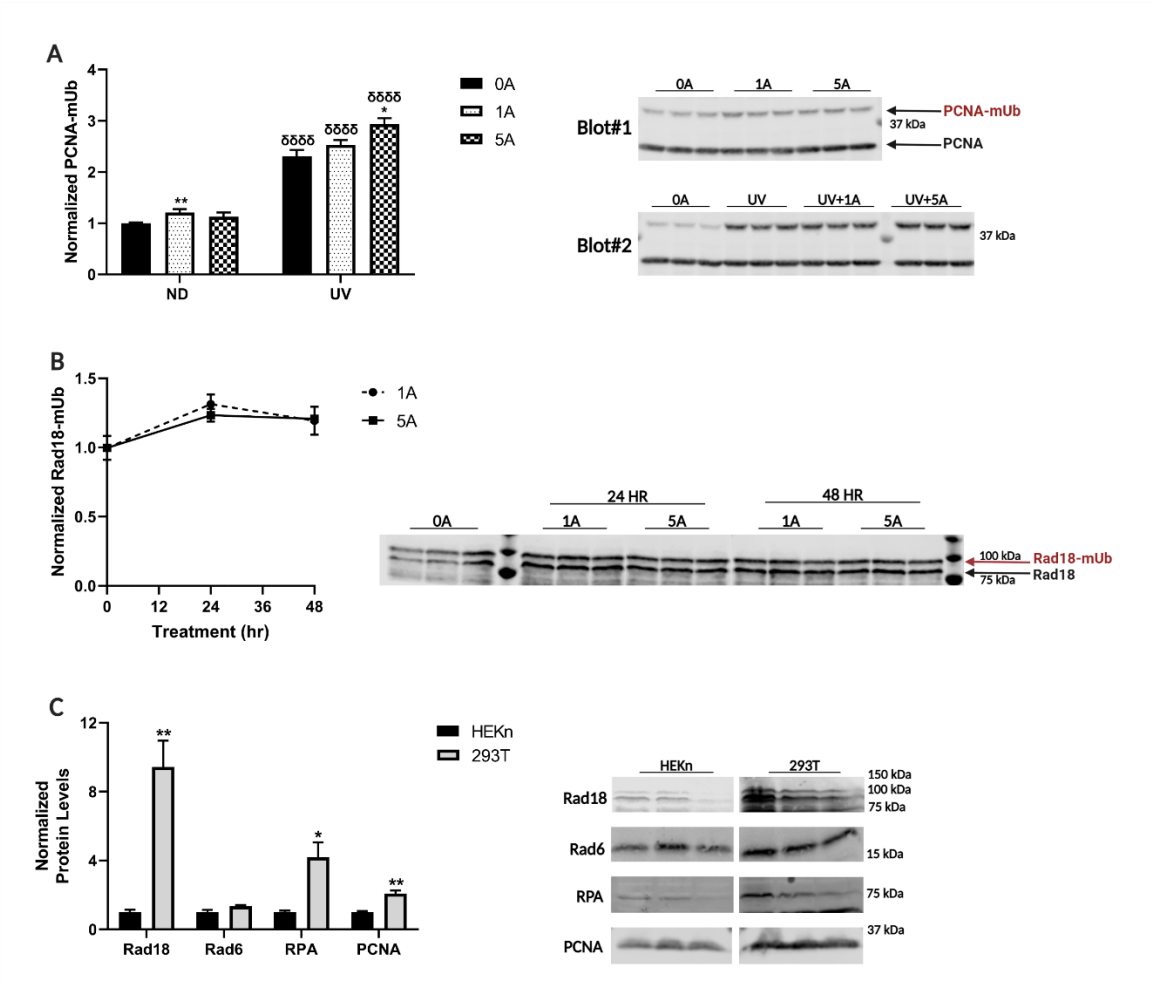

Figure 3.12: Cell line dependent effects. (A) HEK-293T (293T) cells were plated in 60 mm plates at $3x10^5$ cells per plate and cultured for 2 days. Cells were treated without (0A) or with 1 μM (1A) or 5 μM arsenite (5A) for 24 h prior to exposure without (ND) or with 2.8 kJ/m^2 UVB. Whole cell lysates were collected 4 h post UV exposure for western blot analysis. Monoubiquitinated PCNA (Lys164) was normalized to total protein stain and NT control. N≥3. ****p<0.0001, **p<0.01, *p<0.05 compared to corresponding 0A control. $^{\delta\delta\delta\delta}$p<0.0001 comparing ND to UV for arsenite treatment matched groups. **(B)** 293T cells were treated without (0A) or with 1 μM (1A) or 5 μM arsenite (5A) for 24 and 48 h. Whole cell lysates were collected and analyzed via western blot. Monoubiquitinated Rad18 (Rad18-mUb) was normalized to total protein stain and NT control (0 h). N≥3. No significant differences compared to NT. **(C)** Primary HEKn cells and immortalized 293T cells were plated in 100 mm plates and collected for western blot analysis at approximately 80 percent confluence. Each protein was normalized to total protein stain and HEKn cell results. N=3. **p<0.01, *p<0.05 compared to HEKn cells. All values represent mean ± SEM.

3.3 Aim 1 conclusions

In summary, arsenic binds to peptides representing both the RING finger and UBZ domains of Rad18 (**Figure 3.3**) and arsenic exposure promoted zinc loss from endogenous Rad18 (**Figure 3.2**). In contrast to the UBZ peptide, arsenite binding to the RING peptide was evident with zinc coincubation (**Figure 3.4**). These findings suggest arsenite has a higher affinity for the RING finger compared to the UBZ domain and may have more significant effects on RING-dependent functions. This is suggested by concentration dependence for arsenite-induced suppression of RING-dependent PCNA monoubiquitination (**Figure 3.8B**) and Rad18-Rad6B colocalization (**Figure 3.9**) versus UBZ-dependent Rad18 monoubiquitination (**Figure 3.10B**) and foci formation (**Figure 3.11**).

The similarity in results from arsenite and TPEN treated cells further support zinc displacement as the mechanism by which arsenite inhibits Rad18 (**Table 3.1**). The arsenite-induced effect was dependent on cell type, with primary HEKn cells being more vulnerable to Rad18 inhibition compared to immortalized HEK-293T cells (**Figure 3.12**). Altogether, these findings reveal a novel arsenite

target, the UBZ domain, and illustrate a mechanism by which arsenite may influence genome stability through the binding and functional inhibition of the Rad18 zinc fingers. As alterations in the regulation of Rad18 can also impact Rad18-dependent mechanisms such as TLS, it is important to evaluate other effects of arsenite exposure beyond zinc finger inhibition as addressed in the following chapter.

CHAPTER 4

AIM 2: MECHANISMS OF ARSENITE REGULATION OF RAD18

This chapter contains a slightly modified version of "The impact of arsenic on Rad18 and translesion synthesis" by Volk LB, Cooper KL, Jiang T, Paffett ML, and Hudson LG in revision for Toxicology and Applied Pharmacology.

4.1 The minor impact of arsenite on Rad18 expression and phosphorylation

The mechanism of action of arsenic carcinogenesis is exceptionally complex. In the context of DNA repair, arsenite regulates DNA repair pathways and the expression of various DNA repair proteins. Therefore, it is important to distinguish if arsenite inhibition of Rad18 is mediated through zinc finger disruption, altered regulation, or a combination of both. The initiation of TLS through Rad18 is tightly regulated due to the negative implications of error prone DNA damage bypass. Alterations in Rad18 expression (**Figure 4.1A**) and posttranslational modifications, including phosphorylation (**Figure 4.2A**) and ubiquitination (**Figure 3.10A**), in response to DNA damage are important means by which Rad18 modulates TLS (Ma et al., 2020; Vaziri et al., 2016; Zeman et al., 2014).

Arsenite induces a minor increase in Rad18 expression

With regards to expression, arsenite treatment of HEKn cells for 24 h revealed a modest increase in the levels of Rad18 and its binding partner Rad6 but did not change protein levels of two additional TLS proteins (RPA and PCNA)

(**Figure 4.1B**). High levels of Rad18 can overactivate TLS through PCNA monoubiquitination, whereas Rad6 overexpression is associated with increased Rad18 monoubiquitination (Miyase et al., 2005; Yang et al., 2018). However, neither of these effects are observed in arsenite treated HEKn cells (**Figure 3.8B; Figure 3.10B**), further supporting the arsenite mediated inhibition of the Rad18 zinc fingers.

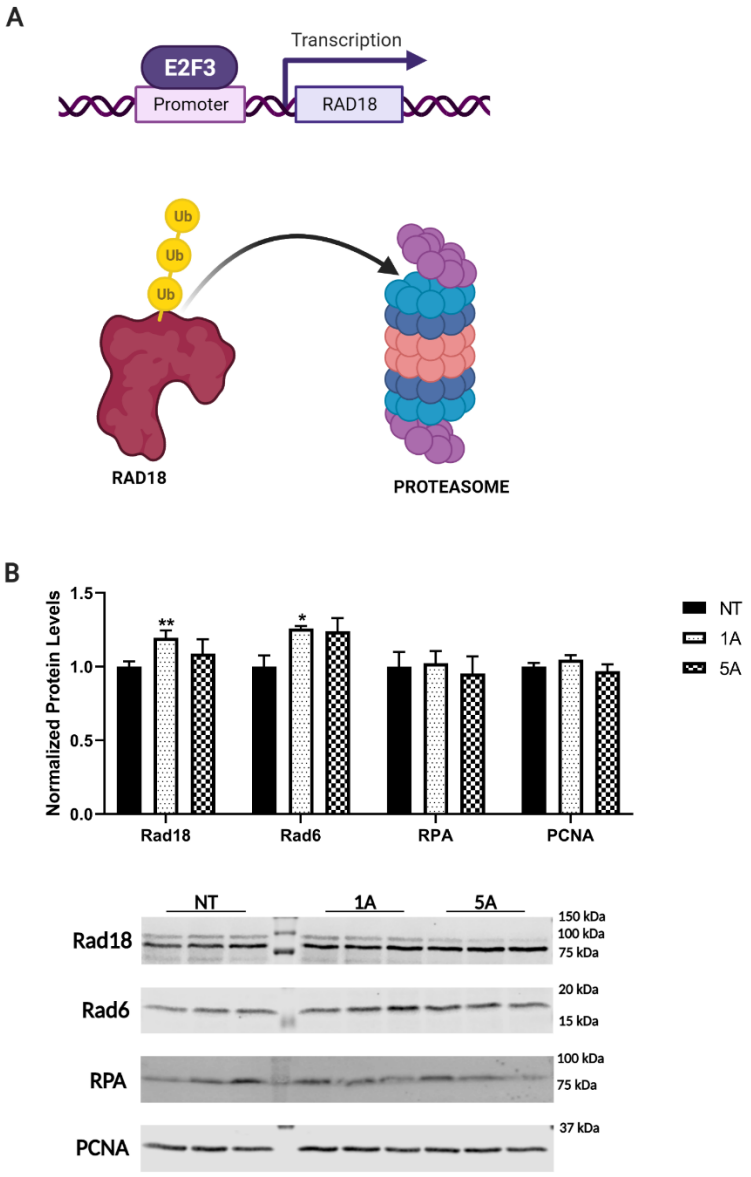

Figure 4.1: Arsenite effect on Rad18 and TLS factor expression. (A) Schematic of Rad18 expression regulation. **(B)** HEKn cells were treated without (NT) or with 1 μM (1A) or 5 μM arsenite (5A) for 24 h. Whole cell lysates were collected and analyzed via western blot. Levels of each protein were normalized to total protein stain and NT control. N≥3. Values represent mean ± SEM. **p<0.01, *p<0.05 compared to NT.

Rad18 phosphorylation is not altered by arsenite exposure

Checkpoint kinase 1 activation of downstream factors leads to the phosphorylation of the Rad18 Polη binding site, which is required for efficient

Polη mediated gap filling during TLS (**Figure 3.7A**) (Barkley et al., 2012; Day et al., 2010). Previous studies have determined arsenite exposure can lead to the inhibition of checkpoint kinase 1, which underlines the importance of evaluating arsenite mediated effects on Rad18 phosphorylation (Hubaux et al., 2013; Muenyi et al., 2015). However, neither basal nor UV-induced Rad18 phosphorylation at the Polη binding site (serine 303) was significantly altered by arsenite treatment (**Figure 4.2B**). Altogether, these findings indicate that arsenite does not inhibit PCNA monoubiquitination as shown in **Figure 3.8** by suppressing Rad18 expression (**Figure 4.1**) or phosphorylation (**Figure 4.2).** However, there are other means of regulating protein activity such as changes in subcellular localization.

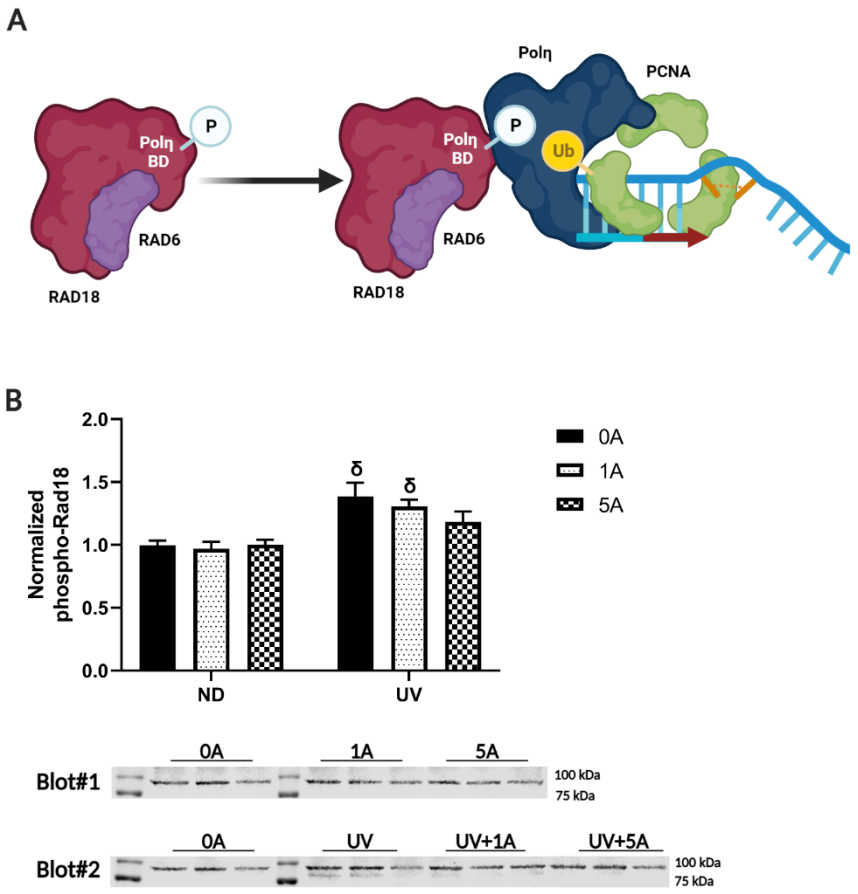

Figure 4.2: Arsenite effect on Rad18 phosphorylation. (A) Schematic of Rad18 phosphorylation. **(B)** HEKn cells were treated without (0A) or with 1 μM (1A) or 5 μM arsenite (5A) for 24 h prior to exposure without (ND) or with 2.8 kJ/m^2 UVB. Whole cell lysates were collected 4 h post UV exposure and analyzed via western blot. Phosphorylated Rad18 (S403) was normalized to total protein stain and NT control. N=3. Values represent mean ± SEM. No significant differences were detected for arsenite treatment compared to corresponding 0A control. $^{\delta}p<0.05$ comparing ND to UV for arsenite treatment matched groups.

4.2 Arsenite decreases the nuclear localization of Rad18

Rad18 and TLS factor localization in response to UV

Alterations in TLS factor localization is another means of TLS regulation (**Figure 4.3A**). Rad18 is predominantly found in the nucleus with a smaller fraction in the cytoplasm. Many factors influence Rad18 localization including cell cycle phase and monoubiquitination (Inagaki et al., 2009; Masuyama et al., 2005;

Miyase et al., 2005). Nuclear localization of Rad18 was significantly decreased by 16% (**Figure 4.3B**) and the cytoplasmic fraction increased by over 3-fold (**Figure 4.4A**) following treatment of HEKn cells with 5 μM arsenite. The reduction of Rad18 in the nucleus and increase in the cytoplasm was evident regardless of exposure to UV.

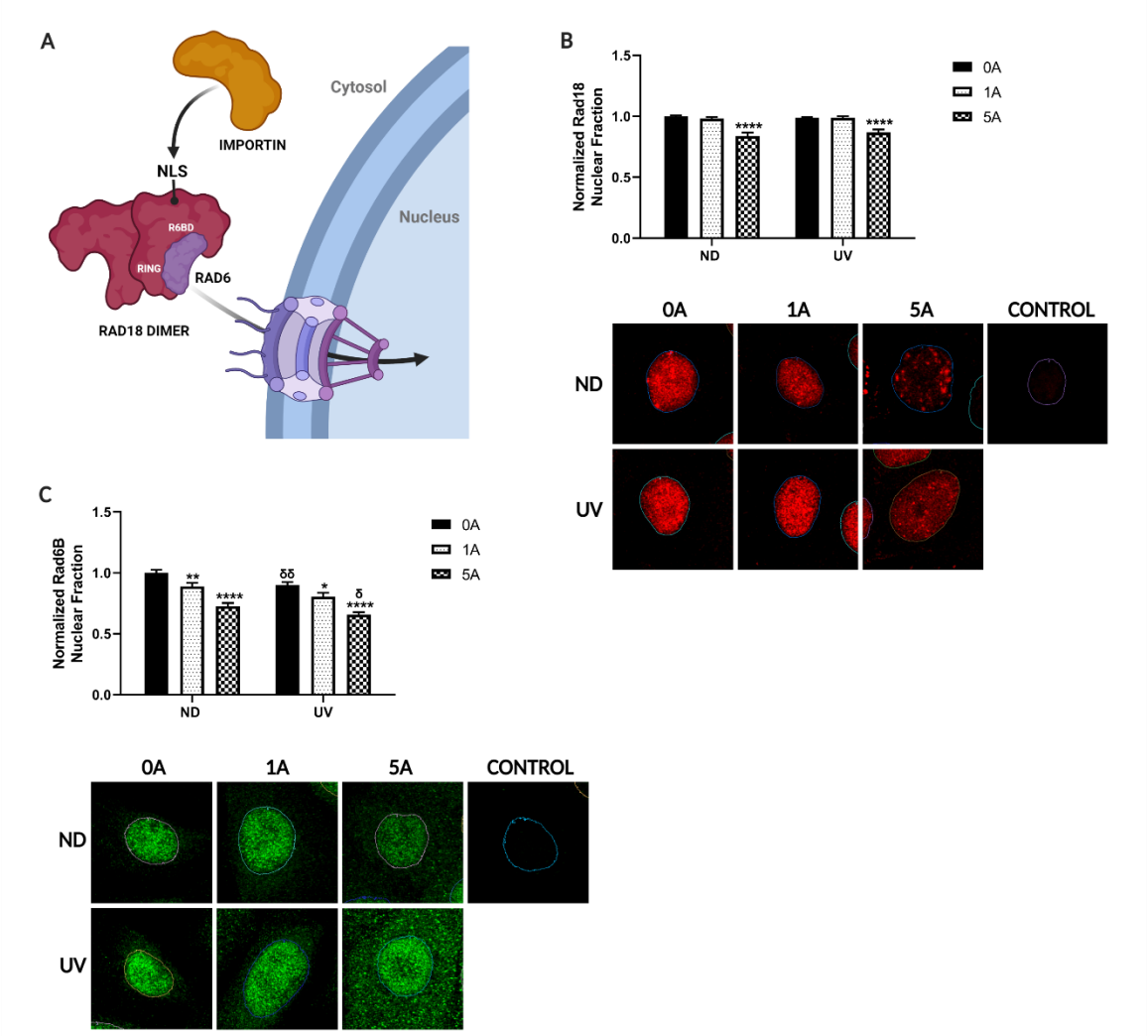

Figure 4.3: Arsenite disrupts the nuclear localization of Rad18 and Rad6B. (A) Schematic of Rad18 and Rad6 nuclear localization. **(B-C)** HEKn cells were treated without (0A) or with 1 μM (1A) or 5 μM arsenite (5A) for 24 h prior to exposure without (ND) or with 2.8 kJ/m^2 UVB. Cells were fixed 4 h post UV exposure and fractional nuclear localization of **(B)** Rad18 and **(C)** Rad6B was measured by immunocytochemistry as described in Methods. MIPs were analyzed for protein nuclear sum of intensity normalized to total sum of intensity and NT control with Slidebook 6. Nuclei are outlined in representative images and secondary only controls (CONTROL) are included. N≥15 images (≥5 cells per image). Values represent mean ± SEM. ****p<0.0001, **p<0.01, *p<0.05 compared to corresponding 0A control. $^{\delta\delta}$p<0.01, $^{\delta}$p<0.05 comparing ND to UV for arsenite treatment matched groups.

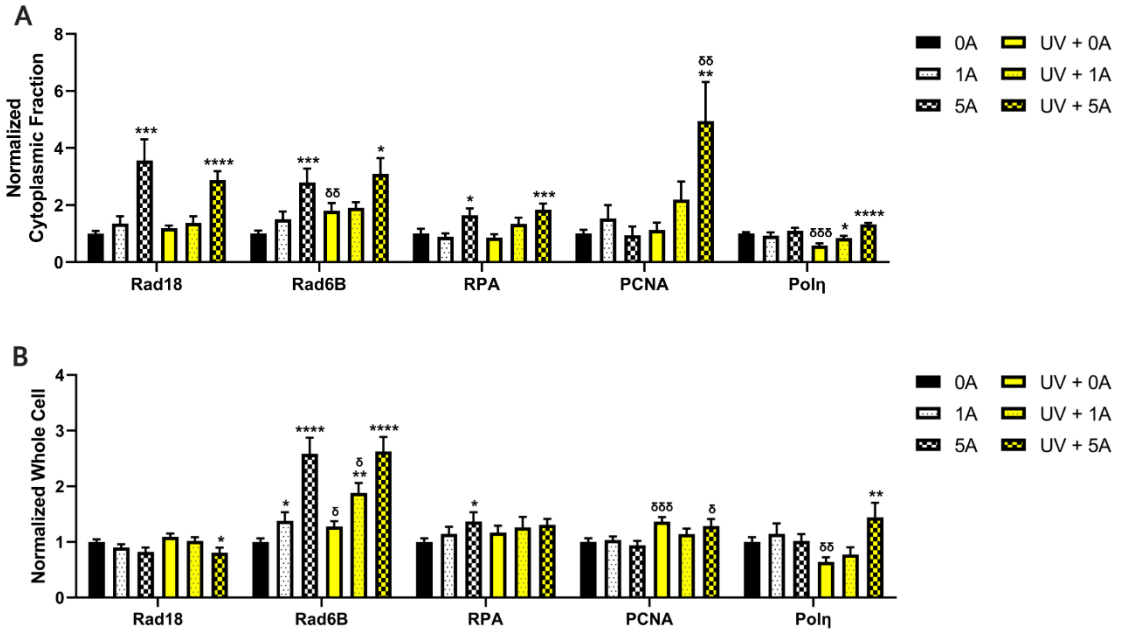

Figure 4.4: Cytoplasmic localization and whole cell signal of TLS factors in response to arsenite and/or UV. HEKn cells were treated without (0A) or with 1 μM (1A) or 5 μM arsenite (5A) for 24 h prior to exposure with or without 2.8 kJ/m^2 UVB. Cells were fixed 4 h post UV exposure and immunocytochemistry performed. MIPs were analyzed for **(A)** protein cytoplasmic sum of intensity normalized to total sum of intensity and NT control and **(B)** protein sum of intensity normalized to number of cells and NT control using Slidebook 6. N≥12 images (≥5 cells per image). Values represent mean ± SEM. ****p<0.0001, ***p<0.001, **p<0.01, *p<0.05 compared to corresponding 0A control. $^{\delta\delta\delta}$p<0.001, $^{\delta\delta}$p<0.01, $^{\delta}$p<0.05 comparing ND to UV for arsenite treatment matched groups.

It is proposed that Rad6 localization is dependent on Rad18 binding and nuclear translocation via the Rad18 nuclear localization signal (Hedglin and Benkovic, 2015). The nuclear localization of the Rad6 human homolog Rad6B was significantly decreased (**Figure 4.3C**), and the cytoplasmic fraction increased (**Figure 4.4A**) in response to arsenite with or without UV. Rad6 binds to Rad18 partially through the Rad18 RING finger (**Figure 3.7A**) and disruption in Rad6 localization may be due to the arsenite mediated inhibition of the Rad18 RING finger (**Chapter 3**).

RPA and PCNA are predominantly located in the nucleus with little detected

in the cytoplasm (**Figure 4.5**). Arsenite caused minor decreases in the nuclear localization of these factors, with corresponding increases in the cytoplasmic fraction (**Figure 4.4A**). The nuclear fraction of Polη was significantly increased by UV exposure (**Figure 4.5**), which was substantially suppressed by arsenite coexposure. Altogether, localization analysis revealed a decrease in the nuclear fraction of several TLS factors which may suppress TLS activity.

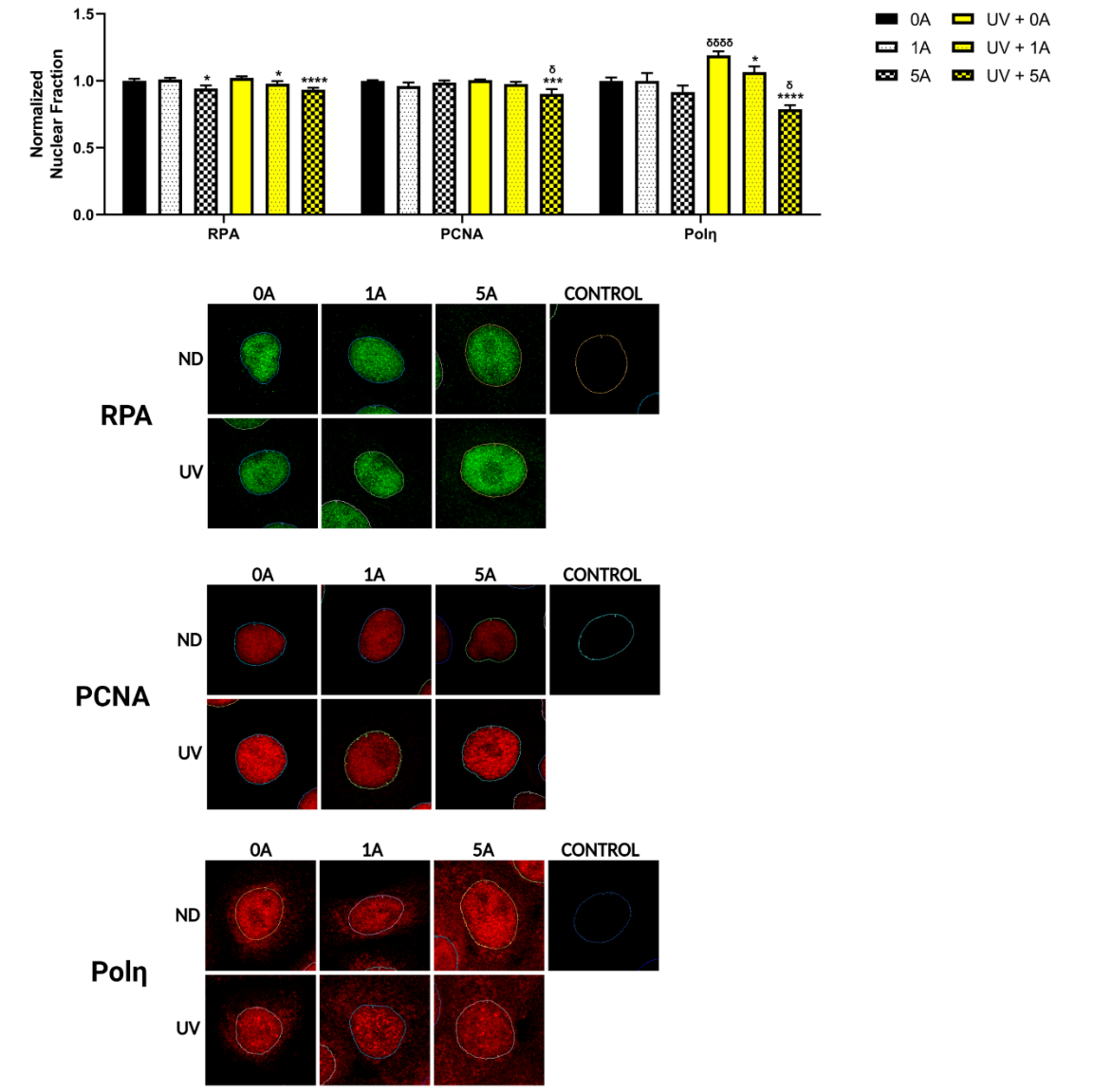

Figure 4.5: Nuclear localization of additional TLS factors in response to arsenite and/or UV. HEKn cells were treated without (0A) or with 1 μM (1A) or 5 μM arsenite (5A) for 24 h prior to exposure without (ND) or with 2.8 kJ/m^2 UVB. Cells were fixed 4 h post UV exposure and immunocytochemistry was performed. MIPs were analyzed for protein nuclear sum of intensity normalized to total sum of intensity and NT control using Slidebook 6. Nuclei are outlined in representative images and secondary only controls (CONTROL) are included. N≥12 images (≥5 cells per image). Values represent mean ± SEM. ****p<0.0001, ***p<0.001, *p<0.05 compared to corresponding 0A control. $^{\delta\delta\delta\delta}$p<0.0001, $^{\delta}$p<0.05 comparing ND to UV for arsenite treatment matched groups.

Rad18 localization in response to IR

As discussed in **Section 3.2**, Rad18 forms distinct nuclear foci in response to

IR. These foci are significantly reduced by arsenite treatment in HEKn cells (**Figure 3.11**). Additionally, the subcellular localization of Rad18 is disrupted by arsenite in IR exposed HEKn cells, with a significant decrease in nuclear localization and increase in the cytoplasmic fraction (**Figure 4.6**). These findings are similar to both UV and unexposed cells, suggesting the mechanism by which arsenite alters the subcellular localization of Rad18 is not DNA damage dependent.

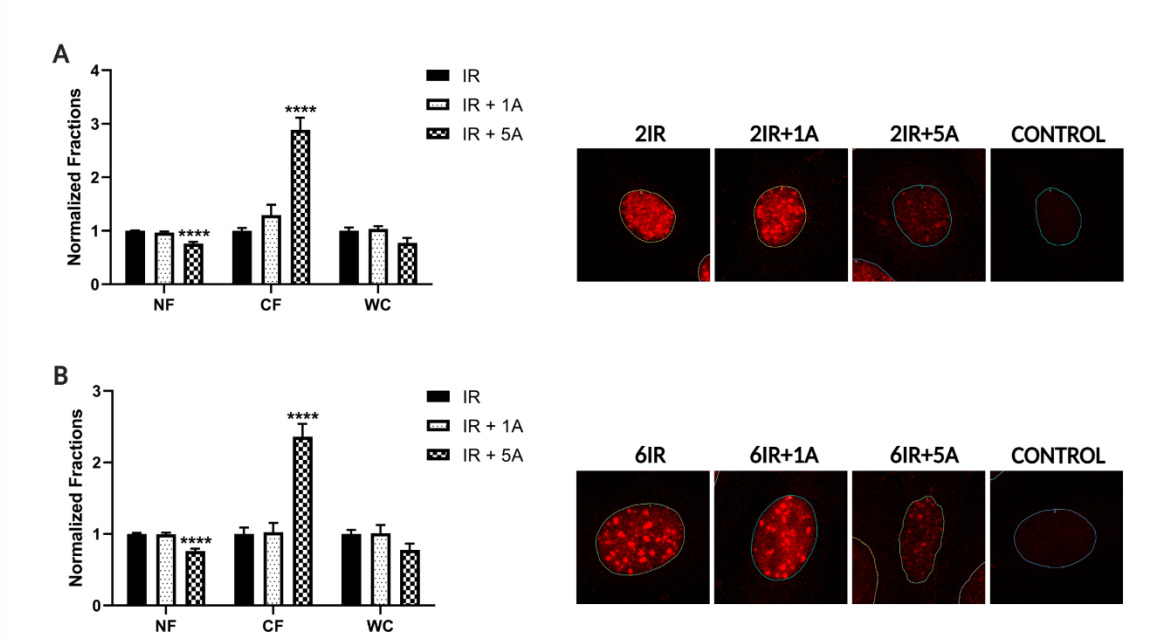

Figure 4.6: Nuclear localization of Rad18 with IR. HEKn cells were treated without (0A) or with 1 μM (1A) or 5 μM arsenite (5A) for 24 h prior to exposure with 5 Gy X-rays. Cells were fixed **(A)** 2 h and **(B)** 6 h post IR exposure and immunocytochemistry performed. MIPs were analyzed for Nuclear Fraction (NF; Rad18 nuclear sum of intensity normalized to total sum of intensity and NT control), Cytoplasmic Fraction (CF; Rad18 cytoplasmic sum of intensity normalized to total sum of intensity and NT control), and Whole Cell (WC; Rad18 sum of intensity normalized to number of cells and NT control) using Slidebook 6. Nuclei are outlined in representative images and secondary only controls (CONTROL) are included. N≥12 images (≥5 cells per image). Values represent mean ± SEM. ****p<0.0001 compared to 0A control for each fraction.

4.3 Arsenite alters Rad18 recruitment to DNA damage

Rad18 and TLS factor recruitment to UV-induced DNA damage

Rad18 recruitment to chromatin is heavily regulated by multiple mechanisms to ensure TLS is initiated only when necessary. RPA and ssDNA are critical factors controlling Rad18 recruitment to stalled replication forks (**Figure 3.7A; Figure 3.8A**) (Li et al., 2020; Ma et al., 2020). Chromatin fractionation of UV exposed HEKn cells revealed a substantial loss in chromatin bound Rad18, Rad6, and RPA upon coexposure to arsenite (**Figure 4.7**). The arsenite-induced decrease in chromatin bound RPA can negatively influence the recruitment of Rad18 and Rad6 to chromatin. RPA contains a zinc finger DBD structurally conducive to arsenite binding which may underly the reduction of RPA on chromatin with arsenite exposure (Bochkareva et al., 2002). The presence of soluble RPA is known to inhibit Rad18 recruitment and thus PCNA monoubiquitination (Ma et al., 2020); however, arsenite did not significantly alter the levels of soluble RPA (data not shown). In contrast to RPA, 5 μM arsenite significantly increased the amount of chromatin bound PCNA by 66% in UV exposed cells.

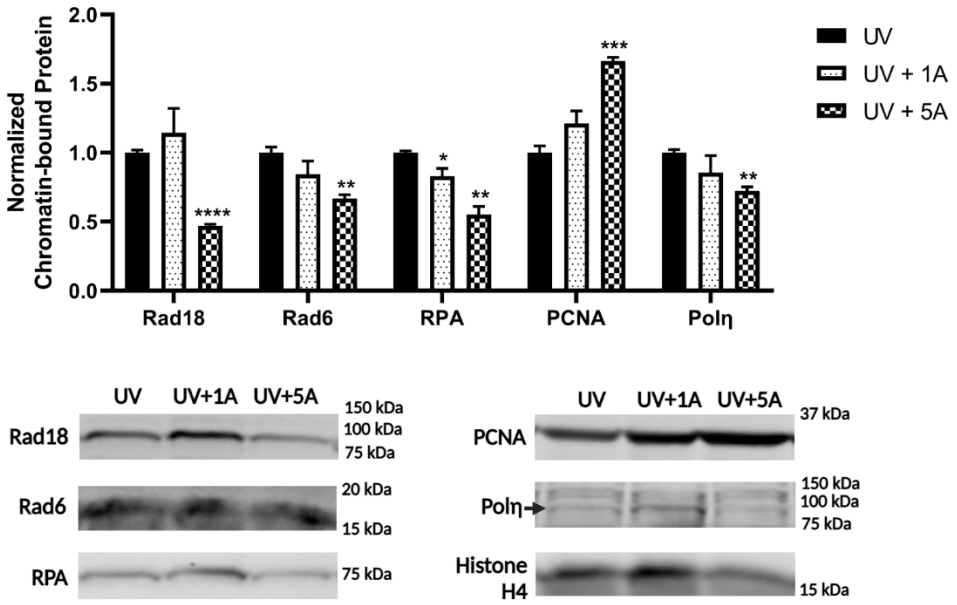

Figure 4.7: Arsenite alters TLS factor chromatin recruitment in response to UV. HEKn cells were treated without (UV) or with 1 μM (UV+1A) or 5 μM (UV+5A) arsenite for 24 h prior to exposure with 2.8 kJ/m^2 UVB. Chromatin fractionation was performed 4 h post UV exposure as described in Methods. TLS proteins in the chromatin fraction were normalized to total protein stain and UV only control. N=3. Values represent mean ± SEM. ****p<0.0001, ***p<0.001, **p<0.01, *p<0.05 compared to UV.

PCNA monoubiquitination by the Rad18-Rad6 complex enhances the recruitment of Polη to stalled replication forks (Ma et al., 2020; Vaziri et al., 2016). Arsenite treatment or Rad18 knockdown significantly decreased PCNA monoubiquitination (**Figure 3.8**). Therefore, it is expected that arsenite exposure will negatively impact the recruitment of Polη to chromatin. Indeed, arsenite treatment decreased the amount of chromatin bound Polη (**Figure 4.7**). The decreased recruitment of critical TLS factors Rad18 and Polη in response to UV was confirmed by colocalization analysis. Colocalization results demonstrated an arsenite-induced reduction in the interaction of Rad18 (**Figure 4.8A**) and Polη (**Figure 4.8B**) with PCNA in UV exposed cells.

Both the inhibition of the Rad18 RING finger domain through arsenite binding and the reduction in nuclear localization and chromatin recruitment of Rad18 could negatively impact TLS initiation, thus impeding the recruitment of Polη to stalled replication forks and increasing replication stress. These findings support a complex mechanism by which arsenite inhibits TLS initiation through Rad18. Though the zinc fingers of Rad18 are not critical in localizing Rad18 to stalled replication forks, the UBZ domain is responsible for Rad18 recruitment to DNA DSBs, such as in the event of replication fork collapse (Huang et al., 2009; Inagaki et al., 2011; Ma et al., 2020; Vaziri et al., 2016).

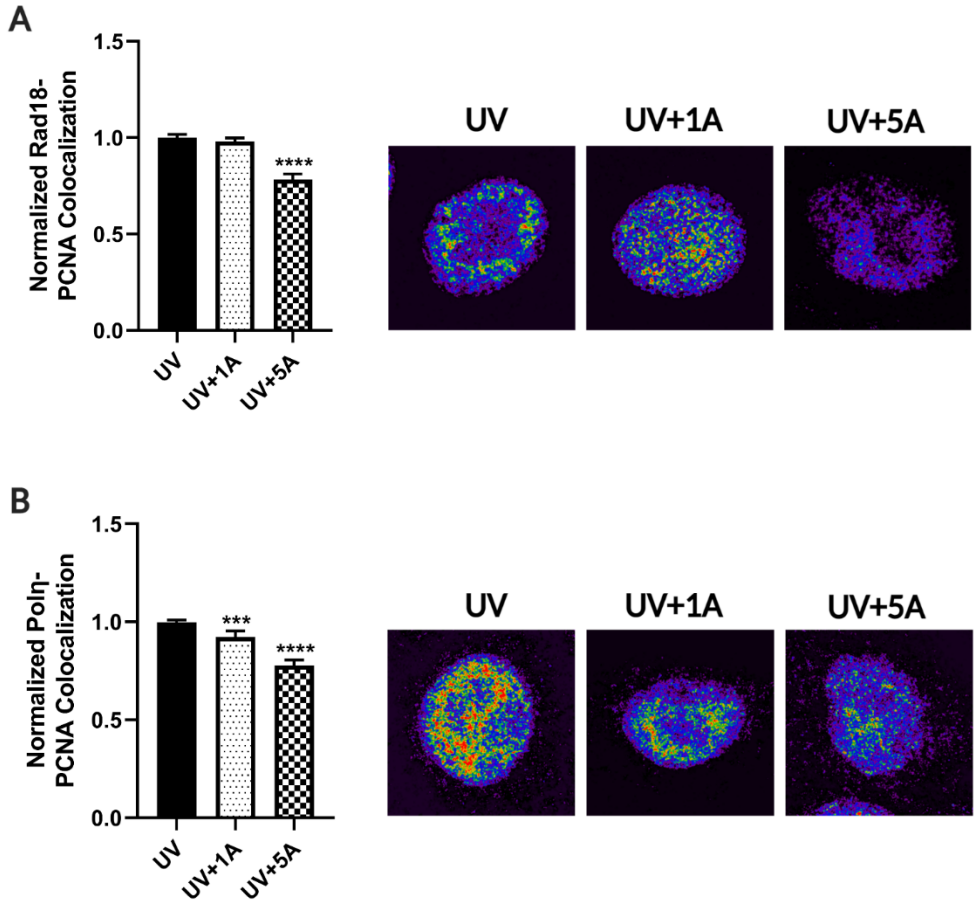

Figure 4.8: Arsenite alters TLS factor colocalization with PCNA in UV exposed cells. HEKn cells were treated without (UV) or with 1 μM (UV+1A) or 5 μM (UV+5A) arsenite for 24 h prior to exposure with 2.8 kJ/m^2 UVB. Cells were fixed 4 h post UV exposure and immunocytochemistry was performed. Pearson's correlation coefficients and colocalization maps for **(A)** Rad18 and **(B)** Polη colocalization with PCNA were obtained with Huygens Colocalization Analyzer. Results were normalized to UV only control. Cells from representative colocalization map MIPs are provided and display false coloring to represent pixel intensity from purple (lowest) < blue < green < yellow < orange < red (highest). N≥18 z-stacks (≥5 cells per z-stack). Values represent mean ± SEM. ****p<0.0001, ***p<0.001 compared to UV.

Rad18 recruitment to IR-induced DNA damage

The Rad18 UBZ domain is critical in localizing Rad18 to DNA DSBs by binding to ubiquitinated factors near the break site such as ubiquityl-histone H2A (**Figure 3.7B**). This process forms large Rad18 foci which are abolished with knockout of the Rad18 UBZ domain (Huang et al., 2009; Inagaki et al., 2011). IR-

induced Rad18 foci formation is negatively impacted by arsenite exposure in HEKn cells (**Figure 3.11**), most likely due to the binding and inhibition of the Rad18 UBZ domain (**Chapter 3**). Due to the decrease in Rad18 foci formation with arsenite, it is expected that Rad18 recruitment to IR-induced DNA damage will also be suppressed by arsenite exposure.

Histone H2AX is rapidly phosphorylated around DNA DSB sites forming distinct PH2AX foci (Mah et al., 2010). The overlap of Rad18 foci with PH2AX foci in IR exposed HEKn cells is significantly decreased with the addition of arsenite at both 2 and 6 h post IR (**Figure 4.9A**). This decrease occurred irrespective of an increase in IR-induced PH2AX foci investigated further in **Section 5.3**. Factors are also ubiquitinated in response to DNA DSBs such as histones H2A and H2AX forming distinct ubiquitin foci, which help facilitate the recruitment of Rad18. Arsenite did not alter ubiquitin foci formation in response to IR (data not shown). However, the overlap of IR-induced Rad18 foci with ubiquitin foci was significantly decreased with arsenite coexposure at 2 h post IR (**Figure 4.9B**). Altogether, results show arsenite disrupts the recruitment of Rad18 to both UV- and IR-induced DNA damage.

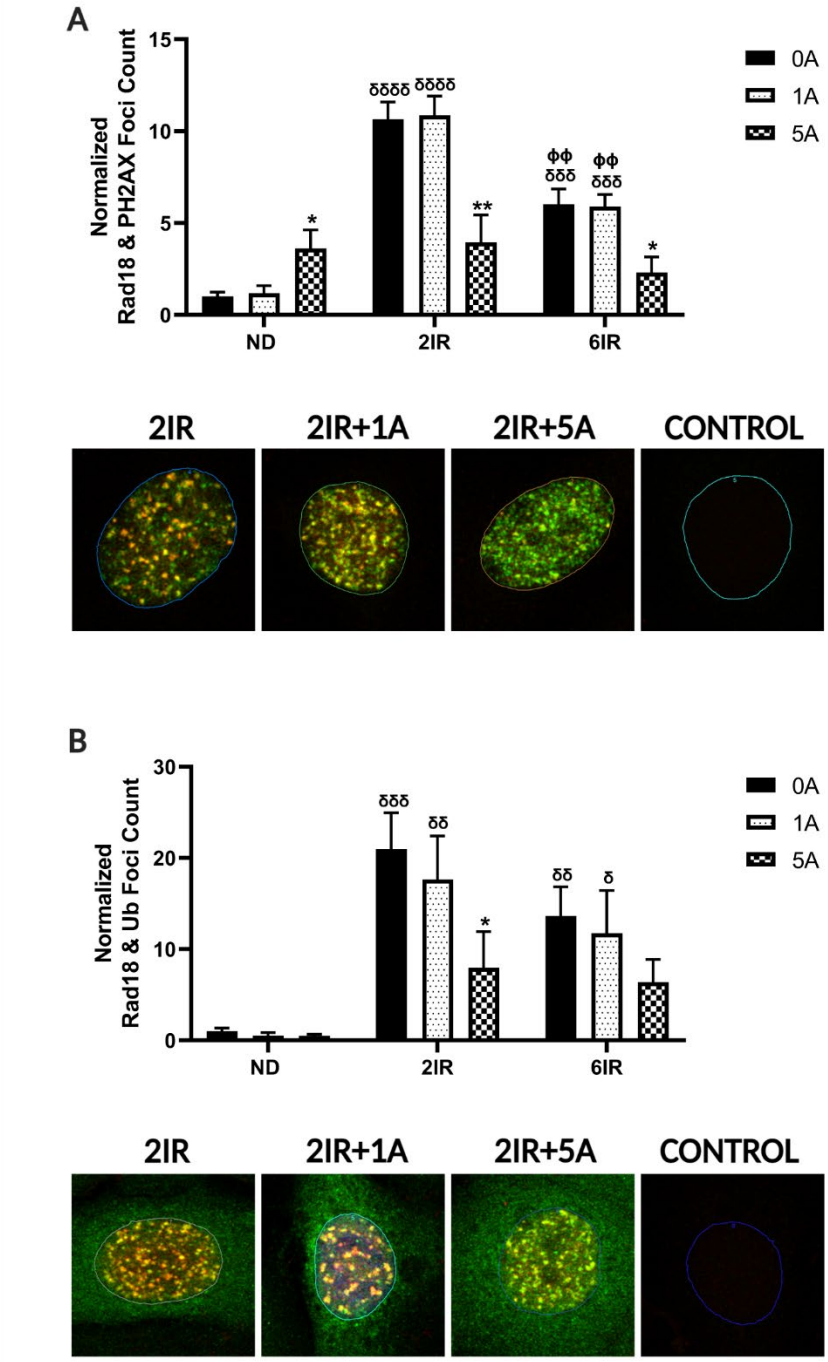
A
Normalized Rad18 & PH2AX Foci Count
15
10
5
0
δδδδ
δδδδ
**
φφ δδδ
φφ δδδ
*
*
ND
2IR
6IR
0A
1A
5A
2IR
2IR+1A
2IR+5A
CONTROL
B
Normalized Rad18 & Ub Foci Count
30
20
10
0
δδδ
δδ
*
δδ
δ
ND
2IR
6IR
0A
1A
5A
2IR
2IR+1A
2IR+5A
CONTROL

Figure 4.9: Rad18 recruitment to IR-induced DNA damage. HEKn cells were treated without (0A) or with 1 μM (1A) or 5 μM arsenite (5A) for 24 h prior to exposure without (ND) or with 5 Gy X-rays. Cells were fixed 2 h (2IR) and 6 h (6IR) post IR and immunocytochemistry was performed. MIPs were analyzed for number of **(A)** Rad18 (red) and PH2AX (green) foci overlap per nuclei normalized to NT control or **(B)** Rad18 (red) and ubiquitin (Ub; green) foci overlap per nuclei normalized to NT control with Slidebook6. Nuclei are outlined in representative images and secondary only controls (CONTROL) are included. N≥5 images (≥5 nuclei per image). **p<0.01, *p<0.05 compared to corresponding 0A control. $^{\delta\delta\delta\delta}$p<0.0001, $^{\delta\delta\delta}$p<0.001, $^{\delta\delta}$p<0.01, $^{\delta}$p<0.05 comparing 2IR and 6IR to ND for arsenite treatment matched groups. $^{\Phi\Phi}$p<0.01 comparing 6IR to 2IR for arsenite treatment matched groups. All values represent mean ± SEM.

4.4 Aim 2 Conclusions

Interestingly, arsenite had a multifaceted impact on Rad18, altering Rad18 subcellular localization and recruitment to chromatin in addition to zinc finger inhibition demonstrated in **Chapter 3**. The nuclear localization of Rad18 and other TLS factors such as Rad6 and Polη were significantly reduced with exposure to higher concentrations of arsenite (**Figure 4.3; Figure 4.5**). The nuclear translocation of Rad6 is dependent on its ability to bind to Rad18, which is partially mediated through the Rad18 RING finger and may be disrupted by arsenite exposure (**Figure 3.9**). Since Rad6 performs many essential functions in the nucleus beyond TLS, these findings may illuminate another mechanism of arsenite carcinogenicity (Roest et al., 2004). For many proteins, mislocalization from the nucleus to the cytoplasmic is a characteristic of carcinogenesis (Wang and Li, 2014).

Chromatin fractionation results show a substantial loss in chromatin bound Rad18, Rad6, RPA, and Polη with arsenite treatment in UV exposed HEKn cells (**Figure 4.7**). Furthermore, UV-induced colocalization of Rad18 and Polη with PCNA was significantly decreased by arsenite treatment (**Figure 4.8**). Since RPA coating along replication gaps encourages Rad18 recruitment to chromatin, the

arsenite-induced loss of chromatin bound RPA may have negatively influenced Rad18 recruitment. The decrease in chromatin bound RPA may be due to arsenite antagonization of the RPA zinc finger DBD. Both the loss of Rad18 RING E3 ubiquitin ligase function and chromatin recruitment may contribute to the arsenite-induced decrease in Polη recruitment to chromatin and colocalization with PCNA. These findings are even more profound considering arsenite exposure increased the amount of chromatin bound PCNA.

Altogether, from arsenite targeting of the Rad18 zinc finger domains to the decrease in TLS factor nuclear localization and chromatin recruitment, findings have supported the inhibition of TLS by arsenite. Additionally, evidence demonstrates the arenite mediated disruption of Rad18 in DSBR through altering Rad18 foci formation (**Figure 3.11**), subcellular localization (**Figure 4.6**), and recruitment to DNA damage (**Figure 4.9**) in IR exposed HEKn cells. The impact of these effects on TLS and DSBR (preliminary) are investigated further in **Chapter 5**.

CHAPTER 5

AIM 3: IMPACTS OF ARSENITE EXPOSURE AND RAD18 DEFICIENCY ON TLS & DSBR

This chapter contains a slightly modified version of "The impact of arsenic on Rad18 and translesion synthesis" by Volk LB, Cooper KL, Jiang T, Paffett ML, and Hudson LG in revision for Toxicology and Applied Pharmacology.

5.1 Arsenite and Rad18 knockdown increase UV-induced replication stress

If not resolved or bypassed, the formation of bulky adducts from UV exposure may induce replication fork stalling, replication gaps, and fork collapse. These outcomes of replication stress can be measured as a decrease in DNA synthesis, increase in ssDNA, and increase in DSBs respectively. Consequently, these events promote apoptosis or mutagenesis. Failure of TLS has been demonstrated to exacerbate replicative stress (Gaillard et al., 2015; Ma et al., 2020; Vaziri et al., 2016).

In order to test the net effect of arsenite on replication stress, HEKn cells were treated with arsenite then UV exposed and the effects on DNA replication (EdU incorporation), DNA strand breaks, and ssDNA gaps were measured. Arsenite treatment of HEKn cells led to a pronounced reduction in EdU incorporation post-UV exposure (**Figure 5.1**). In the absence of UV, 5 μM, but not 1 μM, arsenite decreased EdU incorporation (**Figure 5.2A**). Knockdown of Rad18 led to a 46% decrease in DNA synthesis post-UV (**Figure 5.1**) as has been reported previously (Tateishi et al., 2003, 2000; Yamashita et al., 2002),

and a reduction in EdU incorporation in unexposed cells (**Figure 5.2B**). The addition of arsenite to Rad18 knockdown cells did not significantly alter EdU incorporation when compared to the Scr siRNA control cells, suggesting that the arsenite effect is largely mediated through Rad18. The increase in UV-induced replication stress by arsenite may promote DNA strand breaks through the breakdown of replication forks and gaps (Gaillard et al., 2015; Ma et al., 2020; Vaziri et al., 2016).

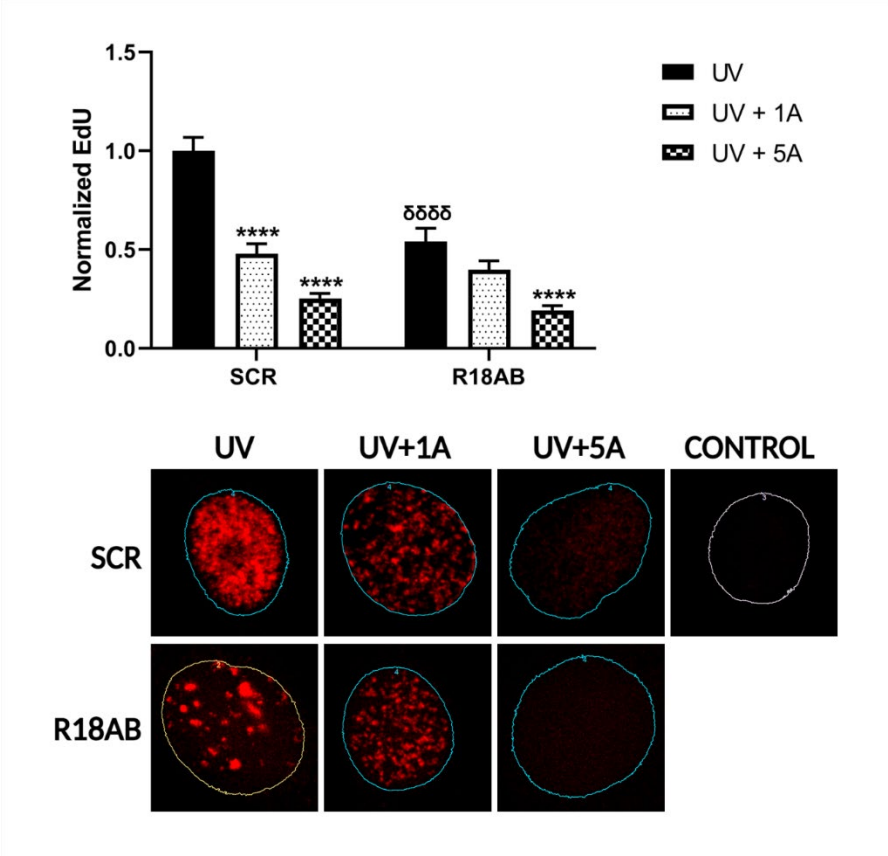

Figure 5.1: Arsenite and Rad18 knockdown increase replication stress. HEKn cells were transfected with 40 nM of universal scrambled control (SCR) or 20 nM each of R18A and R18B (R18AB). One day post transfection, cells were treated without (UV) or with 1 μM (UV+1A) or 5 μM arsenite (UV+5A) for 24 h prior to 2.8 kJ/m^2 UVB. EdU (10 μM) was added 1 h prior to UV. Cells were fixed 4 h post UV exposure and EdU detection was performed as described in Methods. MIPs were analyzed for EdU sum of intensity per nucleus normalized to SCR control. Nuclei are outlined in representative images and a secondary only control (CONTROL) is included. N≥300 nuclei. Values represent mean ± SEM. ****p<0.0001 compared to corresponding UV control. $^{\delta\delta\delta\delta}$p<0.0001 comparing SCR to R18AB for arsenite treatment matched groups.

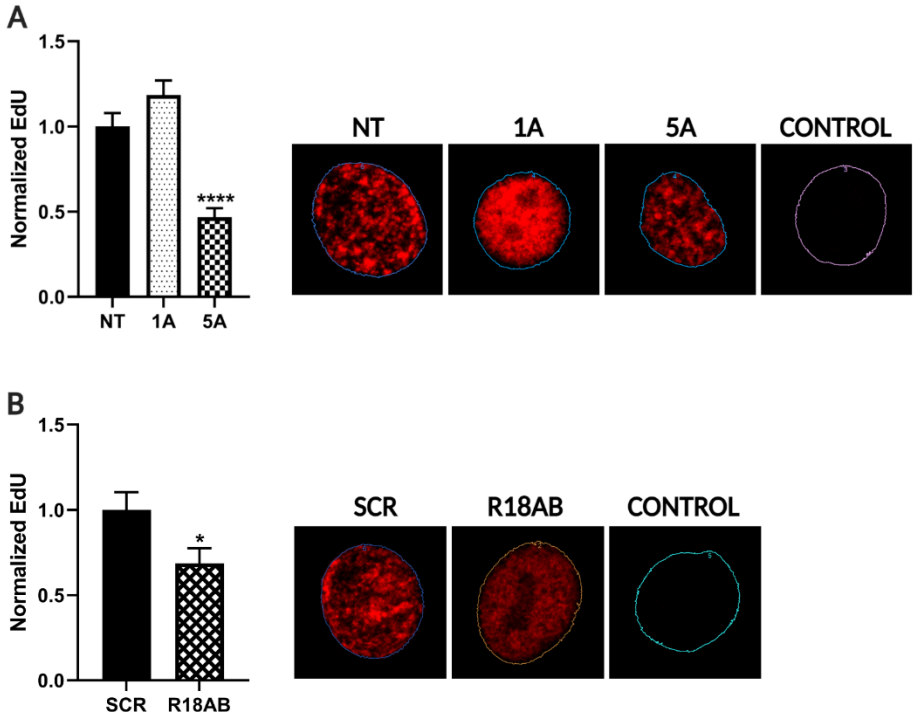

Figure 5.2: Replication stress in response to arsenite or Rad18 knockdown in the absence of UV exposure. (A) HEKn cells were treated without (NT) or with 1 μM (1A) or 5 μM arsenite (5A) for 24 h. EdU (10 μM) was added 5 h prior to fixation and EdU detection was performed. MIPs were analyzed for EdU sum of intensity per nucleus normalized to NT control with Slidebook 6. Nuclei are outlined in representative images and secondary only controls (CONTROL) are included. N≥300 nuclei. ****p<0.0001 compared to NT. **(B)** HEKn cells were transfected with 40 nM of universal scrambled control (SCR) or 20 nM of each R18A and R18B (R18AB). Two days post transfection, EdU detection was performed as in (A). MIPs were analyzed for EdU sum of intensity per nucleus normalized to SCR control. N≥184 nuclei. *p<0.05 compared to SCR. All values represent mean ± SEM.

5.2 Arsenite and Rad18 knockdown enhance the levels of UV-induced DNA strand breaks

Prolonged stalling of replication forks can lead to replication fork collapse

resulting in the formation of mutagenic DNA DSBs (Gaillard et al., 2015; Ma et al., 2020; Vaziri et al., 2016) and PH2AX serves as both a marker of replication stress and DNA strand breaks (Cleaver, 2011; Mognato et al., 2021; Sirbu et al., 2011). Arsenite treatment increased UV-induced PH2AX in a concentration dependent manner (**Figure 5.3, SCR**). Knockdown of Rad18 led to a nearly 3-fold increase in UV-induced PH2AX in the absence of arsenite indicating involvement of Rad18 in the response. Arsenite modestly increased PH2AX in Rad18 knockdown cells, possibly due to inhibition of residual Rad18 (**Figure 2.2**) or through another mechanism. These findings indicate that arsenite treatment and Rad18 knockdown each promote UV-induced replication stress.

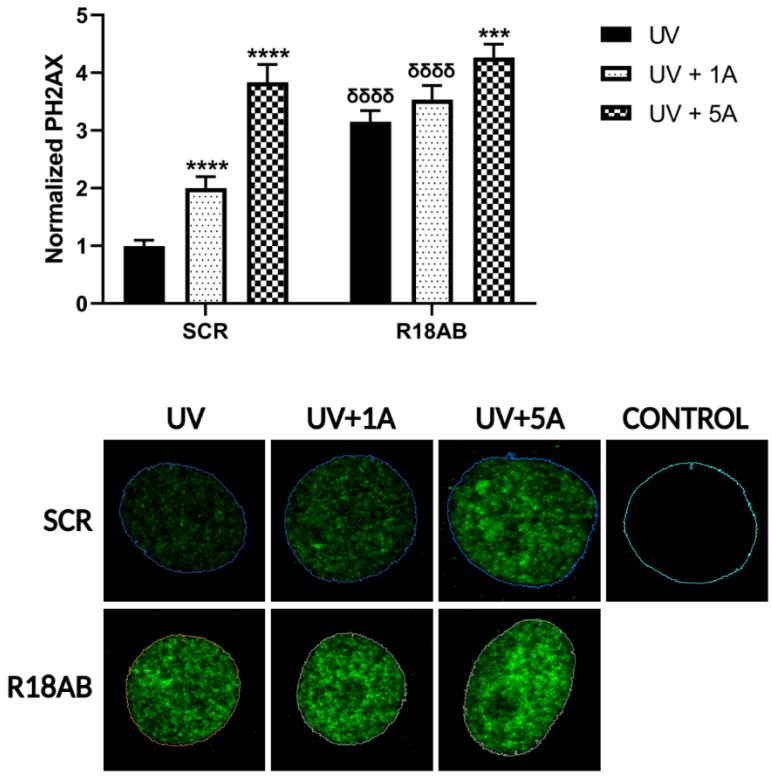

Figure 5.3: UV-induced PH2AX is increased in arsenite and/or Rad18 siRNA treated cells. HEKn cells were treated without (UV) or with 1 μM (UV+1A) or 5 μM arsenite (UV+5A) for 24 h prior to 2.8 kJ/m^2 UVB. Cells were fixed 4 h post UV exposure and immunocytochemistry was performed. MIPs were analyzed for PH2AX (Ser139) sum of intensity per nucleus normalized to SCR control. Nuclei are outlined in representative images and a secondary only control (CONTROL) is included. N≥119 nuclei. Values represent mean ± SEM. ****p<0.0001, ***p<0.0001 compared to corresponding UV control. $^{\delta\delta\delta\delta}$p<0.0001 comparing SCR to R18AB for arsenite treatment matched groups.

Neutral comet assays measure DNA DSBs, and the addition of the S1 nuclease allows for the detection of ssDNA gaps. To capture mutagenic ssDNA gaps and fork collapse events as a consequence of replication stress, UV exposed HEKn cells were tested using a neutral comet assay +/- S1 nuclease (Quinet et al., 2016). Both 1 μM and 5 μM arsenite increased DSBs in UV exposed HEKn cells (**Figure 5.4**). Importantly, the addition of S1 nuclease to arsenite treated cells further increased DSBs indicating the presence of ssDNA. The S1-induced increase in DSBs was not observed in cells untreated with arsenite (**Figure 2.5**). These findings are supportive of an arsenite-induced inhibition of TLS leading to replication stress, ssDNA gaps, and fork collapse events.

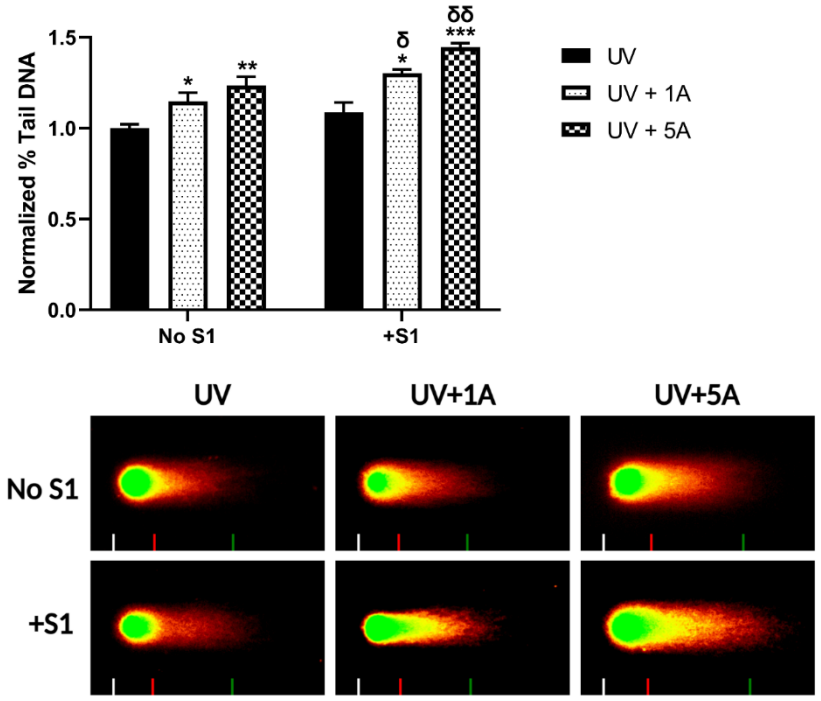

Figure 5.4: Arsenite enhances the levels of UV-induced DNA DSBs and ssDNA gaps. HEKn cells were treated without (UV) or with 1 μM (UV+1A) or 5 μM arsenite (UV+5A) for 24 h prior to 2.8 kJ/m^2 UVB. Neutral comet assay was performed 4 h post UV exposure with or without the addition of S1 nuclease as described in Methods and representative images are shown. Comets were analyzed for percent tail DNA using Trevigen Comet Analysis Software and normalized to UV only control. N≥3. Values represent mean ± SEM. ***p<0.001, **p<0.01, *p<0.05 compared to corresponding UV control. $^{\delta\delta}$p<0.01, $^{\delta}$p<0.01 comparing No S1 to +S1 for arsenite treatment matched groups.

5.3 Preliminary evidence indicating the inhibition of DSBR by arsenite

Thus far, findings strongly support the inhibition of Rad18-dependent TLS by arsenite. Since TS is dependent on Rad18 mediated PCNA monoubiquitination, it reasons that both DDT pathways involved in replication fork maintenance are inhibited by arsenite in HEKn cells (**Figure 1.7**). Consequently, the breakdown of replication forks and gaps lead to the accumulation of DNA DSBs (**Figure 5.3; Figure 5.4**) requiring DSBR for remediation (**Figure 1.7**). Several studies support the inhibition of HR by arsenite (Tam et al., 2020; Zhou et al., 2021). To evaluate

the impact of arsenite on DSBR, IR was utilized as it predominantly contributes to DNA strand breaks (Su et al., 2010). There is a retention in the number of IR-induced PH2AX foci from 2 h to 6 h post IR in HEKn cells exposed to higher concentrations of arsenite (**Figure 5.5A**). Additionally, the size of IR-induced PH2AX foci is increased with arsenite exposure, even at 2 h post IR (**Figure 5.5B**). These findings suggest the inhibition of DSBR by arsenite in HEKn cells, as has been demonstrated in other studies (Tam et al., 2020; Zhou et al., 2021). Further investigation is required to determine the contribution of Rad18 to the retention of IR-induced PH2AX foci and the use of specialized assays for examining HR more specifically.

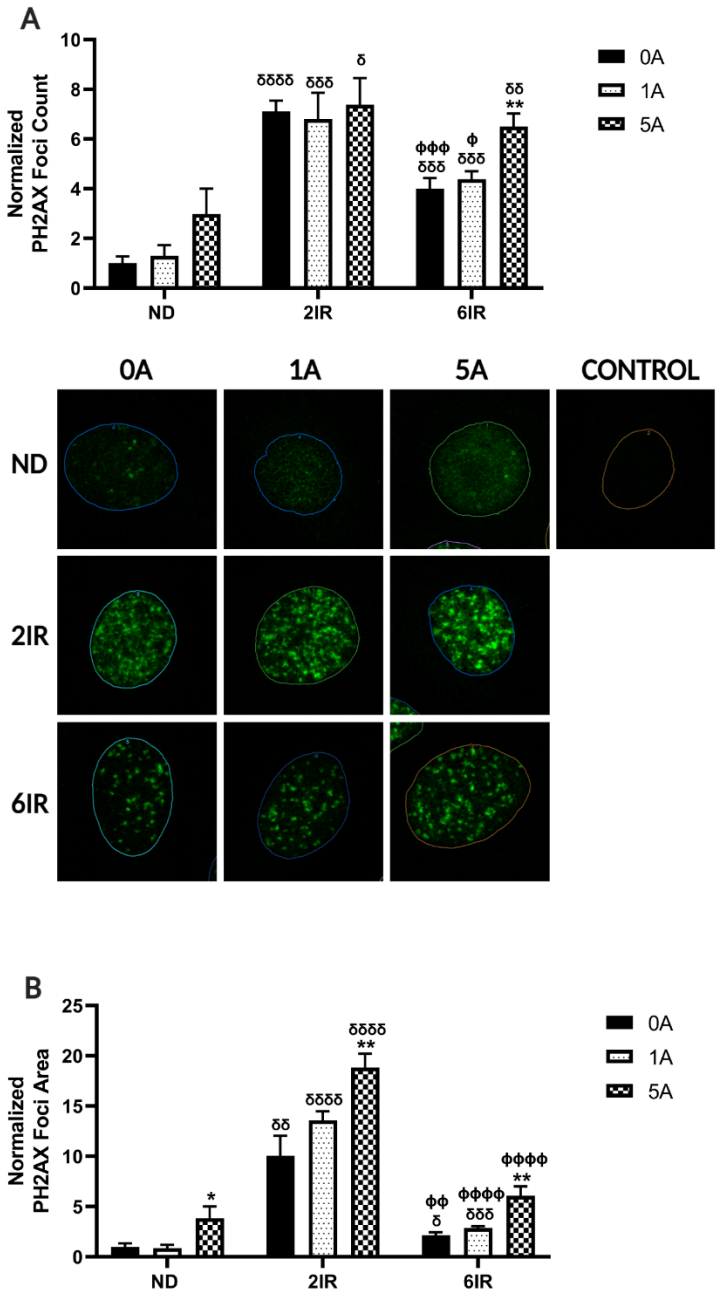

Figure 5.5: Arsenite increases IR-induced PH2AX foci. HEKn cells were treated without (0A) or with 1 μM (1A) or 5 μM arsenite (5A) for 24 h prior to exposure without (ND) or with 5 Gy X-rays. Cells were fixed 2 h (2IR) or 6 h (6IR) post IR exposure and immunocytochemistry was performed. MIPs were analyzed for PH2AX (Ser139) **(A)** foci count and **(B)** foci area per nucleus normalized to NT control with Slidebook 6. Nuclei are outlined in representative images and a secondary only control (CONTROL) is included. N≥5 images (≥5 nuclei per image). Values represent mean ± SEM. **p<0.01, *p<0.05 compared to corresponding 0A control. $^{\delta\delta\delta\delta}$p<0.0001, $^{\delta\delta\delta}$p<0.001, $^{\delta\delta}$p<0.01, $^{\delta}$p<0.05 comparing 2IR and 6IR to ND for arsenite treatment matched groups. $^{\Phi\Phi\Phi\Phi}$p<0.0001, $^{\Phi\Phi\Phi}$p<0.001, $^{\Phi\Phi}$p<0.01, $^{\Phi}$p<0.05 comparing 6IR to 2IR for arsenite treatment matched groups.

5.4 Arsenite inhibits apoptosis

Replication stress activates ATM/ATR mediated phosphorylation of p53 (phospho-p53) promoting apoptosis, which is a characteristic of TLS failure (Gaillard et al., 2015; Huang et al., 2009). Indeed, the knockdown of Rad18 in HEKn cells significantly increased UV-induced phospho-p53 (**Figure 5.6A**) and cleaved caspase-3, a marker of apoptosis (**Figure 5.6B**). Interestingly, 5 μM arsenite suppressed the UV-induced phosphorylation of p53 in Rad18 deficient cells (**Figure 5.6A**), as well as decreased cleaved caspase-3 in UV exposed HEKn cells (**Figure 5.6C**). These findings support previous studies demonstrating the ability of environmentally relevant levels of arsenite to inhibit apoptosis, such as through the inhibition of PARP-1 or p53 (Chen et al., 2005; Qin et al., 2012; Sun et al., 2011; Wu et al., 2005; Zhou et al., 2017). The inhibition of apoptosis by arsenite could further perpetuate genomic instability in cells defective in DDT and repair.

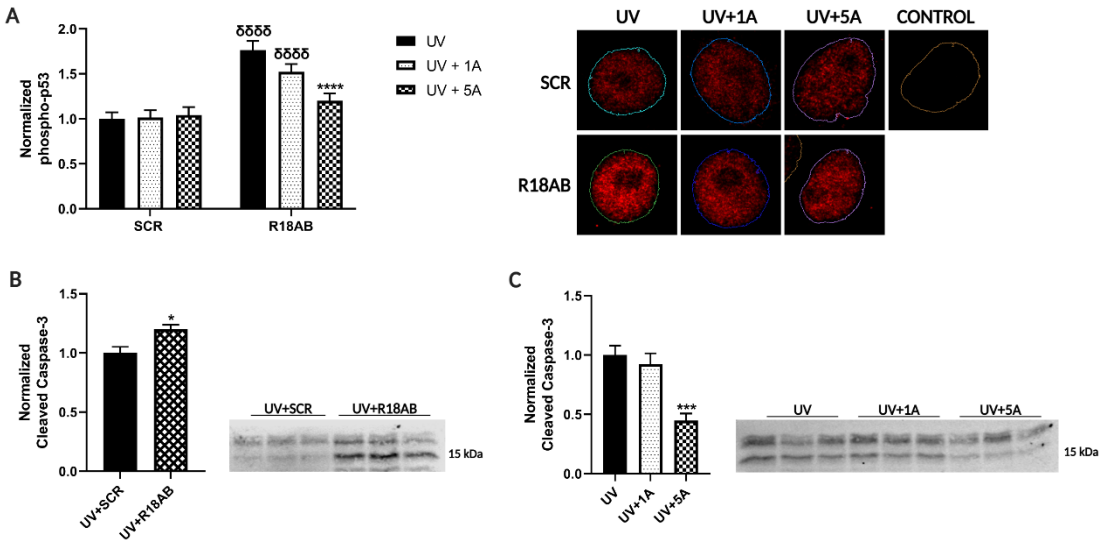

Figure 5.6: Arsenite suppresses UV-induced apoptosis. (A) HEKn cells were transfected with 40 nM of universal scrambled control (SCR) or 20 nM of each R18A and R18B (R18AB). One day post transfection, cells were treated without (UV) or with 1 μM (UV+1A) or 5 μM arsenite (UV+5A) for 24 h prior to 2.8 kJ/m^2 UVB. Cells were fixed 4 h post UV exposure and immunocytochemistry was performed. MIPs were analyzed for phospho-p53 (Ser15) sum of intensity per nucleus normalized to SCR control. Nuclei are outlined in representative images and a secondary only control (CONTROL) is included. N≥119 nuclei. ****p<0.0001 compared to corresponding UV control. $^{\delta\delta\delta\delta}$p<0.0001 comparing SCR to R18AB for arsenite treatment matched groups. **(B)** HEKn cells were treated without (UV) or with 1 μM (UV+1A) or 5 μM arsenite (UV+5A) for 24 h prior to 2.8 kJ/m^2 UVB. Whole cell lysates were collected 4 h post UV exposure and analyzed via western blot. Cleaved caspase-3 was normalized to total protein stain and UV only. N=6. ***p<0.001 compared to UV. **(C)** Cells were transfected with 40 nM SCR (SCR) or 20 nM each of R18A and R18B (R18AB), then exposed to 2.8 kJ/m^2 UVB 2 days later. Whole cell lysates were collected 4 h post UV exposure and analyzed via western blot. Cleaved caspase-3 was normalized to total protein stain and UV+SCR control. N=3. *p<0.05 compared to UV+SCR. All values represent mean ± SEM.

5.5 Aim 3 Conclusions

Rad18 knockdown studies utilized in aim 3 reveal a mechanism by which arsenite induces replication stress through Rad18 in HEKn cells. Both arsenite and Rad18 knockdown reduced post-UV EdU incorporation to a similar degree (**Figure 5.1**), signifying replication fork stalling. Levels of UV-induced PH2AX were elevated in HEKn cells treated with arsenite and/or Rad18 siRNA compared to control (**Figure 5.3**), which further supports replication stress and the potential presence of DNA strand breaks. Comet assay analysis confirmed not only the presence of arsenite-induced DNA DSBs, but also ssDNA gaps in UV exposed HEKn cells (**Figure 5.4**). These potentially mutagenic outcomes support a role for Rad18 and TLS in the cocarcinogenicity of arsenite.

Failure of TLS to bypass DNA lesions during replication can lead to the breakdown of replication forks and gaps inducing the formation of DNA DSBs. These lesions are highly mutagenic and require repair from DSBR mechanisms such as HR and NHEJ (**Figure 1.7**) (Gaillard et al., 2015; Ma et al., 2020; Vaziri et al., 2016). Results suggest arsenite inhibits DSBR due to the increased

retention and size of IR-induced PH2AX foci in arsenite treated HEKn cells (**Figure 5.5**). Further analysis is necessary to determine the contribution of Rad18 and HR to these findings. Aberrant repair of DNA DSBs can lead to the formation of insertions/deletions and chromosomal rearrangements, which are known to be elevated in arsenite treated or Rad18 deficient cells (Despras et al., 2016; Lou et al., 2021; Ma et al., 2020; Saberi et al., 2007; Sasatani et al., 2015; Smith et al., 2004; Zhou et al., 2021, 2021).

Prolonged replication stress and persistent DNA DSBs can trigger apoptosis to prevent mutagenesis (Gaillard et al., 2015). Indeed, knockdown of Rad18 significantly increased UV-induced DNA damage response signaling (**Figure 5.6A**) and levels of cleaved-caspase-3 (**Figure 5.6B**). These findings are consistent with studies showing a decrease in survival with UV in cells deficient in Rad18 or with RING finger mutations (Huang et al., 2009; Saberi et al., 2007; Tateishi et al., 2000; Tian et al., 2013; Watanabe et al., 2004; Yamashita et al., 2002). In contrast, arsenite suppressed DNA damage response signaling and apoptosis (**Figure 5.6**), as has been demonstrated in keratinocytes (Chen et al., 2005; Qin et al., 2012; Sun et al., 2011; Wu et al., 2005; Zhou et al., 2017). The inhibition of apoptosis by arsenite can have grave consequences on the maintenance of genome integrity by allowing the propagation of damaged cells.

CHAPTER 6

DISCUSSION

This chapter contains a slightly modified version of "The impact of arsenic on Rad18 and translesion synthesis" by Volk LB, Cooper KL, Jiang T, Paffett ML, and Hudson LG in revision for Toxicology and Applied Pharmacology.

Elucidating the role of Rad18 and TLS in the mechanism of action of arsenite

This dissertation provides evidence for Rad18 as an arsenic target and for arsenic disruption of Rad18 functions in TLS. A consequence of arsenic inhibition of NER and BER pathways is the retention of UV-induced DNA damage (**Figure 6.1A**) (Holcomb et al., 2017; Muenyi et al., 2015; Tam et al., 2020; Zhou et al., 2021). Unrepaired damage increases replication stress and the burden on DDT pathways including TLS (**Figure 6.1B**). Rad18 regulates TLS initiation and either the under- or over-activation of TLS have deleterious consequences on genomic integrity (Ma et al., 2020; Vaziri et al., 2016). We find that arsenite binds to both zinc finger domains of Rad18 (**Figure 6.1C**) and inhibits RING-dependent PCNA monoubiquitination (**Figure 6.1D**) and Rad6 binding (**Figure 6.1E**), as well as UBZ-dependent Rad18 monoubiquitination (**Figure 6.1F**) and foci formation (**Figure 6.1G**). The arsenite-induced disruption in Rad18 RING finger activity may contribute to the observed decrease in Polη recruitment to chromatin (**Figure 6.1H**), which support an underactivation of TLS leading to replication stress. Indeed, arsenite reduced post-UV DNA replication and increased post-UV

strand breaks as detected by PH2AX and comet assay analysis (**Figure 6.1I**). Not only does arsenite impair a major mechanism to bypass UV-induced DNA damage and prevent replication stress and mutagenic fork collapse, but evidence suggests arsenite inhibits apoptosis in HEKn cells (**Figure 6.1J**), thus further supporting genomic instability and the potential for carcinogenesis.

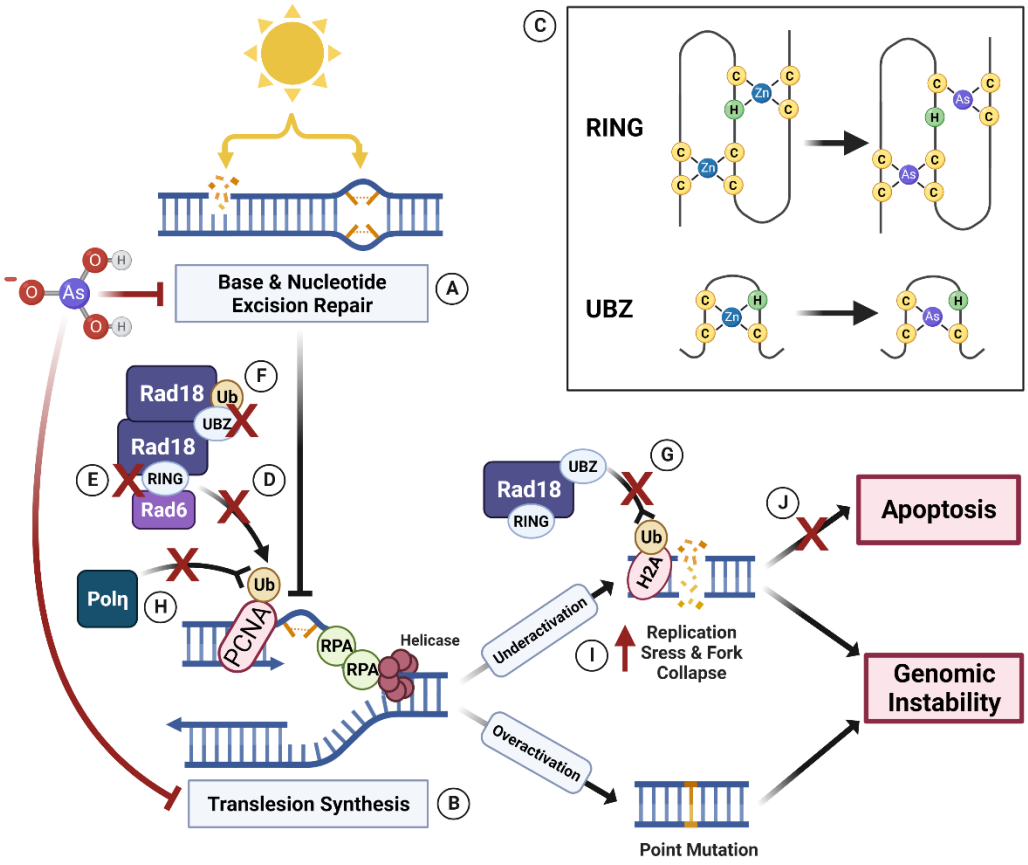

Figure 6.1: Schematic summarizing the impact of arsenic on Rad18 and TLS. (A) Arsenic inhibition of BER and NER pathways increase the retention of UV-induced DNA damage and consequently, **(B)** increases the burden on TLS. **(C)** MS analysis revealed the Rad18 RING finger and UBZ domains as targets of arsenite. Disruption of the Rad18 RING domain may lead to the observed arsenite-induced decrease in **(D)** PCNA monoubiquitination and **(E)** Rad6 binding, whereas disruption of the UBZ domain may contribute to the arsenite-induced decrease in **(F)** Rad18 monoubiquitination and **(G)** foci formation. **(H)** Arsenite exposure decreased UV-induced chromatin recruitment and PCNA colocalization of Rad18 and Polη, further disrupting TLS. **(I)** Rad18 knockdown and arsenite treatment led to a significant decrease in DNA replication and increase in PH2AX post UV, signifying replication stress and potential fork collapse events. Neutral comet assay analysis with S1 nuclease confirmed arsenite-induced ssDNA and DNA DSBs in UV exposed HEKn cells. **(J)** The inhibition of apoptosis by arsenite may further promote genomic instability in HEKn cells. Altogether, these data support the inhibition of Rad18 mediated TLS by arsenite.

Significance of Rad18 zinc finger inhibition by arsenite

Rad18 RING finger

Arsenic binds to peptides representing both the RING and UBZ (UBZ4-type) domains of Rad18 (**Figure 3.3**) and arsenic exposure promoted zinc loss from endogenous Rad18 (**Figure 3.2**). The Rad18 RING finger domain is better characterized than the UBZ domain. A C28F mutation in the RING finger demonstrates that this zinc binding motif is responsible for the UV-induced monoubiquitination of PCNA (Huang et al., 2009; Miyase et al., 2005) and the prevention of UV-induced replication stress (Tateishi et al., 2000) and cell death (Huang et al., 2009; Tateishi et al., 2000). Rad18-dependent PCNA monoubiquitination enhances the recruitment and retention of TLS polymerases including Polη to stalled replication forks and gaps, though evidence suggests this mechanism may differ amongst cell types (Bi et al., 2021; Hendel et al., 2011; Kannouche et al., 2004; Ma et al., 2020; Vaziri et al., 2016; Watanabe et al., 2004).

The effects of Rad18 ablation in previous studies were similar to arsenite treatment in HEKn cells with a significant reduction in UV-induced PCNA

monoubiquitination (**Figure 3.8**) (Huang et al., 2009; Watanabe et al., 2004), Polη recruitment (**Figure 4.7; Figure 4.8B**) (Barkley et al., 2012; Tsuji et al., 2008; Watanabe et al., 2004), and DNA replication post-UV (**Figure 5.1**) (Tateishi et al., 2003; Yamashita et al., 2002). Furthermore, both arsenite and Rad18 knockdown or knockout have been shown to elevate DNA damage-induced strand breaks (**Figure 5.3; Figure 5.4; Figure 5.5**) (Shiomi et al., 2007; Zhou et al., 2021), rate of sister chromatid exchange (Tateishi et al., 2003; Yamashita et al., 2002; Zhou et al., 2021), chromosomal aberrations (Despras et al., 2016; Saberi et al., 2007; Smith et al., 2004; Zhou et al., 2021), micronuclei formation (Sasatani et al., 2015; Zhou et al., 2021), and genomic deletions (Lou et al., 2021; Zhou et al., 2021).

The Rad18 C28F RING mutant decreases Rad6 binding (Inagaki et al., 2011), an interaction necessary for TLS initiation. Colocalization analysis of HEKn cells revealed a dose dependent decrease in the interaction of Rad18 with Rad6B, suggesting disturbance of the Rad18 RING finger binding activity (**Figure 3.9**) (Huang et al., 2009; Inagaki et al., 2011; Miyase et al., 2005). The C28F RING mutant also inhibits the DNA damage-induced recruitment of proteins involved in HR and Fanconi anemia pathway (Huang et al., 2009; Inagaki et al., 2011; Kobayashi et al., 2015; Song et al., 2010; Vaziri et al., 2016; Williams et al., 2011), as has been reported for arsenite exposure (Jiang et al., 2017; Muenyi et al., 2015; Tam et al., 2020; Zhou et al., 2021). Future studies evaluating the DNA damage induced foci formation of factors such as RAD51, RAD51C, Rad9, and FANCD2 in cells treated with or without arsenite or Rad18 siRNA may reveal

further the role of Rad18 in these pathways and the mechanism of action of arsenite.

Rad18 UBZ domain

In contrast to the Rad18 RING finger, the UBZ domain plays a minor role in TLS by sequestering Rad18 through the monoubiquitination and homodimerization of Rad18 (**Figure 3.7A; Figure 3.10A**) (Inagaki et al., 2011; Miyase et al., 2005; Zeman et al., 2014), and higher concentrations of arsenite significantly reduced Rad18 monoubiquitination (**Figure 3.10B**). Rad18 is also implicated in DSBR (**Figure 3.7B**) and higher concentrations of arsenite disrupted the UBZ-dependent recruitment of Rad18 to IR-induced DNA strand breaks (**Figure 3.11**) (Huang et al., 2009; Inagaki et al., 2011). Arsenic bound to the UBZ peptide in the absence, but not the presence, of zinc (**Figure 3.4B-C**) indicating effective zinc competition for arsenic at the UBZ domain peptide. Arsenite binding to the Rad18 UBZ domain may have broader implications given other UBZ4-type proteins are important in the maintenance of genome integrity, including TLS polymerase kappa (Ma et al., 2020; Vilas et al., 2018). Polymerase kappa bypasses BaP generated DNA adducts with high accuracy and efficiency and arsenite is known to enhance BaP-induced DNA damage (**Section 1.5**) (Ma et al., 2020; Zhou et al., 2021)

Rad18 zinc finger comparison

As opposed to the UBZ peptide, arsenite binding to the RING peptide was

evident with zinc coincubation (**Figure 3.4A**). These findings indicate a higher affinity of arsenite for the RING finger compared to the UBZ domain. The concentration dependence for arsenite-induced inhibition of PCNA monoubiquitination (**Figure 3.8B**) and Rad18-Rad6B colocalization (**Figure 3.9**) versus Rad18 monoubiquitination (**Figure 3.10B**) and foci formation (**Figure 3.11**) supports a greater effect of arsenite on the Rad18 RING finger in comparison to the UBZ domain. Results from a kinetics study assessing arsenite binding to the zinc finger peptides of PARP-1 and XPA proposed that three-dimensional structure plays an important role in affinity of arsenite for zinc finger motifs (Huestis et al., 2016). It is possible that the interdigitated structure of the RING finger makes it more conducive to arsenite binding and disruption. In contrast to arsenite, the chelation of zinc by TPEN is non-specific and displayed a negative impact on Rad18 zinc finger activity (**Figure 3.8B; Figure 3.9; Figure 3.10C; Figure 3.11**) further supporting zinc displacement as the mechanism by which arsenite inhibits the activities of Rad18.

Evaluating the impact of Rad18 regulation by arsenite

Localization

Previous studies on arsenite binding often do not consider other mechanisms of inhibition when evaluating the impact of arsenic on a particular protein. In addition to activity, arsenite is known to alter protein expression, post-translational modifications, localization, and recruitment to DNA damage (Muenyi et al., 2015; Tam et al., 2020; Zhou et al., 2021). Indeed, arsenite decreased the

nuclear localization of Rad18 with or without the addition of a DNA damaging agent (**Figure 4.3; Figure 4.6**). This finding along with the decrease in nuclear localization of several other TLS factors (**Figure 4.5**) highlights an interesting avenue for further research. For example, importin 90 involved in nuclear transport has been identified as a target of arsenic binding and may underly the arsenite-induced reduction in protein localization to the nucleus (Zhang et al., 2007).

Recruitment

Chromatin fractionation results revealed a reduction in chromatin bound TLS proteins Rad18, Rad6, RPA, and Polη with arsenite treatment in UV exposed HEKn cells (**Figure 4.7**), as well as a decrease in the UV-induced colocalization of Rad18 (**Figure 4.8A**) and Polη (**Figure 4.8B**) with PCNA. The disruption in RPA chromatin binding may have influenced the recruitment of Rad18 and Rad6 (Ma et al., 2020; Vaziri et al., 2016). Altogether, the inhibition of Rad18 RING function (**Chapter 3**), as well as the reduction in Rad18 nuclear localization and recruitment to DNA damage (**Chapter 4**) may contribute to the arsenite-induced decrease in Polη chromatin binding and colocalization with PCNA.

As Rad18 is also implicated in DSBR, the localization of Rad18 to IR-induced PH2AX and ubiquitin foci was also assessed. Due to the evidence supporting the inhibition of the Rad18 ubiquitin-binding UBZ domain (**Figure 3.3; Figure 3.10; Figure 3.11**), it was expected that IR-induced Rad18 recruitment would be suppressed by arsenite. Indeed, arsenite significantly decreased the overlap of

Rad18 with both PH2AX and ubiquitin. Therefore, despite the presence of UV or IR, arsenite regulates the localization and recruitment of Rad18 to DNA damage, potentially hindering the activities of Rad18 in TLS and DSBR.

The influence of arsenite and Rad18 deficiency on genome integrity

UV-induced replication stress was confirmed in arsenite treated cells, measured as a reduction in post-UV DNA replication (**Figure 5.1**), and increase in ssDNA and DNA strand breaks (**Figure 5.3; Figure 5.4**). Similarities between the findings from arsenite and Rad18 siRNA treated cells suggests arsenite mediates its effects through Rad18. Interestingly, both 5 μM arsenite and Rad18 knockdown in HEKn cells had an impact on the normal replication of HEKn cells (**Figure 5.2**). This may be due to recent findings linking PCNA monoubiquitination to DNA replication origin activation or as a consequence of replication stress (Gaillard et al., 2015; Leung et al., 2022).

The two dominant DDT pathways are the more error prone TLS and template switching which is considered error free; both are dependent on Rad18 mediated PCNA monoubiquitination (**Figure 1.7**) (Gaillard et al., 2015; Ma et al., 2020; Vaziri et al., 2016). Therefore, it reasons that arsenite impinges on both DDT pathways involved in replication fork maintenance. Consequently, stalled replication forks and gaps can collapse forming mutagenic DNA DSBs. These lesions require DSBR for remediation, which preliminary evidence indicates is inhibited with exposure to higher concentrations of arsenite (**Figure 5.5**). Previous studies have shown that arsenite exposure or Rad18 deficiency inhibit

HR, promoting the more error prone NHEJ (Huang et al., 2009; Inagaki et al., 2011; Kobayashi et al., 2015; Saberi et al., 2007; Szüts et al., 2006; Tam et al., 2020; Zhou et al., 2021). Further investigation is needed to elucidate the role of Rad18 and HR to the retention of DNA strand breaks by arsenite.

With severe replication stress and retention of DNA DSBs, cells trigger apoptosis to avoid propagation of DNA damage (Gaillard et al., 2015). The loss of Rad18 is associated with enhanced UV-induced apoptosis (Saberi et al., 2007; Tanoue et al., 2018; Tateishi et al., 2003; Tian et al., 2013; Watanabe et al., 2004; Yamashita et al., 2002) yet arsenic suppressed this response (**Figure 5.6**), supporting previous studies demonstrating the arsenite-induced inhibition of apoptosis in keratinocytes (Chen et al., 2005; Qin et al., 2012; Sun et al., 2011; Wu et al., 2005; Zhou et al., 2017). Arsenite inhibition of apoptosis may promote carcinogenesis by allowing the survival of DNA damaged cells defective in TLS.

Assessing arsenic mutagenesis through Rad18

TLS is associated with different mutagenic pathways, such as when the equilibrium of TLS polymerases is disrupted or Rad18 is overexpressed (Ma et al., 2020; Vaziri et al., 2016). However, there are limited studies on the consequences of Rad18 knockout in UV-induced skin carcinogenesis. Because Rad18 null mice have compensatory signaling by DNA damage response factor checkpoint kinase 2 (Chk2), studies were conducted in Rad18-/-, Chk2-/- and double knockout mice (Tanoue et al., 2018). The number of mice with well-differentiated squamous cell carcinoma after chronic UV exposure was similar in

wild-type (6/20), Rad18-/- (6/19), and Chk2-/- (7/19) mice with significantly more mice bearing tumors in the double knockout (14/20) and a trend toward earlier tumor development in Rad18-/- Chk2-/- mice compared to Chk2-/- mice.

A more detailed *in vivo* analysis reported that Rad18 determines levels of single nucleotide variations (SNVs) versus insertion/deletion (INDEL) mutations during 7,12- dimethylbenz[a]anthracene (DMBA)-induced skin carcinogenesis (Lou et al., 2021). Skin tumor genomes from Rad18+/+ mice revealed that these tumors display mutational signatures with high levels of A(T)>T(A) SNVs. Rad18 expression was also strongly associated with high SNV burdens in human tumor data from The Cancer Genome Atlas. In contrast, tumors from Rad18-/- mice had a mutation pattern characterized by increased numbers of deletions >4 bp and an increased contribution of COSMIC signature 3 also associated with BRCA-mutant tumors (Lou et al., 2021). A study of DMBA-induced hematological malignancies reported that the number of mice with B Cell Lymphoma was significantly higher in the Rad18-/- group (11/23) compared to the Rad18+/+ group (1/20) (Yang et al., 2016). These studies are consistent with other evidence that alterations in the balance of TLS leads to differences in genomic outcomes (**Figure 6.1B**).

With respect to genomic integrity, studies have demonstrated similarities in the consequences of arsenic exposure and Rad18 deficiency, including enhanced DNA damage-induced strand breaks, sister-chromatid exchange, chromosomal aberrations, micronuclei formation, and genomic deletions (**Figure 5.3; Figure 5.4; Figure 5.5**) (Despras et al., 2016; Lou et al., 2021; Muenyi et al.,

2015; Saberi et al., 2007; Sasatani et al., 2015; Shiomi et al., 2007; Smith et al., 2004; Tam et al., 2020; Tanoue et al., 2018; Tateishi et al., 2003; Yamashita et al., 2002; Yang et al., 2016; Zhou et al., 2021, 2021). Unresolved replication stress and fork collapse can contribute these events through aberrant DSBR leading to INDELS and chromosomal rearrangements. Indeed, recent findings have specifically identified arsenite-induced INDELS in UV exposed keratinocytes (unpublished data), which may be a major driver of arsenic cocarcinogenesis.

Findings demonstrate an impact of arsenic on Rad18 and TLS, but the outcomes of arsenic treatment on skin carcinogenesis are expected to differ from those obtained by Rad18 knockout alone. It is possible that Rad18 may still interact with other factors and facilitate functions independent of its zinc finger domains with arsenic exposure. Though perturbed by arsenic, the recruitment of inhibited Rad18 to stalled replication forks and gaps may block the actions of compensatory E3 ubiquitin ligases, such as RNF8 (ring finger protein 8), CRL4Cdt2 (Cullin4-RING ligase (CRL4)-Ddb1-Cdt2), and HLTF (Helicase Like Transcription Factor) (Ma et al., 2020; Tanoue et al., 2018). These E3 ligases also contain RING domains which may be vulnerable to inhibition by arsenic. The reduction in the activity of these redundant mechanisms may shunt cells to more error prone pathways, particularly in the context of UV-induced CPDs where TLS is the predominant tolerance pathway and remarkably accurate (Cohen et al., 2015; Ma et al., 2020).

Future studies to define the effects of arsenic on UV-induced tumor mutational spectrum should shed light on the broader impact of arsenite-induced TLS inhibition. For example, the contribution of Rad18 to arsenic mutagenesis can be determined by treating Rad18+/+ and Rad18-/- mice with arsenite through drinking water, then exposing to solar simulated UV as performed in Cooper and Volk et. al., 2022. Assessing skin tumor burden will reveal the role of Rad18 in UV-induced tumorigenesis by arsenite. Results from this study suggest Rad18 knockout will elevate the number of mice with UV-induced skin tumors and decrease any observed arsenite-induced effects due to the loss of Rad18 in the mechanism of action of arsenite. Whole exome sequencing of lesional and nonlesional skin tissue from the various mouse treatment groups can reveal differences in mutational signatures and illuminate which DNA repair and tolerance pathways may contribute to the cocarcinogenicity of arsenic with UV (Lou et al., 2021). It is important to note that results from this dissertation indicate cell type is an important factor in the alteration of TLS by arsenite (**Figure 3.12**). Therefore, it is necessary to assess if normal mouse keratinocytes display a similar response to arsenite as seen with normal human keratinocytes before experimentation.

Conclusions

In conclusion, results from this study support the novel finding that arsenite exposure in keratinocytes suppresses Rad18 function in TLS, and preliminary evidence supporting the inhibition of Rad18 mediated DSBR. Rad18 is highly

conserved in eukaryotes emphasizing the importance of this protein, and its regulation is critical in preventing TLS imbalance and associated loss of genomic integrity (Gaillard et al., 2015; Ma et al., 2020; Vaziri et al., 2016). Arsenite tips the balance by binding and inhibiting the Rad18 RING finger, which may underly the arsenite-induced reduction in PCNA monoubiquitination, Polη recruitment, post-UV replication, and increase in ssDNA and DNA strand breaks in UV exposed keratinocytes. Overall, results from this study exemplify the complexity of arsenite on DNA damage repair and tolerance and reveal for the first time a potential role of TLS in the cocarcinogenicity of arsenic.

APPENDIX A

CONTRIBUTION OF NADPH OXIDASE TO THE RETENTION OF UVR-INDUCED DNA DAMAGE BY ARSENIC

Karen L. Cooper[a,1], Lindsay B, Volk[a,1], Dayna R. Dominguez[a], Antonia D. Duran[a,b], Ke Jian Liu[a], K.J. and Laurie G. Hudson[a,*]

[a]Department of Pharmaceutical Sciences, College of Pharmacy, University of New Mexico, 1 University of New Mexico, Albuquerque, NM 87131

[b]Current address: Department of Chemistry and Biochemistry, Ohio State University, Columbus, OH 43210

*Corresponding author: MSC09 5360, 1 University of New Mexico Health Sciences Center, Albuquerque, NM 87131, USA; telephone: 505-272-2484; fax: 505-272-0704; e-mail: lhudson@salud.unm.edu

[1]authors contributed equally to the work and are listed alphabetically

Toxicol Appl Pharmacol. 2022 Jan 1;434:115799. doi: 10.1016/j.taap.2021.115799. Epub 2021 Nov 16. PMID: 34798142.

Keywords

Arsenic, oxidative stress, NADPH oxidase, PARP, DNA repair, co-carcinogenesis

Abbreviations

8OHdG, 8-hydroxy-2'-deoxyguanosine; As(III), arsenite; Apo, apocynin; DAB, diaminobenzidine; DAPI, 4’,6-diamino-2-phenylindole; DBD, DNA binding domain; DCFDA, carboxy- 2',7'-dichlorodihydrofluorescein diacetate; HEKn, normal human neonatal epidermal keratinocytes; MED, minimum erythema dose; MnTMPyP, Manganese(III)tetrakis(1-methyl-4-pyridyl)porphyrin; NADPH, reduced nicotinamide adenine dinucleotide phosphate; NOX, NADPH oxidase; PARP, Poly(ADP-ribose) polymerase; PBS, phosphate buffered saline; PH2AX, phospho-histone H2A.X; ROS, reactive oxygen species; Scr, scrambled; siRNA, small interfering RNA; TBHP, tert-butyl hydrogen peroxide; UVR, ultraviolet radiation

ABSTRACT

Arsenic is a naturally occurring element present in food, soil and water and human exposure is associated with increased cancer risk. Arsenic inhibits DNA repair at low, non-cytotoxic concentrations and amplifies the mutagenic and carcinogenic impact of other DNA-damaging agents, such as ultraviolet radiation (UVR). Arsenic exposure leads to oxidation of zinc coordinating cysteine residues, zinc loss and decreased activity of the DNA repair protein poly(ADP)ribose polymerase (PARP)-1. Because arsenic stimulates NADPH oxidase (NOX) activity leading to generation of reactive oxygen species (ROS), the goal of this study was to investigate the role of NOX in arsenic-induced inhibition of PARP activity and retention of DNA damage. NOX involvement in the arsenic response was assessed *in vitro* and *in vivo*. Keratinocytes were treated

with or without arsenite, solar-simulated UVR, NOX inhibitors and/or isoform specific NOX siRNA. Knockdown or inhibition of NOX decreased arsenite-induced ROS, PARP-1 oxidation and DNA damage retention, while restoring arsenite inhibition of PARP-1 activity. The NOX2 isoform was determined to be the major contributor to arsenite-induced ROS generation and DNA damage retention. *In vivo* DNA damage was measured by immunohistochemical staining and analysis of dorsal epidermis sections from C57Bl/6 and p91phox knockout ($NOX2^{-/-}$) mice. There was no significant difference in solar-simulated UVR DNA damage as detected by percent PH2AX positive cells within $NOX2^{-/-}$ mice versus control. In contrast, arsenite-dependent retention of UVR-induced DNA damage was markedly reduced. Altogether, the *in vitro* and *in vivo* findings indicate that NOX is involved in arsenic enhancement of UVR-induced DNA damage.

1. INTRODUCTION

Arsenic exposure is associated with numerous acute and chronic health effects including increased risk of skin, lung and urinary tract cancers (ATSDR, 2016, 2007). In addition to the known direct carcinogenic actions of arsenic, there is substantial evidence that arsenic is a co-carcinogen and amplifies the carcinogenic potential of other DNA-damaging agents such as ultraviolet radiation (UVR) (Hartwig et al., 2020; Rossman et al., 2004; Zhou et al., 2021). In experimental models, Rossman and colleagues demonstrated that non-carcinogenic concentrations of arsenic increased the number of UVR-induced skin lesions in mice, decreased the time to tumor onset and increased tumor size and invasiveness (Burns et al., 2004; Rossman et al., 2004, 2001). The relevance of these findings is supported by human epidemiologic data indicating a relationship between sun exposure and skin cancer in arsenic-exposed populations (Chen et al., 2006, 2003; Melkonian et al., 2011).

Disruption of DNA repair is one mechanism proposed for the observed co-carcinogenic actions of arsenic (Andrew et al., 2006; Hudson et al., 2016; Muenyi et al., 2015; Tam et al., 2020; Zhou et al., 2021). Exposure to low levels of arsenite (As(III)) inhibits base excision repair responsible for the remediation of UVA induced DNA single strand breaks and oxidized DNA bases, and nucleotide excision repair that resolves UVB induced bulky adducts such as cyclobutane pyrimidine dimers and pyrimidine (6-4) pyrimidone photoproducts (Beyersmann and Hartwig, 2008; Cadet and Douki, 2018; Ding et al., 2017; Hartwig et al.,

2020; Muenyi et al., 2015; Tam et al., 2020; Zhou et al., 2021). Thus, arsenic reduces the cellular capacity to repair numerous UVR generated DNA lesions ultimately leading to retention of DNA damage and enhanced mutagenesis.

DNA repair can be disrupted by arsenic through a dual mechanism requiring both 1) the binding of trivalent As(III) to zinc finger DNA binding domains (DBD) of DNA repair protein targets containing three or more zinc coordinating cysteine residues and 2) the subsequent oxidation of the DBD cysteine residues by As(III) stimulated reactive oxygen species (ROS) (Muenyi et al., 2015; Tam et al., 2020; Zhou et al., 2021). Poly (ADP-ribose) polymerase (PARP-1) is a known target of As(III) involved in the remediation of UVR-induced DNA lesions by binding to damaged DNA through its zinc finger containing DBD and stimulating poly ADP-ribosylation for the recruitment of base excision repair, nucleotide excision repair and DNA strand break repair factors (King et al., 2012; Pascal, 2018; Ray Chaudhuri and Nussenzweig, 2017; Reynolds et al., 2015; Wang et al., 2019). We find As(III) binding to the PARP-1 DBD leads to zinc displacem(Zhou et al., 2015)ent and increased susceptibility of the zinc ligands to oxidative damage (Zhou et al., 2015). As(III)-stimulated production of ROS is an important factor in PARP inhibition. Antioxidants and ROS scavengers interfere with As(III)-dependent zinc loss and inhibition of PARP activity (Wang et al., 2013). Further studies found inhibition of NADPH oxidase (NOX) activity blocked PARP-1 DBD zinc displacement and cysteine oxidation in response to As(III) (Zhou et al.,

2015), suggesting As(III) stimulation of NOX is an important pathway for ROS generation related to DNA repair inhibition.

Oxidative stress has long been recognized as a contributing factor to skin carcinogenesis (Alnajjar and Sweasy, 2019; Cadet and Douki, 2018; Nishigori et al., 2004; Rudolf et al., 2018). UVA generates ROS leading to oxidative damage of macromolecules important in the maintenance of genome stability, including DNA and DNA repair proteins (Cadet and Douki, 2018). During DNA replication, the presence of oxidative DNA damage (8-hydroxy-2'-deoxyguanosine; 8-OHdG) can lead to G:C to T:A transversions which are often detected in the mutated *p53* tumor suppressor gene in human skin cancers and UVR-induced mouse skin cancers (Nishigori et al., 2004). Several mechanisms contribute UVR generated ROS including the overactivation of superoxide producing NOX enzymes (de Jager et al., 2017; Raad et al., 2017; Valencia and Kochevar, 2008).

NOX isoforms are detected in the epidermis (Rudolf et al., 2018) and both UVA and As(III) increase overall NOX activity and ROS production in keratinocytes, but with notable differences (Cooper et al., 2009). Exposure of keratinocytes to UVA resulted in rapid and transient NOX activation, whereas the response to As(III) was more pronounced and persistent. NOX inhibitors decreased ROS production in As(III)-treated cells but had little impact on UVA-exposed keratinocytes (Cooper et al., 2009). Collectively, these findings suggest As(III)

stimulation of NOX activity may be a critical pathway for PARP-1 oxidation and inhibition of PARP-1 mediated DNA repair.

In this study we tested the contributions of NOX to As(III)-dependent oxidation of PARP-1, inhibition of PARP-1 activity and enhancement of UVR-induced DNA damage in keratinocytes. We find that NOX inhibition decreases As(III)-induced oxidation of endogenous PARP-1 and significantly rescues As(III) inhibition of PARP-1 activity. NOX2 is expressed at greater levels in human skin than NOX1 (Fagerberg et al., 2014; Uhlen et al., 2015) and results from small interfering RNA (siRNA) knockdown of NOX1 or NOX2 demonstrates NOX2 is the major contributor to As(III)-induced ROS and DNA damage retention in keratinocytes. In addition, we used p91phox knockout ($NOX2^{-/-}$) mice to assess the role of NOX2 in As(III)-dependent responses *in vivo.* As(III) inhibition of UVR-induced PARP activity was not evident in the epidermis of $NOX2^{-/-}$ mice compared to controls. Furthermore, retention of UVR-induced DNA damage by As(III) was decreased in $NOX2^{-/-}$ mice. The findings obtained from this study support a role for NOX2 in mediating the effects of As(III) on UVR-induced DNA damage repair.

2. MATERIALS AND METHODS

2.1 Cell Culture and Materials

Normal human neonatal epidermal keratinocytes (HEKn) and DermaLife K culture medium with supplements were purchased from Lifeline Cell Technologies (Oceanside, CA). Cells were cultured at 37°C in 95% air/5% CO_2

humidified incubator. Sodium arsenite (>99%; As(III)) was purchased from Fluka Chemie (Buchs, Germany). Other chemicals were obtained from Sigma-Aldrich (St. Louis, MO) unless otherwise indicated. Stock solutions of As(III) (10 mM), Manganese(III)tetrakis(1-methyl-4-pyridyl)porphyrin (MnTMPyP; 1mM; Calbiochem; La Jolla, CA), and *tert*-Butyl H_2O_2 (100mM; TBHP; Thermo Fisher; Waltham, MA) were prepared in milliQ water and sterilized using a 0.22-µm syringe filter. Working solutions were prepared by diluting the stock with complete cell growth medium. The ROS indicator carboxy- 2',7'-dichlorodihydrofluorescein diacetate (DCFDA; Thermo Fisher) and apocynin (Apo; Calbiochem) were prepared in dimethyl sulfoxide at 100 mM. Final concentrations of vehicle used to prepare the primary stocks did not exceed 0.1% (v/v) of total volume in the cell culture medium. For experiments involving cell exposures, cells were rinsed and placed in complete medium containing As(III), apocynin, MnTMPyP or TBHP at the concentrations and times indicated in the figure legends. Concentrations of apocynin and MnTMPyP employed did not significantly alter the viability of the HEKn cells at 24 h of treatment (Supplemental Fig. 1) but were sufficient to inhibit ROS induced by As(III) (Supplemental Fig. 2). The NOX1, NOX2 and universal scrambled (Scr) control siRNAs (Supplemental Table 1) were purchased from Origene and HiPerFect Transfection Reagent from Qiagen.

2.2 Ultraviolet Radiation (UVR) Exposure

Solar simulated UVR exposures were performed using an Oriel 1600 Watt Solar Ultraviolet Simulator (Oriel Corp., Stratford, CT). This solar simulator produces a high intensity UVR beam in both the UVA (320-400 nm) and UVB (280-320 nm) spectrum with an emission ratio of 13:1 (UVA:UVB). The proportion and intensity of UVA/UVB was measured using an ILT2400 radiometer equipped with UVA (SED033), UVB (SED240) and UVC (SED270) detectors (International Light Technologies; Peabody, MA). *In vivo* exposures were at 28 kJ/m^2 providing approximately 1 minimum erythema dose (MED). Measurements were made with Erythema UV and UVA intensity meter (Solar Light Co., Inc., Philadelphia, PA) in order to estimate MED. Animal UVR dosing was conducted in groups of 4 or 5 with animals allowed to move freely within the exposure enclosure. Cultured cells were exposed at a dose of 2kJ/m^2 in complete medium with the vessel lids removed. Cells were kept in the dark during transport to and from the UVR exposure lamp.

2.3 Cysteine Oxidation

HEKn cells were treated with As(III) (1 μM) with or without a 30 min pretreatment of either apocynin (Apo; 5 □M) or MnTMPyP (2.5 □M) for 6 h. Cells were harvested in RIPA cell lysis buffer (20 mM Tris, pH 7.5; 150 mM NaCl; 1 mM EDTA; 1 mM EGTA; 1% Triton X-100; 2.5 mM sodium pyrophosphate; 1 mM β-glycerophosphate; 1 mM sodium vanadate) plus 1% Halt Protease Inhibitor Cocktail (Thermo Scientific, Rockford, IL), sonicated and centrifuged at 14,000 rpm for 10 min at 4°C to remove cellular debris. Total protein content was

determined via BCA assay (Pierce, Rockford, IL). Aliquots were prepared and N-ethylmaleimide (NEM; 10 mM; #E3876; Sigma) was added to block free cysteine residues and dimedone (1mM; #A10140; Alfa Aesar; Tewksbury, MA) was added to label SOH functional groups. PARP-1 was immunoprecipitated with anti-PARP1 antibody (#9532; Cell Signaling Technologies; Danvers, MA) from cell lysates (250 □g protein per 500 □l total volume) with Protein A Agarose beads (#15918-014; Invitrogen; Carlsbad, CA) then resolved with 10% SDS-PAGE and transferred to nitrocellulose membrane (PI88018; Fisher Scientific). Immunoblotting was performed with cysteine sulfonic acid (Millipore, #07-2139) antibody to determine level of oxidation. Membranes were stripped and probed for total PARP-1 (#ab75757; Abcam; Cambridge, MA). Quantification of immunoblot results was performed using a FluorChemR image acquisition station (Proteinsimple; Sunnyvale, CA) with the Alpha View FluorChem Q (ver. 3.4.0.0) analysis software. Densitometry of oxidized protein was normalized to PARP-1 protein. All samples were run in duplicate with a minimum of three independent experiments analyzed per treatment. One-way analysis of variance with Tukey's multiple comparison tests conducted using GraphPad Prism 5.03 (San Diego, CA) was used to determine statistical significance.

2.4 NOX1 and NOX2 siRNA Transfection

HEKn cells were transfected with NOX siRNAs according to the manufacturer's instructions. Supplemental Table 1 provides details of each siRNA purchased for these experiments. Briefly, NOX1, NOX2 and Scr negative control siRNAs were

mixed with cell culture medium (10-15% of final volume) and HiPerFect Transfection Reagent (2 µl per ml of final volume; Qiagen) and incubated at room temperature for 10 min. The concentrations of siRNAs used were determined by dose-response experiments and are as follows: NOX1A (10 nM), NOX1C (10 nM), NOX2B (20nM), NOX2C (20 nM) and Scr (20 nM). These resulted in equivalent level of target protein knockdown (approximately 60%) and transfection efficiency was 67.7-79.6% for the siRNAs (Supplemental Fig. 3). Success of the siRNA knockdown was determined for each individual experiment by concurrently plating and transfecting cells in 6 well plates, including Mock, Scr and NOX siRNAs. Cells were incubated for a total of 72 h, total protein collected in RIPA buffer, and immunoblotted for NOX1 and NOX2 proteins. For experiments conducted on cells grown in 60 mm tissue culture plates (i.e., PARP activity and immunoblot analyses), HEKn cells were trypsinized, centrifuged and resuspended in complete medium. 3.5×10^4 cells and transfection complexes were then added to the prepared plates containing 3 ml complete medium. Cells were incubated overnight, medium exchanged for fresh, then incubated for an additional 48 h to allow for adequate protein knockdown (Supplemental Fig. 3) before further analysis as described in sections below. Transfection of cells in 4-well chamber slides was accomplished with slight modifications of cell concentration and volume as described in the following sections. Scr control siRNA prepared as above was used as a negative control. One-way analysis of variance with Tukey's multiple comparison tests conducted using GraphPad

Prism 5.03 was used to determine statistical significance of a minimum of 3 independent experiments.

2.5 ROS Detection

To detect the effects of inhibitors on arsenic-induced ROS production, HEKn cells were pretreated with apocynin (5 μM) or MnTMPyP (2.5 μM), and DCFDA (20 μM) for 30 min., then fresh medium with As(III) (1 μM), inhibitors or As(III) plus inhibitors was added. Plates were incubated for an additional 0.5 h, 2 h or 24 h before detection of ROS. Nuclei were stained with 4',6-diamino-2-phenyindole (0.7 μg/ml; DAPI) and slides immediately imaged using an Olympus IX83 fluorescence microscope equipped with cellSens Dimension (Olympus; v 1.9) imaging software and a DP80 digital camera. A minimum of 10 images per slide were collected per treatment and sum fluorescence intensity was quantified using cellSens Dimension and Count & Measure imaging software (Olympus; v 1.9) and normalized to DAPI fluorescence. To detect the impact of NOX siRNA on arsenic-induced ROS, 2.5 X 10^3 cells were plated in each chamber of 4-well slides (Lab-Tek; Rochester, NY) and incubated overnight. Cells were then transfected as described above with either NOX1, NOX2, NOX1 plus NOX2 or Scr control siRNAs then incubated overnight. Media was changed and slides incubated for an additional 48 h. As(III) (1 μM) and DCFDA (20 μM) were added, and slides returned to the incubator for 0, 5, 30, or 60 min. Nuclei were stained with DAPI, slides imaged and fluorescence quantified as described above. All images were acquired within 3 h of staining to minimize possibility of signal

degradation. Data from at least 3 independent experiments were pooled and statistical significance assessed by one-way ANOVA with Tukey's multiple comparison tests conducted using GraphPad Prism 5.03.

2.6 Detection of PH2AX and 8OHdG

For DNA damage assessment, 2.5 X 10^3 cells were plated and transfected with NOX and control siRNAs as described in 2.4.2 above. Cells were treated with As(III) (1 μM) for 24 h, then exposed to UVR (2 kJ/m^2) to induce DNA damage. As an additional control, cells were incubated with the NOX inhibitor apocynin (5 μM) 30 min prior to the As(III) treatment and subsequent UVR exposure. Results from the non-transfected control were equivalent to the Scr control and therefore were not included in the figures. Slides were fixed with 4% paraformaldehyde at 0 (no UVR), 1 and 6 h post UVR. DNA strand breaks were visualized using antibodies for phospho-histone H2A.X (PH2AX; #2577; 1:800; Cell Signaling Technologies; Danvers MA) or oxidative DNA damage using antibodies for 8OHdG (#ab48508; 1:500; Abcam; Cambridge, MA) by indirect immunofluorescence. Slides were incubated in primary antibody overnight at 4°C followed by a 1 h incubation at room temperature with anti-rabbit FITC conjugated secondary antibody (#6717; 1:1000; Abcam; Cambridge, MA) or anti-mouse Alexa Fluor 647 conjugated secondary antibody (#a32728; 1:1000; Abcam; Cambridge, MA) diluted in blocking buffer (PBS containing 2.5% goat serum, 0.15% triton X-100). Nuclei were stained with DAPI (0.7 μg/ml) and slides were mounted with VectaShield (H-1000; Vector Laboratories; Burlingame, CA)

and visualized with an Olympus IX83 fluorescence microscope equipped with a DP80 digital camera (Olympus America; Center Valley, PA). A minimum of 10 images per slide were collected per treatment and fluorescence intensity was quantified using cellSens Dimension and Count & Measure imaging software (Olympus; v 1.9). Data from at least 3 independent experiments were pooled and statistical significance assessed by one-way ANOVA with Tukey's multiple comparison tests conducted using GraphPad Prism 5.03.

2.7 PARP-1 Activity

Cells were treated as described in the figure legends, then PARP-1 was activated by exposure to UVR (2 kJ/m^2). Whole cell extracts were collected in PAR ELISA lysis buffer (10 mM Tris, pH 7.4, 100 mM sodium chloride, 1 mM EDTA, 1 mM EGTA, 1 mM sodium fluoride, 20 mM sodium pyrophosphate, 2 mM sodium vanadate, 1% triton X-100, 10% glycerol, 0.1% SDS, 0.5% deoxycholate) plus 1% Halt Protease Inhibitor Cocktail (Thermo Scientific, MA, USA) 6 h after UVR exposure. An aliquot of each sample was diluted 1 to 10 in RIPA buffer and total protein content determined via the BCA assay kit. Cell lysates were assayed for PARP activity via the PAR ELISA assay as described in Zhou, X et al. (Zhou et al., 2015). Briefly, PAR standards or total protein (30 µg) were placed in antibody (Trevigen; #4335-MC-100) coated plates in triplicate and incubated overnight at 4°C. Plates were then incubated with polyclonal PAR antibody (Trevigen; #4336-BPC-100) and incubated for 2 h at room temperature followed by an additional 1 h incubation with goat anti-rabbit HRP conjugated antibody at

room temperature. Total PAR content was determined by the addition of SuperSignal ELISA pico substrate (Pierce, Rockford, IL) and luminescence measured on a SpectraMax i3X plate reader equipped with FluorChem Q (ver 3.4.0.0) analysis software (Molecular Devices; Sunnyvale, CA). Luminescence was compared to the standard curve and PAR content reported as nmoles PAR per mg of protein. One-way analysis of variance with Tukey's multiple comparison tests conducted using GraphPad Prism 5.03 was used to determine statistical significance of a minimum of 3 independent experiments.

2.8 In vivo Exposures and Tissue Collection

P91phox (NOX2) knockout breeding pairs (B6.129S-Cybb^{tm1Din}/J; NOX2$^{-/-}$) and C57BL/6 (21–25 days old; CTRL) mice were purchased from Jackson Labs (Bar Harbor, ME). Breeding of the knockout animals was performed by the UNM HSC Animal Research Facility and transferred to the experimental protocol at age 25-27 days old. The difference in age from the background control mice is due to the small size of the knockout animals at day 21. These studies were performed under an approved Institutional Animal Care and Use Committee (IACUC) protocols (#18-200816B-HSC and 18-200864-HSC). Animals were randomly distributed into treatment groups and administered As(III) (5 mg/l) or no addition in the drinking water for 28 days. Water was freshly prepared and changed 3 times per week, consumption monitored and volumes compared to untreated control animals to ensure equivalent water consumption (Supplemental Fig. 4). Controls and treated animals were provided standard mouse chow ad lib.

Animals were anesthetized with isofluorane and the dorsal hair from hips to shoulders removed by shaving and subsequent application of a topical hair remover (Nair™; Church & Dwight Co., Inc.). The animals were given 3 days to recover, then randomly selected from each treatment group for exposure to a single dose (28 kJ/m^2; 1.2 MED of UVR) and euthanized at 0 (no UVR), 1 or 6 h post exposure. These time points were chosen from previously published studies showing time courses from DNA damage initiation through repair (Bykov et al., 1999; Ropolo et al., 2011) and from our previous studies (Cooper et al., 2013; Ding et al., 2008) to reflect the peak damage (1 h) to partial repair (6 h). The UVR exposure reflects a dose to cause significant, but not maximal, DNA damage allowing for detection of As(III) augmented DNA damage (Supplemental Fig. 5) (Cooper et al., 2013). Animals were euthanized using CO_2 followed by cervical dislocation, then the irradiated and UVR naïve dorsal skin was collected and preserved in 10% neutral buffered formalin and paraffin blocks were prepared using standard procedures. A section of skin was quick frozen on a cold block and the epidermis scraped to remove the keratinocytes as previously described (Hudson et al., 2007). These scrapings were then placed in RIPA buffer to extract protein and frozen at -80°C for future analyses.

2.9 PARP Activity in Epidermal Lysates

Lysates obtained from skin scrapings described above were diluted 1:1 in PAR ELISA lysis buffer, vortexed vigorously and sonicated on ice for 3 X 15 sec to fully solubilize proteins. Samples were centrifuged at 14,000 rpm for 10 min at

4°C to remove cellular debris and aliquoted into fresh tubes. BCA assay (Pierce, Rockford, IL) was performed to determine total protein and lysates diluted to 5 □g per 200 □l total volume. PARP activity was determined on 50 µl of sample in triplicate by PARP activity assay as described above. One-way analysis of variance with Tukey's multiple comparison tests conducted using GraphPad Prism 5.03 was used to determine statistical significance.

2.10 Immunohistochemistry and Image Analysis of DNA Damage

Paraffin embedded tissue was sectioned using a rotary microtome (Microm HM315) at a thickness of 10 µm. For staining, slides were deparaffinized with three exchanges of xylene (10 min each) followed by a 1 min exchange in absolute ethanol. Sections were rehydrated by sequential 1 min immersions in 95%, 75%, and 50% ethanol followed by 5 min in water. Slides were treated with 0.125% trypsin for 10 min at room temperature, followed by three rinses with 1X phosphate-buffered saline (PBS), then placed in a 1 N HCl solution for 30 min at room temperature to denature DNA and subsequently rinsed 3 times in 1X PBS. Antigen retrieval was accomplished by immersing slides in hot (90°C) 1 M EDTA, pH 8.0 for 20 min, then peroxidases quenched by immersion in 3% H_2O_2 in methanol for 20 min. For staining of DNA strand breaks, slides were blocked with Background Sniper (Biocare Medical; Concord, CA) 30 min, then incubated with primary antibody against PH2AX (#2577 Cell Signaling, Danvers, MA at 1:300) overnight at 4°C followed by biotinylated anti-rabbit secondary antibody (Vector Labs; Burlingame, CA) at 1:750 for 30 min at room temperature, then incubated

in ABC reagent (Vector Labs) for an additional 30 min. DAB solution (5%; 3,3'-Diaminobenzidine; Sigma) was employed to label positive epitopes with hematoxylin QS (Vector Labs) used as the nuclear counter stain. Sections were dehydrated and coverglass mounted with Permount Mounting Medium (EMS, Hatfield, PA). For analysis, slides were scanned at high-resolution using the Aperio Versa 200 (Lecia Biosystems; Buffalo Grove, IL) automated slide scanner and digitally analyzed with the HALO™ Platform software (v3.0.311.185; Indica Labs; Albuquerque, NM). Tissue sections were annotated with the digital software to differentiate the epidermis from other skin tissue types and to identify positively stained cells. Intensity of positive staining was calibrated to give 0, 1+, 2+ and 3+ levels of staining with 0 being negative staining and 3 being the most intensely stained. ROIs (regions of interest) were drawn around the epidermis of each scanned image to limit the occurrence of false identification of epidermal cells. Percent positive cells was calculated by dividing the number of positive cells for each level by the total number of nuclei from a minimum of 3 separate sections from each mouse. Data from at least five different animals were pooled and two-way ANOVA with Bonferroni post-test was conducted using GraphPad Prism 5.03 to determine statistical significance.

3. RESULTS

3.1 As(III)-induced ROS Through NOX Activation Contributes to PARP-1 Inhibition

As(III) binds to zinc finger domains of PARP-1 leading to zinc displacement and oxidative damage to the zinc coordinating cysteine residues (Ding et al., 2009; Qin et al., 2008b; Wang et al., 2013; Zhou et al., 2011, 2015). Previous work found that NOX inhibition in keratinocytes decreased the As(III)-induced oxidation of cysteine residues within exogenously expressed PARP-1, but effects on PARP-1 activity were not assessed (Zhou et al., 2015). To determine the contributions of NOX and ROS to the oxidation of endogenous PARP-1 and PARP activity, HEKn cells were pretreated with a NOX inhibitor (apocynin, 5 μM) or a ROS scavenger (MnTMPyP, 2.5 μM) prior to exposure to As(III) (1 μM). The concentrations of the NOX inhibitor and ROS scavenger did not significantly alter cellular viability at 24 h post exposure (Supplemental Fig. 1) but effectively inhibited ROS production induced by As(III) at 2 h (Fig. 1A), and at 0.5 and 24 h (Supplemental Fig. 2) post exposure. The consequences of As(III)-induced ROS on PARP-1 cysteine oxidation and enzyme activity were assessed. Oxidation of the PARP-1 cysteine residues was increased by As(III) (1 μM; 6 h), while the pharmacological inhibition of NOX by apocynin resulted in a significant reduction of the observed As(III)-induced effect (Fig. 1B&C). As(III) inhibits UVR (2 kJ/m^2) induced PARP-1 activation (Cooper et al., 2014, 2013; Ding et al., 2009; Qin et al., 2008a, 2008b) and this response is significantly mitigated by the pharmacological inhibition of NOX activity or by the addition of the ROS scavenger (Fig. 1D). Altogether, these results provide evidence that the As(III)-induced production of ROS through NOX is responsible for the oxidation of endogenous PARP-1 and subsequent loss of PARP-1 activity.

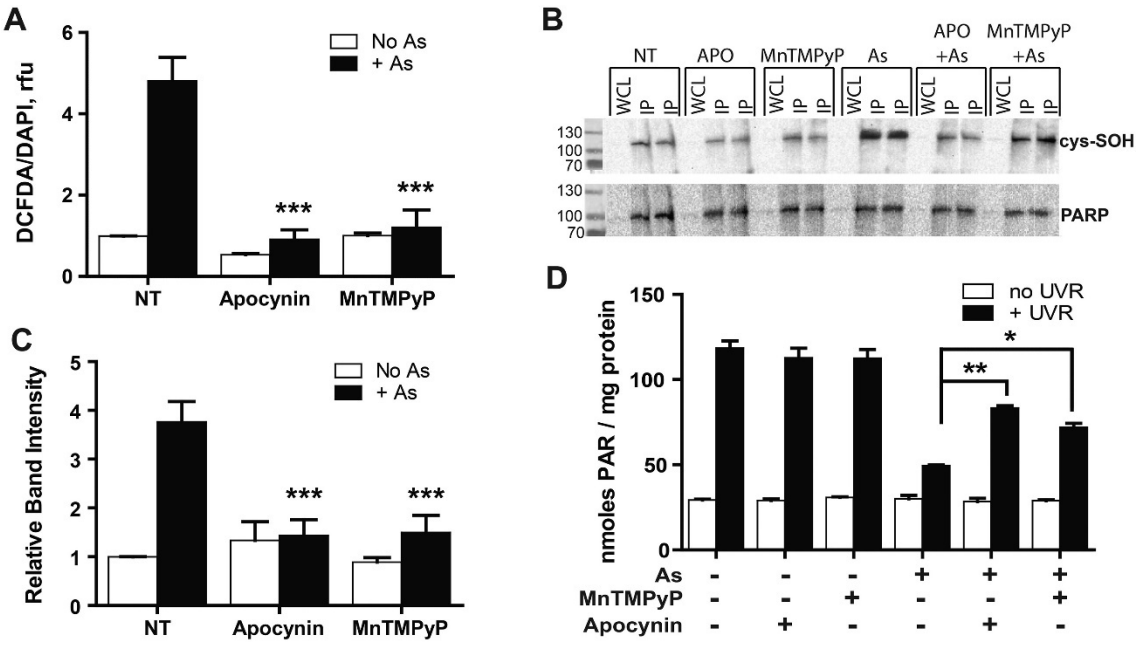

Fig. 1. As(III) stimulates NOX resulting in ROS production, PARP-1 oxidation and reduced PARP-1 activity. A) As(III)-stimulated ROS was measured in the presence or absence of apocynin (5 μM) or MnTMPyP (2.5 μM) and DCFDA (20 μM) for 30 min followed by treatment with As(III) (As; 1 μM) for 2 h. Relative fluorescence intensity values normalized to total DNA fluorescence are shown. Rfu = relative fluorescence units. ***$p < 0.001$ significantly different compared to As(III) only; $n = 3$. B-C) As(III)-stimulated PARP-1 oxidation was measured in the presence or absence of apocynin or MnTMPyP as described in (A) followed by treatment with As(III) (As; 1 μM) for 6 h. B) PARP-1 immunoprecipitated (IP) from whole cell lysate (WCL) and protein oxidation detected by immunoblotting for cysteine sulfenic acid (cys-SOH). Membranes were stripped and reprobed for PARP-1 in order to normalize to total protein immunoprecipitated. C) Graph represents the densitometric quantification of the pooled data from 6 independent experiments. ***p < 0.001 significantly different compared to As(III) only; $n = 6$. D) HEKn cells were treated as in B&C then exposed to a single dose of UVR (UVR; 2 kJ/m^2; black bars) to stimulate PARP activity. Total protein was collected 6 h post UVR exposure and PARP activity determined by ELISA as described in Materials and Methods. *$p < 0.05$, **$p < 0.01$ significantly different between indicated groups; $n = 4$. All graph values represent mean ± SEM.

3.2 Differential Contributions of NOX1 and NOX2 in As(III)-induced ROS and PARP-1 Inhibition

Both NOX1 and NOX2 are expressed in the skin and can be activated by UVR leading to enhanced ROS generation and pathological consequences (Glady et al., 2018; He et al., 2005; Raad et al., 2017; Rudolf et al., 2018; Valencia and Kochevar, 2008). siRNA was used to investigate the individual roles of NOX1 and NOX2 in As(III)-induced NOX activity and PARP-1 inhibition. Immunoblotting

and densitometry confirmed significant knockdown of the NOX1 and NOX2 (p91phox) subunits (Supplemental Fig. 3). To assess As(III)-induced ROS production through NOX1 and NOX2, ROS levels were measured over time in HEKn cells transfected with the individual siRNAs or Scr control. Representative images are shown in Fig. 2A and Supplemental Fig. 6. As(III) (1 μM) treatment in both NOX1 (Fig. 2B) and NOX2 (Fig. 2C) siRNA transfected cells showed a rapid increase in ROS that peaked at 5 min post treatment (6.0 fold and 4.0 fold for NOX1 and NOX2 knockdown cells, respectively), but did not reach the levels observed in the As(III) treated Scr control cells (8.2 fold). Knockdown of each NOX isoform led to a significant reduction of ROS at all three time points investigated; however, NOX2 knockdown had a greater impact on ROS production. The significant differences between NOX1 and NOX2 knockdown at 30 min ($p=0.045$) and 60 min ($p=0.009$) time points indicates that NOX2 is the principal contributor to the sustained production of ROS following As(III) stimulation of keratinocytes (Cooper et al., 2014, 2009, 2007; Qin et al., 2008a; Zhou et al., 2015).

Results from Fig. 1 demonstrated As(III)-induced ROS through NOX activation leads to the oxidation and inhibition of PARP-1. To determine the individual contributions of NOX1 and NOX2 to the inhibition of PARP-1 activity by As(III), knockdown studies were performed. The silencing of both NOX1 (Fig. 2D) and NOX2 (Fig. 2E) resulted in significant restoration of PARP activity following As(III) (1 μM; 24 h) exposure with NOX2 knockdown having a significantly

greater effect than that of NOX1 (45.5% versus 35.6% restoration of activity, respectively; p = 0.042). These results correspond with the findings shown in Fig. 2A-C that indicate NOX2 as the predominant mechanism of As(III)-induced ROS and indicate that NOX2 is capable of mediating As(III) inhibition of PARP activity.

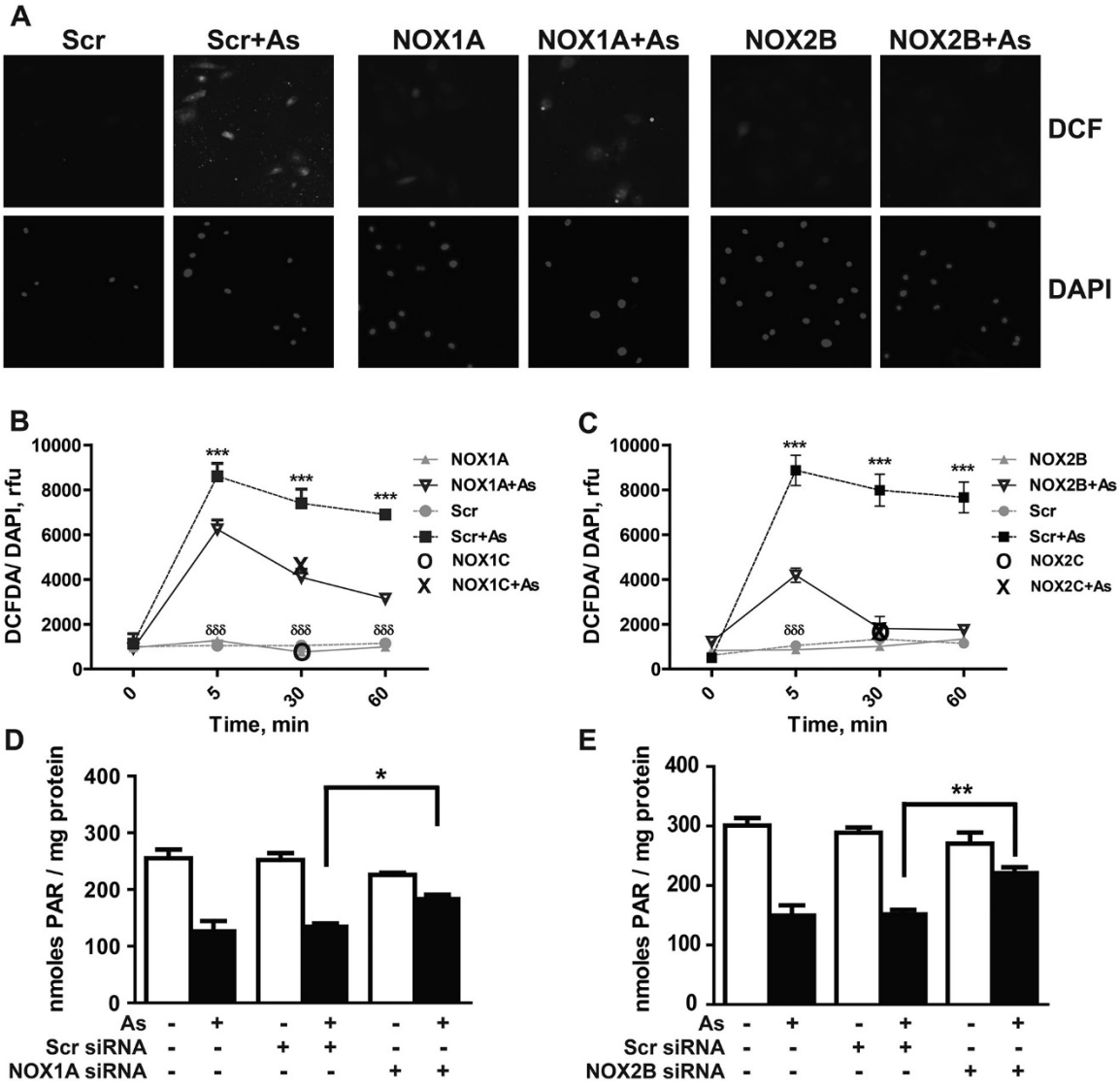

Fig. 2. NOX1 and NOX2 (p91phox) contribute differentially to As(III)-induced ROS production and PARP-1 inhibition. HEKn cells were transfected with NOX1A or C, NOX2B or C or scrambled (Scr) siRNA and cells incubated for 72 h to allow for target protein knockdown. A-C) Measurement of ROS production. DCFDA (DCF, 20 μM) was added with (black lines) and without (gray lines) As(III) (1 μM) and slides were incubated for the indicated times then cells counterstained with DAPI (0.7 μg/ml). Images were collected and relative fluorescence analyzed as described in Materials and Methods. A) Representative images of the 30 min time point. B&C) Graphs show changes in the relative DCFDA fluorescence normalized to DAPI fluorescence in the presence of B) NOX1 or C) NOX2 siRNA (solid lines) as well as the matched Scr siRNA

control (dashed lines). Alternate siRNAs for NOX1 and NOX2 (NOX1C, NOX2C) were used as indicated and designated as “O” without As(III) and “X” with As(III) in the figure key at the 30 min time point to confirm findings. In panel C, NOX2C values −/+ As(III) overlap. There are significant differences between NOX1 (B) and NOX2 (C) knockdown at 30 min ($p = 0.045$) and 60 min ($p = 0.009$). ***$p < 0.001$ significantly different between As(III) treated Scr and NOX siRNA transfected groups; $^{\delta\delta\delta}p < 0.001$ significantly different between As(III) and no As(III) siRNA matched groups; $n \geq 3$. D&E) PARP activity assay. NOX1 (D) and NOX2 (E) siRNA transfected HEKn cells were treated with (black bars) or without (white bars) As(III) (1 μM) for 24 h, then exposed to UVR (UVR; 2 kJ/m^2) to introduce DNA damage. PARP activity was determined by PAR ELISA as described in Materials and Methods. There are significant differences between NOX1 (D) and NOX2 (E) knockdown ($p = 0.042$). *$p < 0.05$, **$p < 0.01$ significantly different between indicated groups; $n \geq 3$. All graph values represent mean ± SEM.

3.3 NOX Activation by As(III) Leads to UVR-induced DNA Damage Retention

Exposure to UVR can generate a variety of DNA lesions including bulky DNA adducts, oxidized bases (i.e. 8OHdG) and single strand breaks (Cadet and Douki, 2018) and As(III) enhances the retention of multiple UVR-induced markers of DNA damage including PH2AX and 8OHdG (Cooper et al., 2014, 2013; Ding et al., 2009, 2017; Qin et al., 2008b). In order to determine the contribution of NOX in As(III) inhibition of DNA repair, the retention of DNA damage was examined in NOX1 and NOX2 siRNA treated HEKn cells. Cells were transfected, treated with As(III) (1 μM; 24 h) then exposed to a single dose of UVR (2 kJ/m^2) to induce DNA damage. Cells were fixed at 0 (no UVR), 1 and 6 h (Fig. 3) post UVR representing time points for detection of DNA damage (1 h) and significant repair of DNA damage (6h). Representative images and graphs of the PH2AX and 8OHdG staining at each time point are shown in Supplemental Fig. 7 and Supplemental Fig. 8 respectively.

At 1h and 6h post UVR, As(III) significantly increased PH2AX and 8OHdG staining compared to UVR alone (Fig. 3, Supplemental Figs. 7&8). Knockdown of

NOX1 or NOX2 by siRNA had little or no impact on UVR-induced DNA damage at the 1h and 6h time points; however, NOX1 and NOX2 silencing significantly decreased the As(III)-dependent retention of UVR-induced DNA damage (Fig. 3). As(III) plus UVR PH2AX staining was reduced 1.8-fold and 2.9-fold by NOX1 and NOX2 siRNA respectively compared to As(III) plus UVR Scr siRNA control at 6h post UVR (Fig. 3). Similarly, 8OHdG staining was reduced 1.3-fold and 2.1-fold by NOX1 and NOX2 siRNAs, respectively. The magnitude of difference between NOX2 and NOX1 was significant (PH2AX $p=0.041$ and 8OHdG $p=0.002$) with NOX2 having a larger effect on reduction of DNA damage retention. Knockdown of both NOX isoforms did not further reduce PH2AX DNA damage retention compared to NOX2 alone ($p=0.596$) and the pharmacological NOX inhibitor, apocynin, reduced levels of PH2AX at 6h post UVR with or without As(III). Collectively, the findings in human keratinocytes demonstrate that NOX2 plays a significant role in As(III)-induced ROS production, PARP-1 inhibition and DNA damage retention.

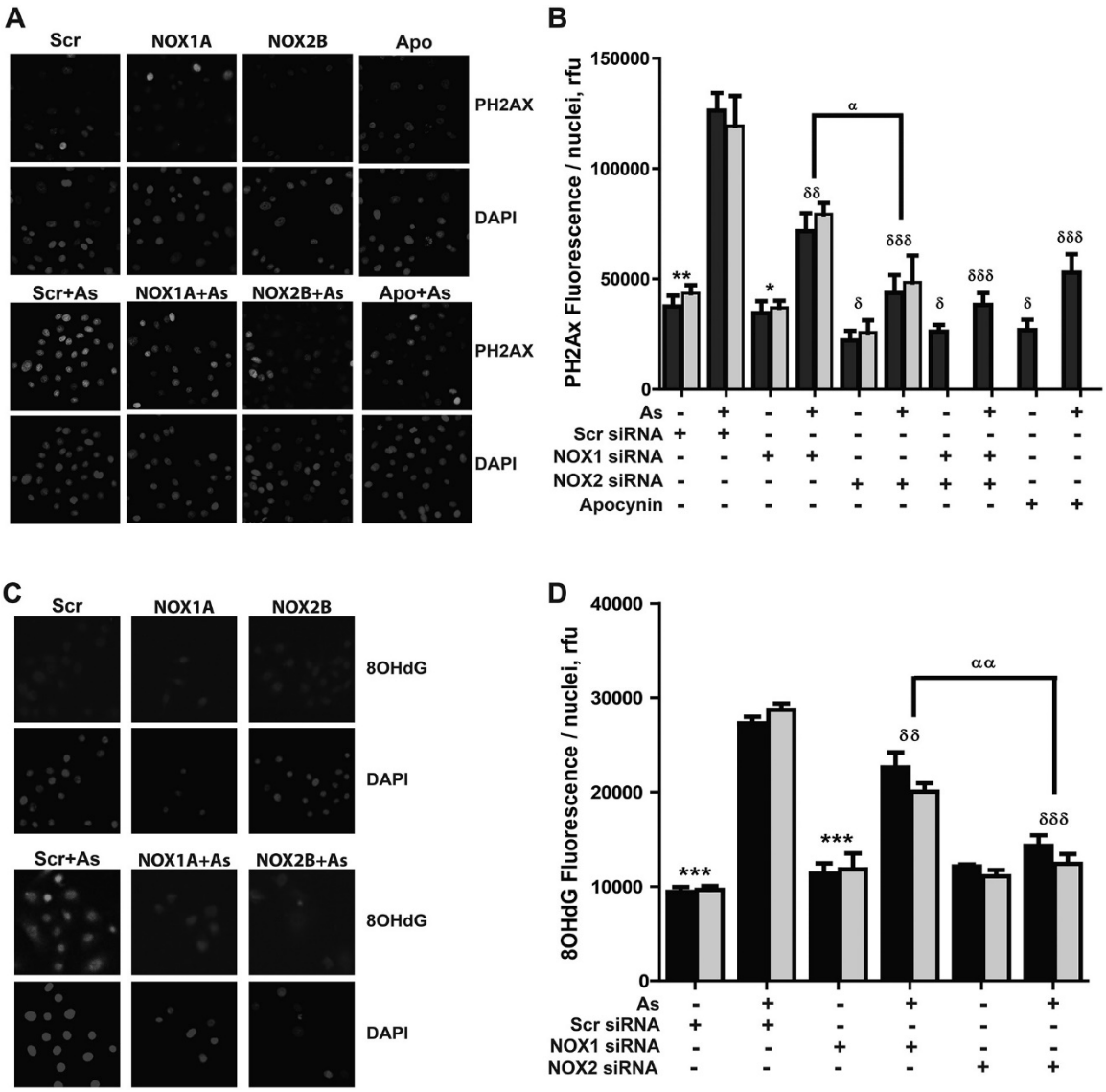

Fig. 3. NOX is a mechanism for the retention of UVR-induced DNA damage in As(III) exposed keratinocytes. HEKn cells were transfected with NOX1A or C, NOX2B or C, both NOX1A and NOX2B siRNAs or scrambled (Scr) as described in Materials and Methods, then treated with As(III) (1 μM) for 24 h, then exposed to UVR (UVR; 2 kJ/m^2) to introduce DNA damage. Apocynin (5 μM; Apo) with and without the addition of As(III) was used as a positive control for NOX inhibition in non-transfected cells (panel B). Slides were fixed and stained for PH2AX (A&B) or 8OHdG (C&D) at 0 (no UVR), 1 and 6 h post UVR exposure; 6 h post UVR exposure is shown here and the other time points are shown in Supplemental Figs. 7 & 8. Images were collected and relative fluorescence analyzed as described in Materials and Methods. A&C) Representative images of PH2AX (A) and 8OHdG (C) staining at 6 h post UVR exposure. B&D) Graphs showing relative fluorescence intensity determined from a minimum of 150 cells per treatment group PH2AX (B) and 8OHdG (D). Results for NOX1A and NOX2B siRNAs are depicted by black bars and the alternate siRNAs (NOX1C, NOX2C) are depicted by the gray bars. *$p < 0.05$, **$p < 0.01$, ***$p < 0.001$ significantly different between no As(III) and plus As(III) siRNA matched groups; $^{\delta}p < 0.05$, $^{\delta\delta}p < 0.01$, $^{\delta\delta\delta}p < 0.001$ significantly different from Scr and treatment matched groups; $^{\alpha}p < 0.05$, $^{\alpha\alpha}p < 0.01$ significantly different from indicated groups; $n \geq 3$. All graph values represent mean ± SEM.

3.4 Role of NOX2 in As(III)-induced inhibition of PARP-1 activity in vivo

It has been demonstrated previously that inhibition of PARP-1 activity by As(III) results in the retention of UVR-induced DNA lesions in both cultured cells (Cooper et al., 2014, 2013; Ding et al., 2009, 2008; Hartwig et al., 2002; Hartwig and Schwerdtle, 2002; Qin et al., 2008a) and *in vivo* (Cooper et al., 2013). To further investigate the role of NOX2 in PARP inhibition and DNA damage retention, experiments were conducted using p91phox knockout mice ($NOX2^{-/-}$). This animal model was chosen as NOX2 (p91phox) is the primary NOX isoform in mouse epidermis and human skin (Bedard and Krause, 2007; Rudolf et al., 2018; Uhlen et al., 2015; Waghela et al., 2021) and there is evidence that As(III) can activate NOX2 leading to enhanced levels of ROS (Fig. 2C) (Chou et al., 2004; Cooper et al., 2009; Lemarie et al., 2008; Lynn et al., 2000; Qian et al., 2005; Zhang et al., 2015).

$NOX2^{-/-}$ mice and background controls (c57bl/6; CTRL) were chronically exposed to As(III) (5 mg/l) in their drinking water for 28 days then exposed to a single dose of UVR (approximately 1.1 MED) to induce DNA damage. Lysates from UVR exposed dorsal epidermis were prepared and protein was analyzed for PARP activity. As observed in cultured keratinocytes, PARP activity was significantly increased at 1 and 6 h post UVR exposure in both the control (Fig. 4A) and $NOX2^{-/-}$ animals (Fig. 4B). The UVR-induced PARP activity was decreased in the presence of As(III) in control mice. In contrast, NOX2 knockout prevented the As(III)-mediated reduction of PARP activity at 6h post UVR

exposure and As(III) transiently increased PARP activity at 1 h post UVR as compared to UVR alone. These findings indicate that As(III) inhibition of UVR-induced PARP activity at the later time point was abrogated in the NOX2$^{-/-}$ epidermis.

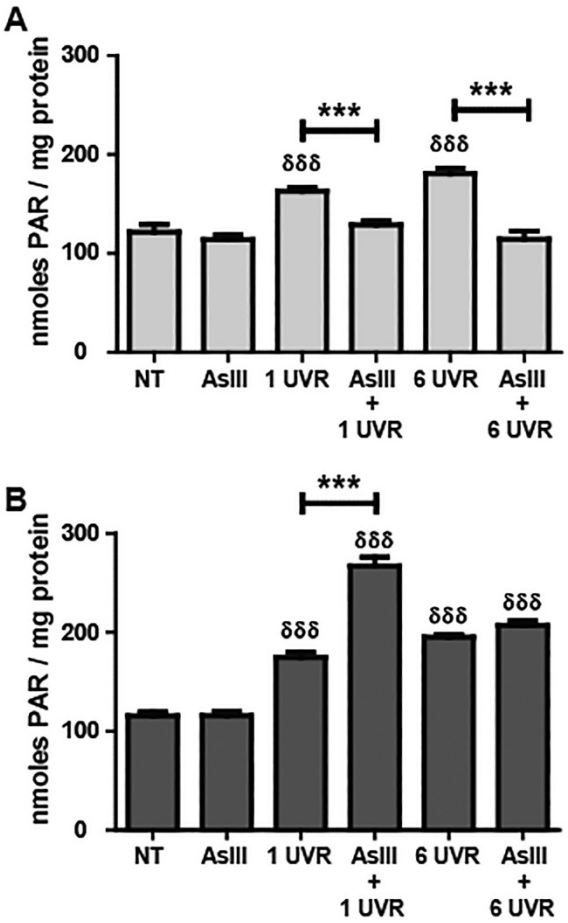

Fig. 4. NOX2 knockout blocks As(III)-dependent inhibition of UVR-stimulated PARP activity *in vivo*. Control (A) and NOX2$^{-/-}$ (B) animals were treated as described in Materials and Methods with the following treatment groups; untreated (NT), As(III) only (As), UVR at 1 h (1 UVR) and 6 h (6 UVR) post exposure; As(III) plus 1 h post UVR (As +1 UVR) and As(III) plus 6 h post UVR (As +6 UVR). Samples were analyzed for PARP activity in triplicate as described in Materials and Methods. ***$p < 0.001$ significantly different between indicated groups; $^{\delta\delta\delta}p < 0.001$ significantly different from untreated control group; $n = 4$. There are significant differences ($p < 0.001$) between the control and the NOX2$^{-/-}$ animals in the As(III) plus UVR at both 1 and 6 h post UVR exposure. All graph values represent mean ± SEM.

3.5 Role of NOX2 in the retention of DNA damage induced by As(III) and UVR in vivo

Based on evidence for an integral role of NOX in As(III)-dependent inhibition of PARP activity, we further investigated the consequences of As(III)-stimulated NOX activity on DNA damage retention *in vivo.* Immunohistochemical staining was performed on dorsal epidermis sections from NOX2$^{-/-}$ and control mice to determine relative amounts of DNA damage marker PH2AX present at 0, 1 and 6 h post UVR exposure. Representative images of the PH2AX immunohistochemical staining with HALO analysis are shown in Fig. 5A (untreated and 6 h post UVR) and Supplemental Fig. 9A-D (As(III) only and 1 h post UVR). Control and NOX2$^{-/-}$ mice showed positive staining at 6 h post UVR. The NOX2$^{-/-}$ mice in the 6 h UVR plus As(III) group exhibited a significant decrease in total positive cells as compared to UVR alone, while the control mice showed a significant increase in positive staining (Fig. 5B). A significant increase in the percentage of total positive nuclei in both control and NOX2$^{-/-}$ mouse strains was observed at 1 h post UVR exposure with a small but significant increase with the combined exposure of UVR and As(III) (Supplemental Fig. 9E).

An in-depth analysis of PH2AX staining intensity profiles was performed. Animals that were not exposed to UVR or As(III) displayed little positive staining and there were no differences detected between the control and NOX2$^{-/-}$ mice (Fig. 5C). PH2AX staining for low (1+) and higher intensity (2+ and 3+) DNA damage was increased with UVR exposure alone in both mouse strains at 6 h post exposure (Fig. 5D). A small, but significant decrease in PH2AX staining was detected in the NOX2$^{-/-}$ mice when compared to control for the low intensity (1+) nuclei but

no differences were noted for the higher intensity (2+ and 3+) nuclei. This suggests that NOX2 alone has limited impact on UVR-induced DNA damage (Fig. 5D).

However, As(III) exposure altered the UVR DNA damage response in NOX2$^{-/-}$ mice when compared to control mice. Exposure to As(III) significantly increased the higher intensity (2+ and 3+) DNA damage at 6 h post UVR exposure in the control mice (gray bars; $p = 0.017$) in contrast to no significant response observed for the NOX2$^{-/-}$ mice (black bars; $p = 0.579$) (Fig. 5D&E). NOX2$^{-/-}$ mice in the As(III) treatment group displayed a significant decrease in low intensity (1+) and high intensity (2+ and 3+) DNA damage compared to control mice at 6 h post UVR (Fig. 5E). This decreased intensity of the DNA damage profile observed at the 6 h time point was also evident in the UVR plus As(III) exposed NOX2$^{-/-}$ mice at 1 h post exposure as compared to control mice (Supplemental Fig. 9H). PH2AX staining was analyzed according to sex in the NOX2$^{-/-}$ group. There were no significant sex differences observed except an increase in low intensity positive nuclei within the males of the As(III) plus 6 h post UVR as compared to the females (Supplemental Fig. 10). These data provide evidence for the involvement of NOX2 in As(III)-dependent retention of UVR-induced DNA damage.

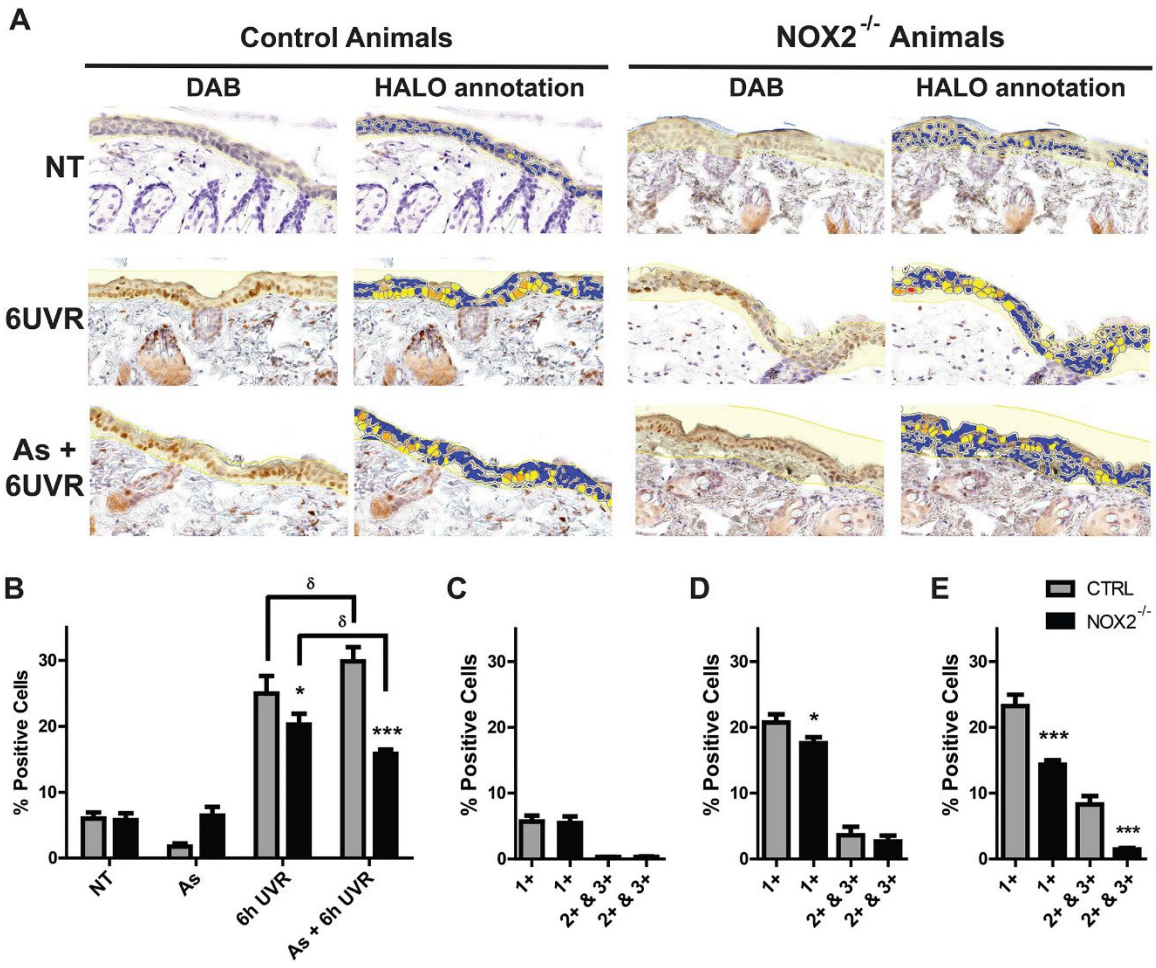

Fig. 5. NOX2 knockout reduces the retention and severity of UVR-induced DNA damage in As (III) treated mice. Control C57Bl/6 and NOX2$^{-/-}$ mice treated and tissues collected as described in the Materials and Methods. The treatment groups shown are defined as follows: untreated (NT), UVR at 6 h (6 UVR) post exposure; As(III) plus 6 h post UVR (As +6UVR). DNA damage was assessed in 10 μm sections using immunohistochemical techniques against the strand break marker, PH2AX, followed by slide scanning and HALO analysis. HALO annotation identifies intensity of positive cells with 0+ in blue, 1+ in yellow, 2+ in orange, and 3+ in red. A) Representative images from the indicated treatment groups showing DAB and HALO annotated sections side by side. B) The percentage of PH2AX positively stained nuclei for each treatment group from both control (gray bars) and NOX2$^{-/-}$ (black bars). C-E) In depth analysis of staining intensity profiles for control (gray bars) and NOX2$^{-/-}$ (black bars) animals, showing percent positive cells in the low positive (1+) compared to the more intensely stained nuclei (2+ and 3+) combined. C) Untreated, D) 6 h post UVR, E) As (III) plus UVR 6 h post exposure. Representative tissue sections prepared from animals from all treatment groups and both time points and stained for PH2AX are shown in Supplemental Fig. 9. *$p < 0.05$, ***$p < 0.001$ significantly different between treatment matched animal strains; $^{\delta}p < 0.05$ significantly different between indicated groups of the same strain; $n \geq 5$ mice per treatment group. (For interpretation of the references to colour in this figure legend, the reader is referred to the web version of this article.)

4.0 DISCUSSION

UVR exposure contributes to approximately 90% of nonmelanoma skin cancers by inducing DNA damage through direct and indirect means (Kim and He, 2014). Highly mutagenic helix distorting DNA lesions such as cyclobutane pyrimidine dimers and pyrimidine (6-4) pyrimidone photoproducts are predominantly generated by exposure to UVB and can lead to replication stress and DNA double-strand breaks if not repaired correctly (Cadet and Douki, 2018; Yajima et al., 2009). UVR-induced ROS can arise through multiple mechanisms including direct interactions with cellular components or photosensitizers and activation of NOX enzymes (de Jager et al., 2017; Fagerberg et al., 2014; Glady et al., 2018; Raad et al., 2017; Rudolf et al., 2018; Valencia and Kochevar, 2008) that lead to DNA oxidation and strand breaks (Cadet and Douki, 2018; Cooper et al., 2009; Glady et al., 2018; Raad et al., 2017; Ray Chaudhuri and Nussenzweig, 2017; Rudolf et al., 2018; Valencia and Kochevar, 2008; Waghela et al., 2021). This study presents evidence that NOX activity is also a key factor in arsenic-dependent inhibition of PARP-1 activity and retention of UVR-induced DNA damage.

Arsenic disrupts select zinc finger protein targets leading to the inhibition of DNA repair, retention of DNA damage and enhanced carcinogenesis (Fig. 6) (Hudson et al., 2016; Rossman et al., 2004; Tam et al., 2020; Zhou et al., 2021, 2015). PARP-1 is a direct molecular target of arsenic and vital in the remediation of a variety of DNA lesions including UVR generated bulky DNA adducts, oxidized bases and DNA strand breaks by recruiting and retaining essential DNA repair

factors (Fig. 6.1) (Cadet and Douki, 2018; King et al., 2012; Pascal, 2018; Ray Chaudhuri and Nussenzweig, 2017; Reynolds et al., 2015; Wang et al., 2019). Indeed, PARP-1 knockout in mice results in enhanced sensitivity to DNA damaging agents, increased genomic instability and a higher incidence of cancer (Ko and Ren, 2012). As(III) inhibits the activity of PARP-1, decreasing its recruitment to chromatin and UVR stimulated PARylation resulting in the retention of UVR-induced DNA lesions (Cooper et al., 2014, 2013; Ding et al., 2017; Zhou et al., 2021). As(III) can selectively bind to the PARP-1 DBD causing the displacement of zinc and increasing the susceptibility of the zinc coordinating cysteine residues to oxidative damage (Cooper et al., 2013; Wang et al., 2013; Zhou et al., 2015, 2011) (Fig. 6.2). As(III) binding capability alone is not sufficient to inhibit PARP activity because antioxidants such as ascorbic acid and catalase or inhibition of NOX significantly rescue PARP-1 activity in As(III) treated keratinocytes (Cooper et al., 2013; Wang et al., 2013; Zhou et al., 2015, 2011). Similarly, ROS generation by As(III) alone is not sufficient to disrupt modified PARP-1 DBD or other DNA repair zinc finger domains lacking the cysteine requirements for As(III) binding (Zhou et al., 2015, 2011). The evidence that As(III)-stimulated ROS is an important facet of PARP-1 inhibition prompted our studies to delineate NOX contributions to As(III) effects on UVR DNA damage repair.

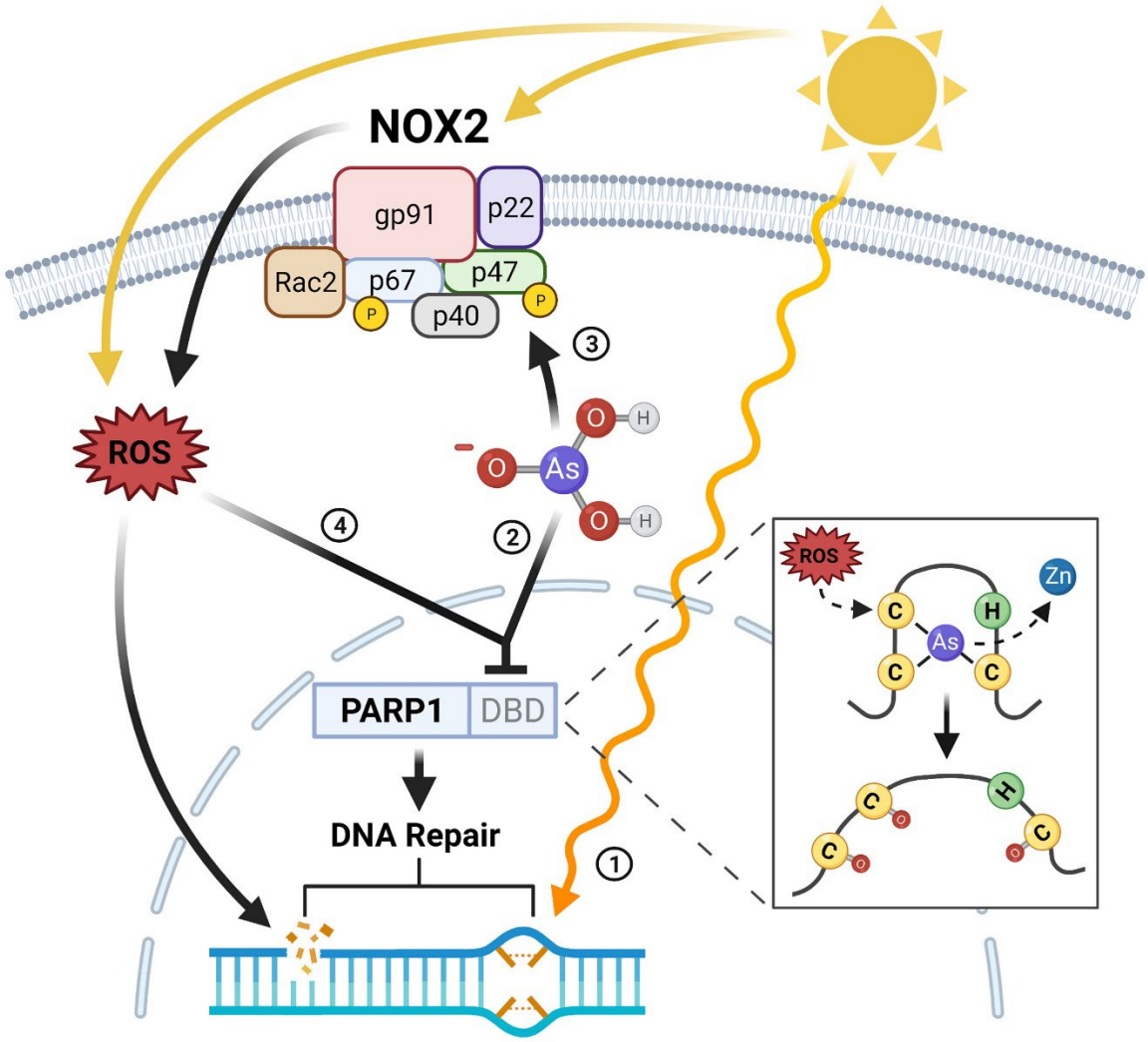

Fig. 6. Schematic representation of the contribution of NOX2 to As(III)-induced PARP-1 inhibition and DNA damage retention. 1) DNA lesions generated from exposure to UVR stimulates PARP-1 activity and the recruitment of DNA repair factors. 2) As(III) binds the PARP-1 DNA binding domain (DBD) increasing the susceptibility of the cysteine residues to oxidative damage. 3) Exposure to As(III) stimulates NOX2 activity leading to ROS production and subsequent damage to DNA and redox sensitive proteins. 4) NOX2 dependent PARP-1 oxidation and inhibition by As(III) results in the retention of UVR-induced DNA damage and can thereby contribute to increased mutagenesis and the development of cancer.

There is considerable evidence that NOX activity is induced by As(III) leading to enhanced production of ROS (Fig. 6.3) (Cooper et al., 2009; Zhang et al., 2015) and NOX activation contributes to zinc loss and DBD oxidation of exogenously expressed PARP-1 (Fig. 6.4) (Zhou et al., 2015). Our current work in human

keratinocytes and mouse skin demonstrates the importance of NOX in As(III)-dependent retention of UVR-induced DNA damage. Pharmacologic inhibition of As(III)-induced NOX activity blocked the rapid and sustained production of ROS (Fig. 1A, Supplemental Fig. 2), the oxidation (Fig. 1B&C) and inhibition (Fig. 1D) of endogenous PARP-1 and reduced the retention of DNA damage as detected by PH2AX (Fig. 3B). Knockdown of NOX1 or NOX2 by siRNA revealed that the consequences of NOX2 knockdown were greater than NOX1 for inhibition of As(III) stimulated ROS production (Fig. 2C), inhibition of PARP activity (Fig. 2E) and retention of DNA damage markers PH2AX and 8OHdG (Fig. 3). The most frequently detected oxidative DNA lesion is 8OHdG and deficits in repair can lead to G:C to T:A mutations (Nishigori et al., 2004). PH2AX is increased in UVR exposed cells and is a biomarker of DNA strand breaks and replication stress (Barnes et al., 2010; Cadet and Douki, 2018; Cleaver, 2011; Yajima et al., 2009). Elevated and sustained levels of PH2AX and 8OHdG are indicative of genomic instability and associated with carcinogenesis (Bonner et al., 2008; Nishigori et al., 2004). The cell based and *in vivo* findings indicate that NOX2 is significantly responsible for the As(III)-dependent actions leading to enhanced DNA damage retention, which can promote carcinogenesis.

NOX1 and NOX2 are the predominant isoforms expressed in the skin and are the major UVR-inducible NOX isoforms in keratinocytes (Fagerberg et al., 2014; Glady et al., 2018; Raad et al., 2017; Rudolf et al., 2018; Valencia and Kochevar, 2008). Neither NOX1 nor NOX2 knockdown modulated the UVR-dependent

generation of 8OHdG at 1h or 6h post-exposure (Fig. 3C&D, Supplemental Fig. 8). In contrast, the knockdown (Fig. 3A&B, Supplemental Fig. 7) or knockout (Fig. 5A,B&D, Supplemental Fig. 9) of NOX2 modestly decreased the levels of UVR induced PH2AX at 6 h post UVR, suggesting involvement of NOX2 in UVR-induced PH2AX retention *in vitro* and *in vivo*. Other studies reported that NOX1 inhibition or knockdown reduced UVB-induced DNA damage as measured by PH2AX or cyclobutane pyrimidine dimers (Glady et al., 2018; Raad et al., 2017; Rudolf et al., 2018). The difference between studies may be due to type of UVR (A, B or solar simulated) or the timing in measuring DNA-damage post-UVR exposure. Though there is much to uncover regarding the role of NOX enzymes in UVR induced DNA damage, our previous studies and current findings clearly demonstrate the importance of NOX activity in As(III) dependent inhibition of DNA repair and retention of DNA damage.

There are several lines of support to account for the observation that NOX2 plays a preferential role in the As(III) responses reported in this study. As(III) upregulates p22phox, a subunit common to NOX1 and NOX2 that is necessary for the regulation of NOX activation (Chou et al., 2004; Cooper et al., 2009; Lynn et al., 2000). Furthermore, As(III) selectively enhances the activity of NOX2 by upregulating the expression of the NOX2 specific subunits p91phox, p47phox, p67phox, p40phox and Rac2 (Chou et al., 2004); increasing the phosphorylation of p47phox and p67phox (Cooper et al., 2009; Lemarie et al., 2008; Qian et al., 2005); and inducing membrane translocation of p47phox and p67phox (Lemarie

et al., 2008; Qian et al., 2005). Collectively, these findings suggest a differential impact of As(III) on NOX2 activity and the *in vivo* studies in NOX2$^{-/-}$ mice confirmed the importance of NOX2 in As(III) inhibition of PARP activity and the retention and severity of UVR-induced DNA damage in As(III) exposed mice (Figs. 4&5).

Altogether, our findings provide evidence linking As(III)-induced PARP-1 oxidation and inhibition to the stimulation of NOX with both *in vitro* and *in vivo* models. UVR activation of NOX and enhanced ROS generation contributes to pathological consequences such as photoaging and the development of squamous cell carcinoma (Rudolf et al., 2018). Our findings demonstrate an additional role for NOX in mechanisms underlying arsenic co-carcinogenesis. The greater influence of NOX2 knockdown on the As(III)-induced effects on PARP activity and retention of UVR-induced DNA damage may be due to the higher expression of NOX2 in the skin and the inducibility of NOX2 by As(III) (Chou et al., 2004; Cooper et al., 2009; Lemarie et al., 2008; Qian et al., 2005). As PARP-1 plays a vital role in the initiation of DNA repair pathways upon exposure to UVR, inhibition of its activities through As(III) stimulated NOX activity may promote mutagenesis and the development of cancer (Cadet and Douki, 2018; King et al., 2012; Ko and Ren, 2012; Pascal, 2018; Ray Chaudhuri and Nussenzweig, 2017; Reynolds et al., 2015; Wang et al., 2019). Many DNA repair proteins beyond PARP-1 are sensitive to oxidative stress (Alnajjar and Sweasy, 2019) and contain domains conducive to As(III) binding and disruption (Tam et

al., 2020; Zhou et al., 2021). Therefore, PARP-1 provides an example of what could be a broader impact of As(III)-induced NOX activity on DNA repair function and carcinogenesis.

Acknowledgements

The authors would like to acknowledge support from the National Institutes of Health 1R01ES021100, 1R01ES030993, 5R25GM060201, UNM METALS Superfund Research Program 1-P42-ES-025589, and the UNM Center for Metals in Biology and Medicine NIH NIGMS P20 GM130422. Additional support was provided by the UNM Comprehensive Cancer Center 2P30 CA118100 through Trainee Matching Funds and support for the Human Tissue Repository and Tissue Analysis Shared Resource in the UNM Department of Pathology. We give special thanks to F. A. Schultz for training and assistance with Immunohistochemical image analysis. Figure 6 was created with BioRender from BioRender.com.

Declaration of Competing Interest

The authors declare no competing interests.

Supplemental Data

Download : **Download Word document (7MB)**

REFERENCES

Abdollahzade, N., Babri, S., Majidinia, M., 2021. Attenuation of chronic arsenic neurotoxicity via melatonin in male offspring of maternal rats exposed to arsenic during conception: Involvement of oxidative DNA damage and inflammatory signaling cascades. Life Sciences 266, 118876. https://doi.org/10.1016/j.lfs.2020.118876

Abuawad, A., Bozack, A.K., Saxena, R., Gamble, M.V., 2021. Nutrition, one-carbon metabolism and arsenic methylation. Toxicology 457, 152803. https://doi.org/10.1016/j.tox.2021.152803

Agre, P., King, L.S., Yasui, M., Guggino, W.B., Ottersen, O.P., Fujiyoshi, Y., Engel, A., Nielsen, S., 2002. Aquaporin water channels – from atomic structure to clinical medicine. The Journal of Physiology 542, 3–16. https://doi.org/10.1113/jphysiol.2002.020818

Ahmad, A., Bhattacharya, P., 2019. Arsenic in Drinking Water: Is 10 µg/L a Safe Limit? Curr Pollution Rep 5, 1–3. https://doi.org/10.1007/s40726-019-0102-7

Ahmad, S., Kitchin, K.T., Cullen, W.R., 2000. Arsenic Species That Cause Release of Iron from Ferritin and Generation of Activated Oxygen. Archives of Biochemistry and Biophysics 382, 195–202. https://doi.org/10.1006/abbi.2000.2023

Alexander, J.L., Orr-Weaver, T.L., 2016. Replication fork instability and the consequences of fork collisions from rereplication. Genes Dev. 30, 2241–2252. https://doi.org/10.1101/gad.288142.116

Alnajjar, K.S., Sweasy, J.B., 2019. A new perspective on oxidation of DNA repair proteins and cancer. DNA Repair (Amst) 76, 60–69. https://doi.org/10.1016/j.dnarep.2019.02.006

Alp, O., Merino, E.J., Caruso, J.A., 2010. Arsenic-induced protein phosphorylation changes in HeLa cells. Anal Bioanal Chem 398, 2099–2107. https://doi.org/10.1007/s00216-010-4128-3

Amin, R.W., Stafford, B., Guttmann, R.P., 2019. A spatial study of bladder cancer mortality and incidence in the contiguous US: 2000–2014. Science of The Total Environment 670, 806–813. https://doi.org/10.1016/j.scitotenv.2019.03.290

Andrew, A.S., Burgess, J.L., Meza, M.M., Demidenko, E., Waugh, M.G., Hamilton, J.W., Karagas, M.R., 2006. Arsenic Exposure Is Associated with Decreased DNA Repair in Vitro and in Individuals Exposed to Drinking Water Arsenic. Environ Health Perspect 114, 1193–1198. https://doi.org/10.1289/ehp.9008

Andrew, A.S., Karagas, M.R., Hamilton, J.W., 2003. Decreased DNA repair gene expression among individuals exposed to arsenic in United States drinking water. International Journal of Cancer 104, 263–268. https://doi.org/10.1002/ijc.10968

Arslan, B., Djamgoz, M.B.A., Akün, E., 2017. ARSENIC: A Review on Exposure Pathways, Accumulation, Mobility and Transmission into the Human Food Chain. Rev Environ Contam Toxicol 243, 27–51. https://doi.org/10.1007/398_2016_18

Asmuss, M., Mullenders, L.H.F., Eker, A., Hartwig, A., 2000. Differential effects of toxic metal compounds on the activities of Fpg and XPA, two zinc finger proteins involved in DNA repair. Carcinogenesis 21, 2097–2104. https://doi.org/10.1093/carcin/21.11.2097

ATSDR, 2016. Addendum to the Toxicological Profile for Arsenic. U.S. Department of Health and Human Services, Atlanta (GA).

ATSDR, 2007. Toxicological profile for Arsenic. U.S. Department of Health and Human Services, Atlanta (GA).

Bach, J., Peremartí, J., Annangi, B., Marcos, R., Hernández, A., 2016. Oxidative DNA damage enhances the carcinogenic potential of in vitro chronic arsenic exposures. Arch Toxicol 90, 1893–1905. https://doi.org/10.1007/s00204-015-1605-7

Bailey, K.A., Wallace, K., Smeester, L., Thai, S.-F., Wolf, D.C., Edwards, S.W., Fry, R.C., 2012. Transcriptional Modulation of the ERK1/2 MAPK and NF-κB Pathways in Human Urothelial Cells After Trivalent Arsenical Exposure: Implications for Urinary Bladder Cancer. J Can Res Updates 1, 57–68.

Banerjee, M., Sarkar, J., Das, J.K., Mukherjee, A., Sarkar, A.K., Mondal, L., Giri, A.K., 2007. Polymorphism in the ERCC2 codon 751 is associated with arsenic-induced premalignant hyperkeratosis and significant chromosome aberrations. Carcinogenesis 28, 672–676. https://doi.org/10.1093/carcin/bgl181

Banerjee, N., Bandyopadhyay, A.K., Dutta, S., Das, J.K., Roy Chowdhury, T., Bandyopadhyay, A., Giri, A.K., 2017. Increased microRNA 21 expression contributes to arsenic induced skin lesions, skin cancers and respiratory distress in chronically exposed individuals. Toxicology 378, 10–16. https://doi.org/10.1016/j.tox.2017.01.006

Bannister, A.J., Kouzarides, T., 2011. Regulation of chromatin by histone modifications. Cell Research 21, 381–395. https://doi.org/10.1038/cr.2011.22

Barchowsky, A., Klei, L.R., Dudek, E.J., Swartz, H.M., James, P.E., 1999. Stimulation of reactive oxygen, but not reactive nitrogen species, in vascular endothelial cells exposed to low levels of arsenite. Free Radical Biology and Medicine 27, 1405–1412. https://doi.org/10.1016/S0891-5849(99)00186-0

Baris, D., Waddell, R., Beane Freeman, L.E., Schwenn, M., Colt, J.S., Ayotte, J.D., Ward, M.H., Nuckols, J., Schned, A., Jackson, B., Clerkin, C., Rothman, N., Moore, L.E., Taylor, A., Robinson, G., Hosain, G.M., Armenti, K.R., McCoy, R., Samanic, C., Hoover, R.N., Fraumeni, J.F., Johnson, A., Karagas, M.R., Silverman, D.T., 2016. Elevated Bladder Cancer in Northern New England: The Role of Drinking Water and Arsenic. J Natl Cancer Inst. https://doi.org/10.1093/jnci/djw099

Barkley, L.R., Palle, K., Durando, M., Day, T.A., Gurkar, A., Kakusho, N., Li, J., Masai, H., Vaziri, C., 2012. c-Jun N-terminal kinase–mediated Rad18 phosphorylation facilitates Polη recruitment to stalled replication forks. Mol Biol Cell 23, 1943–1954. https://doi.org/10.1091/mbc.E11-10-0829

Barnes, L., Dumas, M., Juan, M., Noblesse, E., Tesniere, A., Schnebert, S., Guillot, B., Molès, J.-P., 2010. γH2AX, an Accurate Marker That Analyzes UV Genotoxic Effects on Human Keratinocytes and on Human Skin. Photochemistry and Photobiology 86, 933–941. https://doi.org/10.1111/j.1751-1097.2010.00744.x

Baskar, R., Lee, K.A., Yeo, R., Yeoh, K.-W., 2012. Cancer and Radiation Therapy: Current Advances and Future Directions. Int J Med Sci 9, 193–199. https://doi.org/10.7150/ijms.3635

Bedaiwi, A., Wysong, A., Rogan, E.G., Clarey, D., Arcari, C.M., 2022. Arsenic Exposure and Melanoma Among US Adults Aged 20 or Older, 2003-2016. Public Health Rep 137, 548–556. https://doi.org/10.1177/00333549211008886

Bedard, K., Krause, K.-H., 2007. The NOX Family of ROS-Generating NADPH Oxidases: Physiology and Pathophysiology. Physiological Reviews 87, 245–313. https://doi.org/10.1152/physrev.00044.2005

Beezhold, K., Klei, L.R., Barchowsky, A., 2017. Regulation of cyclin D1 by arsenic and microRNA inhibits adipogenesis. Toxicology Letters 265, 147–155. https://doi.org/10.1016/j.toxlet.2016.12.002

Beyersmann, D., Hartwig, A., 2008. Carcinogenic metal compounds: recent insight into molecular and cellular mechanisms. Arch Toxicol 82, 493–512. https://doi.org/10.1007/s00204-008-0313-y

Bhatia, A., Kumar, Y., 2013. Cancer cell micronucleus: an update on clinical and diagnostic applications. APMIS 121, 569–581. https://doi.org/10.1111/apm.12033

Bhattacharjee, P., Paul, S., Bhattacharjee, S., Giri, A.K., Bhattacharjee, P., 2018a. Association of H3K79 monomethylation (an epigenetic signature) with arsenic-induced skin lesions. Mutation Research/Fundamental and Molecular Mechanisms of Mutagenesis 807, 1–9. https://doi.org/10.1016/j.mrfmmm.2017.11.001

Bhattacharjee, P., Sanyal, T., Bhattacharjee, S., Bhattacharjee, P., 2018b. Epigenetic alteration of mismatch repair genes in the population chronically exposed to arsenic in West Bengal, India. Environmental Research 163, 289–296. https://doi.org/10.1016/j.envres.2018.01.002

Bi, T., Niu, X., Qin, C., Xiao, W., 2021. Genetic and physical interactions between Polη and Rev1 in response to UV-induced DNA damage in mammalian cells. Sci Rep 11, 21364. https://doi.org/10.1038/s41598-021-00878-3

Bi, X., Slater, D.M., Ohmori, H., Vaziri, C., 2005. DNA Polymerase κ Is Specifically Required for Recovery from the Benzo[a]pyrene-Dihydrodiol Epoxide (BPDE)-induced S-phase Checkpoint*. Journal of Biological Chemistry 280, 22343–22355. https://doi.org/10.1074/jbc.M501562200

Birgisdottir, V., Stefansson, O.A., Bodvarsdottir, S.K., Hilmarsdottir, H., Jonasson, J.G., Eyfjord, J.E., 2006. Epigenetic silencing and deletion of

the BRCA1 gene in sporadic breast cancer. Breast Cancer Res 8, R38. https://doi.org/10.1186/bcr1522
Biswas, D., Banerjee, M., Sen, G., Das, J.K., Banerjee, A., Sau, T.J., Pandit, S., Giri, A.K., Biswas, T., 2008. Mechanism of erythrocyte death in human population exposed to arsenic through drinking water. Toxicology and Applied Pharmacology 230, 57–66. https://doi.org/10.1016/j.taap.2008.02.003
Biswas, J., Sinha, D., Mukherjee, S., Roy, S., Siddiqi, M., Roy, M., 2010. Curcumin protects DNA damage in a chronically arsenic-exposed population of West Bengal. Hum Exp Toxicol 29, 513–524. https://doi.org/10.1177/0960327109359020
Bochkareva, E., Korolev, S., Lees-Miller, S.P., Bochkarev, A., 2002. Structure of the RPA trimerization core and its role in the multistep DNA-binding mechanism of RPA. EMBO J 21, 1855–1863. https://doi.org/10.1093/emboj/21.7.1855
Boekelheide, K., Blumberg, B., Chapin, R.E., Cote, I., Graziano, J.H., Janesick, A., Lane, R., Lillycrop, K., Myatt, L., States, J.C., Thayer, K.A., Waalkes, M.P., Rogers, J.M., 2012. Predicting Later-Life Outcomes of Early-Life Exposures. Environ Health Perspect 120, 1353–1361. https://doi.org/10.1289/ehp.1204934
Boffetta, P., Zunarelli, C., Borron, C., 2020. Dose-Response Analysis of Exposure to Arsenic in Drinking Water and Risk of Skin Lesions: A Systematic Review of the Literature. Dose-Response 18, 1559325820957823. https://doi.org/10.1177/1559325820957823
Bolt, H.M., Hengstler, J.G., 2018. Contemporary trends in toxicological research on arsenic. Arch Toxicol 92, 3251–3253. https://doi.org/10.1007/s00204-018-2311-z
Bonner, W.M., Redon, C.E., Dickey, J.S., Nakamura, A.J., Sedelnikova, O.A., Solier, S., Pommier, Y., 2008. γH2AX and cancer. Nat Rev Cancer 8, 957–967. https://doi.org/10.1038/nrc2523
Borgel, J., Tyl, M., Schiller, K., Pusztai, Z., Dooley, C.M., Deng, W., Wooding, C., White, R.J., Warnecke, T., Leonhardt, H., Busch-Nentwich, E.M., Bartke, T., 2017. KDM2A integrates DNA and histone modification signals through a CXXC/PHD module and direct interaction with HP1. Nucleic Acids Res 45, 1114–1129. https://doi.org/10.1093/nar/gkw979
Borrego-Soto, G., Ortiz-López, R., Rojas-Martínez, A., 2015. Ionizing radiation-induced DNA injury and damage detection in patients with breast cancer. Genet Mol Biol 38, 420–432. https://doi.org/10.1590/S1415-475738420150019
Brocato, J., Costa, M., 2013. Basic Mechanics of DNA Methylation and the Unique Landscape of the DNA Methylome in Metal-Induced Carcinogenesis. Crit Rev Toxicol 43. https://doi.org/10.3109/10408444.2013.794769
Burns, F.J., Uddin, A.N., Wu, F., Nádas, A., Rossman, T.G., 2004. Arsenic-induced enhancement of ultraviolet radiation carcinogenesis in mouse

skin: a dose-response study. Environ Health Perspect 112, 599–603. https://doi.org/10.1289/ehp.6655
Bustaffa, E., Stoccoro, A., Bianchi, F., Migliore, L., 2014. Genotoxic and epigenetic mechanisms in arsenic carcinogenicity. Arch Toxicol 88, 1043–1067. https://doi.org/10.1007/s00204-014-1233-7
Bykov, V.J., Hemminki, K., Sheehan, J.M., Young, A.R., 1999. In Situ Repair of Cyclobutane Pyrimidine Dimers and 6–4 Photoproducts in Human Skin Exposed to Solar Simulating Radiation. Journal of Investigative Dermatology 112, 326–331. https://doi.org/10.1046/j.1523-1747.1999.00523.x
Cadet, J., Douki, T., 2018. Formation of UV-induced DNA damage contributing to skin cancer development. Photochem. Photobiol. Sci. 17, 1816–1841. https://doi.org/10.1039/c7pp00395a
Cajuso, T., Sulo, P., Tanskanen, T., Katainen, R., Taira, A., Hänninen, U.A., Kondelin, J., Forsström, L., Välimäki, N., Aavikko, M., Kaasinen, E., Ristimäki, A., Koskensalo, S., Lepistö, A., Renkonen-Sinisalo, L., Seppälä, T., Kuopio, T., Böhm, J., Mecklin, J.-P., Kilpivaara, O., Pitkänen, E., Palin, K., Aaltonen, L.A., 2019. Retrotransposon insertions can initiate colorectal cancer and are associated with poor survival. Nature Communications 10, 4022. https://doi.org/10.1038/s41467-019-11770-0
Cao, Y., Yu, S.-L., Wang, Y., Guo, G.-Y., Ding, Q., An, R.-H., 2011. MicroRNA-dependent regulation of PTEN after arsenic trioxide treatment in bladder cancer cell line T24. Tumor Biol. 32, 179–188. https://doi.org/10.1007/s13277-010-0111-z
Cassandri, M., Smirnov, A., Novelli, F., Pitolli, C., Agostini, M., Malewicz, M., Melino, G., Raschella, G., 2017. Zinc-finger proteins in health and disease. Cell Death Discov 3, 17071. https://doi.org/10.1038/cddiscovery.2017.71
Ćavar, S., Bošnjak, Z., Klapec, T., Barišić, K., Čepelak, I., Jurasović, J., Milić, M., 2010. Blood selenium, glutathione peroxidase activity and antioxidant supplementation of subjects exposed to arsenic via drinking water. Environmental Toxicology and Pharmacology 29, 138–143. https://doi.org/10.1016/j.etap.2009.12.008
Chakraborty, T., De, M., 2009. Clastogenic effects of inorganic arsenic salts on human chromosomes in vitro. Drug and Chemical Toxicology 32, 169–173. https://doi.org/10.1080/01480540802594509
Chanda, S., Dasgupta, U.B., GuhaMazumder, D., Gupta, M., Chaudhuri, U., Lahiri, S., Das, S., Ghosh, N., Chatterjee, D., 2006. DNA Hypermethylation of Promoter of Gene p53 and p16 in Arsenic-Exposed People with and without Malignancy. Toxicological Sciences 89, 431–437. https://doi.org/10.1093/toxsci/kfj030
Chang, C.-W., Ou, C.-H., Yu, C.-C., Lo, C.-W., Tsai, C.-Y., Cheng, P.-Y., Chen, Y.-T., Huang, H.-C., Wu, C.-C., Li, C.-C., Lee, H.-Y., 2021. Comparative analysis of patients with upper urinary tract urothelial carcinoma in black-foot disease endemic and non-endemic area. BMC Cancer 21, 80. https://doi.org/10.1186/s12885-021-07799-4

Chang, J.-S., Gu, M.B., Kim, K.-W., 2009. Effect of arsenic on p53 mutation and occurrence of teratogenic salamanders: their potential as ecological indicators for arsenic contamination. Chemosphere 75, 948–954. https://doi.org/10.1016/j.chemosphere.2009.01.002

Chatterjee, N., Walker, G.C., 2017. Mechanisms of DNA damage, repair, and mutagenesis. Environ Mol Mutagen 58, 235–263. https://doi.org/10.1002/em.22087

Chayapong, J., Madhyastha, H., Madhyastha, R., Nurrahmah, Q.I., Nakajima, Y., Choijookhuu, N., Hishikawa, Y., Maruyama, M., 2017. Arsenic trioxide induces ROS activity and DNA damage, leading to G0/G1 extension in skin fibroblasts through the ATM-ATR-associated Chk pathway. Environ Sci Pollut Res 24, 5316–5325. https://doi.org/10.1007/s11356-016-8215-7

Chen, C.-L., Chiou, H.-Y., Hsu, L.-I., Hsueh, Y.-M., Wu, M.-M., Chen, C.-J., 2010. Ingested arsenic, characteristics of well water consumption and risk of different histological types of lung cancer in northeastern Taiwan. Environmental Research, 2nd International Congress, As 2008: Arsenic from Nature to Humans (Valencia, Spain, May 21-23) 110, 455–462. https://doi.org/10.1016/j.envres.2009.08.010

Chen, C.-L., Hsu, L.-I., Chiou, H.-Y., Hsueh, Y.-M., Chen, S.-Y., Wu, M.-M., Chen, C.-J., Blackfoot Disease Study Group, for the, 2004. Ingested Arsenic, Cigarette Smoking, and Lung Cancer Risk: A Follow-up Study in Arseniasis-Endemic Areas in Taiwan. JAMA 292, 2984. https://doi.org/10.1001/jama.292.24.2984

Chen, P.-H., Lan, C.-C.E., Chiou, M.-H., Hsieh, M.-C., Chen, G.-S., 2005. Effects of arsenic and UVB on normal human cultured keratinocytes: impact on apoptosis and implication on photocarcinogenesis. Chem Res Toxicol 18, 139–144. https://doi.org/10.1021/tx049834b

Chen, Q.Y., Costa, M., 2021. Arsenic: A Global Environmental Challenge. Annu Rev Pharmacol Toxicol 61, 47–63. https://doi.org/10.1146/annurev-pharmtox-030220-013418

Chen, Y., Graziano, J.H., Parvez, F., Hussain, I., Momotaj, H., van Geen, A., Howe, G.R., Ahsan, H., 2006. Modification of Risk of Arsenic-Induced Skin Lesions by Sunlight Exposure, Smoking, and Occupational Exposures in Bangladesh. Epidemiology 17, 459–467. https://doi.org/10.1097/01.ede.0000220554.50837.7f

Chen, Y.-C., Guo, Y.-L.L., Su, H.-J.J., Hsueh, Y.-M., Smith, T.J., Ryan, L.M., Lee, M.-S., Chao, S.-C., Lee, J.Y.-Y., Christiani, D.C., 2003. Arsenic methylation and skin cancer risk in southwestern Taiwan. J Occup Environ Med 45, 241–248. https://doi.org/10.1097/01.jom.0000058336.05741.e8

Cheng, P.-S., Weng, S.-F., Chiang, C.-H., Lai, F.-J., 2016. Relationship between arsenic-containing drinking water and skin cancers in the arseniasis endemic areas in Taiwan. The Journal of Dermatology 43, 181–186. https://doi.org/10.1111/1346-8138.13058

Chervona, Y., Hall, M.N., Arita, A., Wu, F., Sun, H., Tseng, H.-C., Ali, E., Uddin, M.N., Liu, X., Zoroddu, M.A., Gamble, M.V., Costa, M., 2012. Associations between Arsenic Exposure and Global Posttranslational Histone

Modifications among Adults in Bangladesh. Cancer Epidemiol Biomarkers Prev 21, 2252–2260. https://doi.org/10.1158/1055-9965.EPI-12-0833
Chou, W.-C., Jie, C., Kenedy, A.A., Jones, R.J., Trush, M.A., Dang, C.V., 2004. Role of NADPH oxidase in arsenic-induced reactive oxygen species formation and cytotoxicity in myeloid leukemia cells. Proc. Natl. Acad. Sci. U.S.A. 101, 4578–4583. https://doi.org/10.1073/pnas.0306687101
Choudhury, Md.I.M., Shabnam, N., Ahsan, T., Ahsan, S.M.A., Kabir, Md.S., Khan, R.Md., Miah, Md.A., Uddin, Mohd.K., Liton, Md.A.R., 2018. Cutaneous Malignancy due to Arsenicosis in Bangladesh: 12-Year Study in Tertiary Level Hospital. Biomed Res Int 2018, 4678362. https://doi.org/10.1155/2018/4678362
Chung, C.-J., Huang, Y.-L., Huang, Y.-K., Wu, M.-M., Chen, S.-Y., Hsueh, Y.-M., Chen, C.-J., 2013. Urinary arsenic profiles and the risks of cancer mortality: A population-based 20-year follow-up study in arseniasis-endemic areas in Taiwan. Environmental Research 122, 25–30. https://doi.org/10.1016/j.envres.2012.11.007
Clauson, C., Schärer, O.D., Niedernhofer, L., 2013. Advances in Understanding the Complex Mechanisms of DNA Interstrand Cross-Link Repair. Cold Spring Harb Perspect Biol 5, a012732. https://doi.org/10.1101/cshperspect.a012732
Cleaver, J.E., 2011. γH2Ax: Biomarker of Damage or Functional Participant in DNA Repair “All that Glitters Is not Gold!” Photochemistry and Photobiology 87, 1230–1239. https://doi.org/10.1111/j.1751-1097.2011.00995.x
Cohen, I.S., Bar, C., Paz-Elizur, T., Ainbinder, E., Leopold, K., de Wind, N., Geacintov, N., Livneh, Z., 2015. DNA lesion identity drives choice of damage tolerance pathway in murine cell chromosomes. Nucleic Acids Res 43, 1637–1645. https://doi.org/10.1093/nar/gku1398
Colognato, R., Coppedè, F., Ponti, J., Sabbioni, E., Migliore, L., 2007. Genotoxicity induced by arsenic compounds in peripheral human lymphocytes analysed by cytokinesis-block micronucleus assay. Mutagenesis 22, 255–261. https://doi.org/10.1093/mutage/gem010
Cooper, K., Yager, J., Hudson, L., 2014. Melanocytes and keratinocytes have distinct and shared responses to ultraviolet radiation and arsenic. Toxicol Lett 224, 407–415. https://doi.org/10.1016/j.toxlet.2013.11.010
Cooper, K.L., King, B.S., Sandoval, M.M., Liu, K.J., Hudson, L.G., 2013. Reduction of arsenite-enhanced ultraviolet radiation-induced DNA damage by supplemental zinc. Toxicol Appl Pharmacol 269, 81–88. https://doi.org/10.1016/j.taap.2013.03.008
Cooper, K.L., Liu, K.J., Hudson, L.G., 2009. Enhanced ROS production and redox signaling with combined arsenite and UVA exposure: Contribution of NADPH oxidase. Free Radic Biol Med 47, 381–388. https://doi.org/10.1016/j.freeradbiomed.2009.04.034
Cooper, K.L., Liu, K.J., Hudson, L.G., 2007. Contributions of reactive oxygen species and mitogen-activated protein kinase signaling in arsenite-

stimulated hemeoxygenase-1 production. Toxicol Appl Pharmacol 218, 119–127. https://doi.org/10.1016/j.taap.2006.09.020
Cooper, K.L., Volk, L.B., Dominguez, D.R., Duran, A.D., Ke Jian Liu, K.J., Hudson, L.G., 2022. Contribution of NADPH oxidase to the retention of UVR-induced DNA damage by arsenic. Toxicology and Applied Pharmacology 434, 115799. https://doi.org/10.1016/j.taap.2021.115799
Corsini, E., Asti, L., Viviani, B., Marinovich, M., Galli, C.L., 1999. Sodium Arsenate Induces Overproduction of Interleukin-1α in Murine Keratinocytes: Role of Mitochondria. J Invest Dermatol 113, 760–765. https://doi.org/10.1046/j.1523-1747.1999.00748.x
Costes, A., Lambert, S.A.E., 2012. Homologous recombination as a replication fork escort: fork-protection and recovery. Biomolecules 3, 39–71. https://doi.org/10.3390/biom3010039
Dasari, S., Tchounwou, P.B., 2014. Cisplatin in cancer therapy: molecular mechanisms of action. Eur J Pharmacol 0, 364–378. https://doi.org/10.1016/j.ejphar.2014.07.025
Day, T.A., Palle, K., Barkley, L.R., Kakusho, N., Zou, Y., Tateishi, S., Verreault, A., Masai, H., Vaziri, C., 2010. Phosphorylated Rad18 directs DNA Polymerase η to sites of stalled replication. Journal of Cell Biology 191, 953–966. https://doi.org/10.1083/jcb.201006043
de Jager, T.L., Cockrell, A.E., Du Plessis, S.S., 2017. Ultraviolet Light Induced Generation of Reactive Oxygen Species. Adv Exp Med Biol 996, 15–23. https://doi.org/10.1007/978-3-319-56017-5_2
de la Rosa, R., Steinmaus, C., Akers, N.K., Conde, L., Ferreccio, C., Kalman, D., Zhang, K.R., Skibola, C.F., Smith, A.H., Zhang, L., Smith, M.T., 2017. Associations between arsenic (+3 oxidation state) methyltransferase (AS3MT) and N-6 adenine-specific DNA methyltransferase 1 (N6AMT1) polymorphisms, arsenic metabolism, and cancer risk in a chilean population. Environ Mol Mutagen 58, 411–422. https://doi.org/10.1002/em.22104
De Zio, D., Cianfanelli, V., Cecconi, F., 2013. New Insights into the Link Between DNA Damage and Apoptosis. Antioxid Redox Signal 19, 559–571. https://doi.org/10.1089/ars.2012.4938
Delgado, D.A., Chernoff, M., Huang, L., Tong, L., Chen, L., Jasmine, F., Shinkle, J., Cole, S.A., Haack, K., Kent, J., Umans, J., Best, L.G., Nelson, H., Griend, D.V., Graziano, J., Kibriya, M.G., Navas-Acien, A., Karagas, M.R., Ahsan, H., Pierce, B.L., 2021. Rare, Protein-Altering Variants in AS3MT and Arsenic Metabolism Efficiency: A Multi-Population Association Study. Environ Health Perspect 129, 47007. https://doi.org/10.1289/EHP8152
Despras, E., Sittewelle, M., Pouvelle, C., Delrieu, N., Cordonnier, A.M., Kannouche, P.L., 2016. Rad18-dependent SUMOylation of human specialized DNA polymerase eta is required to prevent under-replicated DNA. Nat Commun 7, 13326. https://doi.org/10.1038/ncomms13326
Di, Y., Tamás, M.J., 2007. Regulation of the arsenic-responsive transcription factor Yap8p involves the ubiquitin-proteasome pathway. Journal of Cell Science 120, 256–264. https://doi.org/10.1242/jcs.03346

Ding, W., Hudson, L.G., Liu, K.J., 2005a. Inorganic arsenic compounds cause oxidative damage to DNA and protein by inducing ROS and RNS generation in human keratinocytes. Mol Cell Biochem 279, 105–112. https://doi.org/10.1007/s11010-005-8227-y

Ding, W., Hudson, L.G., Liu, K.J., 2005b. Inorganic arsenic compounds cause oxidative damage to DNA and protein by inducing ROS and RNS generation in human keratinocytes. Mol. Cell. Biochem. 279, 105–112. https://doi.org/10.1007/s11010-005-8227-y

Ding, W., Hudson, L.G., Sun, X., Feng, C., Liu, K.J., 2008. As(III) inhibits ultraviolet radiation-induced cyclobutane pyrimidine dimers repair via generation of nitric oxide in human keratinocytes. Free Radic Biol Med 45, 1065–1072. https://doi.org/10.1016/j.freeradbiomed.2008.06.022

Ding, W., Liu, W., Cooper, K.L., Qin, X.-J., de Souza Bergo, P.L., Hudson, L.G., Liu, K.J., 2009. Inhibition of Poly(ADP-ribose) Polymerase-1 by Arsenite Interferes with Repair of Oxidative DNA Damage. J Biol Chem 284, 6809–6817. https://doi.org/10.1074/jbc.M805566200

Ding, X., Zhang, A., Li, C., Ma, L., Tang, S., Wang, Q., Yang, G., Li, J., 2020. The role of H3K9me2-regulated base excision repair genes in the repair of DNA damage induced by arsenic in HaCaT cells and the effects of Ginkgo biloba extract intervention. Environ Toxicol n/a. https://doi.org/10.1002/tox.23088

Ding, X., Zhou, X., Cooper, K.L., Huestis, J., Hudson, L.G., Liu, K.J., 2017. Differential sensitivities of cellular XPA and PARP-1 to arsenite inhibition and zinc rescue. Toxicol Appl Pharmacol 331, 108–115. https://doi.org/10.1016/j.taap.2017.05.031

Dong, J., Wang, J., Qian, Q., Li, G., Yang, D., Jiang, C., 2019. Micronucleus assay for monitoring the genotoxic effects of arsenic in human populations: A systematic review of the literature and meta-analysis. Mutation Research/Reviews in Mutation Research, Epigenetic mechanisms in DNA repair and cancer 780, 1–10. https://doi.org/10.1016/j.mrrev.2019.02.002

Dreval, K., Tryndyak, V., Kindrat, I., Twaddle, N.C., Orisakwe, O.E., Mudalige, T.K., Beland, F.A., Doerge, D.R., Pogribny, I.P., 2018. Cellular and Molecular Effects of Prolonged Low-Level Sodium Arsenite Exposure on Human Hepatic HepaRG Cells. Toxicological Sciences 162, 676–687. https://doi.org/10.1093/toxsci/kfx290

Drobna, Z., Styblo, M., Thomas, D.J., 2009. An Overview of Arsenic Metabolism and Toxicity. Current Protocols in Toxicology 42, 4.31.1-4.31.6. https://doi.org/10.1002/0471140856.tx0431s42

Duan, J., Gaffrey, M.J., Qian, W.-J., 2017. Quantitative proteomic characterization of redox-dependent post-translational modifications on protein cysteines. Mol. BioSyst. 13, 816–829. https://doi.org/10.1039/C6MB00861E

Dutta, K., Prasad, P., Sinha, D., 2015. Chronic low level arsenic exposure evokes inflammatory responses and DNA damage. International Journal

of Hygiene and Environmental Health 218, 564–574. https://doi.org/10.1016/j.ijheh.2015.06.003
Ebert, F., Weiss, A., Bültemeyer, M., Hamann, I., Hartwig, A., Schwerdtle, T., 2011. Arsenicals affect base excision repair by several mechanisms. Mutation Research/Fundamental and Molecular Mechanisms of Mutagenesis 715, 32–41. https://doi.org/10.1016/j.mrfmmm.2011.07.004
Eom, K.S., Cheong, J.S., Lee, S.J., 2016. Structural Analyses of Zinc Finger Domains for Specific Interactions with DNA. J Microbiol Biotechnol 26, 2019–2029. https://doi.org/10.4014/jmb.1609.09021
Ezeh, P.C., Lauer, F.T., Liu, K.J., Hudson, L.G., Burchiel, S.W., 2015. Arsenite interacts with DBC at low levels to suppress bone marrow lymphoid progenitors in mice. Biol Trace Elem Res 166, 82–88. https://doi.org/10.1007/s12011-015-0279-6
Fadda, E., 2015. Role of the XPA protein in the NER pathway: A perspective on the function of structural disorder in macromolecular assembly. Comput Struct Biotechnol J 14, 78–85. https://doi.org/10.1016/j.csbj.2015.11.007
Fagerberg, L., Hallström, B.M., Oksvold, P., Kampf, C., Djureinovic, D., Odeberg, J., Habuka, M., Tahmasebpoor, S., Danielsson, A., Edlund, K., Asplund, A., Sjöstedt, E., Lundberg, E., Szigyarto, C.A.-K., Skogs, M., Takanen, J.O., Berling, H., Tegel, H., Mulder, J., Nilsson, P., Schwenk, J.M., Lindskog, C., Danielsson, F., Mardinoglu, A., Sivertsson, Å., von Feilitzen, K., Forsberg, M., Zwahlen, M., Olsson, I., Navani, S., Huss, M., Nielsen, J., Ponten, F., Uhlén, M., 2014. Analysis of the Human Tissue-specific Expression by Genome-wide Integration of Transcriptomics and Antibody-based Proteomics. Mol Cell Proteomics 13, 397–406. https://doi.org/10.1074/mcp.M113.035600
Faita, F., Cori, L., Bianchi, F., Andreassi, M.G., 2013. Arsenic-Induced Genotoxicity and Genetic Susceptibility to Arsenic-Related Pathologies. Int J Environ Res Public Health 10, 1527–1546. https://doi.org/10.3390/ijerph10041527
Farzan, S.F., Shahriar, M., Kibriya, M.G., Jasmine, F., Sarwar, G., Slavkovic, V., Graziano, J.H., Ahsan, H., Argos, M., 2021. Urinary arsenic and relative telomere length in 5–7 year old children in Bangladesh. Environment International 156, 106765. https://doi.org/10.1016/j.envint.2021.106765
Federico, M.B., Vallerga, M.B., Radl, A., Paviolo, N.S., Bocco, J.L., Giorgio, M.D., Soria, G., Gottifredi, V., 2016. Chromosomal Integrity after UV Irradiation Requires FANCD2-Mediated Repair of Double Strand Breaks. PLOS Genetics 12, e1005792. https://doi.org/10.1371/journal.pgen.1005792
Fernández, M.I., Valdebenito, P., Delgado, I., Segebre, J., Chaparro, E., Fuentealba, D., Castillo, M., Vial, C., Barroso, J.P., Ziegler, A., Bustamante, A., 2020. Impact of arsenic exposure on clinicopathological characteristics of bladder cancer: A comparative study between patients from an arsenic-exposed region and nonexposed reference sites. Urol Oncol 38, 40.e1-40.e7. https://doi.org/10.1016/j.urolonc.2019.09.013

Fernández-Medarde, A., Santos, E., 2011. Ras in Cancer and Developmental Diseases. Genes Cancer 2, 344–358. https://doi.org/10.1177/1947601911411084
Ferreccio, C., Smith, A.H., Durán, V., Barlaro, T., Benítez, H., Valdés, R., Aguirre, J.J., Moore, L.E., Acevedo, J., Vásquez, M.I., Pérez, L., Yuan, Y., Liaw, J., Cantor, K.P., Steinmaus, C., 2013a. Case-control study of arsenic in drinking water and kidney cancer in uniquely exposed Northern Chile. Am J Epidemiol 178, 813–818. https://doi.org/10.1093/aje/kwt059
Ferreccio, C., Yuan, Y., Calle, J., Benítez, H., Parra, R.L., Acevedo, J., Smith, A.H., Liaw, J., Steinmaus, C., 2013b. Arsenic, Tobacco Smoke, and Occupation. Epidemiology 24, 898–905. https://doi.org/10.1097/EDE.0b013e31829e3e03
Flora, S.J., 1999. Arsenic-Induced Oxidative Stress and Its Reversibility Following Combined Administration of N-Acetylcysteine and Meso 2,3–Dimercaptosuccinic Acid in Rats. Clinical and Experimental Pharmacology and Physiology 26, 865–869. https://doi.org/10.1046/j.1440-1681.1999.03157.x
Foglizzo, M., Middleton, A.J., Day, C.L., 2016. Structure and Function of the RING Domains of RNF20 and RNF40, Dimeric E3 Ligases that Monoubiquitylate Histone H2B. Journal of Molecular Biology 428, 4073–4086. https://doi.org/10.1016/j.jmb.2016.07.025
Fu, M., Blackshear, P.J., 2017. RNA-binding proteins in immune regulation: a focus on CCCH zinc finger proteins. Nat Rev Immunol 17, 130–143. https://doi.org/10.1038/nri.2016.129
Gaillard, H., García-Muse, T., Aguilera, A., 2015. Replication stress and cancer. Nat Rev Cancer 15, 276–289. https://doi.org/10.1038/nrc3916
Gamboa-Loira, B., Cebrián, M.E., Franco-Marina, F., López-Carrillo, L., 2017. Arsenic metabolism and cancer risk: A meta-analysis. Environ Res 156, 551–558. https://doi.org/10.1016/j.envres.2017.04.016
Ganapathy, S., Liu, J., Xiong, R., Yu, T., Makriyannis, A., Chen, C., 2019. Chronic low dose arsenic exposure preferentially perturbs mitotic phase of the cell cycle. Genes Cancer 10, 39–51. https://doi.org/10.18632/genesandcancer.185
Gao, J., Wen, S., Zhou, H., Feng, S., 2015. De-methylation of displacement loop of mitochondrial DNA is associated with increased mitochondrial copy number and nicotinamide adenine dinucleotide subunit 2 expression in colorectal cancer. Molecular Medicine Reports 12, 7033–7038. https://doi.org/10.3892/mmr.2015.4256
Germolec, D.R., Yoshida, T., Gaido, K., Wilmer, J.L., Simeonova, P.P., Kayama, F., Burleson, F., Dong, W., Lange, R.W., Luster, M.I., 1996. Arsenic induces overexpression of growth factors in human keratinocytes. Toxicology and Applied Pharmacology 141, 308–318. https://doi.org/10.1016/S0041-008X(96)80037-8
Ghosh, S., Basu, M., Banerjee, K., Chaudhury, S.P., Paul, T., Bera, D.K., Pal, D.K., Sk, U.H., Panda, C.K., Ghosh, A., 2021. Arsenic level in bladder tumor of patients from an exposed population: association with

progression and prognosis. Future Oncol 17, 1311–1323. https://doi.org/10.2217/fon-2020-0154
Gibson, T.J., Postma, J.P., Brown, R.S., Argos, P., 1988. A model for the tertiary structure of the 28 residue DNA-binding motif ('zinc finger') common to many eukaryotic transcriptional regulatory proteins. Protein Eng 2, 209–18. https://doi.org/10.1093/protein/2.3.209
Glady, A., Tanaka, M., Moniaga, C.S., Yasui, M., Hara-Chikuma, M., 2018. Involvement of NADPH oxidase 1 in UVB-induced cell signaling and cytotoxicity in human keratinocytes. Biochem Biophys Rep 14, 7–15. https://doi.org/10.1016/j.bbrep.2018.03.004
Gossai, A., Zens, M.S., Punshon, T., Jackson, B.P., Perry, A.E., Karagas, M.R., 2017. Rice Consumption and Squamous Cell Carcinoma of the Skin in a United States Population. Environ Health Perspect 125, 097005. https://doi.org/10.1289/EHP1065
Gu, S., Lai, Y., Chen, H., Liu, Y., Zhang, Z., 2017. miR-155 mediates arsenic trioxide resistance by activating Nrf2 and suppressing apoptosis in lung cancer cells. Scientific Reports 7, 12155. https://doi.org/10.1038/s41598-017-06061-x
Gundert-Remy, U., Damm, G., Foth, H., Freyberger, A., Gebel, T., Golka, K., Röhl, C., Schupp, T., Wollin, K.-M., Hengstler, J.G., 2015. High exposure to inorganic arsenic by food: the need for risk reduction. Arch Toxicol 89, 2219–2227. https://doi.org/10.1007/s00204-015-1627-1
Guo, H.-R., Wang, N.-S., Hu, H., Monson, R.R., 2004. Cell type specificity of lung cancer associated with arsenic ingestion. Cancer Epidemiol Biomarkers Prev 13, 638–643.
Harmon, M.E., Lewis, J., Miller, C., Hoover, J., Ali, A.-M.S., Shuey, C., Cajero, M., Lucas, S., Pacheco, B., Erdei, E., Ramone, S., Nez, T., Campen, M.J., Gonzales, M., 2018. Arsenic association with circulating oxidized low-density lipoprotein in a Native American community. Journal of Toxicology and Environmental Health, Part A 81, 535–548. https://doi.org/10.1080/15287394.2018.1443860
Hartwig, A., Arand, M., Epe, B., Guth, S., Jahnke, G., Lampen, A., Martus, H.-J., Monien, B., Rietjens, I.M.C.M., Schmitz-Spanke, S., Schriever-Schwemmer, G., Steinberg, P., Eisenbrand, G., 2020. Mode of action-based risk assessment of genotoxic carcinogens. Arch Toxicol 94, 1787–1877. https://doi.org/10.1007/s00204-020-02733-2
Hartwig, A., Asmuss, M., Ehleben, I., Herzer, U., Kostelac, D., Pelzer, A., Schwerdtle, T., Bürkle, A., 2002. Interference by toxic metal ions with DNA repair processes and cell cycle control: molecular mechanisms. Environ. Health Perspect. 110 Suppl 5, 797–799. https://doi.org/10.1289/ehp.02110s5797
Hartwig, A., Blessing, H., Schwerdtle, T., Walter, I., 2003. Modulation of DNA repair processes by arsenic and selenium compounds. Toxicology, DNA Repair in Toxicology 193, 161–169. https://doi.org/10.1016/j.tox.2003.08.004

Hartwig, A., Schwerdtle, T., 2002. Interactions by carcinogenic metal compounds with DNA repair processes: toxicological implications. Toxicol. Lett. 127, 47–54. https://doi.org/10.1016/s0378-4274(01)00482-9
Hassani, S., Khaleghian, A., Ahmadian, S., Alizadeh, S., Alimoghaddam, K., Ghavamzadeh, A., Ghaffari, S.H., 2018. Redistribution of cell cycle by arsenic trioxide is associated with demethylation and expression changes of cell cycle related genes in acute promyelocytic leukemia cell line (NB4). Ann Hematol 97, 83–93. https://doi.org/10.1007/s00277-017-3163-y
Hayakawa, T., Kobayashi, Y., Cui, X., Hirano, S., 2005. A new metabolic pathway of arsenite: arsenic–glutathione complexes are substrates for human arsenic methyltransferase Cyt19. Arch Toxicol 79, 183–191. https://doi.org/10.1007/s00204-004-0620-x
Hayes, J.D., Dinkova-Kostova, A.T., Tew, K.D., 2020. Oxidative Stress in Cancer. Cancer Cell 38, 167–197. https://doi.org/10.1016/j.ccell.2020.06.001
Hays, A.M., Srinivasan, D., Witten, M.L., Carter, D.E., Lantz, R.C., 2006. Arsenic and Cigarette Smoke Synergistically Increase DNA Oxidation in the Lung. Toxicol Pathol 34, 396–404. https://doi.org/10.1080/01926230600824926
He, Y.-Y., Huang, J.-L., Block, M.L., Hong, J.-S., Chignell, C.F., 2005. Role of Phagocyte Oxidase in UVA-Induced Oxidative Stress and Apoptosis in Keratinocytes. Journal of Investigative Dermatology 125, 560–566. https://doi.org/10.1111/j.0022-202X.2005.23851.x
Heck, J.E., Andrew, A.S., Onega, T., Rigas, J.R., Jackson, B.P., Karagas, M.R., Duell, E.J., 2009. Lung cancer in a U.S. population with low to moderate arsenic exposure. Environ Health Perspect 117, 1718–1723. https://doi.org/10.1289/ehp.0900566
Hedglin, M., Benkovic, S.J., 2015. Regulation of Rad6/Rad18 Activity During DNA Damage Tolerance. Annu Rev Biophys 44, 207–228. https://doi.org/10.1146/annurev-biophys-060414-033841
Hei, T.K., Liu, S.X., Waldren, C., 1998. Mutagenicity of arsenic in mammalian cells: Role of reactive oxygen species. PNAS 95, 8103–8107. https://doi.org/10.1073/pnas.95.14.8103
Hendel, A., Krijger, P.H.L., Diamant, N., Goren, Z., Langerak, P., Kim, J., Reißner, T., Lee, K., Geacintov, N.E., Carell, T., Myung, K., Tateishi, S., D'Andrea, A., Jacobs, H., Livneh, Z., 2011. PCNA Ubiquitination Is Important, But Not Essential for Translesion DNA Synthesis in Mammalian Cells. PLoS Genet 7. https://doi.org/10.1371/journal.pgen.1002262
Holcomb, N., Goswami, M., Han, S.G., Scott, T., D'Orazio, J., Orren, D.K., Gairola, C.G., Mellon, I., 2017. Inorganic arsenic inhibits the nucleotide excision repair pathway and reduces the expression of XPC. DNA Repair (Amst) 52, 70–80. https://doi.org/10.1016/j.dnarep.2017.02.009
Hossain, M.B., Vahter, M., Concha, G., Broberg, K., 2012. Environmental arsenic exposure and DNA methylation of the tumor suppressor gene p16 and the DNA repair gene MLH1: effect of arsenic metabolism and genotype. Metallomics 4, 1167–1175. https://doi.org/10.1039/c2mt20120h

Hou, D., Liu, Z., Xu, X., Liu, Q., Zhang, X., Kong, B., Wei, J.-J., Gong, Y., Shao, C., 2018. Increased oxidative stress mediates the antitumor effect of PARP inhibition in ovarian cancer. Redox Biology 17, 99–111. https://doi.org/10.1016/j.redox.2018.03.016

Howe, C.G., Gamble, M.V., 2016. Influence of Arsenic on Global Levels of Histone Posttranslational Modifications: a Review of the Literature and Challenges in the Field. Curr Envir Health Rpt 3, 225–237. https://doi.org/10.1007/s40572-016-0104-1

Hu, Y., Li, J., Lou, B., Wu, R., Wang, G., Lu, C., Wang, H., Pi, J., Xu, Y., 2020. The Role of Reactive Oxygen Species in Arsenic Toxicity. Biomolecules 10. https://doi.org/10.3390/biom10020240

Hu, Y., Su, L., Snow, E.T., 1998. Arsenic toxicity is enzyme specific and its affects on ligation are not caused by the direct inhibition of DNA repair enzymes. Mutat Res 408, 203–218. https://doi.org/10.1016/s0921-8777(98)00035-4

Huang, A., Hibbert, R.G., de Jong, R.N., Das, D., Sixma, T.K., Boelens, R., 2011. Symmetry and asymmetry of the RING-RING dimer of Rad18. J. Mol. Biol. 410, 424–435. https://doi.org/10.1016/j.jmb.2011.04.051

Huang, C., Ke, Q., Costa, M., Shi, X., 2004. Molecular mechanisms of arsenic carcinogenesis. Mol Cell Biochem 255, 57–66. https://doi.org/10.1023/B:MCBI.0000007261.04684.78

Huang, C.-Y., Lin, Y.-C., Shiue, H.-S., Chen, W.-J., Su, C.-T., Pu, Y.-S., Ao, P.-L., Hsueh, Y.-M., 2018. Comparison of arsenic methylation capacity and polymorphisms of arsenic methylation genes between bladder cancer and upper tract urothelial carcinoma. Toxicol Lett 295, 64–73. https://doi.org/10.1016/j.toxlet.2018.05.035

Huang, H.-H., Huang, J.-Y., Lung, C.-C., Wu, C.-L., Ho, C.-C., Sun, Y.-H., Ko, P.-C., Su, S.-Y., Chen, S.-C., Liaw, Y.-P., 2013. Cell-type specificity of lung cancer associated with low-dose soil heavy metal contamination in Taiwan: an ecological study. BMC Public Health 13, 330. https://doi.org/10.1186/1471-2458-13-330

Huang, J., Huen, M.S.Y., Kim, H., Leung, C.C.Y., Glover, J.N.M., Yu, X., Chen, J., 2009. RAD18 transmits DNA damage signalling to elicit homologous recombination repair. Nat Cell Biol 11, 592–603. https://doi.org/10.1038/ncb1865

Hubaux, R., Becker-Santos, D.D., Enfield, K.S., Rowbotham, D., Lam, S., Lam, W.L., Martinez, V.D., 2013. Molecular features in arsenic-induced lung tumors. Molecular Cancer 12, 20. https://doi.org/10.1186/1476-4598-12-20

Hudson, L.G., Choi, C., Newkirk, K.M., Parkhani, J., Cooper, K.L., Lu, P., Kusewitt, D.F., 2007. Ultraviolet radiation stimulates expression of Snail family transcription factors in keratinocytes. Mol Carcinog 46, 257–268. https://doi.org/10.1002/mc.20257

Hudson, L.G., Cooper, K.L., Atlas, S.R., King, B.S., Liu, K.J., 2016. Arsenic Interaction with Zinc Finger Motifs, in: States, J.C. (Ed.), Arsenic: Exposure Sources, Health Risks, and Mechanisms of Toxicity. John Wiley & Sons, Inc, Hoboken, NJ.

Huestis, J., Zhou, X., Chen, L., Feng, C., Hudson, L.G., Liu, K.J., 2016. KINETICS AND THERMODYNAMICS OF ZINC(II) AND ARSENIC(III) BINDING TO XPA AND PARP-1 ZINC FINGER PEPTIDES. J Inorg Biochem 163, 45–52. https://doi.org/10.1016/j.jinorgbio.2016.08.003

Hughes, M.F., 2002. Arsenic toxicity and potential mechanisms of action. Toxicology Letters 133, 1–16. https://doi.org/10.1016/S0378-4274(02)00084-X

Hughes, M.F., Beck, B.D., Chen, Y., Lewis, A.S., Thomas, D.J., 2011. Arsenic Exposure and Toxicology: A Historical Perspective. Toxicol Sci 123, 305–332. https://doi.org/10.1093/toxsci/kfr184

Hughes, M.F., Kenyon, E.M., Edwards, B.C., Mitchell, C.T., Razo, L.M.D., Thomas, D.J., 2003. Accumulation and metabolism of arsenic in mice after repeated oral administration of arsenate. Toxicology and Applied Pharmacology 191, 202–210. https://doi.org/10.1016/S0041-008X(03)00249-7

Hunt, K.M., Srivastava, R.K., Elmets, C.A., Athar, M., 2014. The mechanistic basis of arsenicosis: pathogenesis of skin cancer. Cancer Lett 354, 211–219. https://doi.org/10.1016/j.canlet.2014.08.016

IARC, 2004. Some drinking-water disinfectants and contaminants, including arsenic. IARC Monogr Eval Carcinog Risks Hum 84, 1–477.

Inagaki, A., Sleddens-Linkels, E., Cappellen, W.A. van, Hibbert, R.G., Sixma, T.K., Hoeijmakers, J.H.J., Grootegoed, J.A., Baarends, W.M., 2011. Human RAD18 Interacts with Ubiquitylated Chromatin Components and Facilitates RAD9 Recruitment to DNA Double Strand Breaks. PLOS ONE 6, e23155. https://doi.org/10.1371/journal.pone.0023155

Inagaki, A., van Cappellen, W.A., van der Laan, R., Houtsmuller, A.B., Hoeijmakers, J.H.J., Grootegoed, J.A., Baarends, W.M., 2009. Dynamic localization of human RAD18 during the cell cycle and a functional connection with DNA double-strand break repair. DNA Repair (Amst) 8, 190–201. https://doi.org/10.1016/j.dnarep.2008.10.008

Ince, S., Kucukkurt, I., Acaroz, U., Arslan-Acaroz, D., Varol, N., 2019. Boron ameliorates arsenic-induced DNA damage, proinflammatory cytokine gene expressions, oxidant/antioxidant status, and biochemical parameters in rats. Journal of Biochemical and Molecular Toxicology 33, e22252. https://doi.org/10.1002/jbt.22252

Jacobson, T., Navarrete, C., Sharma, S.K., Sideri, T.C., Ibstedt, S., Priya, S., Grant, C.M., Christen, P., Goloubinoff, P., Tamás, M.J., 2012. Arsenite interferes with protein folding and triggers formation of protein aggregates in yeast. J Cell Sci 125, 5073–5083. https://doi.org/10.1242/jcs.107029

Jeanne, M., Lallemand-Breitenbach, V., Ferhi, O., Koken, M., Le Bras, M., Duffort, S., Peres, L., Berthier, C., Soilihi, H., Raught, B., de Thé, H., 2010. PML/RARA oxidation and arsenic binding initiate the antileukemia response of As2O3. Cancer Cell 18, 88–98. https://doi.org/10.1016/j.ccr.2010.06.003

Jiang, G., Gong, Z., Li, X.-F., Cullen, W.R., Le, X.C., 2003. Interaction of trivalent arsenicals with metallothionein. Chem. Res. Toxicol. 16, 873–880. https://doi.org/10.1021/tx034053g

Jiang, J., Bellani, M., Li, L., Wang, P., Seidman, M.M., Wang, Y., 2017. Arsenite Binds to the RING Finger Domain of FANCL E3 Ubiquitin Ligase and Inhibits DNA Interstrand Crosslink Repair. ACS Chem. Biol. 12, 1858–1866. https://doi.org/10.1021/acschembio.6b01135

Jomova, K., Jenisova, Z., Feszterova, M., Baros, S., Liska, J., Hudecova, D., Rhodes, C.J., Valko, M., 2011. Arsenic: toxicity, oxidative stress and human disease. Journal of Applied Toxicology 31, 95–107. https://doi.org/10.1002/jat.1649

Kannouche, P.L., Wing, J., Lehmann, A.R., 2004. Interaction of Human DNA Polymerase η with Monoubiquitinated PCNA: A Possible Mechanism for the Polymerase Switch in Response to DNA Damage. Molecular Cell 14, 491–500. https://doi.org/10.1016/S1097-2765(04)00259-X

Kao, Y.-T., Wu, C.-H., Wu, S.-Y., Lan, S.-H., Liu, H.-S., Tseng, Y.-S., 2017. Arsenic treatment increase Aurora-A overexpression through E2F1 activation in bladder cells. BMC Cancer 17, 277. https://doi.org/10.1186/s12885-017-3253-1

Karagas, M.R., Gossai, A., Pierce, B., Ahsan, H., 2015. Drinking Water Arsenic Contamination, Skin Lesions, and Malignancies: A Systematic Review of the Global Evidence. Curr Environ Health Rep 2, 52–68. https://doi.org/10.1007/s40572-014-0040-x

Karagas, M.R., Punshon, T., Davis, M., Bulka, C.M., Slaughter, F., Karalis, D., Argos, M., Ahsan, H., 2019. Rice Intake and Emerging Concerns on Arsenic in Rice: a Review of the Human Evidence and Methodologic Challenges. Curr Environ Health Rep 6, 361–372. https://doi.org/10.1007/s40572-019-00249-1

Karagas, M.R., Tosteson, T.D., Morris, J.S., Demidenko, E., Mott, L.A., Heaney, J., Schned, A., 2004. Incidence of transitional cell carcinoma of the bladder and arsenic exposure in New Hampshire. Cancer Causes Control 15, 465–472. https://doi.org/10.1023/B:CACO.0000036452.55199.a3

Kato, K., Hayashi, H., Hasegawa, A., Yamanaka, K., Okada, S., 1994. DNA damage induced in cultured human alveolar (L-132) cells by exposure to dimethylarsinic acid. Environ Health Perspect 102 Suppl 3, 285–288. https://doi.org/10.1289/ehp.94102s3285

Kayajanian, G., 2003. Arsenic, cancer, and thoughtless policy. Ecotoxicology and Environmental Safety 55, 139–142. https://doi.org/10.1016/S0147-6513(02)00042-8

Kenyon, E.M., Del Razo, L.M., Hughes, M.F., 2005. Tissue Distribution and Urinary Excretion of Inorganic Arsenic and Its Methylated Metabolites in Mice Following Acute Oral Administration of Arsenate. Toxicological Sciences 85, 468–475. https://doi.org/10.1093/toxsci/kfi107

Kessel, M., Liu, S.X., Xu, A., Santella, R., Hei, T.K., 2002. Arsenic induces oxidative DNA damage in mammalian cells. Mol Cell Biochem 234, 301–308. https://doi.org/10.1023/A:1015927406142

Kim, T.-H., Seo, J.-W., Hong, Y.-S., Song, K.-H., 2017. Case–control study of chronic low-level exposure of inorganic arsenic species and non-melanoma skin cancer. The Journal of Dermatology 44, 1374–1379. https://doi.org/10.1111/1346-8138.13993
Kim, Y., He, Y.-Y., 2014. Ultraviolet radiation-induced non-melanoma skin cancer: Regulation of DNA damage repair and inflammation. Genes Dis 1, 188–198. https://doi.org/10.1016/j.gendis.2014.08.005
King, B.S., Cooper, K.L., Liu, K.J., Hudson, L.G., 2012. Poly(ADP-ribose) contributes to an association between poly(ADP-ribose) polymerase-1 and xeroderma pigmentosum complementation group A in nucleotide excision repair. J Biol Chem 287, 39824–39833. https://doi.org/10.1074/jbc.M112.393504
Kitchin, K.T., Wallace, K., 2006a. Dissociation of arsenite-peptide complexes: Triphasic nature, rate constants, half-lives, and biological importance. Journal of Biochemical and Molecular Toxicology 20, 48–56. https://doi.org/10.1002/jbt.20108
Kitchin, K.T., Wallace, K., 2006b. Arsenite binding to synthetic peptides: The effect of increasing length between two cysteines. Journal of Biochemical and Molecular Toxicology 20, 35–38. https://doi.org/10.1002/jbt.20112
Klug, A., 2010. The discovery of zinc fingers and their development for practical applications in gene regulation and genome manipulation. Q Rev Biophys 43, 1–21. https://doi.org/10.1017/S0033583510000089
Ko, H.L., Ren, E.C., 2012. Functional Aspects of PARP1 in DNA Repair and Transcription. Biomolecules 2, 524–548. https://doi.org/10.3390/biom2040524
Kobayashi, S., Kasaishi, Y., Nakada, S., Takagi, T., Era, S., Motegi, A., Chiu, R.K., Takeda, S., Hirota, K., 2015. Rad18 and Rnf8 facilitate homologous recombination by two distinct mechanisms, promoting Rad51 focus formation and suppressing the toxic effect of nonhomologous end joining. Oncogene 34, 4403–4411. https://doi.org/10.1038/onc.2014.371
Koutros, S., Baris, D., Waddell, R., Beane Freeman, L.E., Colt, J.S., Schwenn, M., Johnson, A., Ward, M.H., Hosain, G.M., Moore, L.E., Stolzenberg-Solomon, R., Rothman, N., Karagas, M.R., Silverman, D.T., 2018. Potential effect modifiers of the arsenic-bladder cancer risk relationship. Int J Cancer 143, 2640–2646. https://doi.org/10.1002/ijc.31720
Krajewski, A.K., Jimenez, M.P., Rappazzo, K.M., Lobdell, D.T., Jagai, J.S., 2021. Aggregated cumulative county arsenic in drinking water and associations with bladder, colorectal, and kidney cancers, accounting for population served. J Expo Sci Environ Epidemiol 31, 979–989. https://doi.org/10.1038/s41370-021-00314-8
Krishna, S.S., Majumdar, I., Grishin, N.V., 2003. Structural classification of zinc fingersSURVEY AND SUMMARY. Nucleic Acids Res 31, 532–550. https://doi.org/10.1093/nar/gkg161
Kumagai, Y., Sumi, D., 2007. Arsenic: Signal Transduction, Transcription Factor, and Biotransformation Involved in Cellular Response and Toxicity. Annu.

Rev. Pharmacol. Toxicol. 47, 243–262. https://doi.org/10.1146/annurev.pharmtox.47.120505.105144
Kumar, P., Gao, Q., Ning, Y., Wang, Z., Krebsbach, P.H., Polverini, P.J., 2008. Arsenic trioxide enhances the therapeutic efficacy of radiation treatment of oral squamous carcinoma while protecting bone. Mol Cancer Ther 7, 2060–2069. https://doi.org/10.1158/1535-7163.MCT-08-0287
Kuo, Y.-C., Lo, Y.-S., Guo, H.-R., 2017. Lung Cancer Associated with Arsenic Ingestion: Cell-type Specificity and Dose Response. Epidemiology 28 Suppl 1, S106–S112. https://doi.org/10.1097/EDE.0000000000000743
Kwon, M., Leibowitz, M.L., Lee, J.-H., 2020. Small but mighty: the causes and consequences of micronucleus rupture. Experimental & Molecular Medicine 52, 1777–1786. https://doi.org/10.1038/s12276-020-00529-z
Lake, R.J., Geyko, A., Hemashettar, G., Zhao, Y., Fan, H.-Y., 2010. UV-induced association of the CSB remodeling protein with chromatin requires ATP-dependent relief of N-terminal autorepression. Mol Cell 37, 235–246. https://doi.org/10.1016/j.molcel.2009.10.027
Lamm, S.H., Boroje, I.J., Ferdosi, H., Ahn, J., 2021. A review of low-dose arsenic risks and human cancers. Toxicology 456, 152768. https://doi.org/10.1016/j.tox.2021.152768
Langston, M.E., Brown, H.E., Lynch, C.F., Roe, D.J., Dennis, L.K., 2022. Ambient UVR and Environmental Arsenic Exposure in Relation to Cutaneous Melanoma in Iowa. International Journal of Environmental Research and Public Health 19, 1742. https://doi.org/10.3390/ijerph19031742
Lee, C.-H., Wu, S.-B., Hong, C.-H., Chen, G.-S., Wei, Y.-H., Yu, H.-S., 2013. Involvement of mtDNA Damage Elicited by Oxidative Stress in the Arsenical Skin Cancers. Journal of Investigative Dermatology 133, 1890–1900. https://doi.org/10.1038/jid.2013.55
Lemarie, A., Bourdonnay, E., Morzadec, C., Fardel, O., Vernhet, L., 2008. Inorganic arsenic activates reduced NADPH oxidase in human primary macrophages through a Rho kinase/p38 kinase pathway. J Immunol 180, 6010–6017. https://doi.org/10.4049/jimmunol.180.9.6010
Leung, W., Baxley, R.M., Thakar, T., Chang, Y.-C., Rogers, C.B., Wang, L., Durrett, W., Tella, A., Moldovan, G.-L., Shima, N., Bielinsky, A.-K., 2022. A PCNA-K164R mutation impinges on origin activation and mitotic DNA synthesis. https://doi.org/10.1101/2020.06.25.172361
Li, D., Morimoto, K., Takeshita, T., Lu, Y., 2001. Arsenic induces DNA damage via reactive oxygen species in human cells. Environ Health Prev Med 6, 27–32. https://doi.org/10.1007/BF02897306
Li, F., Mao, G., Tong, D., Huang, J., Gu, L., Yang, W., Li, G.-M., 2013. The Histone Mark H3K36me3 Regulates Human DNA Mismatch Repair through its Interaction with MutSα. Cell 153, 590–600. https://doi.org/10.1016/j.cell.2013.03.025
Li, G.-M., 2008. Mechanisms and functions of DNA mismatch repair. Cell Research 18, 85–98. https://doi.org/10.1038/cr.2007.115

Li, H., Lin, J., Li, Y., Yan, J., Li, B., Zhang, W., Dong, Z., Chen, C., 2013. [Distribution of arsenic species and its DNA damage in subchronic arsenite-exposed mice]. Wei Sheng Yan Jiu 42, 764–769, 776.
Li, J., Packianathan, C., Rossman, T.G., Rosen, B.P., 2017. Nonsynonymous Polymorphisms in the Human AS3MT Arsenic Methylation Gene: Implications for Arsenic Toxicity. Chem. Res. Toxicol. 30, 1481–1491. https://doi.org/10.1021/acs.chemrestox.7b00113
Li, M., Sengupta, B., Benkovic, S.J., Lee, T.H., Hedglin, M., 2020. PCNA Monoubiquitination Is Regulated by Diffusion of Rad6/Rad18 Complexes along RPA Filaments. Biochemistry 59, 4694–4702. https://doi.org/10.1021/acs.biochem.0c00849
Liaw, J., Marshall, G., Yuan, Y., Ferreccio, C., Steinmaus, C., Smith, A.H., 2008. Increased childhood liver cancer mortality and arsenic in drinking water in northern Chile. Cancer Epidemiol Biomarkers Prev 17, 1982–1987. https://doi.org/10.1158/1055-9965.EPI-07-2816
Lieber, M.R., Gu, J., Lu, H., Shimazaki, N., Tsai, A.G., 2010. Nonhomologous DNA End Joining (NHEJ) and Chromosomal Translocations in Humans. Subcell Biochem 50, 279–296. https://doi.org/10.1007/978-90-481-3471-7_14
Lin, Y.-C., Chen, W.-J., Huang, C.-Y., Shiue, H.-S., Su, C.-T., Ao, P.-L., Pu, Y.-S., Hsueh, Y.-M., 2018. Polymorphisms of Arsenic (+3 Oxidation State) Methyltransferase and Arsenic Methylation Capacity Affect the Risk of Bladder Cancer. Toxicol Sci 164, 328–338. https://doi.org/10.1093/toxsci/kfy087
Linke, K., Mace, P.D., Smith, C.A., Vaux, D.L., Silke, J., Day, C.L., 2008. Structure of the MDM2/MDMX RING domain heterodimer reveals dimerization is required for their ubiquitylation in trans. Cell Death Differ 15, 841–8. https://doi.org/10.1038/sj.cdd.4402309
Liu, Z., Boles, E., Rosen, B.P., 2004. Arsenic Trioxide Uptake by Hexose Permeases in Saccharomyces cerevisiae*. Journal of Biological Chemistry 279, 17312–17318. https://doi.org/10.1074/jbc.M314006200
Liu, Z., Sanchez, M.A., Jiang, X., Boles, E., Landfear, S.M., Rosen, B.P., 2006. Mammalian glucose permease GLUT1 facilitates transport of arsenic trioxide and methylarsonous acid. Biochemical and Biophysical Research Communications 351, 424–430. https://doi.org/10.1016/j.bbrc.2006.10.054
Liu, Z., Shen, J., Carbrey, J.M., Mukhopadhyay, R., Agre, P., Rosen, B.P., 2002. Arsenite transport by mammalian aquaglyceroporins AQP7 and AQP9. Proceedings of the National Academy of Sciences 99, 6053–6058. https://doi.org/10.1073/pnas.092131899
Lou, J., Yang, Y., Gu, Q., Price, B.A., Qiu, Y., Fedoriw, Y., Desai, S., Mose, L.E., Chen, B., Tateishi, S., Parker, J.S., Vaziri, C., Wu, D., 2021. Rad18 mediates specific mutational signatures and shapes the genomic landscape of carcinogen-induced tumors in vivo. NAR Cancer 3, zcaa037. https://doi.org/10.1093/narcan/zcaa037
Lynn, S., Gurr, J.R., Lai, H.T., Jan, K.Y., 2000. NADH oxidase activation is involved in arsenite-induced oxidative DNA damage in human vascular

smooth muscle cells. Circ. Res. 86, 514–519. https://doi.org/10.1161/01.res.86.5.514
Lynn Shugene, Gurr Jia-Ran, Lai Hsien-Tsung, Jan Kun-Yan, 2000. NADH Oxidase Activation Is Involved in Arsenite-Induced Oxidative DNA Damage in Human Vascular Smooth Muscle Cells. Circulation Research 86, 514–519. https://doi.org/10.1161/01.RES.86.5.514
Ma, B., Stepanov, I., Hecht, S.S., 2019. Recent Studies on DNA Adducts Resulting from Human Exposure to Tobacco Smoke. Toxics 7. https://doi.org/10.3390/toxics7010016
Ma, X., Tang, T.-S., Guo, C., 2020. Regulation of translesion DNA synthesis in mammalian cells. Environmental and Molecular Mutagenesis 61, 680–692. https://doi.org/10.1002/em.22359
Mah, L.-J., El-Osta, A., Karagiannis, T.C., 2010. γH2AX: a sensitive molecular marker of DNA damage and repair. Leukemia 24, 679–686. https://doi.org/10.1038/leu.2010.6
Mahata, J., Argos, M., Verret, W., Kibriya, M.G., Santella, R.M., Ahsan, H., 2007. Effect of Selenium and Vitamin E Supplementation on Plasma Protein Carbonyl Levels in Patients With Arsenic-Related Skin Lesions. Nutrition and Cancer 60, 55–60. https://doi.org/10.1080/01635580701761282
Mahata, J., Basu, A., Ghoshal, S., Sarkar, J.N., Roy, A.K., Poddar, G., Nandy, A.K., Banerjee, A., Ray, K., Natarajan, A.T., Nilsson, R., Giri, A.K., 2003. Chromosomal aberrations and sister chromatid exchanges in individuals exposed to arsenic through drinking water in West Bengal, India. Mutation Research/Genetic Toxicology and Environmental Mutagenesis 534, 133–143. https://doi.org/10.1016/S1383-5718(02)00255-3
Maier, A., Schumann, B.L., Chang, X., Talaska, G., Puga, A., 2002. Arsenic co-exposure potentiates benzo[a]pyrene genotoxicity. Mutation Research/Genetic Toxicology and Environmental Mutagenesis 517, 101–111. https://doi.org/10.1016/S1383-5718(02)00057-8
Mailand, N., Gibbs-Seymour, I., Bekker-Jensen, S., 2013. Regulation of PCNA–protein interactions for genome stability. Nature Reviews Molecular Cell Biology 14, 269–282. https://doi.org/10.1038/nrm3562
Mäki-Paakkanen, J., Kurttio, P., Paldy, A., Pekkanen, J., 1998. Association between the clastogenic effect in peripheral lymphocytes and human exposure to arsenic through drinking water. Environ Mol Mutagen 32, 301–313. https://doi.org/10.1002/(sici)1098-2280(1998)32:4<301::aid-em3>3.0.co;2-i
Manna, P., Sinha, M., Sil, P.C., 2008. Protection of arsenic-induced testicular oxidative stress by arjunolic acid. Redox Report 13, 67–77. https://doi.org/10.1179/135100008X259169
Mar Wai, K., Umezaki, M., Mar, O., Umemura, M., Watanabe, C., 2019. Arsenic exposure through drinking Water and oxidative stress Status: A cross-sectional study in the Ayeyarwady region, Myanmar. Journal of Trace Elements in Medicine and Biology 54, 103–109. https://doi.org/10.1016/j.jtemb.2019.04.009

Marshall, G., Ferreccio, C., Yuan, Y., Bates, M.N., Steinmaus, C., Selvin, S., Liaw, J., Smith, A.H., 2007. Fifty-year study of lung and bladder cancer mortality in Chile related to arsenic in drinking water. J Natl Cancer Inst 99, 920–928. https://doi.org/10.1093/jnci/djm004

Martin, E.M., Fry, R.C., 2018. Environmental Influences on the Epigenome: Exposure- Associated DNA Methylation in Human Populations. Annu. Rev. Public Health 39, 309–333. https://doi.org/10.1146/annurev-publhealth-040617-014629

Martinez, V.D., Buys, T.P.H., Adonis, M., Benítez, H., Gallegos, I., Lam, S., Lam, W.L., Gil, L., 2010. Arsenic-related DNA copy-number alterations in lung squamous cell carcinomas. British Journal of Cancer 103, 1277–1283. https://doi.org/10.1038/sj.bjc.6605879

Martinez, V.D., Lam, W.L., 2021. Health Effects Associated With Pre- and Perinatal Exposure to Arsenic. Front Genet 12, 664717. https://doi.org/10.3389/fgene.2021.664717

Marty, M.T., Baldwin, A.J., Marklund, E.G., Hochberg, G.K.A., Benesch, J.L.P., Robinson, C.V., 2015. Bayesian Deconvolution of Mass and Ion Mobility Spectra: From Binary Interactions to Polydisperse Ensembles. Anal. Chem. 87, 4370–4376. https://doi.org/10.1021/acs.analchem.5b00140

Masuyama, S., Tateishi, S., Yomogida, K., Nishimune, Y., Suzuki, K., Sakuraba, Y., Inoue, H., Ogawa, M., Yamaizumi, M., 2005. Regulated expression and dynamic changes in subnuclear localization of mammalian Rad18 under normal and genotoxic conditions. Genes to Cells 10, 753–762. https://doi.org/10.1111/j.1365-2443.2005.00874.x

Matthews, J.M., Bhati, M., Lehtomaki, E., Mansfield, R.E., Cubeddu, L., Mackay, J.P., 2009. It takes two to tango: the structure and function of LIM, RING, PHD and MYND domains. Curr Pharm Des 15, 3681–96. https://doi.org/10.2174/138161209789271861

Matthews, N.H., Fitch, K., Li, W.-Q., Morris, J.S., Christiani, D.C., Qureshi, A.A., Cho, E., 2019. Exposure to Trace Elements and Risk of Skin Cancer: A Systematic Review of Epidemiologic Studies. Cancer Epidemiol Biomarkers Prev 28, 3–21. https://doi.org/10.1158/1055-9965.EPI-18-0286

Mauro, M., Caradonna, F., Klein, C.B., 2016. Dysregulation of DNA Methylation Induced by Past Arsenic Treatment Causes Persistent Genomic Instability in Mammalian Cells. Environ Mol Mutagen 57, 137–150. https://doi.org/10.1002/em.21987

Mayer, J.E., Goldman, R.H., 2016. Arsenic and skin cancer in the USA: the current evidence regarding arsenic-contaminated drinking water. International Journal of Dermatology 55, e585–e591. https://doi.org/10.1111/ijd.13318

Medda, N., De, S.K., Maiti, S., 2021. Different mechanisms of arsenic related signaling in cellular proliferation, apoptosis and neo-plastic transformation. Ecotoxicology and Environmental Safety 208, 111752. https://doi.org/10.1016/j.ecoenv.2020.111752

Melak, D., Ferreccio, C., Kalman, D., Parra, R., Acevedo, J., Pérez, L., Cortés, S., Smith, A.H., Yuan, Y., Liaw, J., Steinmaus, C., 2014. Arsenic methylation and lung and bladder cancer in a case-control study in northern Chile. Toxicol Appl Pharmacol 274, 225–231. https://doi.org/10.1016/j.taap.2013.11.014

Melkonian, S., Argos, M., Pierce, Brandon L., Chen, Y., Islam, T., Ahmed, A., Syed, E.H., Parvez, F., Graziano, J., Rathouz, P.J., Ahsan, H., 2011. A Prospective Study of the Synergistic Effects of Arsenic Exposure and Smoking, Sun Exposure, Fertilizer Use, and Pesticide Use on Risk of Premalignant Skin Lesions in Bangladeshi Men. Am J Epidemiol. 173, 183–191. https://doi.org/10.1093/aje/kwq357

Mendez, W.M., Eftim, S., Cohen, J., Warren, I., Cowden, J., Lee, J.S., Sams, R., 2017. Relationships between arsenic concentrations in drinking water and lung and bladder cancer incidence in U.S. counties. J Expo Sci Environ Epidemiol 27, 235–243. https://doi.org/10.1038/jes.2016.58

Meng, R., Zhou, J., Sui, M., Li, Z., Feng, G., Yang, B., 2010. Arsenic trioxide promotes mitochondrial DNA mutation and cell apoptosis in primary APL cells and NB4 cell line. Sci. China Life Sci. 53, 87–93. https://doi.org/10.1007/s11427-010-0004-9

Miller, D.M., Thomas, S.D., Islam, A., Muench, D., Sedoris, K., 2012. c-Myc and Cancer Metabolism. Clin Cancer Res 18, 5546–5553. https://doi.org/10.1158/1078-0432.CCR-12-0977

Miodragović, Đ., Swindell, E.P., Sattar Waxali, Z., Bogachkov, A., O'Halloran, T.V., 2019. Beyond cisplatin: Combination therapy with arsenic trioxide. Inorganica Chimica Acta 496, 119030. https://doi.org/10.1016/j.ica.2019.119030

Miyase, S., Tateishi, S., Watanabe, K., Tomita, K., Suzuki, K., Inoue, H., Yamaizumi, M., 2005. Differential Regulation of Rad18 through Rad6-dependent Mono- and Polyubiquitination*. Journal of Biological Chemistry 280, 515–524. https://doi.org/10.1074/jbc.M409219200

Mo, J., Xia, Y., Wade, T.J., Schmitt, M., Le, X.C., Dang, R., Mumford, J.L., 2006. Chronic Arsenic Exposure and Oxidative Stress: OGG1 Expression and Arsenic Exposure, Nail Selenium, and Skin Hyperkeratosis in Inner Mongolia. Environ Health Perspect 114, 835–841. https://doi.org/10.1289/ehp.8723

Mognato, M., Burdak-Rothkamm, S., Rothkamm, K., 2021. Interplay between DNA replication stress, chromatin dynamics and DNA-damage response for the maintenance of genome stability. Mutation Research/Reviews in Mutation Research 787, 108346. https://doi.org/10.1016/j.mrrev.2020.108346

Mokhtari, R.B., Homayouni, T.S., Baluch, N., Morgatskaya, E., Kumar, S., Das, B., Yeger, H., 2017. Combination therapy in combating cancer. Oncotarget 8, 38022–38043. https://doi.org/10.18632/oncotarget.16723

Moloudi, K., Neshasteriz, A., Hosseini, A., Eyvazzadeh, N., Shomali, M., Eynali, S., Mirzaei, E., Azarnezhad, A., 2017. Synergistic Effects of Arsenic

Trioxide and Radiation: Triggering the Intrinsic Pathway of Apoptosis. Iran Biomed J 21, 330–337. https://doi.org/10.18869/acadpub.ibj.21.5.330
Moore, L.E., Smith, A.H., Eng, C., Kalman, D., DeVries, S., Bhargava, V., Chew, K., Moore II, D., Ferreccio, C., Rey, O.A., Waldman, F.M., 2002. Arsenic-Related Chromosomal Alterations in Bladder Cancer. JNCI: Journal of the National Cancer Institute 94, 1688–1696. https://doi.org/10.1093/jnci/94.22.1688
Morales, M.E., Derbes, R.S., Ade, C.M., Ortego, J.C., Stark, J., Deininger, P.L., Roy-Engel, A.M., 2016. Heavy Metal Exposure Influences Double Strand Break DNA Repair Outcomes. PLOS ONE 11, e0151367. https://doi.org/10.1371/journal.pone.0151367
Moslehi, R., Stagnar, C., Srinivasan, S., Radziszowski, P., Carpenter, D.O., 2021. The possible role of arsenic and gene-arsenic interactions in susceptibility to breast cancer: a systematic review. Rev Environ Health 36, 523–534. https://doi.org/10.1515/reveh-2020-0080
Muenyi, C.S., Ljungman, M., States, J.C., 2015. Arsenic Disruption of DNA Damage Responses—Potential Role in Carcinogenesis and Chemotherapy. Biomolecules 5, 2184–2193. https://doi.org/10.3390/biom5042184
Muenyi, C.S., States, V.A., Masters, J.H., Fan, T.W., Helm, C.W., States, J.C., 2011. Sodium arsenite and hyperthermia modulate cisplatin-DNA damage responses and enhance platinum accumulation in murine metastatic ovarian cancer xenograft after hyperthermic intraperitoneal chemotherapy (HIPEC). J Ovarian Res 4, 9. https://doi.org/10.1186/1757-2215-4-9
Nandi, D., Patra, R.C., Swarup, D., 2005. Effect of cysteine, methionine, ascorbic acid and thiamine on arsenic-induced oxidative stress and biochemical alterations in rats. Toxicology 211, 26–35. https://doi.org/10.1016/j.tox.2005.02.013
Natarajan V, Scribner W M, al-Hassani M, Vepa S, 1998. Reactive oxygen species signaling through regulation of protein tyrosine phosphorylation in endothelial cells. Environmental Health Perspectives 106, 1205–1212. https://doi.org/10.1289/ehp.98106s51205
Naujokas, M.F., Anderson, B., Ahsan, H., Aposhian, H.V., Graziano, J.H., Thompson, C., Suk, W.A., 2013. The Broad Scope of Health Effects from Chronic Arsenic Exposure: Update on a Worldwide Public Health Problem. Environ Health Perspect 121, 295–302. https://doi.org/10.1289/ehp.1205875
Navasumrit, P., Chaisatra, K., Promvijit, J., Parnlob, V., Waraprasit, S., Chompoobut, C., Binh, T.T., Hai, D.N., Bao, N.D., Hai, N.K., Kim, K.-W., Samson, L.D., Graziano, J.H., Mahidol, C., Ruchirawat, M., 2019. Exposure to arsenic in utero is associated with various types of DNA damage and micronuclei in newborns: a birth cohort study. Environ Health 18. https://doi.org/10.1186/s12940-019-0481-7
Nishigori, C., Hattori, Y., Toyokuni, S., 2004. Role of reactive oxygen species in skin carcinogenesis. Antioxid Redox Signal 6, 561–570. https://doi.org/10.1089/152308604773934314

Nohara, K., Nakabayashi, K., Okamura, K., Suzuki, T., Suzuki, S., Hata, K., 2020. Gestational arsenic exposure induces site-specific DNA hypomethylation in active retrotransposon subfamilies in offspring sperm in mice. Epigenetics & Chromatin 13, 53. https://doi.org/10.1186/s13072-020-00375-3

Nohara, K., Suzuki, T., Okamura, K., Matsushita, J., Takumi, S., 2017. Tumor-augmenting effects of gestational arsenic exposure on F1 and F2 in mice. Genes and Environment 39, 3. https://doi.org/10.1186/s41021-016-0069-1

Nohara, K., Tateishi, Y., Suzuki, T., Okamura, K., Murai, H., Takumi, S., Maekawa, F., Nishimura, N., Kobori, M., Ito, T., 2012. Late-onset increases in oxidative stress and other tumorigenic activities and tumors with a Ha-ras mutation in the liver of adult male C3H mice gestationally exposed to arsenic. Toxicol Sci 129, 293–304. https://doi.org/10.1093/toxsci/kfs203

Nollen, M., Ebert, F., Moser, J., Mullenders, L.H.F., Hartwig, A., Schwerdtle, T., 2009. Impact of arsenic on nucleotide excision repair: XPC function, protein level, and gene expression. Molecular Nutrition & Food Research 53, 572–582. https://doi.org/10.1002/mnfr.200800480

Norbury, C.J., Zhivotovsky, B., 2004. DNA damage-induced apoptosis. Oncogene 23, 2797–2808. https://doi.org/10.1038/sj.onc.1207532

Noureddine, A., Paffett, M.L., Franco, S., Chan, A.E., Pallikkuth, S., Lidke, K., Serda, R.E., 2021. Endolysosomal Mesoporous Silica Nanoparticle Trafficking along Microtubular Highways. Pharmaceutics 14, 56. https://doi.org/10.3390/pharmaceutics14010056

Nunez, N., Clifton, M.M.K., Funnell, A.P.W., Artuz, C., Hallal, S., Quinlan, K.G.R., Font, J., Vandevenne, M., Setiyaputra, S., Pearson, R.C.M., Mackay, J.P., Crossley, M., 2011. The multi-zinc finger protein ZNF217 contacts DNA through a two-finger domain. J Biol Chem 286, 38190–38201. https://doi.org/10.1074/jbc.M111.301234

Oberoi, S., Barchowsky, A., Wu, F., 2014. The global burden of disease for skin, lung, and bladder cancer caused by arsenic in food. Cancer Epidemiol Biomarkers Prev 23, 1187–1194. https://doi.org/10.1158/1055-9965.EPI-13-1317

Ortega, J., Li, J.Y., Lee, S., Tong, D., Gu, L., Li, G.-M., 2015. Phosphorylation of PCNA by EGFR inhibits mismatch repair and promotes misincorporation during DNA synthesis. PNAS 112, 5667–5672. https://doi.org/10.1073/pnas.1417711112

Osmond, M.J., Kunz, B.A., Snow, E.T., 2010. Age and exposure to arsenic alter base excision repair transcript levels in mice. Mutagenesis 25, 517–522. https://doi.org/10.1093/mutage/geq037

Palma-Lara, I., Martínez-Castillo, M., Quintana-Pérez, J.C., Arellano-Mendoza, M.G., Tamay-Cach, F., Valenzuela-Limón, O.L., García-Montalvo, E.A., Hernández-Zavala, A., 2020. Arsenic exposure: A public health problem leading to several cancers. Regul Toxicol Pharmacol 110, 104539. https://doi.org/10.1016/j.yrtph.2019.104539

Pant, N., Murthy, R.C., Srivastava, S.P., 2004. Male reproductive toxicity of sodium arsenite in mice. Hum Exp Toxicol 23, 399–403. https://doi.org/10.1191/0960327104ht467oa
Partridge, M.A., Huang, S.X.L., Hernandez-Rosa, E., Davidson, M.M., Hei, T.K., 2007. Arsenic Induced Mitochondrial DNA Damage and Altered Mitochondrial Oxidative Function: Implications for Genotoxic Mechanisms in Mammalian Cells. Cancer Res 67, 5239–5247. https://doi.org/10.1158/0008-5472.CAN-07-0074
Pascal, J.M., 2018. The comings and goings of PARP-1 in response to DNA damage. DNA Repair (Amst.) 71, 177–182. https://doi.org/10.1016/j.dnarep.2018.08.022
Petushkova, A.I., Zamyatnin, A.A., 2020. Redox-Mediated Post-Translational Modifications of Proteolytic Enzymes and Their Role in Protease Functioning. Biomolecules 10, 650. https://doi.org/10.3390/biom10040650
Pfeifer, G.P., Hainaut, P., 2003. On the origin of G→T transversions in lung cancer. Mutation Research/Fundamental and Molecular Mechanisms of Mutagenesis 526, 39–43. https://doi.org/10.1016/S0027-5107(03)00013-7
Piberger, A.L., Krüger, C.T., Strauch, B.M., Schneider, B., Hartwig, A., 2018. BPDE-induced genotoxicity: relationship between DNA adducts, mutagenicity in the in vitro PIG-A assay, and the transcriptional response to DNA damage in TK6 cells. Arch Toxicol 92, 541–551. https://doi.org/10.1007/s00204-017-2003-0
Podgorski, J., Berg, M., 2020. Global threat of arsenic in groundwater. Science 368, 845–850. https://doi.org/10.1126/science.aba1510
Pournara, A., Kippler, M., Holmlund, T., Ceder, R., Grafström, R., Vahter, M., Broberg, K., Wallberg, A.E., 2016. Arsenic alters global histone modifications in lymphocytes in vitro and in vivo. Cell Biol Toxicol 32, 275–284. https://doi.org/10.1007/s10565-016-9334-0
Qian, Y., Liu, K.J., Chen, Y., Flynn, D.C., Castranova, V., Shi, X., 2005. Cdc42 regulates arsenic-induced NADPH oxidase activation and cell migration through actin filament reorganization. J. Biol. Chem. 280, 3875–3884. https://doi.org/10.1074/jbc.M403788200
Qin, X.-J., Hudson, L.G., Liu, W., Ding, W., Cooper, K.L., Liu, K.J., 2008a. Dual actions involved in arsenite-induced oxidative DNA damage. Chem Res Toxicol 21, 1806–1813. https://doi.org/10.1021/tx8001548
Qin, X.-J., Hudson, L.G., Liu, W., Timmins, G.S., Liu, K.J., 2008b. Low concentration of arsenite exacerbates UVR-induced DNA strand breaks by inhibiting PARP-1 activity. Toxicol Appl Pharmacol 232, 41–50. https://doi.org/10.1016/j.taap.2008.05.019
Qin, X.-J., Liu, W., Li, Y.-N., Sun, X., Hai, C.-X., Hudson, L.G., Liu, K.J., 2012. Poly(ADP-Ribose) Polymerase-1 Inhibition by Arsenite Promotes the Survival of Cells With Unrepaired DNA Lesions Induced by UV Exposure. Toxicological Sciences 127, 120–129. https://doi.org/10.1093/toxsci/kfs099
Quinet, A., Martins, D.J., Vessoni, A.T., Biard, D., Sarasin, A., Stary, A., Menck, C.F.M., 2016. Translesion synthesis mechanisms depend on the nature of

DNA damage in UV-irradiated human cells. Nucleic Acids Res 44, 5717–5731. https://doi.org/10.1093/nar/gkw280
Raad, H., Serrano-Sanchez, M., Harfouche, G., Mahfouf, W., Bortolotto, D., Bergeron, V., Kasraian, Z., Dousset, L., Hosseini, M., Taieb, A., Rezvani, H.R., 2017. NADPH Oxidase-1 Plays a Key Role in Keratinocyte Responses to UV Radiation and UVB-Induced Skin Carcinogenesis. Journal of Investigative Dermatology 137, 1311–1321. https://doi.org/10.1016/j.jid.2016.12.027
Ray Chaudhuri, A., Nussenzweig, A., 2017. The multifaceted roles of PARP1 in DNA repair and chromatin remodelling. Nat Rev Mol Cell Biol 18, 610–621. https://doi.org/10.1038/nrm.2017.53
Razin, S.V., Borunova, V.V., Maksimenko, O.G., Kantidze, O.L., 2012. Cys2His2 zinc finger protein family: classification, functions, and major members. Biochemistry (Mosc) 77, 217–26. https://doi.org/10.1134/S0006297912030017
Rea, M., Eckstein, M., Eleazer, R., Smith, C., Fondufe-Mittendorf, Y.N., 2017. Genome-wide DNA methylation reprogramming in response to inorganic arsenic links inhibition of CTCF binding, DNMT expression and cellular transformation. Scientific Reports 7, 41474. https://doi.org/10.1038/srep41474
Reichard, J.F., Puga, A., 2010. Effects of arsenic exposure on DNA methylation and epigenetic gene regulation. Epigenomics 2, 87–104. https://doi.org/10.2217/epi.09.45
Reichard, J.F., Schnekenburger, M., Puga, A., 2007. Long term low-dose arsenic exposure induces loss of DNA methylation. Biochemical and Biophysical Research Communications 352, 188–192. https://doi.org/10.1016/j.bbrc.2006.11.001
Rengarajan, T., Rajendran, Peramaiyan, Nandakumar, N., Lokeshkumar, B., Rajendran, Palaniswami, Nishigaki, I., 2015. Exposure to polycyclic aromatic hydrocarbons with special focus on cancer. Asian Pacific Journal of Tropical Biomedicine 5, 182–189. https://doi.org/10.1016/S2221-1691(15)30003-4
Reynolds, P., Cooper, S., Lomax, M., O'Neill, P., 2015. Disruption of PARP1 function inhibits base excision repair of a sub-set of DNA lesions. Nucleic Acids Res 43, 4028–4038. https://doi.org/10.1093/nar/gkv250
Rizzo, A.A., Salerno, P.E., Bezsonova, I., Korzhnev, D.M., 2014. NMR structure of the human Rad18 zinc finger in complex with ubiquitin defines a class of UBZ domains in proteins linked to the DNA damage response. Biochemistry 53, 5895–5906. https://doi.org/10.1021/bi500823h
Rocha, C.R.R., Silva, M.M., Quinet, A., Cabral-Neto, J.B., Menck, C.F.M., 2018. DNA repair pathways and cisplatin resistance: an intimate relationship. Clinics (Sao Paulo) 73. https://doi.org/10.6061/clinics/2018/e478s
Roest, H.P., Baarends, W.M., de Wit, J., van Klaveren, J.W., Wassenaar, E., Hoogerbrugge, J.W., van Cappellen, W.A., Hoeijmakers, J.H.J., Grootegoed, J.A., 2004. The Ubiquitin-Conjugating DNA Repair Enzyme HR6A Is a Maternal Factor Essential for Early Embryonic Development in

Mice. Mol Cell Biol 24, 5485–5495. https://doi.org/10.1128/MCB.24.12.5485-5495.2004
Rogers, H.W., Weinstock, M.A., Feldman, S.R., Coldiron, B.M., 2015. Incidence Estimate of Nonmelanoma Skin Cancer (Keratinocyte Carcinomas) in the U.S. Population, 2012. JAMA Dermatol 151, 1081–1086. https://doi.org/10.1001/jamadermatol.2015.1187
Ropolo, M., Cappelli, E., Foresta, M., Poggi, A., Proietti-De-Santis, L., Frosina, G., 2011. Defective resolution of pH2AX foci and enhanced DNA breakage in ionizing radiation-treated cockayne syndrome B cells. IUBMB Life 63, 272–276. https://doi.org/10.1002/iub.445
Rossman, T.G., Uddin, A.N., Burns, F.J., 2004. Evidence that arsenite acts as a cocarcinogen in skin cancer. Toxicol Appl Pharmacol 198, 394–404. https://doi.org/10.1016/j.taap.2003.10.016
Rossman, T.G., Uddin, A.N., Burns, F.J., Bosland, M.C., 2001. Arsenite is a cocarcinogen with solar ultraviolet radiation for mouse skin: an animal model for arsenic carcinogenesis. Toxicol Appl Pharmacol 176, 64–71. https://doi.org/10.1006/taap.2001.9277
Roy, N.K., Murphy, A., Costa, M., 2020. Arsenic Methyltransferase and Methylation of Inorganic Arsenic. Biomolecules 10, E1351. https://doi.org/10.3390/biom10091351
Roy, P., Mukherjee, A., Giri, S., 2016. Evaluation of genetic damage in tobacco and arsenic exposed population of Southern Assam, India using buccal cytome assay and comet assay. Ecotoxicology and Environmental Safety 124, 169–176. https://doi.org/10.1016/j.ecoenv.2015.10.019
Rudolf, J., Raad, H., Taieb, A., Rezvani, H.R., 2018. NADPH Oxidases and Their Roles in Skin Homeostasis and Carcinogenesis. Antioxidants & Redox Signaling 28, 1238–1261. https://doi.org/10.1089/ars.2017.7282
Ruíz-Vera, T., Ochoa-Martínez, Á.C., Zarazúa, S., Carrizales-Yáñez, L., Pérez-Maldonado, I.N., 2019. Circulating miRNA-126, -145 and -155 levels in Mexican women exposed to inorganic arsenic via drinking water. Environmental Toxicology and Pharmacology 67, 79–86. https://doi.org/10.1016/j.etap.2019.02.004
Saberi, A., Hochegger, H., Szuts, D., Lan, L., Yasui, A., Sale, J.E., Taniguchi, Y., Murakawa, Y., Zeng, W., Yokomori, K., Helleday, T., Teraoka, H., Arakawa, H., Buerstedde, J.-M., Takeda, S., 2007. RAD18 and Poly(ADP-Ribose) Polymerase Independently Suppress the Access of Nonhomologous End Joining to Double-Strand Breaks and Facilitate Homologous Recombination-Mediated Repair. Mol Cell Biol 27, 2562–2571. https://doi.org/10.1128/MCB.01243-06
Saha, B., Salemi, M., Williams, G.L., Oh, S., Paffett, M.L., Phinney, B., Mandell, M.A., 2022. Interactomic analysis reveals a homeostatic role for the HIV restriction factor TRIM5α in mitophagy. Cell Rep 39, 110797. https://doi.org/10.1016/j.celrep.2022.110797
Saint-Jacques, N., Brown, P., Nauta, L., Boxall, J., Parker, L., Dummer, T.J.B., 2018. Estimating the risk of bladder and kidney cancer from exposure to

low-levels of arsenic in drinking water, Nova Scotia, Canada. Environment International 110, 95–104. https://doi.org/10.1016/j.envint.2017.10.014
Saint-Jacques, N., Parker, L., Brown, P., Dummer, T.J., 2014. Arsenic in drinking water and urinary tract cancers: a systematic review of 30 years of epidemiological evidence. Environ Health 13, 44. https://doi.org/10.1186/1476-069X-13-44
Sakumi, K., Tominaga, Y., Furuichi, M., Xu, P., Tsuzuki, T., Sekiguchi, M., Nakabeppu, Y., 2003. Ogg1 Knockout-associated Lung Tumorigenesis and Its Suppression by Mth1 Gene Disruption. Cancer Res 63, 902–905.
Salnikow, K., Zhitkovich, A., 2008. Genetic and Epigenetic Mechanisms in Metal Carcinogenesis and Cocarcinogenesis: Nickel, Arsenic and Chromium. Chemical research in toxicology 21, 28–44. https://doi.org/10.1021/tx700198a
Samuel, S., Kathirvel, R., Jayavelu, T., Chinnakkannu, P., 2005. Protein oxidative damage in arsenic induced rat brain: influence of dl-α-lipoic acid. Toxicology Letters 155, 27–34. https://doi.org/10.1016/j.toxlet.2004.08.001
Sanyal, T., Bhattacharjee, P., Bhattacharjee, S., Bhattacharjee, P., 2018. Hypomethylation of mitochondrial D-loop and ND6 with increased mitochondrial DNA copy number in the arsenic-exposed population. Toxicology 408, 54–61. https://doi.org/10.1016/j.tox.2018.06.012
Sasatani, M., Xu, Y., Kawai, H., Cao, L., Tateishi, S., Shimura, T., Li, J., Iizuka, D., Noda, A., Hamasaki, K., Kusunoki, Y., Kamiya, K., 2015. RAD18 Activates the G2/M Checkpoint through DNA Damage Signaling to Maintain Genome Integrity after Ionizing Radiation Exposure. PLOS ONE 10, e0117845. https://doi.org/10.1371/journal.pone.0117845
Sattar, A., Xie, S., Hafeez, M.A., Wang, X., Hussain, H.I., Iqbal, Z., Pan, Y., Iqbal, M., Shabbir, M.A., Yuan, Z., 2016. Metabolism and toxicity of arsenicals in mammals. Environmental Toxicology and Pharmacology 48, 214–224. https://doi.org/10.1016/j.etap.2016.10.020
Saxena, R., Bozack, A.K., Gamble, M.V., 2018. Nutritional Influences on One-Carbon Metabolism: Effects on Arsenic Methylation and Toxicity. Annu Rev Nutr 38, 401–429. https://doi.org/10.1146/annurev-nutr-082117-051757
Schärer, O.D., 2013. Nucleotide Excision Repair in Eukaryotes. Cold Spring Harb Perspect Biol 5. https://doi.org/10.1101/cshperspect.a012609
Selmin, O.I., Donovan, M.G., Skovan, B., Paine-Murieta, G.D., Romagnolo, D.F., 2019. Arsenic-induced BRCA1 CpG promoter methylation is associated with the downregulation of ER[alpha] and resistance to tamoxifen in MCF7 breast cancer cells and mouse mammary tumor xenografts. International Journal of Oncology 54, 869–879. https://doi.org/10.3892/ijo.2019.4687
Shao, K., Zhou, Z., Xun, P., Cohen, S.M., 2021. Bayesian benchmark dose analysis for inorganic arsenic in drinking water associated with bladder and lung cancer using epidemiological data. Toxicology 455, 152752. https://doi.org/10.1016/j.tox.2021.152752

Sheldon, L.A., 2017. Inhibition of E2F1 activity and cell cycle progression by arsenic via retinoblastoma protein. Cell Cycle 16, 2058–2072. https://doi.org/10.1080/15384101.2017.1338221
Shen, L., Zhang, Guangshun, Lou, Z., Xu, G., Zhang, Guangji, 2017. Cryptotanshinone enhances the effect of Arsenic trioxide in treating liver cancer cell by inducing apoptosis through downregulating phosphorylated-STAT3 in vitro and in vivo. BMC Complementary and Alternative Medicine 17, 106. https://doi.org/10.1186/s12906-016-1548-4
Shi, H., Hudson, L.G., Ding, W., Wang, S., Cooper, K.L., Liu, S., Chen, Y., Shi, X., Liu, K.J., 2004a. Arsenite causes DNA damage in keratinocytes via generation of hydroxyl radicals. Chem Res Toxicol 17, 871–878. https://doi.org/10.1021/tx049939e
Shi, H., Hudson, L.G., Liu, K.J., 2004b. Oxidative stress and apoptosis in metal ion-induced carcinogenesis. Free Radical Biology and Medicine 37, 582–593. https://doi.org/10.1016/j.freeradbiomed.2004.03.012
Shiomi, N., Mori, M., Tsuji, H., Imai, T., Inoue, H., Tateishi, S., Yamaizumi, M., Shiomi, T., 2007. Human RAD18 is involved in S phase-specific single-strand break repair without PCNA monoubiquitination. Nucleic Acids Res 35, e9. https://doi.org/10.1093/nar/gkl979
Singh, K.P., Kumari, R., Treas, J., DuMond, J.W., 2011. Chronic Exposure to Arsenic Causes Increased Cell Survival, DNA Damage, and Increased Expression of Mitochondrial Transcription Factor A (mtTFA) in Human Prostate Epithelial Cells. Chem. Res. Toxicol. 24, 340–349. https://doi.org/10.1021/tx1003112
Sirbu, B.M., Couch, F.B., Feigerle, J.T., Bhaskara, S., Hiebert, S.W., Cortez, D., 2011. Analysis of protein dynamics at active, stalled, and collapsed replication forks. Genes Dev. 25, 1320–1327. https://doi.org/10.1101/gad.2053211
Smeester, L., Fry, R.C., 2018. Long-Term Health Effects and Underlying Biological Mechanisms of Developmental Exposure to Arsenic. Curr Envir Health Rpt 5, 134–144. https://doi.org/10.1007/s40572-018-0184-1
Smith, A.H., Marshall, G., Liaw, J., Yuan, Y., Ferreccio, C., Steinmaus, C., 2012. Mortality in Young Adults following in Utero and Childhood Exposure to Arsenic in Drinking Water. Environ Health Perspect 120, 1527–1531. https://doi.org/10.1289/ehp.1104867
Smith, A.H., Marshall, G., Yuan, Y., Ferreccio, C., Liaw, J., von, E.O., Steinmaus, C., Bates, M.N., Selvin, S., 2006. Increased Mortality from Lung Cancer and Bronchiectasis in Young Adults after Exposure to Arsenic in Utero and in Early Childhood. Environmental Health Perspectives 114, 1293–1296. https://doi.org/10.1289/ehp.8832
Smith, K.R., Klei, L.R., Barchowsky, A., 2001. Arsenite stimulates plasma membrane NADPH oxidase in vascular endothelial cells. American Journal of Physiology-Lung Cellular and Molecular Physiology 280, L442–L449. https://doi.org/10.1152/ajplung.2001.280.3.L442
Smith, S., Hwang, J.-Y., Banerjee, S., Majeed, A., Gupta, A., Myung, K., 2004. Mutator genes for suppression of gross chromosomal rearrangements

identified by a genome-wide screening in Saccharomyces cerevisiae. PNAS 101, 9039–9044. https://doi.org/10.1073/pnas.0403093101
Song, I.Y., Palle, K., Gurkar, A., Tateishi, S., Kupfer, G.M., Vaziri, C., 2010. Rad18-mediated Translesion Synthesis of Bulky DNA Adducts Is Coupled to Activation of the Fanconi Anemia DNA Repair Pathway *. Journal of Biological Chemistry 285, 31525–31536. https://doi.org/10.1074/jbc.M110.138206
Song, Y., Jin, D., Chen, J., Liang, W., Liu, X., 2020. Effects of Arsenic (+3 Oxidation State) Methyltransferase Gene Polymorphisms and Expression on Bladder Cancer: Evidence from a Systematic Review, Meta-analysis and TCGA Dataset. Toxicol Sci 177, 27–40. https://doi.org/10.1093/toxsci/kfaa087
Soriano, C., Creus, A., Marcos, R., 2007. Gene-mutation induction by arsenic compounds in the mouse lymphoma assay. Mutation Research/Genetic Toxicology and Environmental Mutagenesis 634, 40–50. https://doi.org/10.1016/j.mrgentox.2007.05.014
Souza, K., Maddock, D.A., Zhang, Q., Chen, J., Chiu, C., Mehta, S., Wan, Y., 2001. Arsenite Activation of PI3K/AKT Cell Survival Pathway is Mediated by p38 in Cultured Human Keratinocytes. Mol Med 7, 767–772. https://doi.org/10.1007/BF03401967
Srinivas, N., Rachakonda, S., Hielscher, T., Calderazzo, S., Rudnai, P., Gurzau, E., Koppova, K., Fletcher, T., Kumar, R., 2019. Telomere length, arsenic exposure and risk of basal cell carcinoma of skin. Carcinogenesis 40, 715–723. https://doi.org/10.1093/carcin/bgz059
Steinmaus, C., Ferreccio, C., Acevedo, J., Yuan, Y., Liaw, J., Durán, V., Cuevas, S., García, J., Meza, R., Valdés, R., Valdés, G., Benítez, H., VanderLinde, V., Villagra, V., Cantor, K.P., Moore, L.E., Perez, S.G., Steinmaus, S., Smith, A.H., 2014. Increased lung and bladder cancer incidence in adults after in utero and early-life arsenic exposure. Cancer Epidemiol Biomarkers Prev 23, 1529–1538. https://doi.org/10.1158/1055-9965.EPI-14-0059
Su, C.-C., Lu, J.-L., Tsai, K.-Y., Lian, I.-B., 2011. Reduction in arsenic intake from water has different impacts on lung cancer and bladder cancer in an arseniasis endemic area in Taiwan. Cancer Causes Control 22, 101–108. https://doi.org/10.1007/s10552-010-9679-2
Su, Y., Meador, J.A., Geard, C.R., Balajee, A.S., 2010. Analysis of ionizing radiation-induced DNA damage and repair in three-dimensional human skin model system. Exp Dermatol 19, e16–e22. https://doi.org/10.1111/j.1600-0625.2009.00945.x
Sun, X., Zhan, L., Chen, Y., Wang, G., He, L., Wang, Q., Zhou, F., Yang, F., Wu, J., Wu, Y., Xing, J., He, X., Huang, Q., 2018. Increased mtDNA copy number promotes cancer progression by enhancing mitochondrial oxidative phosphorylation in microsatellite-stable colorectal cancer. Signal Transduction and Targeted Therapy 3, 1–9. https://doi.org/10.1038/s41392-018-0011-z

Sun, X., Zhou, X., Du, L., Liu, W., Liu, Y., Hudson, L.G., Liu, K.J., 2014. Arsenite binding-induced zinc loss from PARP-1 is equivalent to zinc deficiency in reducing PARP-1 activity, leading to inhibition of DNA repair. Toxicol Appl Pharmacol 274, 313–318. https://doi.org/10.1016/j.taap.2013.11.010

Sun, Y., Kojima, C., Chignell, C., Mason, R., Waalkes, M.P., 2011. Arsenic Transformation Predisposes Human Skin Keratinocytes To UV-induced DNA Damage Yet Enhances Their Survival Apparently by Diminishing Oxidant Response. Toxicol Appl Pharmacol 255, 242–250. https://doi.org/10.1016/j.taap.2011.07.006

Sykora, P., Snow, E.T., 2008. Modulation of DNA polymerase beta-dependent base excision repair in cultured human cells after low dose exposure to arsenite. Toxicology and Applied Pharmacology 228, 385–394. https://doi.org/10.1016/j.taap.2007.12.019

Szüts, D., Simpson, L.J., Kabani, S., Yamazoe, M., Sale, J.E., 2006. Role for RAD18 in Homologous Recombination in DT40 Cells. Molecular and Cellular Biology 26, 8032–8041. https://doi.org/10.1128/MCB.01291-06

Taeger, D., Johnen, G., Wiethege, T., Tapio, S., Möhner, M., Wesch, H., Tannapfel, A., Müller, K.-M., Brüning, T., Pesch, B., 2009. Major histopathological patterns of lung cancer related to arsenic exposure in German uranium miners. Int Arch Occup Environ Health 82, 867–875. https://doi.org/10.1007/s00420-008-0386-1

Takahashi, M., Barrett, J.C., Tsutsui, T., 2002. Transformation by inorganic arsenic compounds of normal Syrian hamster embryo cells into a neoplastic state in which they become anchorage-independent and cause tumors in newborn hamsters. International Journal of Cancer 99, 629–634. https://doi.org/10.1002/ijc.10407

Takahashi, S., Takeda, E., Kubota, Y., Okayasu, R., 2000. Inhibition of Repair of Radiation-Induced DNA Double-Strand Breaks by Nickel and Arsenite. Radiation Research 154, 686–691.

Tam, L.M., Jiang, J., Wang, P., Li, L., Miao, W., Dong, X., Wang, Y., 2017. Arsenite Binds to the Zinc Finger Motif of TIP60 Histone Acetyltransferase and Induces Its Degradation via the 26S Proteasome. Chem. Res. Toxicol. 30, 1685–1693. https://doi.org/10.1021/acs.chemrestox.7b00146

Tam, L.M., Price, N.E., Wang, Y., 2020. Molecular Mechanisms of Arsenic-Induced Disruption of DNA Repair. Chem. Res. Toxicol. 33, 709–726. https://doi.org/10.1021/acs.chemrestox.9b00464

Tamás, M.J., Sharma, S.K., Ibstedt, S., Jacobson, T., Christen, P., 2014. Heavy Metals and Metalloids As a Cause for Protein Misfolding and Aggregation. Biomolecules 4, 252–267. https://doi.org/10.3390/biom4010252

Tanoue, Y., Toyoda, T., Sun, J., Mustofa, Md.K., Tateishi, C., Endo, S., Motoyama, N., Araki, K., Wu, D., Okuno, Y., Tsukamoto, T., Takeya, M., Ihn, H., Vaziri, C., Tateishi, S., 2018. Differential Roles of Rad18 and Chk2 in Genome Maintenance and Skin Carcinogenesis Following UV Exposure. Journal of Investigative Dermatology 138, 2550–2557. https://doi.org/10.1016/j.jid.2018.05.015

Tateishi, S., Niwa, H., Miyazaki, J.-I., Fujimoto, S., Inoue, H., Yamaizumi, M., 2003. Enhanced Genomic Instability and Defective Postreplication Repair in RAD18 Knockout Mouse Embryonic Stem Cells. Mol Cell Biol 23, 474–481. https://doi.org/10.1128/MCB.23.2.474-481.2003

Tateishi, S., Sakuraba, Y., Masuyama, S., Inoue, H., Yamaizumi, M., 2000. Dysfunction of human Rad18 results in defective postreplication repair and hypersensitivity to multiple mutagens. PNAS 97, 7927–7932. https://doi.org/10.1073/pnas.97.14.7927

Tehrani, S.S., Hosseini, H.M., Yousefi, T., Abolghasemi, M., Qujeq, D., Maniati, M., Amani, J., 2019. The crosstalk between trace elements with DNA damage response, repair, and oxidative stress in cancer. Journal of Cellular Biochemistry 120, 1080–1105. https://doi.org/10.1002/jcb.27617

Thompson, J.A., White, C.C., Cox, D.P., Chan, J.Y., Kavanagh, T.J., Fausto, N., Franklin, C.C., 2009. Distinct Nrf1/2-independent mechanisms mediate As3+-induced glutamate-cysteine ligase subunit gene expression in murine hepatocytes. Free Radical Biology and Medicine 46, 1614–1625. https://doi.org/10.1016/j.freeradbiomed.2009.03.016

Thompson, S.L., Compton, D.A., 2011. Chromosomes and cancer cells. Chromosome Res 19, 433–444. https://doi.org/10.1007/s10577-010-9179-y

Tian, F., Sharma, S., Zou, J., Lin, S.-Y., Wang, B., Rezvani, K., Wang, H., Parvin, J.D., Ludwig, T., Canman, C.E., Zhang, D., 2013. BRCA1 promotes the ubiquitination of PCNA and recruitment of translesion polymerases in response to replication blockade. Proc Natl Acad Sci U S A 110, 13558–13563. https://doi.org/10.1073/pnas.1306534110

Tong, D., Ortega, J., Kim, C., Huang, J., Gu, L., Li, G.-M., 2015. Arsenic Inhibits DNA Mismatch Repair by Promoting EGFR Expression and PCNA Phosphorylation. J Biol Chem 290, 14536–14541. https://doi.org/10.1074/jbc.M115.641399

Tran, H.-P., Prakash, Arungundrum.S., Barnard, R., Chiswell, B., Ng, J.C., 2002. Arsenic inhibits the repair of DNA damage induced by benzo(a)pyrene. Toxicology Letters 133, 59–67. https://doi.org/10.1016/S0378-4274(02)00088-7

Tsai, T.-L., Kuo, C.-C., Hsu, L.-I., Tsai, S.-F., Chiou, H.-Y., Chen, C.-J., Hsu, K.-H., Wang, S.-L., 2021. Association between arsenic exposure, DNA damage, and urological cancers incidence: A long-term follow-up study of residents in an arseniasis endemic area of northeastern Taiwan. Chemosphere 266, 129094. https://doi.org/10.1016/j.chemosphere.2020.129094

Tseng, L.-M., Yin, P.-H., Chi, C.-W., Hsu, C.-Y., Wu, C.-W., Lee, L.-M., Wei, Y.-H., Lee, H.-C., 2006. Mitochondrial DNA mutations and mitochondrial DNA depletion in breast cancer. Genes, Chromosomes and Cancer 45, 629–638. https://doi.org/10.1002/gcc.20326

Tsuda, T., Babazono, A., Yamamoto, E., Kurumatani, N., Mino, Y., Ogawa, T., Kishi, Y., Aoyama, H., 1995. Ingested arsenic and internal cancer: a

historical cohort study followed for 33 years. Am J Epidemiol 141, 198–209. https://doi.org/10.1093/oxfordjournals.aje.a117421
Tsuji, J.S., Chang, E.T., Gentry, P.R., Clewell, H.J., Boffetta, P., Cohen, S.M., 2019. Dose-response for assessing the cancer risk of inorganic arsenic in drinking water: the scientific basis for use of a threshold approach. Critical Reviews in Toxicology 49, 36–84. https://doi.org/10.1080/10408444.2019.1573804
Tsuji, Y., Watanabe, K., Araki, K., Shinohara, M., Yamagata, Y., Tsurimoto, T., Hanaoka, F., Yamamura, K., Yamaizumi, M., Tateishi, S., 2008. Recognition of forked and single-stranded DNA structures by human RAD18 complexed with RAD6B protein triggers its recruitment to stalled replication forks. Genes to Cells 13, 343–354. https://doi.org/10.1111/j.1365-2443.2008.01176.x
Tu, W., Liu, Y., Xie, C., Zhou, X., 2018. Arsenite downregulates H3K4 trimethylation and H3K9 dimethylation during transformation of human bronchial epithelial cells. Journal of Applied Toxicology 38, 480–488. https://doi.org/10.1002/jat.3555
Turner, C.E., Miller, J.T., 1994. Primary sequence of paxillin contains putative SH2 and SH3 domain binding motifs and multiple LIM domains: identification of a vinculin and pp125Fak-binding region. J Cell Sci 107 (Pt 6), 1583–91.
Uhlen, M., Fagerberg, L., Hallstrom, B.M., Lindskog, C., Oksvold, P., Mardinoglu, A., Sivertsson, A., Kampf, C., Sjostedt, E., Asplund, A., Olsson, I., Edlund, K., Lundberg, E., Navani, S., Szigyarto, C.A.-K., Odeberg, J., Djureinovic, D., Takanen, J.O., Hober, S., Alm, T., Edqvist, P.-H., Berling, H., Tegel, H., Mulder, J., Rockberg, J., Nilsson, P., Schwenk, J.M., Hamsten, M., von Feilitzen, K., Forsberg, M., Persson, L., Johansson, F., Zwahlen, M., von Heijne, G., Nielsen, J., Ponten, F., 2015. Tissue-based map of the human proteome. Science 347, 1260419–1260419. https://doi.org/10.1126/science.1260419
United States Environmental Protection Agency, 2000. Arsenic in drinking water rule economic analysis [WWW Document].
Valencia, A., Kochevar, I.E., 2008. Nox1-Based NADPH Oxidase Is the Major Source of UVA-Induced Reactive Oxygen Species in Human Keratinocytes. Journal of Investigative Dermatology 128, 214–222. https://doi.org/10.1038/sj.jid.5700960
Varanasi, L., Do, P.M., Goluszko, E., Martinez, L.A., 2012. Rad18 is a transcriptional target of E2F3. Cell Cycle 11, 1131–1141. https://doi.org/10.4161/cc.11.6.19558
Vaziri, C., Tateishi, S., Mutter-Rottmayer, E., Gao, Y., 2016. Chapter 16 - Roles of RAD18 in DNA Replication and Postreplication Repair, in: Kovalchuk, I., Kovalchuk, O. (Eds.), Genome Stability. Academic Press, Boston, pp. 257–273. https://doi.org/10.1016/B978-0-12-803309-8.00016-1
Vilas, C.K., Emery, L.E., Denchi, E.L., Miller, K.M., 2018. Caught with one's zinc fingers in the genome integrity cookie jar. Trends Genet 34, 313–325. https://doi.org/10.1016/j.tig.2017.12.011

Vogt, B.L., Rossman, T.G., 2001. Effects of arsenite on p53, p21 and cyclin D expression in normal human fibroblasts — a possible mechanism for arsenite's comutagenicity. Mutation Research/Fundamental and Molecular Mechanisms of Mutagenesis 478, 159–168. https://doi.org/10.1016/S0027-5107(01)00137-3

Waalkes, M.P., Liu, J., Diwan, B.A., 2007. Transplacental arsenic carcinogenesis in mice. Toxicology and Applied Pharmacology, Research and Risk Assessment for Arsenic 222, 271–280. https://doi.org/10.1016/j.taap.2006.12.034

Waghela, B.N., Vaidya, F.U., Agrawal, Y., Santra, M.K., Mishra, V., Pathak, C., 2021. Molecular insights of NADPH oxidases and its pathological consequences. Cell Biochem Funct 39, 218–234. https://doi.org/10.1002/cbf.3589

Walter, I., Schwerdtle, T., Thuy, C., Parsons, J.L., Dianov, G.L., Hartwig, A., 2007. Impact of arsenite and its methylated metabolites on PARP-1 activity, PARP-1 gene expression and poly(ADP-ribosyl)ation in cultured human cells. DNA Repair 6, 61–70. https://doi.org/10.1016/j.dnarep.2006.08.008

Wang, C.-K., Lee, H.-L., Chang, H., Tsai, M.-H., Kuo, Y.-C., Lin, P., 2012. Enhancement between environmental tobacco smoke and arsenic on emphysema-like lesions in mice. Journal of Hazardous Materials 221–222, 256–263. https://doi.org/10.1016/j.jhazmat.2012.04.042

Wang, F., Zhou, X., Liu, W., Sun, X., Chen, C., Hudson, L.G., Jian Liu, K., 2013. Arsenite-induced ROS/RNS generation causes zinc loss and inhibits the activity of poly(ADP-ribose) polymerase-1. Free Radical Biology and Medicine 61, 249–256. https://doi.org/10.1016/j.freeradbiomed.2013.04.019

Wang, T.-C., Jan, K.-Y., Wang, A.S.S., Gurr, J.-R., 2007. Trivalent arsenicals induce lipid peroxidation, protein carbonylation, and oxidative DNA damage in human urothelial cells. Mutation Research/Fundamental and Molecular Mechanisms of Mutagenesis 615, 75–86. https://doi.org/10.1016/j.mrfmmm.2006.10.003

Wang, X., Li, S., 2014. Protein mislocalization: mechanisms, functions and clinical applications in cancer. Biochim Biophys Acta 1846, 13–25. https://doi.org/10.1016/j.bbcan.2014.03.006

Wang, Yijie, Luo, W., Wang, Yingfei, 2019. PARP-1 and its associated nucleases in DNA damage response. DNA Repair (Amst) 81, 102651. https://doi.org/10.1016/j.dnarep.2019.102651

Watanabe, K., Iwabuchi, K., Sun, J., Tsuji, Y., Tani, T., Tokunaga, K., Date, T., Hashimoto, M., 2009. RAD18 promotes DNA double-strand break repair during G1 phase through chromatin retention of 53BP1. Nucleic Acids Res 2176–2193.

Watanabe, K., Tateishi, S., Kawasuji, M., Tsurimoto, T., Inoue, H., Yamaizumi, M., 2004. Rad18 guides polη to replication stalling sites through physical interaction and PCNA monoubiquitination. The EMBO Journal 23, 3886–3896. https://doi.org/10.1038/sj.emboj.7600383

Watanabe, M., Funakoshi, T., Unuma, K., Aki, T., Uemura, K., 2014. Activation of the ubiquitin–proteasome system against arsenic trioxide cardiotoxicity involves ubiquitin ligase Parkin for mitochondrial homeostasis. Toxicology 322, 43–50. https://doi.org/10.1016/j.tox.2014.04.008
Wei, S., Zhang, H., Tao, S., 2019. A review of arsenic exposure and lung cancer. Toxicol Res (Camb) 8, 319–327. https://doi.org/10.1039/c8tx00298c
Wetzler, M., Brady, M.T., Tracy, E., Li, Z.-R., Donohue, K.A., O'Loughlin, K.L., Cheng, Y., Mortazavi, A., McDonald, A.A., Kunapuli, P., Wallace, P.K., Baer, M.R., Cowell, J.K., Baumann, H., 2006. Arsenic Trioxide Affects Signal Transducer and Activator of Transcription Proteins through Alteration of Protein Tyrosine Kinase Phosphorylation. Clin Cancer Res 12, 6817–6825. https://doi.org/10.1158/1078-0432.CCR-06-1354
Whitaker, A.M., Schaich, M.A., Smith, M.S., Flynn, T.S., Freudenthal, Bret.D., 2017. Base excision repair of oxidative DNA damage: from mechanism to disease. Front Biosci (Landmark Ed) 22, 1493–1522.
Williams, S.A., Longerich, S., Sung, P., Vaziri, C., Kupfer, G.M., 2011. The E3 ubiquitin ligase RAD18 regulates ubiquitylation and chromatin loading of FANCD2 and FANCI. Blood 117, 5078–5087. https://doi.org/10.1182/blood-2010-10-311761
Wong, C., Roberts, S.M., Saab, I.N., 2022. Review of regulatory reference values and background levels for heavy metals in the human diet. Regulatory Toxicology and Pharmacology 130, 105122. https://doi.org/10.1016/j.yrtph.2022.105122
World Health Organization, 2018. WHO housing and health guidelines. World Health Organization, Geneva.
Wu, F., Burns, F.J., Zhang, R., Uddin, A.N., Rossman, T.G., 2005. Arsenite-Induced Alterations of DNA Photodamage Repair and Apoptosis After Solar-Simulation UVR in Mouse Keratinocytes in Vitro. Environ Health Perspect 113, 983–986. https://doi.org/10.1289/ehp.7846
Xu, H., Lauer, F.T., Liu, K.J., Hudson, L.G., Burchiel, S.W., 2016. Editor's Highlight: Interactive Genotoxicity Induced by Environmentally Relevant Concentrations of Benzo(a)Pyrene Metabolites and Arsenite in Mouse Thymus Cells. Toxicological Sciences 154, 153–161. https://doi.org/10.1093/toxsci/kfw151
Yager, J.W., Erdei, E., Myers, O., Siegel, M., Berwick, M., 2016. Arsenic and ultraviolet radiation exposure: melanoma in a New Mexico non-Hispanic white population. Environ Geochem Health 38, 897–910. https://doi.org/10.1007/s10653-015-9770-4
Yajima, H., Lee, K.-J., Zhang, S., Kobayashi, J., Chen, B.P.C., 2009. DNA double-strand break formation upon UV-induced replication stress activates ATM and DNA-PKcs kinases. J Mol Biol 385, 800–810. https://doi.org/10.1016/j.jmb.2008.11.036
Yamanaka, K., Hoshino, M., Okamoto, M., Sawamura, R., Hasegawa, A., Okada, S., 1990. Induction of DNA damage by dimethylarsine, a metabolite of inorganic arsenics, is for the major part likely due to its peroxyl radical.

Biochemical and Biophysical Research Communications 168, 58–64. https://doi.org/10.1016/0006-291X(90)91674-H
Yamashita, Y.M., Okada, T., Matsusaka, T., Sonoda, E., Zhao, G.Y., Araki, K., Tateishi, S., Yamaizumi, M., Takeda, S., 2002. RAD18 and RAD54 cooperatively contribute to maintenance of genomic stability in vertebrate cells. EMBO J 21, 5558–5566. https://doi.org/10.1093/emboj/cdf534
Yan, W., Jung, Y.-S., Zhang, Y., Chen, X., 2014. Arsenic Trioxide Reactivates Proteasome-Dependent Degradation of Mutant p53 Protein in Cancer Cells in Part via Enhanced Expression of Pirh2 E3 Ligase. PLoS One 9. https://doi.org/10.1371/journal.pone.0103497
Yang, C., Hao, R., Lan, Y.F., Chen, Y.J., Wang, C., Bu, N., Wang, Q.Q., Hussain, L., Ma, L.Y., Maimaitiyiming, Y., Lu, X.Y., Naranmandura, H., 2019. Integrity of zinc finger motifs in PML protein is necessary for inducing its degradation by antimony. Metallomics 11, 1419–1429. https://doi.org/10.1039/C9MT00102F
Yang, Y., Gao, Y., Zlatanou, A., Tateishi, S., Yurchenko, V., Rogozin, I.B., Vaziri, C., 2018. Diverse roles of RAD18 and Y-family DNA polymerases in tumorigenesis. Cell Cycle 17, 833–843. https://doi.org/10.1080/15384101.2018.1456296
Yang, Y., Poe, J.C., Yang, L., Fedoriw, A., Desai, S., Magnuson, T., Li, Z., Fedoriw, Y., Araki, K., Gao, Y., Tateishi, S., Sarantopoulos, S., Vaziri, C., 2016. Rad18 confers hematopoietic progenitor cell DNA damage tolerance independently of the Fanconi Anemia pathway in vivo. Nucleic Acids Res 44, 4174–4188. https://doi.org/10.1093/nar/gkw072
Ye, C.J., Sharpe, Z., Heng, H.H., 2020. Origins and Consequences of Chromosomal Instability: From Cellular Adaptation to Genome Chaos-Mediated System Survival. Genes (Basel) 11. https://doi.org/10.3390/genes11101162
Yin, Y., Meng, F., Sui, C., Jiang, Y., Zhang, L., 2019. Arsenic enhances cell death and DNA damage induced by ultraviolet B exposure in mouse epidermal cells through the production of reactive oxygen species. Clinical and Experimental Dermatology 44, 512–519. https://doi.org/10.1111/ced.13834
Ying, S., Myers, K., Bottomley, S., Helleday, T., Bryant, H.E., 2009. BRCA2-dependent homologous recombination is required for repair of Arsenite-induced replication lesions in mammalian cells. Nucleic Acids Res 37, 5105–5113. https://doi.org/10.1093/nar/gkp538
Yu, M., Zhou, Y., Shi, Y., Ning, L., Yang, Y., Wei, X., Zhang, N., Hao, X., Niu, R., 2007. Reduced mitochondrial DNA copy number is correlated with tumor progression and prognosis in Chinese breast cancer patients. IUBMB Life 59, 450–457. https://doi.org/10.1080/15216540701509955
Yuan, Y., Marshall, G., Ferreccio, C., Steinmaus, C., Liaw, J., Bates, M., Smith, A.H., 2010. Kidney cancer mortality: fifty-year latency patterns related to arsenic exposure. Epidemiology 21, 103–108. https://doi.org/10.1097/EDE.0b013e3181c21e46

Zeman, M.K., Lin, J.-R., Freire, R., Cimprich, K.A., 2014. DNA damage-specific deubiquitination regulates Rad18 functions to suppress mutagenesis. J. Cell Biol. 206, 183–197. https://doi.org/10.1083/jcb.201311063
Zhang, A., Li, H., Xiao, Y., Chen, L., Zhu, X., Li, J., Ma, L., Pan, X., Chen, W., He, Z., 2017. Aberrant methylation of nucleotide excision repair genes is associated with chronic arsenic poisoning. Biomarkers 22, 429–438. https://doi.org/10.1080/1354750X.2016.1217933
Zhang, F., Paramasivam, M., Cai, Q., Dai, X., Wang, P., Lin, K., Song, J., Seidman, M.M., Wang, Y., 2014. Arsenite binds to the RING finger domains of RNF20-RNF40 histone E3 ubiquitin ligase and inhibits DNA double-strand break repair. J. Am. Chem. Soc. 136, 12884–12887. https://doi.org/10.1021/ja507863d
Zhang, N., Wu, Z.-M., McGowan, E., Shi, J., Hong, Z.-B., Ding, C.-W., Xia, P., Di, W., 2009. Arsenic trioxide and cisplatin synergism increase cytotoxicity in human ovarian cancer cells: Therapeutic potential for ovarian cancer. Cancer Science 100, 2459–2464. https://doi.org/10.1111/j.1349-7006.2009.01340.x
Zhang, W., Liu, Y., An, Z., Huang, D., Qi, Y., Zhang, Y., 2011. Mediating effect of ROS on mtDNA damage and low ATP content induced by arsenic trioxide in mouse oocytes. Toxicology in Vitro 25, 979–984. https://doi.org/10.1016/j.tiv.2011.03.009
Zhang, X., Yang, F., Shim, J.-Y., Kirk, K.L., Anderson, D.E., Chen, X., 2007. Identification of arsenic-binding proteins in human breast cancer cells. Cancer Lett 255, 95–106. https://doi.org/10.1016/j.canlet.2007.03.025
Zhang, Y., Bi, X., Jiang, F., 2015. Cytotoxin-induced NADPH oxides activation: roles in regulation of cell death. Arch. Toxicol. 89, 991–1006. https://doi.org/10.1007/s00204-015-1476-y
Zhou, L., Liu, Y., Liu, Shaobo, Yin, Y., Zeng, G., Tan, X., Hu, Xi, Hu, Xinjiang, Jiang, L., Ding, Y., Liu, Shaoheng, Huang, X., 2016. Investigation of the adsorption-reduction mechanisms of hexavalent chromium by ramie biochars of different pyrolytic temperatures. Bioresource Technology 218, 351–359. https://doi.org/10.1016/j.biortech.2016.06.102
Zhou, X., Cooper, K.L., Huestis, J., Xu, H., Burchiel, S.W., Hudson, L.G., Liu, K.J., 2016. S-nitrosation on zinc finger motif of PARP-1 as a mechanism of DNA repair inhibition by arsenite. Oncotarget 7, 80482–80492. https://doi.org/10.18632/oncotarget.12613
Zhou, X., Cooper, K.L., Sun, X., Liu, K.J., Hudson, L.G., 2015. Selective Sensitization of Zinc Finger Protein Oxidation by Reactive Oxygen Species through Arsenic Binding. J. Biol. Chem. 290, 18361–18369. https://doi.org/10.1074/jbc.M115.663906
Zhou, X., Ding, X., Shen, J., Yang, D., Hudson, L.G., Liu, K.J., 2019. Peroxynitrite contributes to arsenic-induced PARP-1 inhibition through ROS/RNS generation. Toxicology and Applied Pharmacology 378, 114602. https://doi.org/10.1016/j.taap.2019.114602
Zhou, X., Medina, S., Bolt, A.M., Zhang, H., Wan, G., Xu, H., Lauer, F.T., Wang, S.C., Burchiel, S.W., Liu, K.J., 2020. Inhibition of red blood cell

development by arsenic-induced disruption of GATA-1. Sci Rep 10, 19055. https://doi.org/10.1038/s41598-020-76118-x

Zhou, X., Speer, R.M., Volk, L., Hudson, L.G., Liu, K.J., 2021. Arsenic co-carcinogenesis: Inhibition of DNA repair and interaction with zinc finger proteins. Seminars in Cancer Biology. https://doi.org/10.1016/j.semcancer.2021.05.009

Zhou, X., Sun, X., Cooper, K.L., Wang, F., Liu, K.J., Hudson, L.G., 2011. Arsenite Interacts Selectively with Zinc Finger Proteins Containing C3H1 or C4 Motifs. J Biol Chem 286, 22855–22863. https://doi.org/10.1074/jbc.M111.232926

Zhou, X., Sun, X., Mobarak, C., Gandolfi, A.J., Burchiel, S.W., Hudson, L.G., Liu, K.J., 2014. Differential Binding of Monomethylarsonous Acid Compared to Arsenite and Arsenic Trioxide with Zinc Finger Peptides and Proteins. Chem. Res. Toxicol. 27, 690–698. https://doi.org/10.1021/tx500022j

Zhou, Y., Zeng, W., Qi, M., Duan, Y., Su, J., Zhao, S., Zhong, W., Gao, M., Li, F., He, Y., Hu, X., Xu, X., Chen, X., Peng, C., Zhang, J., 2017. Low dose arsenite confers resistance to UV induced apoptosis via p53-MDM2 pathway in ketatinocytes. Oncogenesis 6, e370. https://doi.org/10.1038/oncsis.2017.67